MAP 1 ROCCAMONFINA VOLCANO

Distribution of analysed samples and main lava groups.

- T–P — Trias–Palaeocene Limestones
- Main Lava Flows of Strato–Volcano
- tf — Tephritic Flank Eruptions
- tlp — Tephr. Lc. Phono./ Lc. Phonolite
- Caldera Wall
- Road
- β° — Olivine Basalt
- β¹ — Trachybasalt
- Lba — Latite
- •56 — Sample Location

0 1 2 3 Kms.

R.Garigliano

N

M.Friello

Conca d. Campania

Fortinella

Sipicciano

M.S.Antonio

La Cerchiara

M.Lattani

M.S.Croce

M.S.Maria

Terracorpo

Marzano Appio

M.Atano

Capitola

Carbonara

S.Lorenzo

Tuoro Piccolo

Ponte Grottoni

M.Casi

Teano

Fontanelle

M.Canneto

S.Giuliano

M.Ofelio

Sessa Aurunca

THE PETROLOGY OF THE POTASSIUM-RICH LAVAS OF THE ROCCAMONFINA VOLCANO, ITALY

by

J.D. APPLETON, B.Sc.(Dunelm)

Thesis presented for the Degree of Doctor of Philosophy of the University of Edinburgh in the Faculty of Science.

1970



ABSTRACT

The Roccamonfina volcano is situated 50 km NNW of Naples, W. Italy, and is one of the major volcanic centres in the Roman Region. The volcanic rocks of the Roman Region are characterised by their high potassium content, though there is a wide variation in the level of K enrichment in the different volcanic sequences. Published information concerning the Roccamonfina volcano indicated the presence of two significantly different lava series which can be distinguished on the basis of age, petrography and chemistry. The first series (referred to in this thesis as the High K series) includes the undersaturated ne and lc normative leucite bearing lavas of the main strato volcano, whilst the second series (Low K series) consists of ne/hy/Qz normative olivine basalts, trachybasalts, and biotite augite latites. Even in the Low K series, the K_2O/Na_2O ratio (mean = 1·5) is much higher than in the majority of basic volcanic rocks.

Major and trace element analyses of 117 samples from the Roccamonfina volcano show that the lavas of the High K series are enriched in K, P, Ba, Zr, Sr, Rb, Th, and Ce relative to the lavas of the Low K series. An analysis of the chemical variation in the primitive lavas indicates an almost parallel enrichment in K and associated elements. This relationship is also characteristic of the Roman Region primitive lavas. The compositional variation observed in the lavas of the Roman Region can be related to two main differentiation processes. Process A produces the parental magma

with a specific level of enrichment in K and associated elements. This is an intermediate or high pressure differentiation process. Process B (low pressure crystal-liquid fractionation) controls the evolution towards salic derivatives.

The low pressure differentiation of the lavas of the Roccamonfina High K series can be explained by the fractionation of the assemblage biotite-clinopyroxene-plagioclase-ore-apatite at c. 1·5 - 2·5kb P_{H2O} followed by the release of pressure and equilibration with the atmospheric pressure mineral assemblages. Fractionation of leucite slightly modifies the composition of some of the liquids derived from the earlier fractionation event. The variation in the lavas of the Low K series can be explained by the fractionation of olivine gabbro followed by the biotite-plagioclase-clinopyroxene-ore assemblage.

It is concluded that crustal assimilation and vapour transfer processes, and partial melting of a postulated upper mantle composition, cannot account for the variation observed in the primitive lavas of the Roman Region nor for the geochemical characteristics of potassic undersaturated rocks in general. It is proposed that high pressure eclogite fractionation, zone refining or mantle wall-rock reaction may produce the high levels of enrichment of K and associated elements observed in the lavas of the Roman Region.

PRELIMINARY NOTE ON UNITS

Unless otherwise stated, oxides are quoted as weight percent (wt.%) and elements as parts per million (ppm.)

C O N T E N T S

		Page
CHAPTER 1	INTRODUCTION	1
1:1	Potassium-rich lavas of the Roman Region	2
1:2	Roccamonfina - General Geology and Previous Research	5
1:3	Present Research	10
1:4	Plan of the Thesis	12
CHAPTER 2	PETROGRAPHY	13
2:1	High K Series	13
	Introduction	13
	Leucitites	15
	Tephritic leucitites	16
	Transitional tephritic leucitites	19
	Leucite tephrites	21
	Phonolitic leucite tephrites	21
	Tephritic leucite phonolites	23
	Leucite phonolites	23
	Trachyte	24
2:2	Low K Series	24
	Olivine basalts	24
	Trachybasalts	26
	Biotite augite latites	27
	Trachytic grey ash flow	28
2:3	Biotite Gabbro nodules	29
PLATES 1 - 50		
CHAPTER 3	MINERALOGY	30
3:1	Introduction	30
3:2	Leucite	30
3:3	Clinopyroxene	35
3:4	Phlogopite and Biotite	37
3:5	Plagioclase	39
3:6	Olivine	40

		Page
CHAPTER 4	CHEMISTRY OF THE LAVAS	41
4:1	Introduction	41
4:2	Frequency Distribution of Major and Trace Element Data	43
4:3	C.I.P.W. Norms	43
4:4	Chemical Variation	44
4:4:1	Correlation Coefficients	44
4:4:2	Variation Diagrams	46
	Introduction	46
	Roccamonfina Variation Diagrams	48
	K and associated elements enrichment and analysis of the K_2O v. SiO_2 plot for the lavas of the Roman Region	51
	Composition and sequence of lavas erupted at each of the volcanic centres	56
4:4:3	K/Rb relationship	57
4:4:4	Niobium	58
CHAPTER 5	DIFFERENTIATION OF THE LAVAS	59
5:1	Roccamonfina High K Series	59
	Introduction	59
	Phenocryst assemblages and other petrographic features relevant to the differentiation of the lavas of the High K series	60
	Nodules as possible crystal extracts	63
	Variation diagrams and extract calculations	65
	Leucite fractionation	69
	Leucite stability	71
5:2	Roccamonfina Low K Series	74
	Phenocryst assemblages	74
	Differentiation	74
5:3	Differentiation of some of the other volcanic sequences in the Roman Region	76
5:4	Summary	78

		Page
CHAPTER 6	ENRICHMENT PROCESSES	80
6:1	Introduction	80
6:2	Enrichment processes involving crustal assimilation	81
6:2:1	Introduction	81
6:2:2	Carbonate assimilation	82
6:2:3	Assimilation and hybridisation	85
6:2:4	Significance of Sr_{87}/Sr_{86} data	88
6:2:5	Crustal wall-rock reaction	90
6:3	Gaseous transfer	92
6:4	Upper mantle enrichment processes	94
6:4:1	Enrichment factors	94
6:4:2	Partial melting	97
6:4:3	Crystal-liquid fractionation	98
6:4:4	Zone refining and mantle wall-rock reaction	99
6:5	Conclusions	101
ACKNOWLEDGEMENTS		103
BIBLIOGRAPHY		104
APPENDIX A	Sample preparation and analytical methods	
APPENDIX B	Modal data and petrographic notes for the Roccamonfina lavas	
APPENDIX C	Tables of chemical data for the Roccamonfina lavas	
APPENDIX D	Correlation matrices	
APPENDIX E	Miscellaneous data	

CHAPTER 1

INTRODUCTION

Potassium-rich basic and ultrabasic volcanic rocks are of very limited occurrence, being mainly confined to continental areas. Some of the best known examples include the Roman Region of Italy (Washington, 1906; Rittman, 1933), the Laacher See area of Germany (Brauns, 1922, 1928; Frechen, 1962), the Birunga and Toro Ankole regions of Central Africa (Holmes and Harwood, 1937; Holmes, 1950; Higazy, 1954; Bell and Powell, 1969), the West Kimberly district of Australia (Wade and Prider, 1940), and the Leucite Hills of Wyoming (Cross, 1897; Carmichael, 1967). Less well known are the potassic undersaturated lavas of Java (Brouwer, 1945), and of the U.S.S.R. (Vorobieva, 1960). The only truly oceanic occurrence of leucite bearing lavas is Tristan da Cunha (Baker et al., 1964).

These very distinctive potassium-rich lavas are all characterised by high K_2O content, high K_2O/Na_2O ratio, and relatively low SiO_2 content, which is usually reflected in the appearance of feldspathoids, especially leucite. The trace element data available for some of these lavas indicates extreme enrichment in K and associated elements (Higazy, 1954; Bell and Powell, 1969). The term K and associated elements (Jamieson and Clark, 1970) refers to those elements (K,P,Ba,Zr,Sr,Rb,Th,U,Pb, and the Rare Earths) which are thought to be largely rejected by the main silicate phases in the zone of magma generation of the Upper Mantle (Harris, 1957; Oxburgh, 1964; Griffin and Murthy, 1969). These elements will be

preferentially concentrated in the liquid formed on partial melting of mantle peridotite and will remain in the liquid during subsequent periods of crystal-liquid fractionation. Jamieson and Clark (1970) review some of the processes which could affect the level of enrichment of K and associated elements in tholeiites, but it should be noted that these processes are equally applicable to lavas showing extreme enrichment in K and associated elements.

This thesis is mainly concerned with the petrology of the potassium-rich lavas of the Roccamonfina volcano (W. Italy), though data are also presented for comparative purposes, for lavas from some of the other volcanic centres of the Roman Region.

1:1 Potassium-rich lavas of the Roman Region

The Roman Region (Washington, 1906) consists of seven volcanic centres to the west of the Appennines (see Fig. 1-1). Although the main Plio-Pleistocene volcanic activity occurred to the west of the Appennines, leucite-bearing lavas are also found in a small area to the east of this mountain range (i.e. in the Mte. Vulture area.) The petrography and chemistry of the Vulture lavas is distinctly different from the lavas of the volcanic centres of Western Italy. Vulture lavas are characterised by the presence of hauyne, high SO_3, and relatively low K_2O/Na_2O ratios (Imbo, 1967). When trace element data becomes available for these lavas, their relationship to the more abundant leucite-bearing lavas of W. Italy may become more clear. Marinelli (1967) has discussed the general succession of volcanic activity in Italy

Fig. 1-1.

Volcanic centres of the Roman Region, W. Italy

(The map also shows the position of the
Mte. Vulture volcanic centre)

Vu = Vulsini

Ci = Cimini (includes the Vico volcano)

Sa = Sabatini

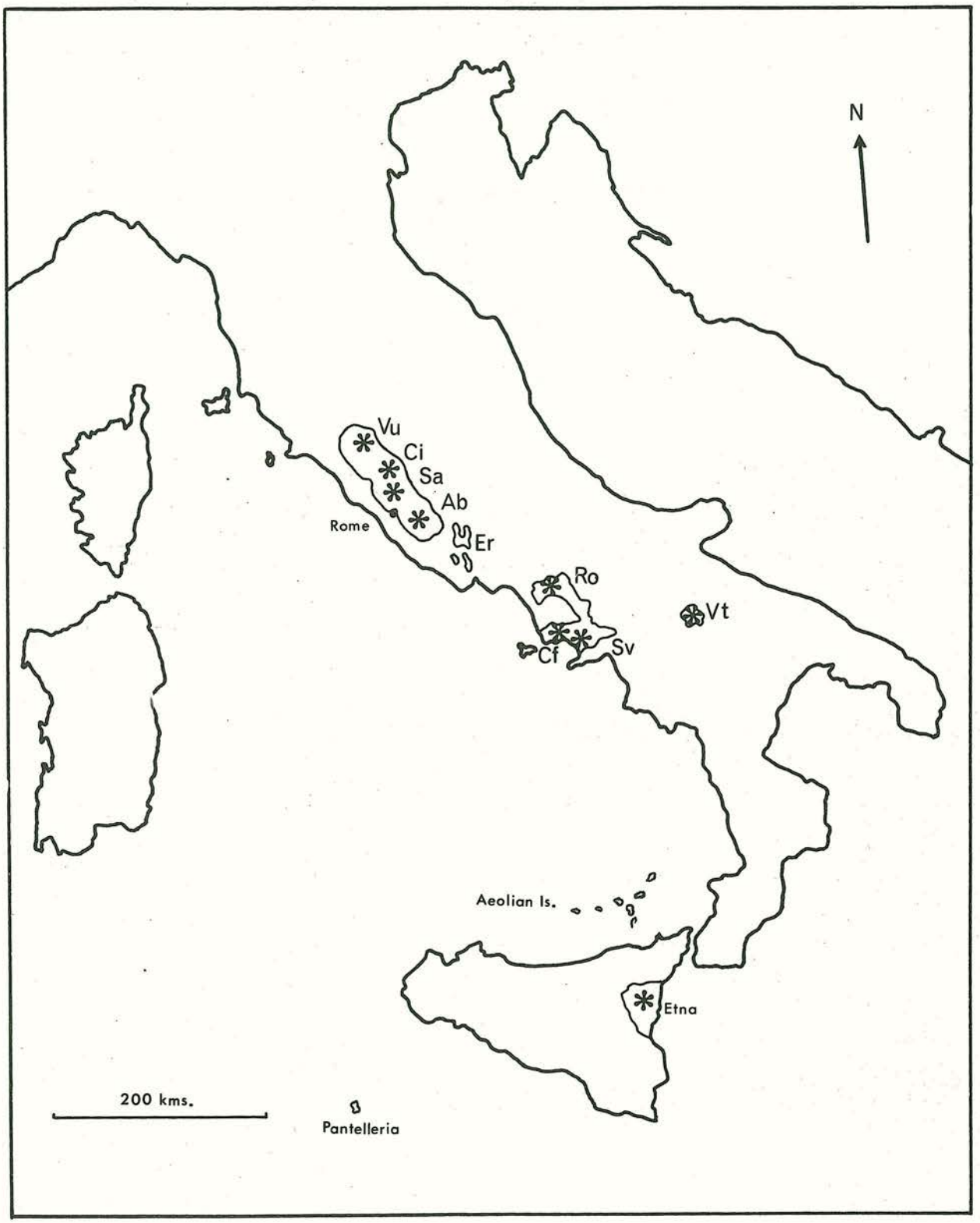
Ab = Albani (= Alban Hills)

Er = Ernici

Ro = Roccamonfina (= Auruncan district)

Cf = Phlegrean Fields)
) Campanian district
Sv = Somma-Vesuvius)

Vt = Vulture


N
Vu
Ci
Sa
Ab
Rome
Er
Ro
Vt
Cf
Sv
Aeolian Is.
Etna
200 kms.
Pantelleria

from the Mesozoic to the Pleistocene; the interested reader is referred to this work for further information.

K-Ar age determinations of the Italian Plio-Pleistocene volcanic rocks (Gasparini and Adams, 1969) show that the lavas of the Roman Region were erupted between 1·18 m.y. ago and the present day (the last eruption of Vesuvius being in 1944).

The volcanoes of the Roman Region exhibit a wide range of rock types, though the situation has been considerably confused by the use of complicated local terminology (Washington, 1906; Rittman, 1933). As well as the undersaturated leucite-bearing lavas (leucite basanites, leucitites, tephritic leucitites, leucite tephrites, phonolitic leucite tephrites, tephritic leucite phonolites, and leucite phonolites -- terminology according to Streckeisen, 1964, 1966) there are also potash-rich hy and Q normative lavas (e.g. the olivine basalts, trachybasalts, and latites of Roccamonfina (Arevalo et al., 1962; Gianetti, 1964) and Latera-Vulsini (Schneider, 1965; Triglia, 1966). These hy and Q normative lavas have distinctly lower K_2O contents when compared with the leucite-bearing lavas, but they still have abnormally high K_2O/Na_2O ratios (>1) when compared with "normal" alkaline lavas. It seems possible that the process that has produced the K-enrichment in the leucite-bearing lavas of the Roman Region has operated less efficiently to produce the hy and Q normative lavas. It should be noted that the eruption in the same volcanic region of lava series showing different K_2O/Na_2O ratios is not confined to the Roman Region (Joplin, 1968). For

example, in Indonesia, leucite-bearing lavas are found in the same region as calcalkaline lavas and lavas of the absarokite-shoshonite-banakite series, whilst in the Bufumbira area of Uganda (Holmes and Harwood, 1937; Bell and Powell, 1969), lavas of the absarokite-shoshonite-banakite series are found in association with leucite-bearing mafic lavas.

In order to document the differentiation of the leucite-phyric and leucite-free lavas of the Roman Region, and to assess quantitatively the enrichment level of K and associated elements, it was decided to carry out a detailed major and trace element geochemical study, backed up by petrographic and mineralogical data, of the lavas of the Roccamonfina volcano. The Roccamonfina volcano was chosen because published data (Panichi, 1922; Arevalo et al., 1962; Gianetti, 1964, 1965; Tedesco, 1965) indicated the presence of a relatively wide range of rock types and also the presence of two significantly different lava series. The two lava series can be distinguished on the basis of age, petrography, and chemistry. The first series includes undersaturated leucitites, tephritic leucitites, leucite tephrites, phonolitic leucite tephrites, tephritic leucite phonolites, and leucite phonolites, while the second series is a lower K series of ne/hy/Q normative olivine basalts, trachybasalts, and biotite augite latites. Even in the low K series, the K_2O/Na_2O ratio (mean = 1·5) is much higher than in the majority of volcanic rocks. These two lava series are referred to as the High K and the Low K series in this thesis.

It was thought that by quantitatively assessing enrichment

levels for K and associated elements in the Roccamonfina lavas, it might be possible to suggest an enrichment mechanism and to decide which of the many theories proposed to explain the geochemistry of potassic undersaturated lavas (recently reviewed by Bell and Powell, 1969) is the most plausible.

1:2 Roccamonfina - General Geology and Previous Research

The extinct volcano of Roccamonfina (last recorded eruption 276 B.C.) is located 50 km. N.N.W. of Naples (see Fig. 1-1). It is surrounded by fault-bounded mountains of Mesozoic and Cenozoic limestones, and is made up of a number of distinct morphological units which document its volcanic evolution (Tedesco, 1965; Fig. 1-2 and Map 1). These are:

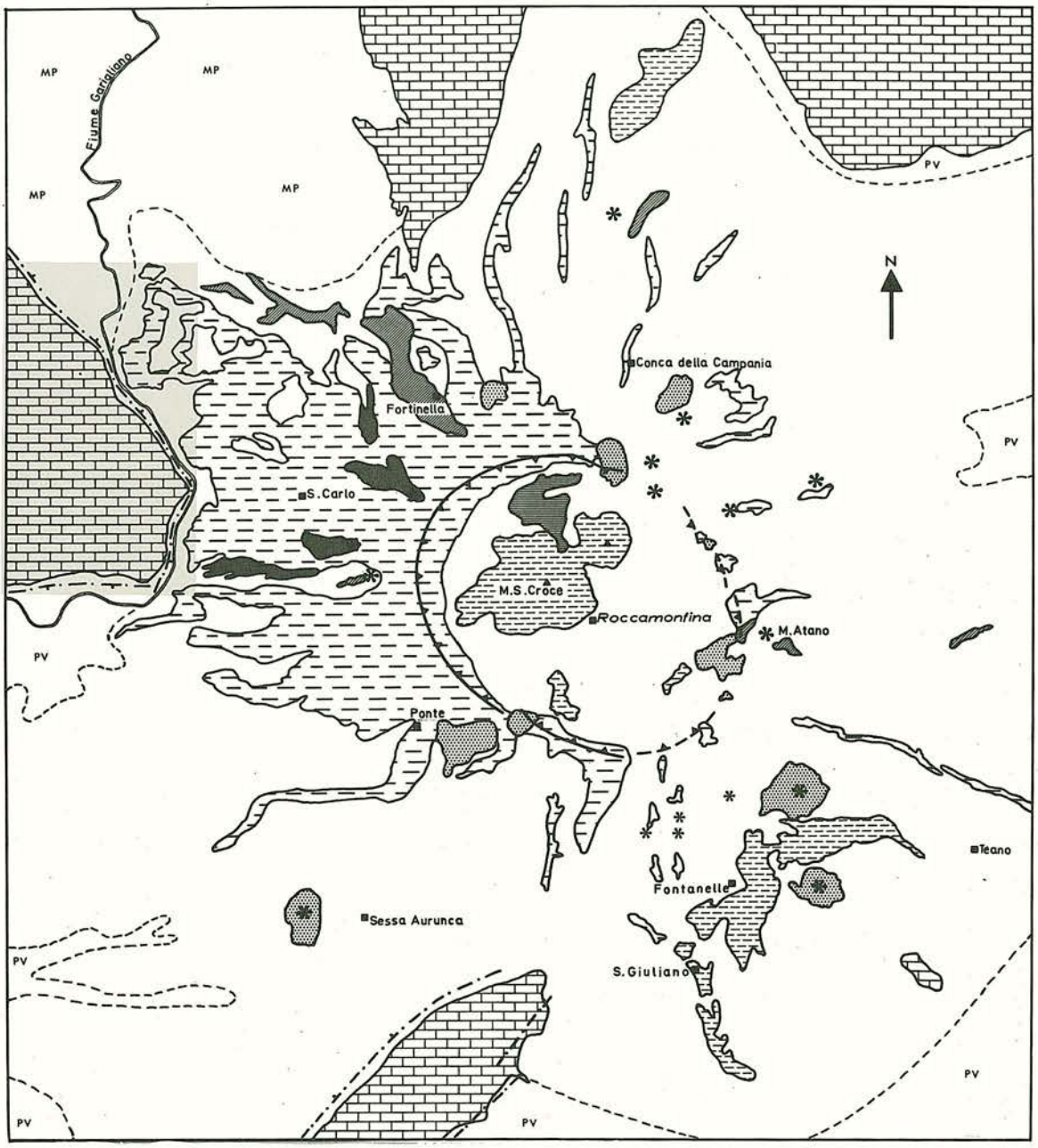
(1) The main strato volcano built up mainly of interstratified leucite-bearing lavas and tuffs. The thickest flows occur along the west flank bordering the Garigliano fault, where a fine grained tephritic leucitite/leucite tephrite (R. 81-83) reaches 20 m. in thickness. Most of the macroporphyritic lava flows are thinner (down to 1 m.), though at Ponte Grottoni a leucite macrophyric flow reaches over 8 m. in thickness.

(2) Adventive cones and flank eruptions of largely indeterminate age. These include the tephritic flows of the western flank (R. 37, 42, 53), the adventive cones of Mte. Casi, Mte. Canneto, Mte. Friello, Mte. Ofelio, the latite flows of the south-east flank near S. Giuliano and Fontanelle, and the olivine basalt flow of Sipicciano-Fortinella. The age of these flows and adventive

Fig. 1-2.

Simplified geological map of the Roccamonfina volcano

Adapted with slight modifications from the Italian Geological Survey Maps (Sheets 160, 161, 171, 172). The distribution of the grey ash flow is not shown. Map 1 (back pocket of this thesis) shows the distribution of the main lava groups in greater detail.



KEY

- Trias–Palaeocene Lsts.
- MP — Miocene–Pliocene Sediments
- Main Lava Flows of Strato–Volcano
- Pyroclastics
- Tephritic Flank Eruptions
- Tephr. Lc. Phona/ Lc. Phonolite
- Olivine Basalt
- Trachybasalt
- Latite
- PV — Post–Volcanic Sediments
- Adventive Cone
- Caldera Wall
- Fault
- Approx. Boundary of Strato–Volcano

5 Kms.

cones relative to the caldera collapse (Stage 3) is not precisely known, but they are thought to have been erupted after the main leucitic lava flows of the strato volcano (Tedesco, 1965; Gianetti, 1964, 1965).

(3) The caldera wall was formed as a result of the collapse of the central part of the volcano. It is very prominent along the west side, rising 290m. above the flat plain inside the caldera, but along the east side it is considerably dissected. The vast outpourings of mudflows and pyroclastic flows following the main leucitic lavas of the strato volcano are probably related to the period of caldera collapse (Tedesco, 1965).

(4) Extrusion in the centre of the caldera of the twin latite domes of Mte. S. Croce and Mte. Lattani followed the caldera collapse. The base of the caldera is filled with lacustrine deposits which are thought to predate the extrusion of the latite domes.

(5) The main trachybasalt flow of La Cerchiara was extruded in the depression between the latite domes of Mte. S. Croce and Mte. Lattani.

(6) According to Tedesco (1965), the Grey ash flow is the final eruption from the Roccamonfina caldera. J. Keller (personal communication), however, suggests that the Grey ash flow may have been erupted from a fissure to the east of the main Roccamonfina volcano and that the ash flow was moving so rapidly that it was able to climb the flanks of the strato volcano and flow into the caldera. The precise age and origin of the Grey ash flow is not particularly important to the present study.

Although the age of the basalt (Sipicciano-Fortinella, Mte. Friello, Mte. Atano) and latite (S. Giuliano-Fontanelle) flank eruptions is not precisely known, the fact that the central latite and trachybasalt eruptions definitely occurred after the collapse of the central caldera, and also the fact that leucite-bearing lavas are never seen overlying them suggests that all the lavas of the Low K series (olivine basalt, trachybasalt, latite sequence) were probably erupted after the eruption of the leucitic lavas and after the caldera collapse.

Petrographic studies of the Roccamonfina lavas have been carried out by Washington (1897, 1906), Panichi (1922), Seifert (1942), Aiello (1962), Arevalo et al. (1962), and Gianetti (1964, 1965, 1966). Both Arevalo et al. (1962) and Gianetti (1964, 1965) recognised the presence of at least two distinctive lava series on the basis of age, petrography, and chemistry. Arevalo et al. (1962) identified three lava series on the basis of 27 chemical analyses. They subdivide the High K series (as defined in this thesis) into two groups, the first including the main tephritic leucitite flows of the strato volcano, and the second including the biotite phonolitic tephrites (R.37,42,53 - Table B-1, Appendix B), and the tephritic phonolites/leucite phonolites of the adventive cones and flank eruptions (marked T on the Italian Geological Survey maps.) The differences between these two leucite-bearing series is small compared with the differences between the High K and Low K series as defined in this thesis.

Gianetti (1964) described some of the basalt, trachybasalt, and latite lavas of the Low K series, and in his second paper (1965) he described some of the most salic lavas of the High K series (tephritic leucite phonolites/leucite phonolites). On visiting some of the exposures described by Gianetti (1965), the present author found some of them to be extremely small and the rocks were very weathered (which probably explains the presence of 3·63%, 4·4%, and 9·6% H_2O in three of Gianetti's analyses).

The Italian Geological Survey maps of the Roccamonfina area suggest that the tephritic leucite phonolites and leucite phonolites (marked T on the maps) are the first eruptive products of the Roccamonfina volcano, being unconformably overlain by the tephritic leucitite flows of the main strato volcano. The present author has not found any evidence to confirm this, and Gianetti (1965) suggests that these phonolitic lavas were erupted after the caldera collapse. On the basis of the limited field evidence collected by the present author, the phonolitic lavas are thought to occur either as an integral part of the general sequence of leucitic lavas and tuffs which make up the main stratovolcano (e.g. R.179 is found interstratified with tephritic leucitite lavas and tuffs on the north flank of the volcano), or they represent a period of eruption after the collapse of the caldera (Gianetti, 1965), or during the later stages of the evolution of the strato volcano.

The lack of crucial exposures makes it very difficult to determine the exact age relationships between some of the lava types. However, the general sequence of (1) the eruption of the

leucite-bearing lavas of the strato volcano, followed by (2) caldera collapse, and (3) extrusion of olivine basalt, trachybasalt, and latite lavas within the caldera and on the flanks of the strato volcano is accepted by most authors (Arevalo et al., 1962; Gianetti, 1964, 1965; Tedesco, 1965).

Gianetti (1966) has also published a short note concerning two tephritic leucitite dykes which are exposed on the northern flank of the strato volcano (R.181,182).

Civetta and Rapolla (1965) and Imbo et al. (1968) have presented K, Th, and U data for some of the Roccamonfina lavas. The Th data (X.R.F.) presented in this thesis are in good agreement with the Th data (Gamma spectrometry) of these authors and confirms the high level of enrichment of Th in the Roccamonfina lavas.

Following the ideas of Rittman (1933), both Arevalo et al., (1962) and Gianetti (1964, 1965) concluded that the Roccamonfina leucite-bearing lavas "resulted from the primary Tyrhennian magma, which is known to be of trachybasaltic composition, by carbonate syntexis followed by normal gravitative differentiation, whereas the oversaturated rocks of the third (Low K) series represent a late rise of slightly differentiated but not desilicated melts". (Arevalo et al., 1962, p. 237). The various theories proposed to explain the peculiar geochemical features of the potassium-rich lavas of Roccamonfina in particular, and the Roman Region in general, will be discussed in Chapter 6.

1:3 Present Research

When this project was started in October 1967, there was no published trace element data for the lavas of the Roccamonfina volcano, and there were no modal petrographic data available for most of the analysed lavas. It was decided to collect a wide range of samples from the Roccamonfina volcano and to determine their major and trace element chemistry. It was hoped that this detailed major and trace element study, backed up by petrographic and mineralogical studies, might provide enough evidence to elucidate the differentiation of the two lava series, and also to put limitations on the possible mechanisms for enrichment in K_2O.

Since the project was started, there has been a rapid increase in the number of chemical analyses (major, trace, and isotopic) available for the lavas of the Roman Region (Savelli, 1967; Locardi and Mittempergher, 1967; Hoefs and Wedepohl, 1969) and for potassic lavas in general (Bell and Powell, 1969, 1970). However, no data have yet been published to illustrate the relationship between the undersaturated leucite-bearing lavas and the leucite-free lavas of the Roman Region in general, and Roccamonfina in particular.

Detailed mineralogical studies were not attempted due to the lack of electron-microprobe facilities.

During April-May 1968, 210 specimens were collected from the Roccamonfina area in an attempt to obtain a selection of samples encompassing the complete range of lava types. Use was made of the Italian Geological Survey maps (Sheets 160,161,171,172) and the

Italian topographic maps (Sheets 160 IISE, 160 IISO, 171 ISE, 171 INE, 172 IVSO, 172 IVNO) for locating the best exposures. The location of the analysed samples is shown on the geological map (Map 1); the basic geological boundaries of the various lava types being taken with slight modifications from the Italian Geological Survey maps. The majority of the samples were collected from roadside and quarry exposures as these were the only two types of exposure where fresh samples could be obtained.

A few specimens were also collected from the Alban Hills, Latera (Vulsini), Vesuvius, and Radicofani. Data concerning the location of these specimens, their petrography, and chemistry are presented in Appendix E. By collecting from more than one volcano it was hoped to compare the Roccamonfina lavas (especially the level of enrichment of K and associated elements) with the lavas from the other volcanic centres of the Roman Region. Comparisons based solely on trace element data taken from the literature may be complicated by the fact that different analytical techniques were used.

Thin sections of all the samples were examined and 117 whole rock samples from the Roccamonfina volcano were analysed for 12 major and 7 trace elements. A few were also analysed for Ce, and Nb. Leucite is the main phenocryst phase, so in order to see if there was any systematic variation in its major/trace element chemistry, 12 macrophyric lavas were selected and the leucite phenocrysts and groundmasses were separated and analysed.

1:4 Plan of the thesis

The petrographic, mineralogical, and chemical data are presented, interpreted and discussed in the main part of the thesis. Details of analytical methods, together with modal data, and most of the chemical analyses are presented in Appendices A to E.

CHAPTER 2

PETROGRAPHY

As noted in Chapter 1, the Roccamonfina volcano has two main series of lavas which are easily distinguished on the basis of age, petrography, and chemistry. The distribution of the various lava types and the location of analysed specimens are shown on the map of the Roccamonfina area (Map 1). A modal analysis and brief petrographic notes for each of the analysed specimens is presented in Appendix B. In this chapter, the main petrographic features of each of the major lava groups are noted, together with an explanation of the classificatory criteria. The relationship between the petrography and chemistry of the Roccamonfina lavas is shown in Fig. 2-1. Photomicrographs (Plates 1-50) referred to in the text can be found at the end of this chapter.

2:1 High K Series

Introduction

Following the recommendations of Rittman (1952) and Streckeisen (1964, 1966), the lavas of the High K series were classified according to the approximate modal proportions of the felsic constituents - leucite, plagioclase, and alkai feldspar (sanidine). The specifications of the petrographic classification used in this study are as follows:

```
                                                                    ;
                                                                    ;
                                                                    ;
```

Fig. 2-1.

K_2O v. SiO_2 plot showing the relationship between the petrography and chemistry of the Roccamonfina lavas. (Chemical analyses of the lavas are presented in Appendix C).

L : Leucitites

TL : Tephritic Leucitites

TG : Transitional Group - Tephritic Leucitites/ Leucite Tephrites/Phonolitic Leucite Tephrites.

PLT : Phonolitic Leucite Tephrites

TLP : Tephritic Leucite Phonolites

LP : Leucite Phonolites

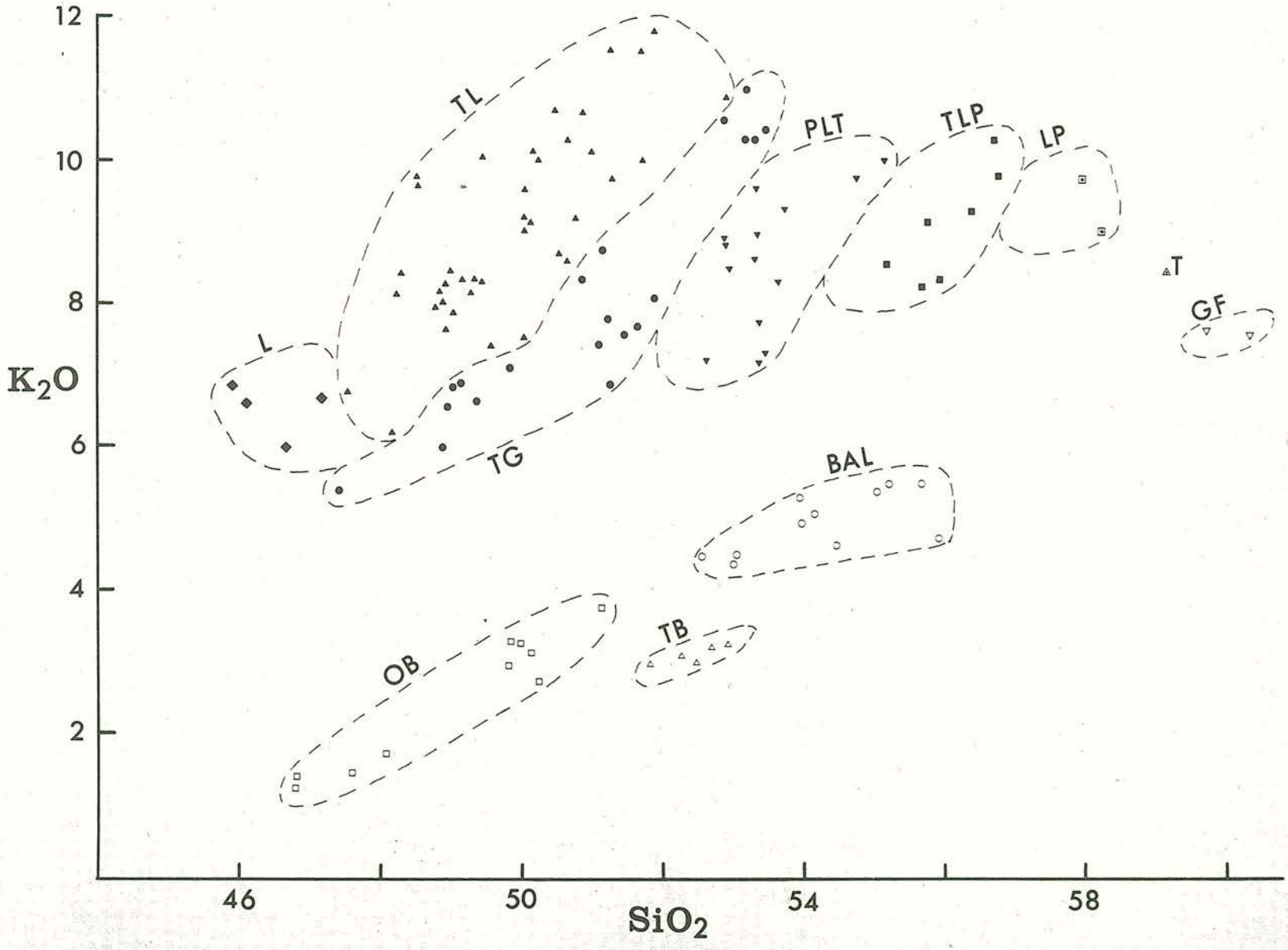
T : Trachyte

OB : Olivine Basalts

TB : Trachybasalts

BAL : Biotite Augite Latites

GF : Grey Ash Flow


12
10
8
6
4
2
K_2O
46
50
54
58
SiO_2
TL
PLT
TLP
LP
T
GF
L
TG
BAL
OB
TB

Leucitite — leucite + <10% total feldspar

Tephritic leucitite — leucite>plagioclase; sanidine <10%

Leucite tephrite — plagioclase>leucite; sanidine <10%

Phonolitic leucite tephrite — leucite + plagioclase + sanidine; plag.>sanidine

Tephritic leucite phonolite — leucite + plagioclase + sanidine; sanidine > plag.

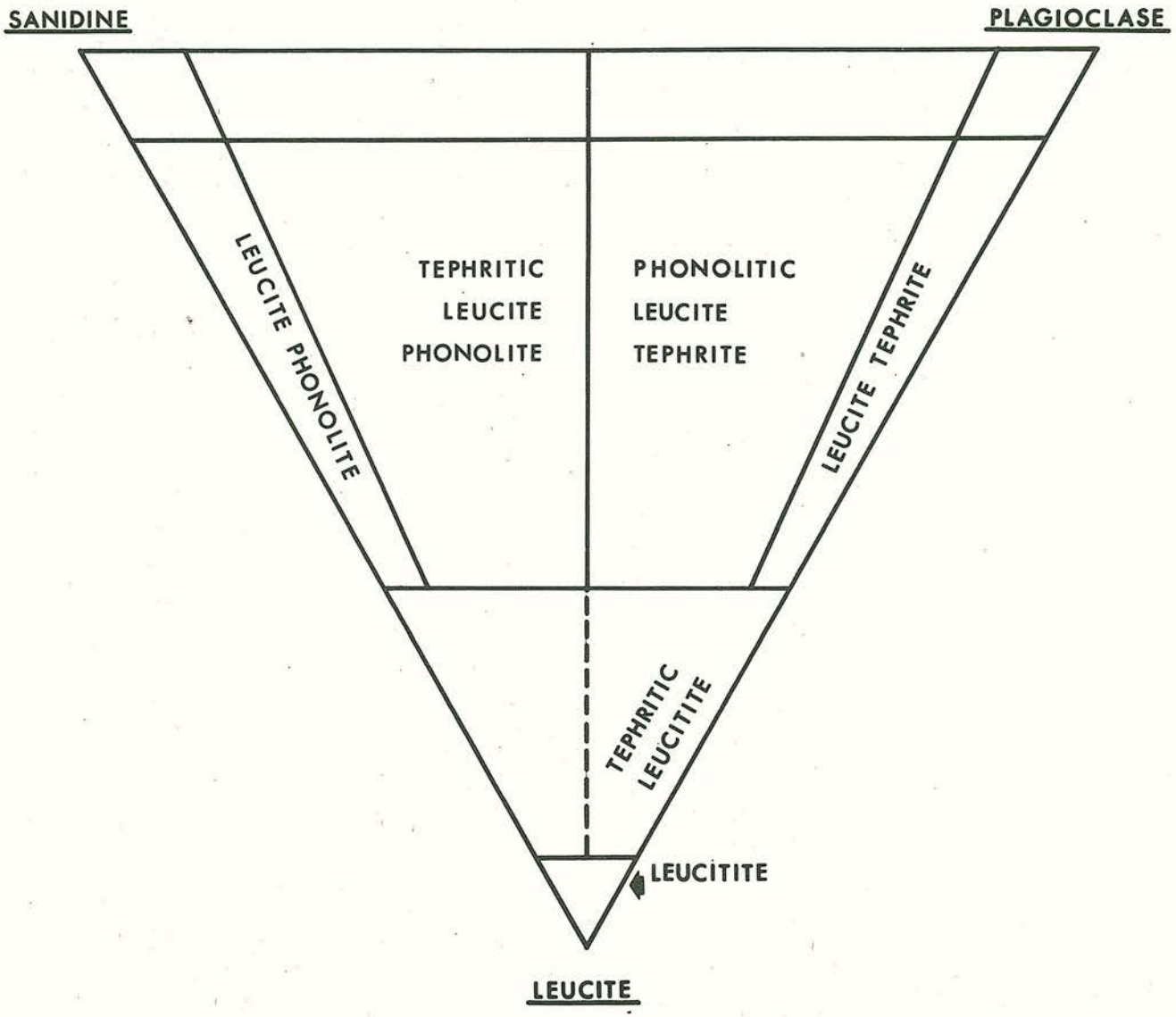
Leucite phonolite — sanidine > leucite; plagioclase <10%

Reference to Fig. 2-2, shows that the classification used in this study is very similar to the classification proposed by Streckeisen (1966).

In the petrographic notes (Appendix B), each of the analysed specimens is given a name according to the above classification; transitional types are labelled tephritic leucitite/leucite tephrite etc. When using a classificatory system based on the modal proportions of certain minerals, it is obviously very difficult to classify transitional types accurately. Indeed, there seems little point in using anything more than a rough classification when the classification is used solely as a descriptive aid. Savelli (1967) used a combination of X.R.D. and point-counting techniques to calculate the modal proportions of leucite, plagioclase, and sanidine in the Somma-Vesuvius lavas. However, quantitative analysis by X.R.F. is very imprecise (D.H. Doff, personal communication) so it was decided to calculate the modal proportions of the felsic constituents by point-counting the

Fig. 2-2

Classification of potassic volcanic rocks according to Streckeisen (1966).


SANIDINE
PLAGIOCLASE
LEUCITE PHONOLITE
TEPHRITIC
LEUCITE
PHONOLITE
PHONOLITIC
LEUCITE
TEPHRITE
LEUCITE TEPHRITE
TEPHRITIC
LEUCITITE
LEUCITITE
LEUCITE

phenocrysts and estimating the groundmass composition "by-eye". Estimation of the proportion of leucite in the groundmass is facilitated by using a combination of crossed-nicols, sensitive tint plate, and partially closed sub-stage diaphragm.

It should be noted that the compositional "cloud" or "continuum" seen in the K_2O v. SiO_2 plot for Roccamonfina (Fig. 2-1) and for the Roman Region (Fig. 4-8) is also reflected in a continuum of modal proportions of the felsic constituents - leucite, plagioclase, and sanidine.

Leucitites

Leucitites are rare in the Roccamonfina area. The two main flows are the clinopyroxene-olivine phyric leucitites of Conca della Campania (R. 153,154) and Teano (R. 112). These are sparsely porphyritic with eusubhedral phenocrysts of faintly pleochroic (α-yellow green, β and γ-pale green), zoned clinopyroxene ($c \wedge n\gamma = -45^\circ$). The zoning is variable; some of the phenocrysts have dark green cores, others have dark green margins, and some have zones clouded with ore (Plate 1). Rare, marginally iddingsitised, partially resorbed olivine is the only other phenocryst phase. An ore pseudomorph after biotite was noted in R.112. The groundmass is composed of prismatic microphenocrysts of clinopyroxene in a matrix of equidimensional leucite, granular clinopyroxene, ore, and 10% plagioclase. Interstitial phlogopitic mica (Plate 2) and partially iddingsitised olivine (R.153) are other groundmass phases. Apatite is a common accessory, often being found as prismatic crystals in the clinopyroxene phenocrysts.

Tephritic leucitites

Forty tephritic leucitites were analysed. As with Vesuvius (Savelli, 1967), tephritic leucitites form the bulk of the lava flows of the strato volcano. There is a wide range of crystallinity from aphyric to coarsely porphyritic types containing leucite phenocrysts 10mm. in diameter. The main phenocryst phases are leucite and clinopyroxene, with subsidiary amounts of basic plagioclase (labradorite-bytownite), ore, biotite, and apatite. Modally leucite>plagioclase and sanidine < 10%.

(a) Aphyric tephritic leucitites

Plate 3 shows a typical aphyric tephritic leucitite from a dyke cutting leucitic tuffs on the north flank of the volcano. It contains very rare macrophenocrysts of leucite (→ 4mm.) with more numerous leucite and clinopyroxene (→ 1mm.) microphenocrysts. The bulk of the rock is composed of "quench" leucite, pale green prismatic clinopyroxene, plagioclase microlites and ore. Apatite is a common accessory. The complex "star-shaped" growth forms of the rapidly chilled leucite is caused by the symmetrically arranged inclusions of clinopyroxene, ore, and glass. Rare fluid inclusions have been found in similar lavas from the Alban Hills area (Roedder and Coombs, 1967), but none were found in the rapidly chilled Roccamonfina lavas. In another tephritic leucitite (R.8), late-stage poikilitic potash feldspar is seen replacing the leucite. The poikilitic K-feldspar still retains the symmetrically arranged inclusions from the primary leucite (Plates 4,5,6).

R.137 and R.139 are more plagioclase-rich tephritic leucitites.

They contain rare subhedral, pale green, slightly pleochroic clinopyroxene phenocrysts (max. 3mm.), rare glomerophyric aggregates of cpx-plagioclase-ore-apatite, partially resorbed biotite (Plate 7), and partially iddingsitised olivine (Plate 8) as common accessories. The phenocrysts are set in a groundmass composed of leucite (± 0·2mm.), prismatic and granular pale green clinopyroxene, oscillatory zoned plagioclase ($An_{66,68,75}$), ore, and poikilitic patches of K-feldspar, occasionally showing Carlsbad twinning. Interstitial olivine also occurs as a minor groundmass phase.

(b) Leucite-clinopyroxene macrophyric tephritic leucitites

Plates 9, 11, and 12 show typical leucite-cpx macrophyric tephritic leucitites. In R.39 (Plate 9), euhedral leucite (0·5-5·0mm.) and eu-subhedral clinopyroxene (→ 2mm.) phenocrysts are set in a finely crystalline groundmass of leucite, cpx, plagioclase, and ore. Rare microphenocrysts of plagioclase (An_{77}) are also found. The leucite icositetrahedra show typical polysynthetic twinning (Plate 12). Clinopyroxene phenocrysts are faintly pleochroic (α-yellow green, β and γ-pale green; $c\wedge n\gamma = -44^{\circ}$), showing oscillatory zoning, hourglass structure, and rare twinning parallel to (100). Both the leucite and the clinopyroxene occur as single phenocrysts and as glomerophyric aggregates. Plate 10 shows prismatic apatite inclusions in a clinopyroxene phenocryst, and the circular arrangement of cpx-apatite inclusions in a leucite phenocryst is shown in Plate 13. Both these features are typical of the macrophyric tephritic leucitites. Plates 9, 11, 12, and 13 illustrate the extremely wide variation in size of the leucite phenocrysts.

(c) Leucite-cpx-plagioclase macrophyric tephritic leucitites

Plagioclase is present only in small quantities as a phenocryst phase in the tephritic leucitites. R.44 with < 2% is the most plagioclase-phyric lava in this group (Plate 14). The plagioclase phenocrysts occur as small laths (→ 0·5mm.), rarely zoned, and albite-twinned (An_{77}, An_{86} core-An_{49} margin). Microphenocrysts of ore (± 0·1mm.) are also found in this rock together with a wide range of leucite (0·5 - 8·0mm.) and clinopyroxene (0·25 - 4·0mm.) phenocrysts. A clinopyroxene phenocryst from a lc-cpx-plag macrophyric tephritic leucitite (R.35) shows oscillatory zoning and hourglass structure (Plate 15).

(d) Cpx-plagioclase-ore+ apatite glomerophyric aggregates

In some of the tephritic leucitites, glomerophyric aggregates of cpx-plagioclase-ore± apatite are found. R.44 and R.183 are good examples. Plate 14 (R.44) shows a glomerophyric aggregate of plagioclase (An_{77}), pale green clinopyroxene (containing prisms and needles of apatite), and ore, enclosed by "late" leucite phenocrysts. Plate 16 (R.183) shows another glomeroaggregate, mainly composed of plagioclase (An_{76}), with accessory clinopyroxene, ore, and apatite. R.131 (Plate 17) contains a cpx-plagioclase-biotite-ore-apatite glomerophyric aggregate; the biotite is almost totally altered to magnetite. At the contact between the plagioclase and "late" leucite in some of these glomerophyric aggregates, a complex intergrowth of a low birefrigent, felsic mineral occurs (e.g. R.15, R.44). Its R.I. is less than plagioclase and greater than leucite, and it is probably K-feldspar.

The fact that some of these glomeroaggregates of cpx-plagioclase-ore are surrounded by leucite phenocrysts (the reverse situation has not been noted) is thought to be of significance (see Chapter 5).

(e) Biotite-Cpx phyric tephritic leucitites

Only one example of a Biotite-cpx phyric tephritic leucitite was found in the Roccamonfina area (R.140 from a lava flow below Terracorpo, near Marzano Appio.). Small (0·25 - 2·0 mm.) pale green-yellow green, slightly pleochroic, zoned, clinopyroxene phenocrysts together with biotite (± 0·5mm., partially to totally resorbed to magnetite and 2^{o} phlogopitic mica) and rare microphenocrysts of plagioclase (An_{75}) occur in a groundmass of leucite, clinopyroxene, plagioclase, and ore. Rare phenocrysts of apatite (max. 0·5mm., frequently associated with biotite, and clouded with ore particles), marginally iddingsitised olivine, and leucite are also found in this lava.

Transitional tephritic leucitites

Some of the lavas are transitional between the tephritic leucitites and the leucite tephrites or phonolitic leucite tephrites. The thick, fine-grained flow exposed on the west flank of the volcano near the Garigliano river is a transitional tephritic leucitite/leucite tephrite with a plagioclase to leucite ratio of about 1:1. It contains rare phenocrysts of clinopyroxene (max. 2mm.), leucite (0·5mm.), olivine, and plagioclase (An_{78}) in a groundmass of "quench" leucite, plagioclase, granular clinopyroxene,

and dendritic combs of ore. Secondary interstitial carbonate characterises these lava flows near the Garigliano fault, which is the only present day site of hot springs and carbonate tuffa deposits in the Roccamonfina area. It is interesting to note that the oldest lavas of the Alban Hills volcano are also characterised by 2° carbonation (Fornaseri et al., 1963).

The presence of a glomerophyric aggregate of plagioclase in R.59 (Plate 18) and the presence of plagioclase phenocrysts in R.60 is important because it marks the entry of plagioclase into the phenocryst assemblage (see Chapter 5). R.60 is interesting because it contains phenocrysts of cpx., plagioclase, biotite, ore, and leucite (Plate 19). Its chemical composition is very similar to the aphyric lavas R.81,82,83. The eu-subhedral clinopyroxene phenocrysts (± 1·5mm.) are faintly pleochroic in tints of pale green-yellow green, and frequently show oscillatory zoning, hourglass structure, and polysynthetic twinning. Leucite is euhedral (→ 2mm.), often glomerophyric and sometimes enclosing clinopyroxene. Biotite is marginally to totally resorbed and plagioclase (An_{72}, An_{89}-An_{81}-An_{75} zoned) shows faint normal and oscillatory zoning. Plagioclase-cpx-ore glomerophyric aggregates are common.

Plate 20 (R.61) shows a transitional tephritic leucitite/phonolitic leucite tephrite containing a glomeroaggregate of cpx-plagioclase (An_{70},An_{81} with sanidine mantles)-leucite. Groundmass plagioclase composition is An_{62}.

Leucite tephrites

There are very few leucite tephrites in the Roccamonfina area. R.163 is a good example (Plate 21), with rare euhedral macrophenocrysts of leucite (→ 6mm.) and rare microphenocrysts of leucite, pale green clinopyroxene, and plagioclase (An_{79}), in a fairly coarse groundmass of leucite (0·1mm.), clinopyroxene, plagioclase (An_{70}), ore and interstitial K-feldspar.

Phonolitic leucite tephrites

Two main groups of phonolitic tephrites can be recognised

(1) Lower K_2O group with biotite-cpx-plagioclase-ore+rare leucite phenocrysts (part of BCPO group; see Chapter 5).

(a) Transitional leucite tephrites phonolitic leucite tephrites (R.106,107,108,170,209).

(b) Phonolitic leucite tephrites sensu stricto (R.37,42,47, 53)

(2) Higher K_2O group with leucite-cpx-plagioclase-ore phenocrysts

(a) Macroporphyritic (R.21,72,73,91,129)

(b) Aphyric (R.122,123,128)

(1a) Clinopyroxene (→ 2·5mm.), plagioclase (An_{77}, zoned An_{89-54}), partially resorbed biotite and ore occur as single phenocrysts and in glomeroaggregates (Plate 22). Rare leucite phenocrysts and apatite (ore clouded prisms in cpx phenocrysts) also occur in R.170 and R.209. The groundmass plagioclase composition is An_{60}. In R.106-108 some of the plagioclase phenocrysts have sanidine mantles and glomeroaggregates of plagioclase are common (Plate 23).

Olivine with a rim of clinopyroxene, ore, and biotite phenocrysts were also noted in these lavas.

(1b) Lavas of this group are confined to two lava flows on the west flank of the volcano (see Map 1). Eu-subhedral (→ 2mm.), zoned, slightly pleochroic clinopyroxene, plagioclase (An_{72}) with sanidine mantles, partially to totally resorbed biotite, and accessory ore and ore clouded apatite (Plate 24) occur in a finely crystalline, sometimes trachytic, groundmass of leucite, plagioclase, sanidine, clinopyroxene, and ore. Sanidine is more abundant than in R.170 - R.209, forming mantles to phenocryst and groundmass plagioclase, as well as interstitial patches. Glomeroaggregates of one or more of the phenocryst phases are particularly common (Plate 25).

(2a) As with the macrophyric tephritic leucitites, there is a wide range in the percentage and size distribution of the leucite phenocrysts. In R.148, individual leucite phenocrysts range up to 25 - 30mm. in diameter. Leucite phenocrysts have been reported in the Roccamonfina area to reach dimensions of 40mm. (Eigenfeld, 1967). Glomeroaggregates of cpx-plagioclase-ore-leucite are common in these lavas. R.21 has pegmatitic veins of K-feldspar with accessory aegirine-augite and ore traversing it (Plates 26, 27). Some of the leucite phenocrysts in this lava are partially to totally replaced by K-feldspar (Plate 28), presumably as a result of subsolidus reaction.

(2b) These lavas are the aphyric equivalents of group (2a).

Tephritic leucite phonolites

This group of lavas (R.11,14,29,64,105,111,134,179) is characterised by phenocrysts of basic plagioclase, clinopyroxene, ore, ± leucite ± sanidine in a groundmass containing more sanidine than plagioclase. Biotite and apatite are common accessories. In some of the tephritic leucite phonolites, leucite is the dominant phenocryst phase (R.179), and in R.111 there is 4% of unaltered red-brown biotite phenocrysts. R.64 (Plate 29) contains large phenocrysts of zoned, Carlsbad twinned sanidine (→ 4mm.), zoned plagioclase (An_{74}) with sanidine mantles, small pale green clinopyroxene ($c\wedge\gamma = -42^{\circ}$), ore, and resorbed biotite phenocrysts, often in glomeroaggregates, in a fine grained trachytic groundmass composed mainly of K-feldspar with < 5% cpx, < 20% leucite, and rare plagioclase with mantles of K-feldspar. R.134 (Plate 30) is very similar - the clinopyroxene is marginally altered to 2° hornblende, and ore clouded apatite is a common accessory.

Leucite phonolites

Only two leucite phonolites were analysed. The Mte. Canneto phonolite (R.99 - Plate 31) is composed of sanidine crystals (0·2 - 1·0mm.), leucite (± 0·05mm.) and accessory ore + aegirine-augite + plagioclase with sanidine mantles. The other phonolite is from the dome of the Capitolo (R.121), on the eastern margin of the caldera. This contains rare phenocrysts of sanidine (→ 3mm.), zoned plagioclase (→ 0·5mm., An_{73}) with sanidine mantles, aegirine-augite, sphene (Plate 32), and hauyne. The groundmass is trachytic. For more details concerning the petrography of the

tephritic leucite phonolites and leucite phonolites of Tuoro Piccolo, dome of the Capitolo, Mte. S. Antonio, and Mte. S. Maria, the reader is referred to Gianetti (1965).

Trachyte

A block of trachytic composition (R.97) was found in a stratified adventive ash/cinder cone. It contains phenocrysts of sanidine (→ 10mm.), plagioclase (→ 2mm., An_{75}), aegirine-augite, fresh dark brown biotite, and ore in a trachytic matrix composed mainly of alkali feldspar. It is difficult to know which of the two Roccamonfina lava series this trachyte belongs to. It has < 1% ne in its norm.

2:2 Low K Series

In classifying the lavas of the Low K series, the terminology used by previous authors (Panichi, 1922; Seifert, 1942; Arevalo et al., 1962; Gianetti, 1964) has been adopted. Four main groups are recognised on the basis of petrographic criteria:

(1) Olivine basalts

(2) Trachybasalts

(3) Biotite augite latites

(4) Trachytic grey ash flow

The phenocryst assemblages and occurrences of each of these groups are presented in Table 2-1.

Olivine basalts

At Mte. Atano, dark, red-weathering, scoriaceous blocks showing varying degress of vesicularity and some bombs of ropey

TABLE 2-1

ROCCAMONFINA LOW K SERIES - ROCK CLASSIFICATION

Rock Type	Phenocrysts - in approx. order of abundance	Occurrence
Olivine Basalt	clinopyroxene olivine plagioclase	q.682 (R.184) Fortinella-Sippiciano (R.56,57,86) Mte. Atano (R.117,119) Mte. Friello (R.157,158,160) Carbonara (R.114)
Trachybasalt	plagioclase clinopyroxene olivine	La Cerchiara (R.186,187,188,189) S. Lorenzo (R.101)
Biotite Augite Latite	plagioclase clinopyroxene biotite ore	Mte. S. Croce - Mte. Lattani (R.191,192,193,195) San Giuliano-Fontanelle (R.95,96,98,109) Caldera wall (R.104) Inside caldera (R.90) N. of Mte. Friello (R.162)
Trachytic Grey Ash Flow	- - - - -	see Italian Geological Survey Maps

lava are found. In thin section, the rock is fine grained, vesicular, with euhedral phenocrysts of clinopyroxene (± 0·25mm., colourless to pale green), and olivine (often skeletal, quenched, and with iddingsitised margins). Microphenocrysts of clinopyroxene and olivine are common, and the groundmass is composed of plagioclase (An_{65}), cpx, and finely disseminated ore. Some of the olivine phenocrysts show evidence of high temperature oxidation (Plate 33). Similar basaltic scoria is found on the northern rim of the caldera, near q.682.

The Carbonara basalt is composed of eu-subhedral phenocrysts of pale green clinopyroxene (± 1mm.), subhedral olivine, and small phenocrysts of plagioclase (An_{72-75}), in a coarse groundmass of plagioclase (0·1 - 0·2mm.), granular clinopyroxene, iddingsitised olivine, and ore. Rare glomeroaggregates of cpx-plagioclase are also found (Plate 34). Small plates of secondary red-brown biotite occurs in some of the vesicles of the Carbonara basalt.

The Mte. Friello basaltic scoria and lava flows contain phenocrysts of clinopyroxene and olivine (→ 1mm.) with numerous microphenocrysts of cpx and olivine in a fine granular matrix composed of cpx, plagioclase, olivine and ore.

The largest olivine basalt lava flow found in the Roccamonfina area is the Fortinella-Sipicciano flow (see Map 1). It is a porphyritic vesicular olivine basalt containing eu-subhedral phenocrysts (1 - 3mm.) of colourless to pale green, frequently polysynthetically twinned, clinopyroxene; subhedral (partially iddingsitised) phenocrysts of olivine (Fo_{87}); plagioclase (An_{71}),

and rare, dark brown, partially resorbed, plates of biotite (sometimes enclosing cpx). The groundmass has an intergranular texture and is composed of cpx, iddingsitised olivine, plagioclase (An_{66}), and ore. Glomeroaggregates of cpx-plagioclase-olivine (Plate 35) and rare, large, corroded olivines with cpx coronas (Plate 36) are also found. A single glomeroaggregate of pale green clinopyroxene containing small crystals of red spinel was seen in R.57 (Plate 37).

Trachybasalts

Trachybasalts are found as scoria near S. Lorenzo and as scoria and a lava flow at Fontana La Cerchiara between the twin latite domes of Mte. S. Croce and Mte. Lattani (see Map 1). The trachybasalt from La Cerchiara is dark grey, finely vesicular, with abundant olivine and feldspar phenocrysts (1 - 2 mm.) apparent in hand specimen. In thin section (Plate 39), plagioclase phenocrysts (An_{62-68}, 0·25 - 1·0mm.) are abundant. The larger phenocrysts sometimes have a spongy texture due to magmatic resorption, and some show oscillatory zoning. Clinopyroxene occurs as eu-subhedral, colourless to pale green-brown phenocrysts (0·5 - 1·0mm.) and is rarely found in glomeroaggregates and as coronas to resorbed olivine. Skeletal quench olivine (→ 0·5mm.) phenocrysts are sometimes marginally iddingsitised. The groundmass is composed of microcrystalline plagioclase (An_{50-54}), cpx, ore, and olivine, in a brown devitrified glassy matrix. R.189 contains rare, red-brown, corroded plates of biotite.

Biotite augite latites

The main latite occurrences in the Roccamonfina area are the domes of Mte. S. Croce - Mte. Lattani (R.191,192,193,195) and the flows on the south-east flank of the volcano near S. Giuliano-Fontanelle (R.95,96,98,109). Subsidiary occurrences are a flow north of Mte. Friello (R.162), and at the S.E. margin of the caldera wall (R.104).

A typical biotite augite latite from Mte. Lattani (R.196 - Plate 41) and Mte. S. Croce (R.191) is porphyritic with phenocrysts of plagioclase, clinopyroxene, biotite and ore in a trachytic groundmass. The plagioclase (An_{70-77}) occurs as euhedral, polysynthetically twinned, oscillatory zoned phenocrysts, 0·5 - 2·0 mm. in size (Plate 42). Many of the plagioclase phenocrysts have spongy cores as a result of magmatic resorption, and some are partially altered to a micaceous mineral. They are also frequently clouded with zones of inclusions of cpx, glass and indeterminate particles. Many of the plagioclase phenocrysts have sanidine mantles (Plate 43). The pale green, eu-subhedral clinopyroxene phenocrysts (0·5 - 1·0mm.; $c\wedge n\gamma = -43^{\circ}$) are occasionally zoned. They frequently contain inclusions of ore, biotite, and plagioclase, and occasionally form coronas to rare, resorbed olivine phenocrysts. Biotite phenocrysts (0·5 - 1·0mm.) are pleochroic pale yellow brown to dark red brown and are commonly partially to totally altered to ore. Frequently the former presence of biotite can only be ascertained by the platey habit of the ore pseudomorphs. In the latites where the biotite is most strongly resorbed

(e.g. R.195), the plagioclase phenocrysts also show a very "spongy" texture, suggesting late stage alteration. Small ore phenocrysts (→ 0·2mm.) were found together with accessory apatite. Plagioclase, cpx, biotite and ore commonly occur as glomero-aggregates (Plate 41), though the proportion of each mineral in the aggregate can vary considerably. The trachytic groundmass is composed of plagioclase (An_{58}), and sanidine with minor amounts of cpx and ore. The latites of the south east flank of the volcano are sparsely porphyritic with eu-subhedral phenocrysts of plagioclase, clinopyroxene, and biotite in a trachytic groundmass of plagioclase, K-feldspar, cpx, and ore. In R.96 plagioclase phenocrysts (0·5 - 2·0mm; An_{71}) are occasionally zoned with sanidine mantles and frequently have a "spongy" texture. The clinopyroxene phenocrysts (→ 1mm.) are pale green, and biotite is commonly altered to ore. Plagioclase, cpx, biotite, and ore frequently occur as glomeroaggregates. R.95 contains rare iddingsitised and resorbed olivine phenocrysts. The groundmass of these latites is either trachytic or is composed of granular cpx and ore in a mesh of plagioclase and K-feldspar. Accessory apatite is sometimes associated with the biotite. In R.98 a large plate of biotite is seen enclosing tabular plagioclase crystals (Plate 45).

Trachytic grey ash flow

An X.R.D. trace of the grey ash flow suggests that it is composed mainly of K-feldspar. Tedesco (1965, p. 15) has described the petrography of the ash flow in detail.

2:3 Biotite Gabbro nodules

One specimen of biotite gabbro (R.103) was collected from superficial tuffaceous deposits on the southern margin of the caldera (see Map 1). Similar specimens have been collected from tuffs near Sessa Aurunca by Arevalo et al. (1962). In hand specimen it is holocrystalline with an average grain size of 1 - 2mm. Biotite, pyroxene, plagioclase, and ore are recognisable; the biotite shows a pronounced sub-parallel alignment in both hand specimen and thin section (Plate 47). Microscopically (Plate 48) the gabbro is seen to consist of a subhedral to anhedral aggregate of faintly pleochroic pale green clinopyroxene (α = yellow green, β and γ = green; $c \wedge n\gamma = -44^{\circ}$), subhedral plagioclase (An_{93} - β index determination), strongly pleochroic brown biotite, anhedral magnetite, and prismatic crystals of apatite ($\rightarrow$ 0·5mm.). Biotite often shows an ophitic relationship to plagioclase (Plate 49).

PLATES 1 - 50

Key to plates:

A = Apatite

B = Biotite

C = Clinopyroxene

L = Leucite

M = Magnetite/Ore

O = Olivine

P = Plagioclase

Ph = Phlogopite

S = Sanidine

PLATE 1

R.112: Clinopyroxene-olivine phyric leucitite

Note ore clouded zone in clinopyroxene phenocryst and rim of cpx + ore surrounding the olivine

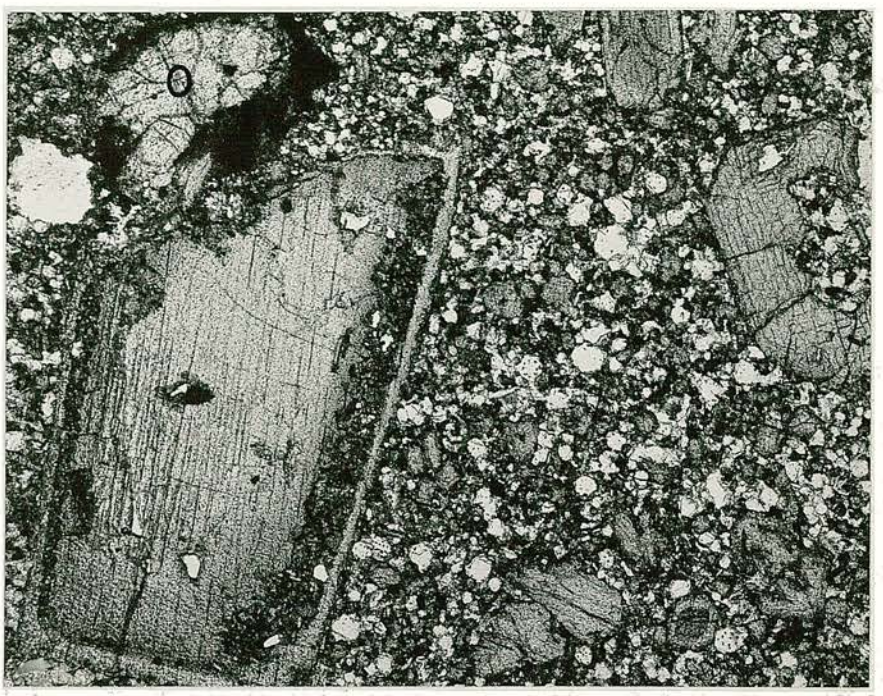
X 30

PLATE 2

R.154: Leucitite

Note interstitial phlogopite, and apatite needles in the leucite

X 150


O

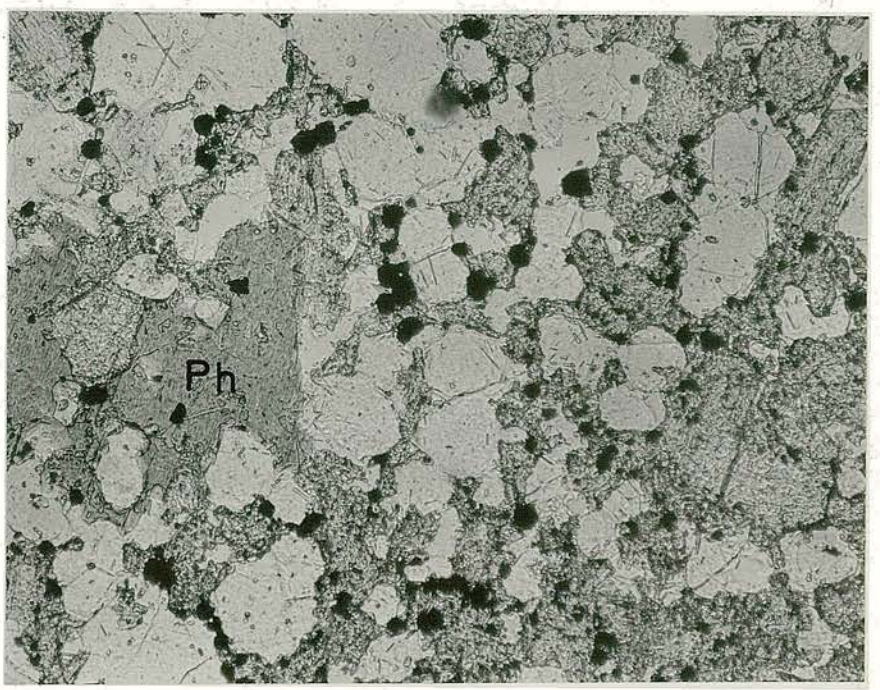

Ph

PLATE 3

R.180: Tephritic Leucitite

Note "star" shaped growth form of the "quench" leucite

X 160

PLATE 4

R.8: Potash feldspar replacing primary "quench" leucite in a Tephritic Leucitite

X 150

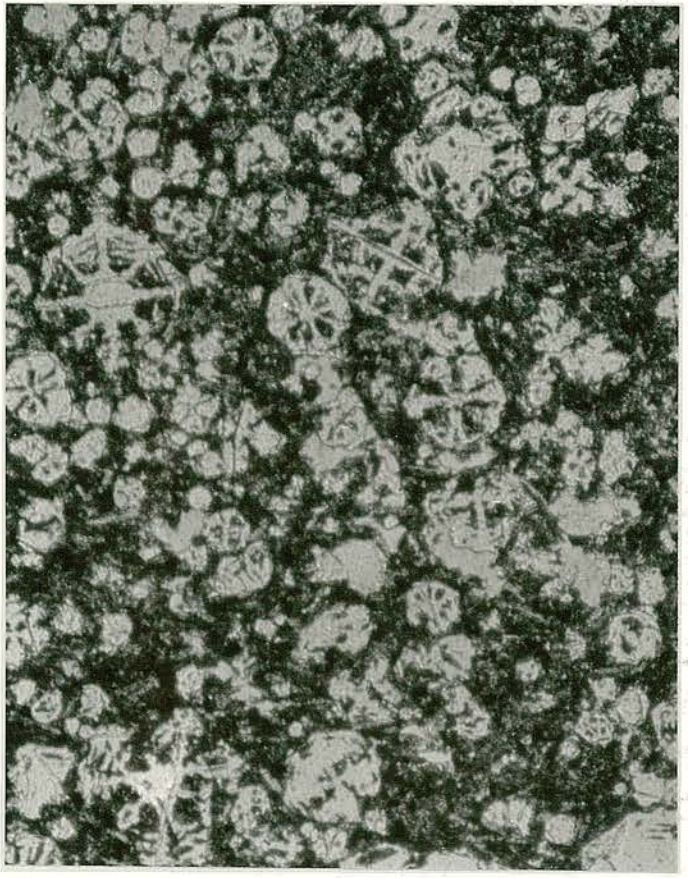




PLATE 5

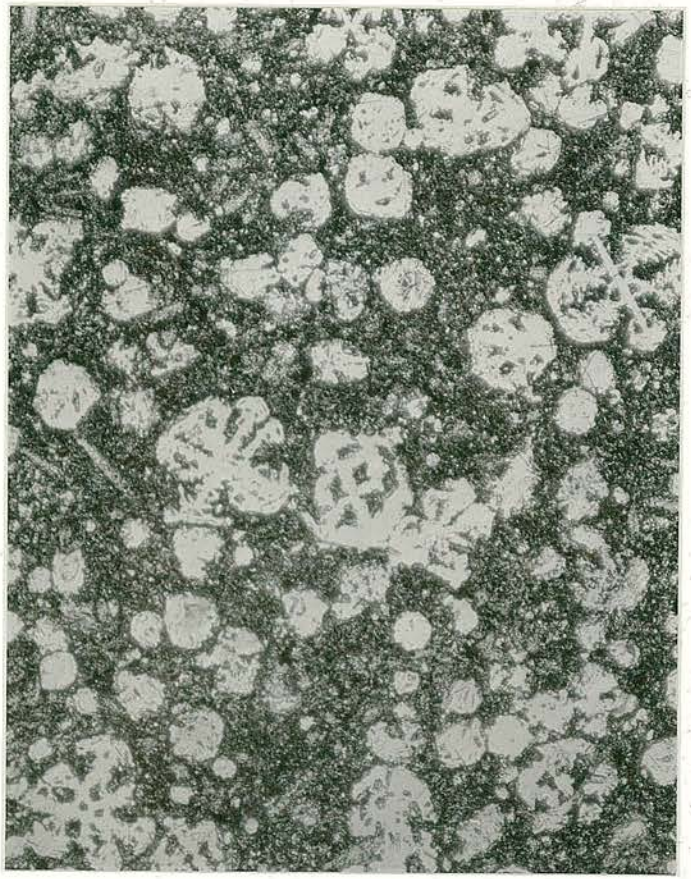
R.8: "Star" shaped growth forms of "quench" leucite in Tephritic Leucitite.

X 60

PLATE 6

R.8: Same as Plate 5, but with crossed nicols. Note Carlsbad twinned K-feldspar replacing some of the primary leucite.

X 60



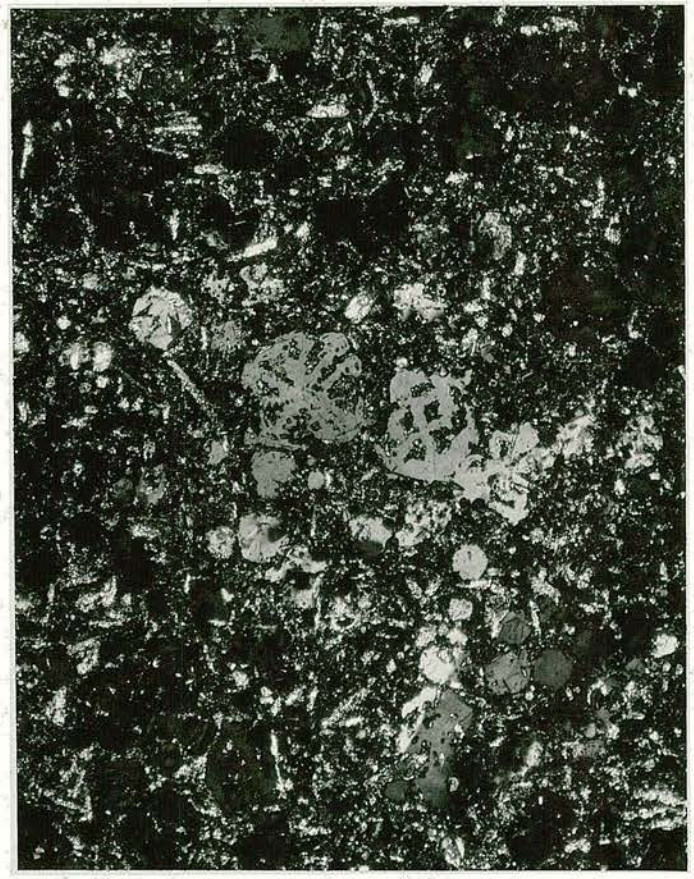


PLATE 7

R.137: Partially resorbed biotite in Tephritic Leucitite.

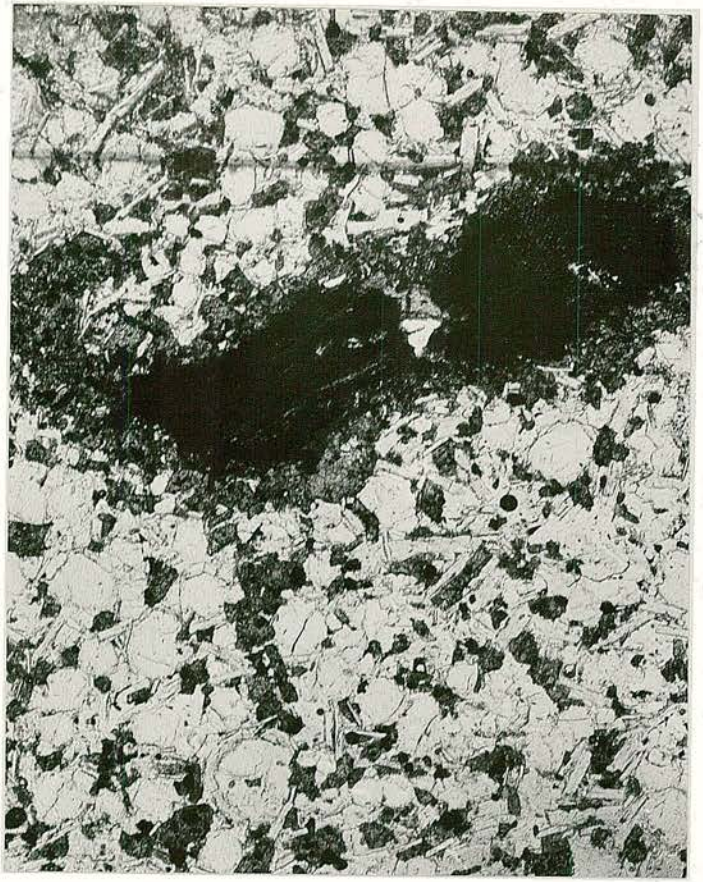
Note rim of cpx + ore

X 30

PLATE 8

R.139: Marginally iddingsitised olivine in Tephritic Leucitite

X 60



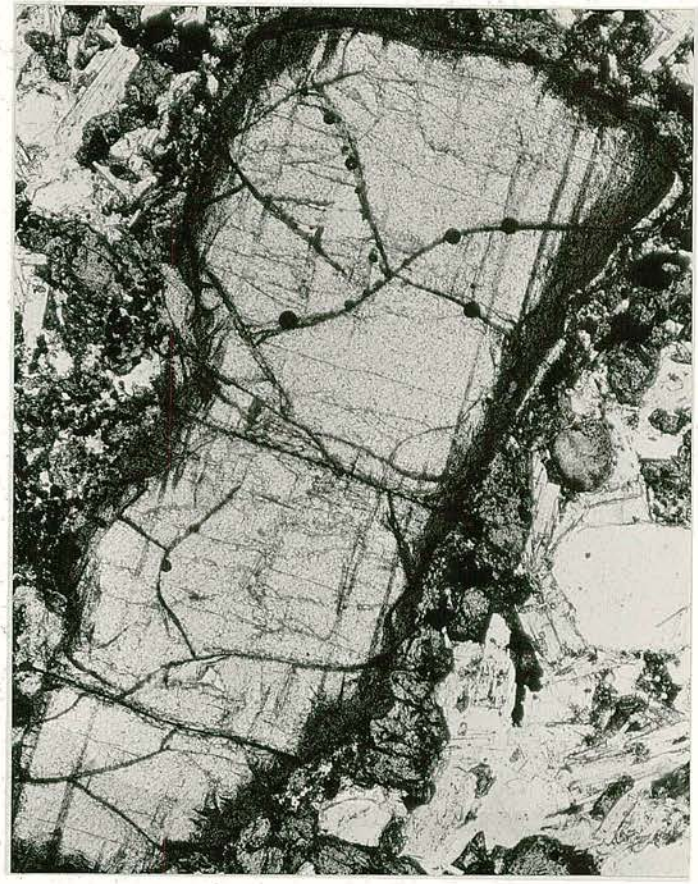


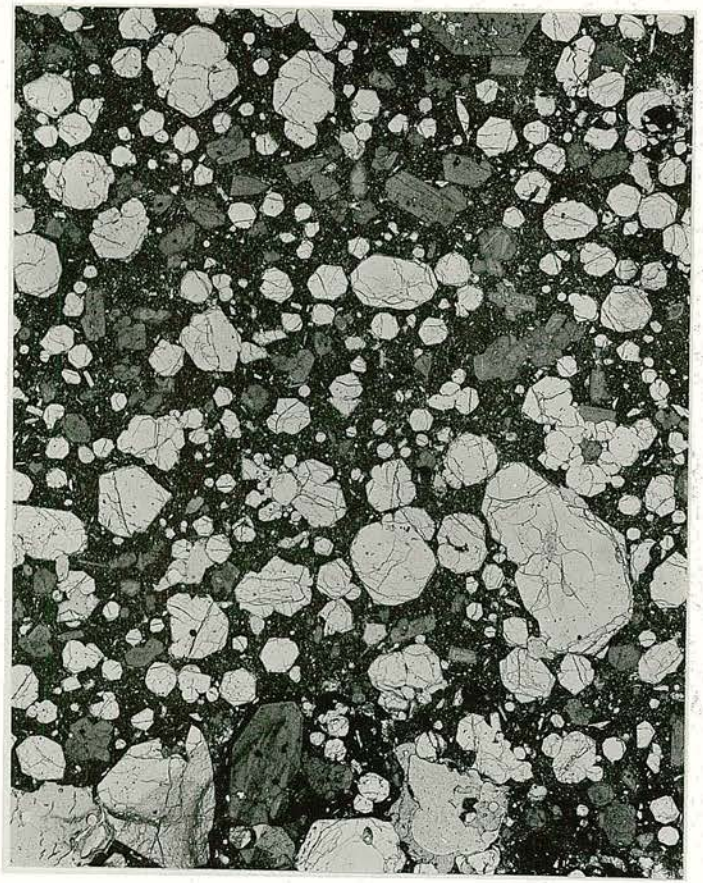
PLATE 9

R.39: Leucite-clinopyroxene macrophyric Tephritic Leucitite.

X 7

PLATE 10

R.185: Apatite inclusions in clinopyroxene phenocryst.



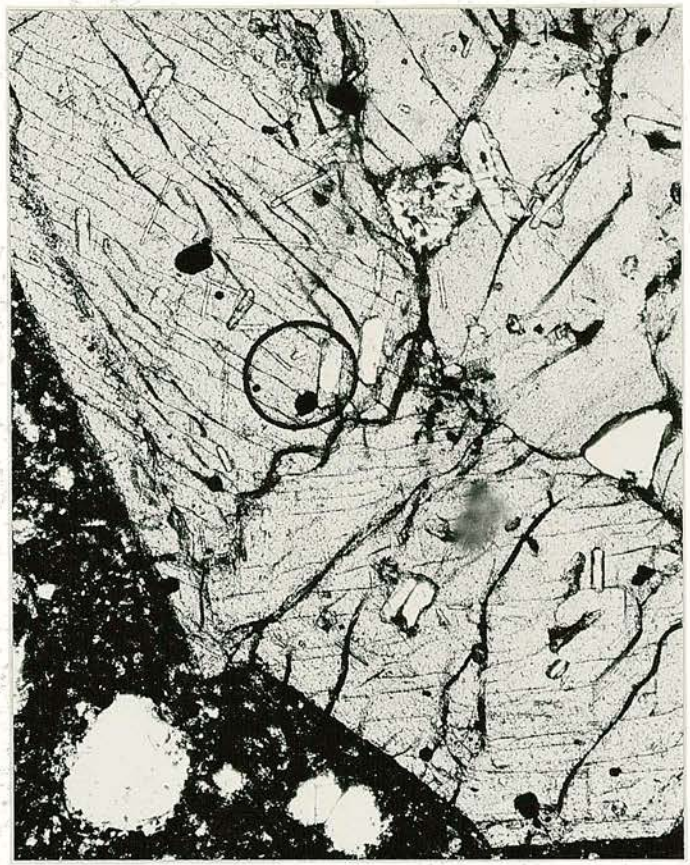


PLATE 11

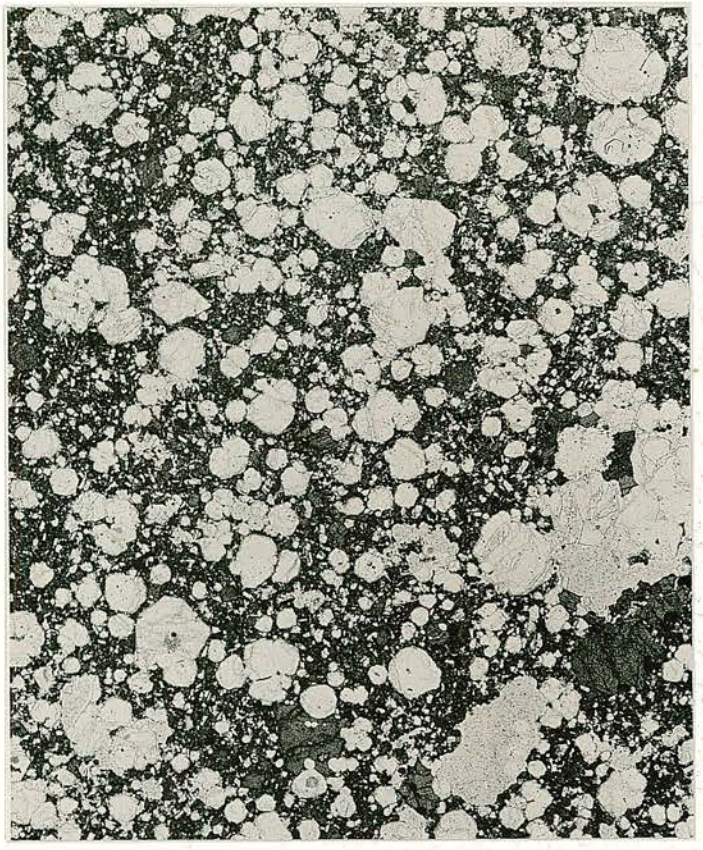
R.23: Leucite-clinopyroxene phyric Tephritic Leucitite.

X 8

PLATE 12

R.23: Polysynthetically twinned leucite phenocrysts in Tephritic Leucitite.

X 7 crossed nicols



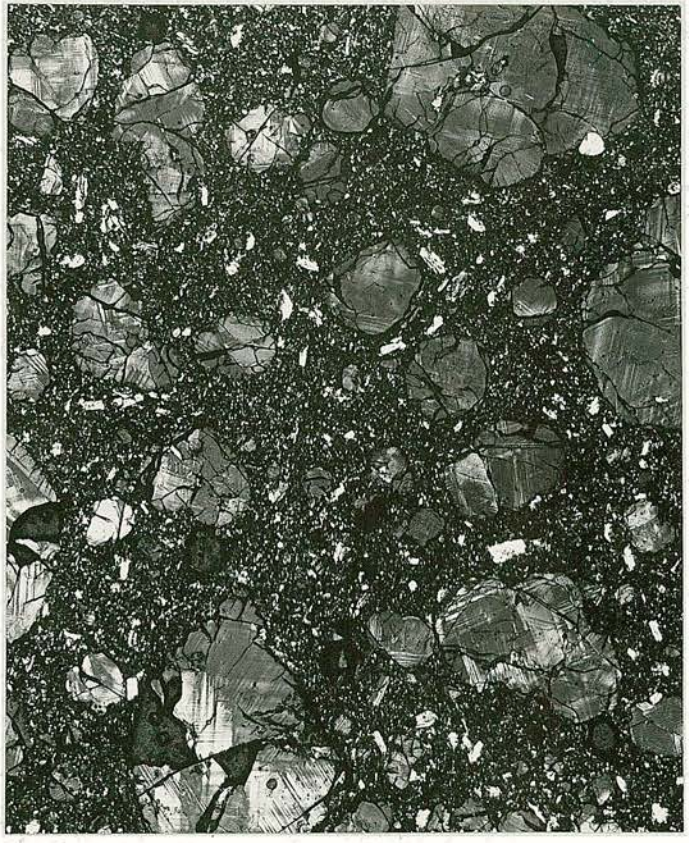


PLATE 13

R.185: Leucite-clinopyroxene macrophyric Tephritic Leucitite

Note (1) circular arrangement of cpx-apatite inclusions in large leucite phenocryst (centre)

(2) wide variation in size of leucite phenocrysts.

X 14

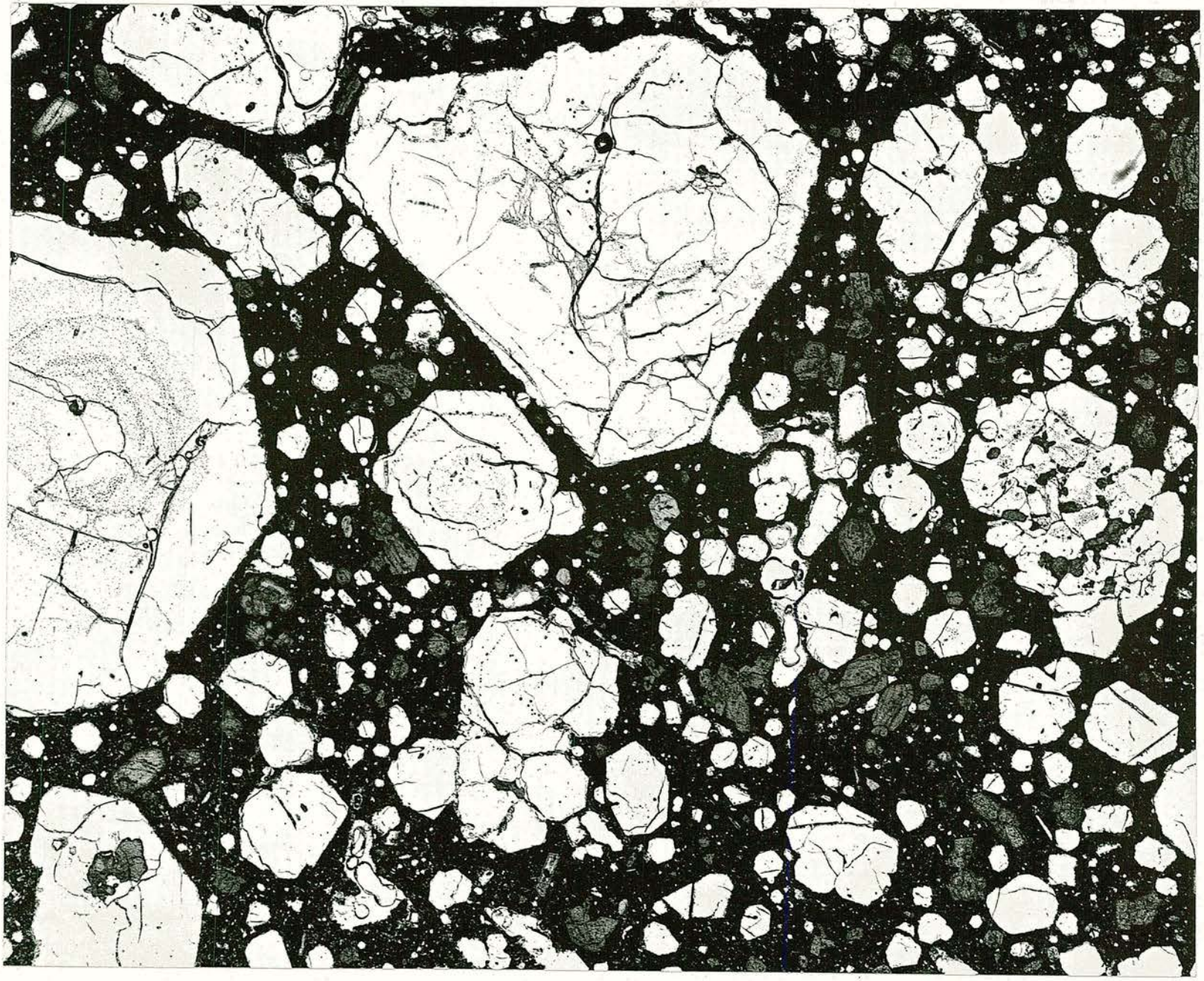


PLATE 14

R.44: Cpx-plagioclase-ore glomerophyric aggregate enclosed by leucite phenocrysts in a Tephritic Leucitite.

X 14

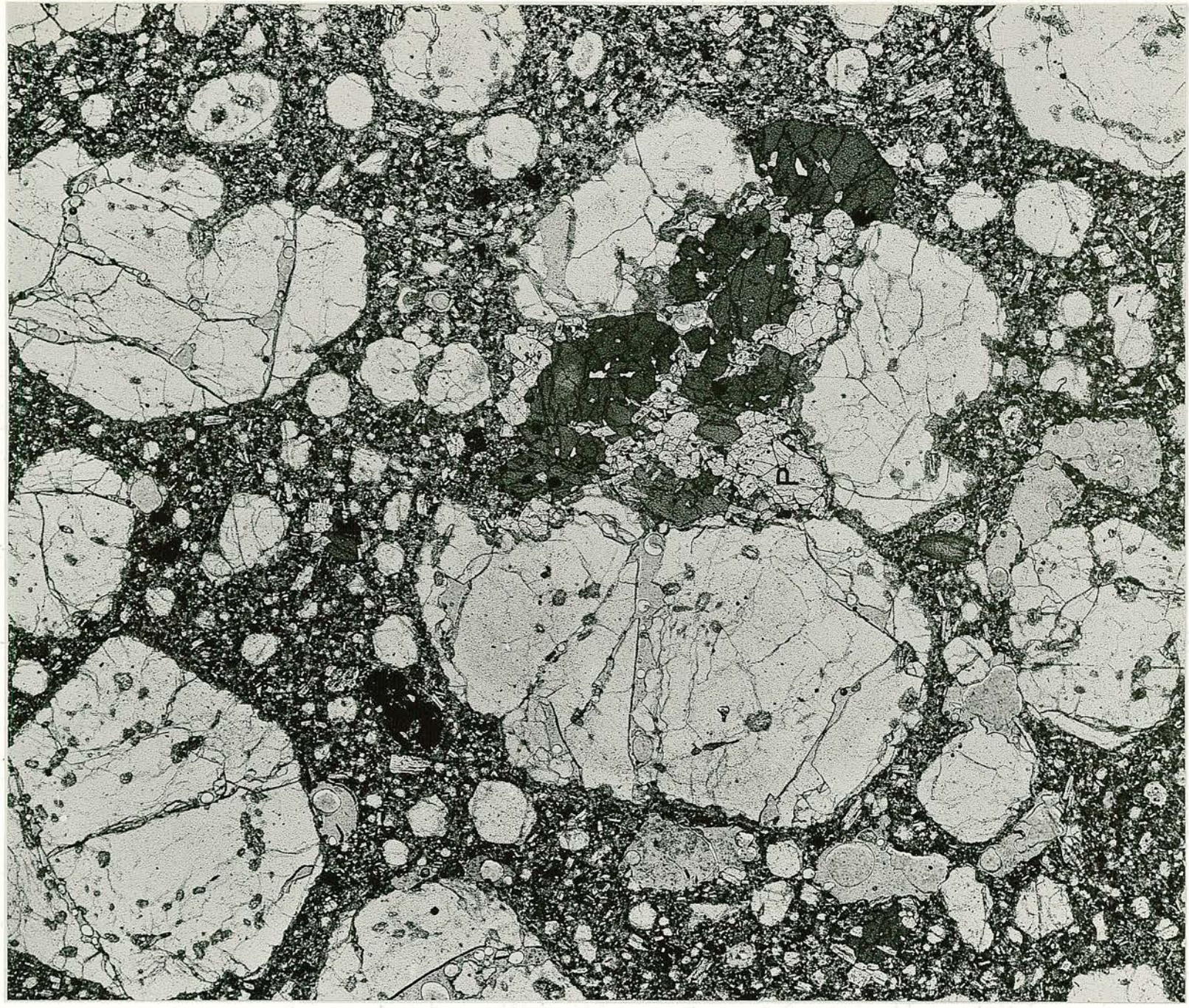

P

PLATE 15

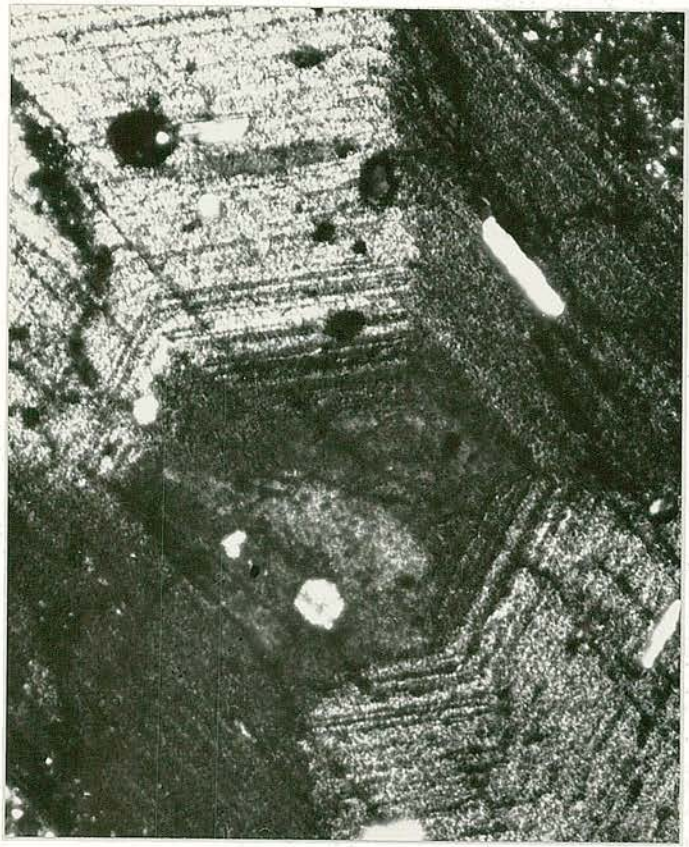
R.35: Clinopyroxene phenocryst showing oscillatory zoning and hourglass structure.

X 60 crossed nicols

PLATE 16

R.183: Glomerophyric aggregate of plagioclase, plus accessory cpx, ore, and apatite in a Tephritic Leucitite.

X 60 crossed nicols




C
A

PLATE 17

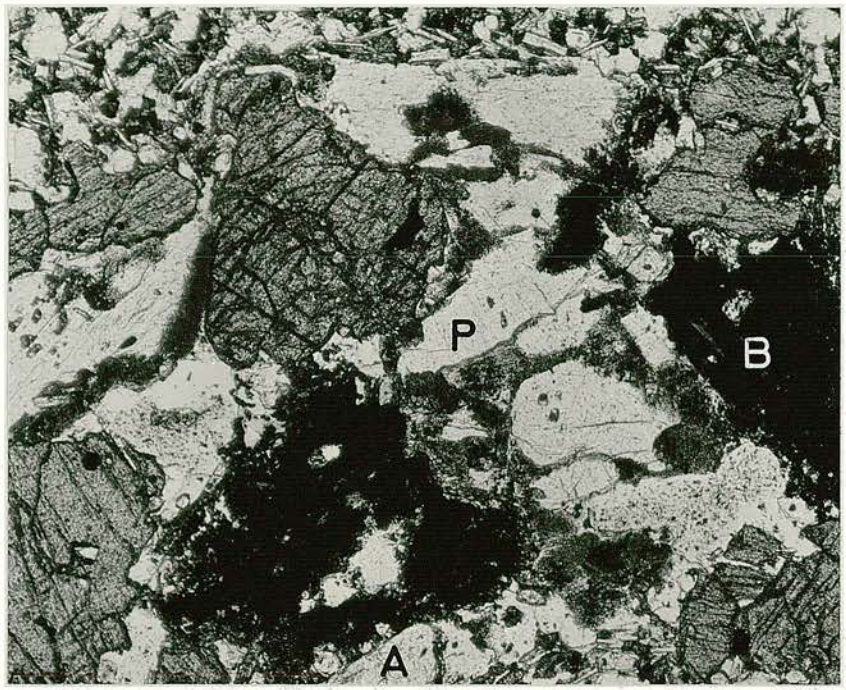
R.131: Glomeroaggregate of cpx-plagioclase-partially resorbed biotite-ore in a Tephritic Leucitite.

X 60

PLATE 18

R.59: Glomeroaggregate of plagioclase in a Tephritic Leucitite/Leucite Tephrite.

X 60 crossed nicols


P
B
A

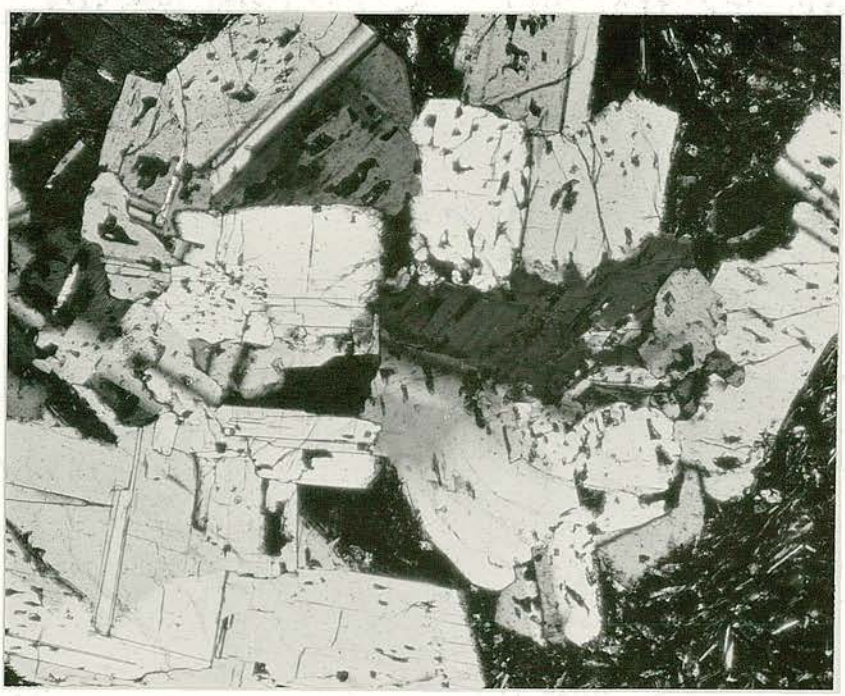


PLATE 19

R.60: Leucite-cpx-biotite-plagioclase-ore-phenocrysts in a transitional Tephritic Leucitite/Leucite Tephrite.

X 8

PLATE 20

R.61: Cpx-plagioclase-apatite-ore-leucite glomeroaggregate in a transitional Tephritic Leucitite/Phonolitic Leucite Tephrite.

X 7



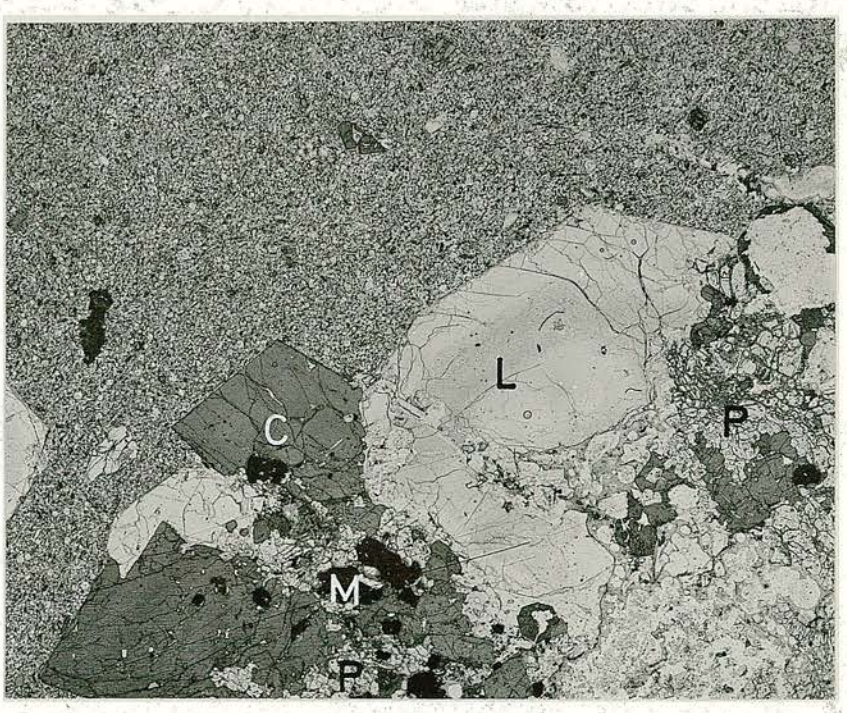

L
C
P
M
P

PLATE 21

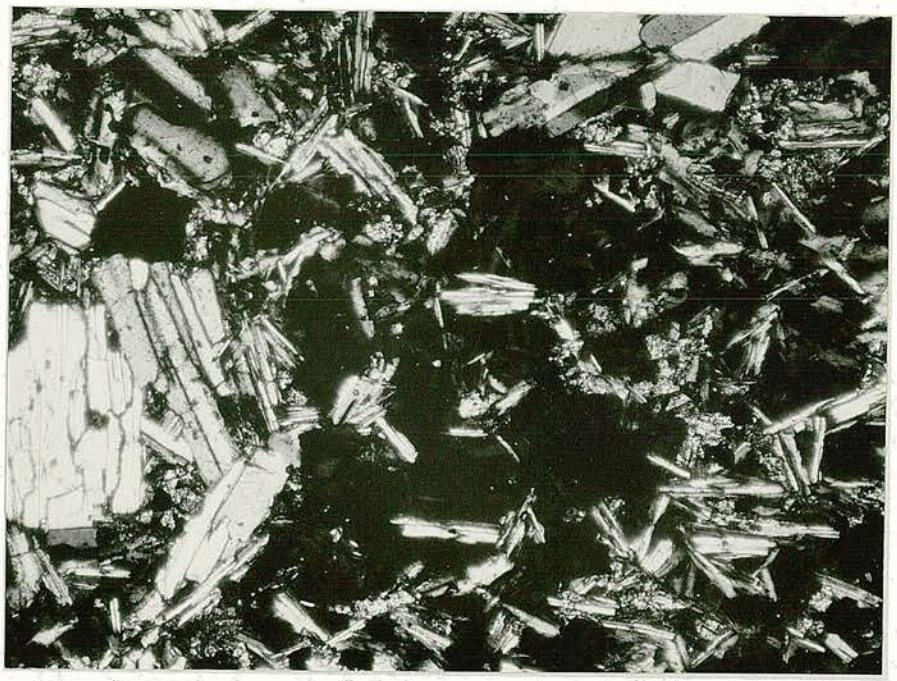
R.163: Leucite Tephrite

X 60 crossed nicols

PLATE 22

R.209: Cpx-plagioclase-biotite (altered to ore)-ore glomeroaggregate in transitional Leucite Tephrite/Phonolitic Leucite Tephrite.

X 30



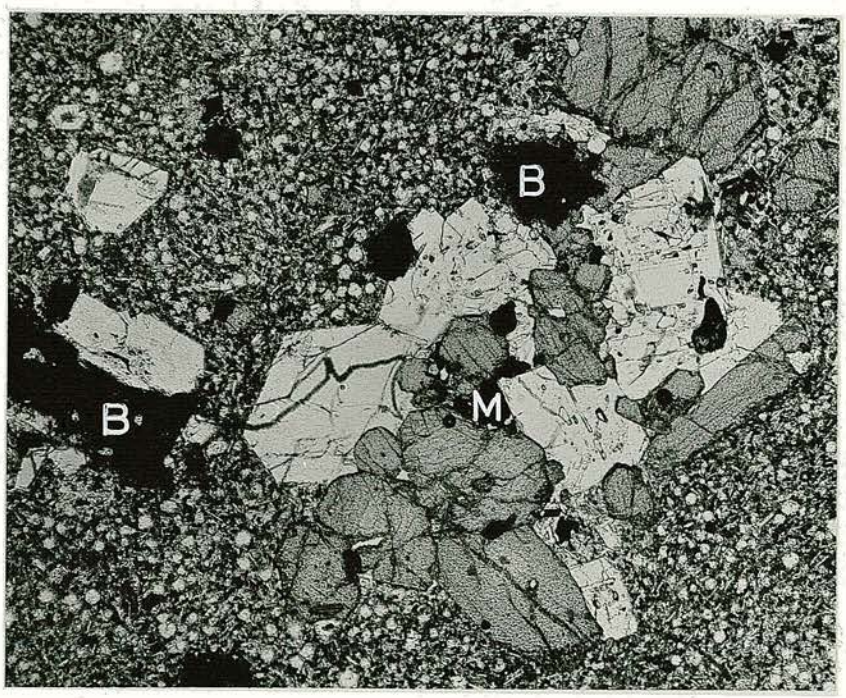

B
B
M

PLATE 23

R.107: Glomeroaggregate of plagioclase in a biotite-cpx-plagioclase-ore-rare leucite phyric Phonolitic Leucite Tephrite.

X 30 crossed nicols

PLATE 24

R.47: Apatite phenocryst clouded with ore particles.

X 150



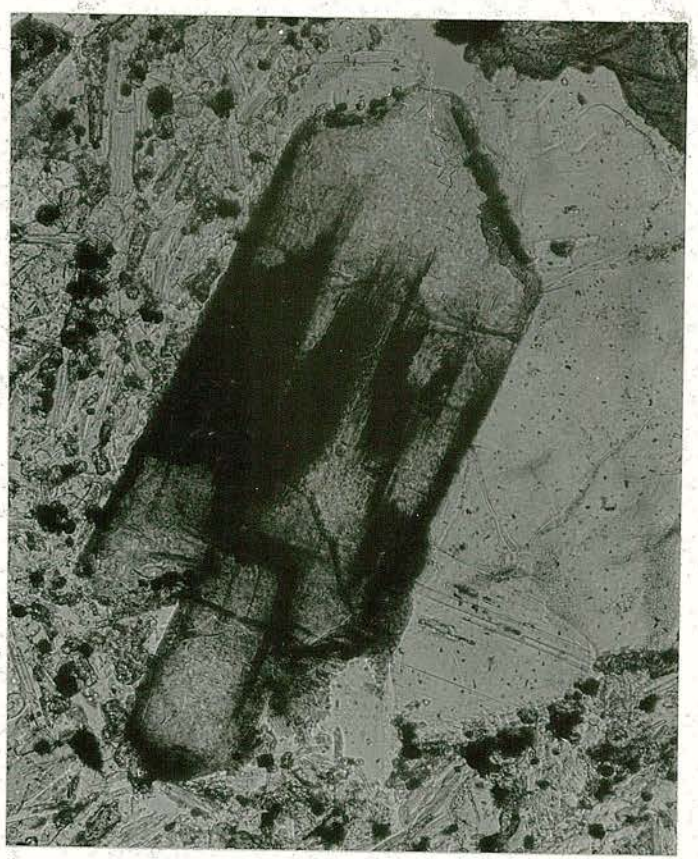


PLATE 25

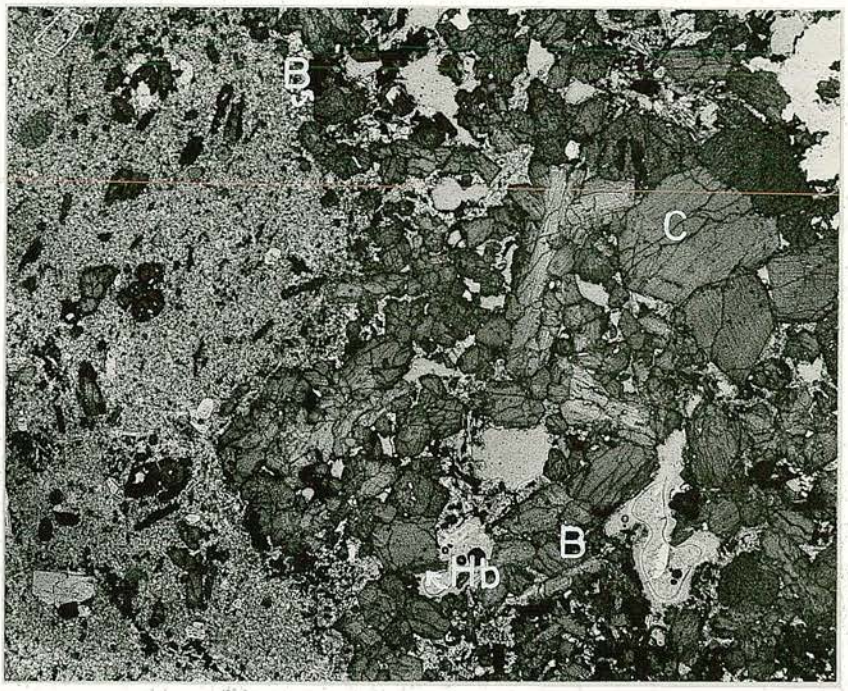
R.38: Clinopyroxene (2^{o} hornblende)-biotite aggregate in a Phonolitic Leucite Tephrite.

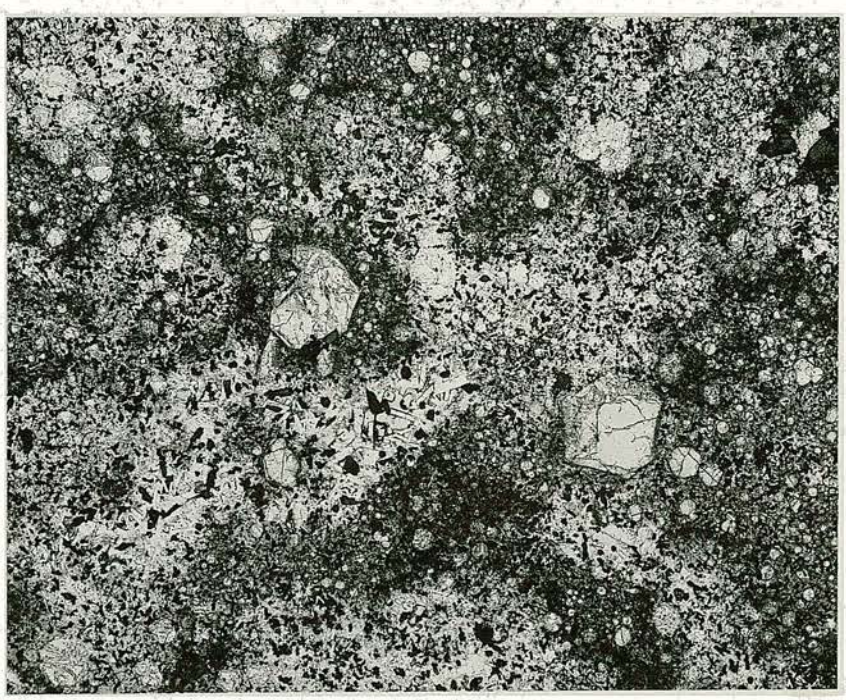
X 8

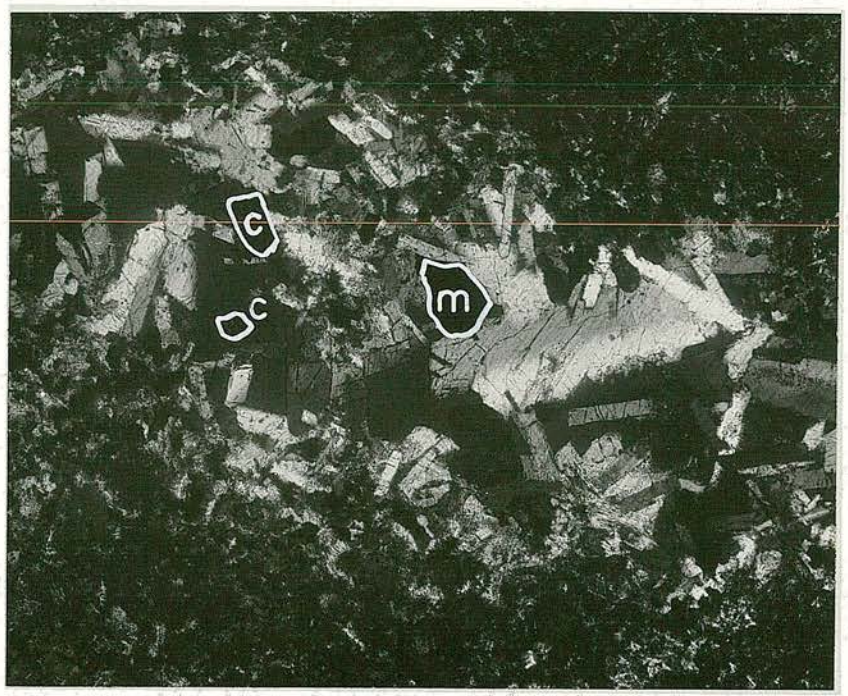
PLATE 26

R.21: Phonolitic Leucite Tephrite containing pegmatitic veins of K-feldspar and aegirine-augite.

X 8


B
C
B
Hb




c
c
m

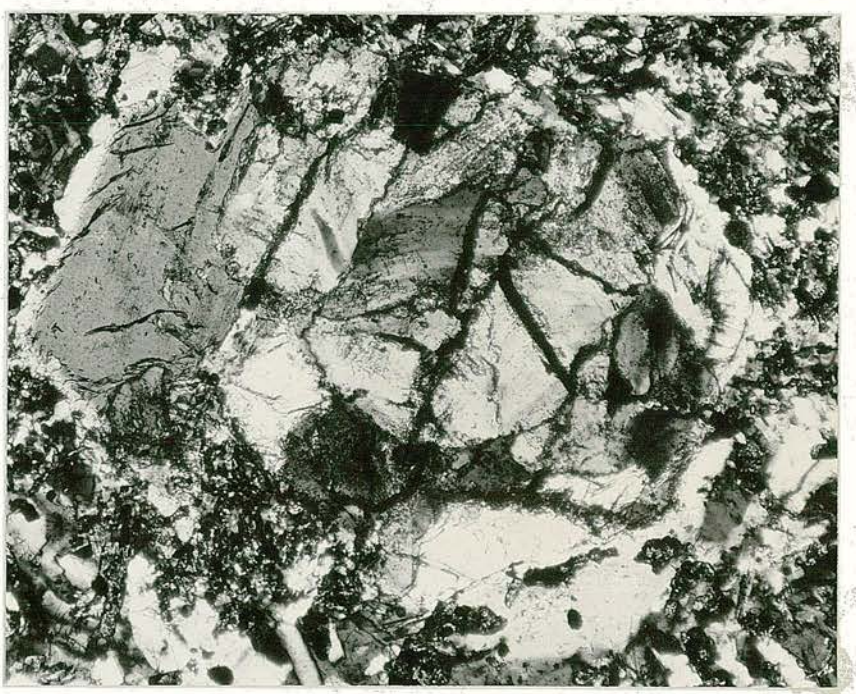


PLATE 27

R.21: Vein of K-feldspar plus accessory aegirine-augite and ore in a Phonolitic Leucite Tephrite.

X 30 crossed nicols

PLATE 28

R.21: Leucite phenocryst replaced by K-feldspar in a Phonolitic Leucite Tephrite.

X 60 crossed nicols

PLATE 29

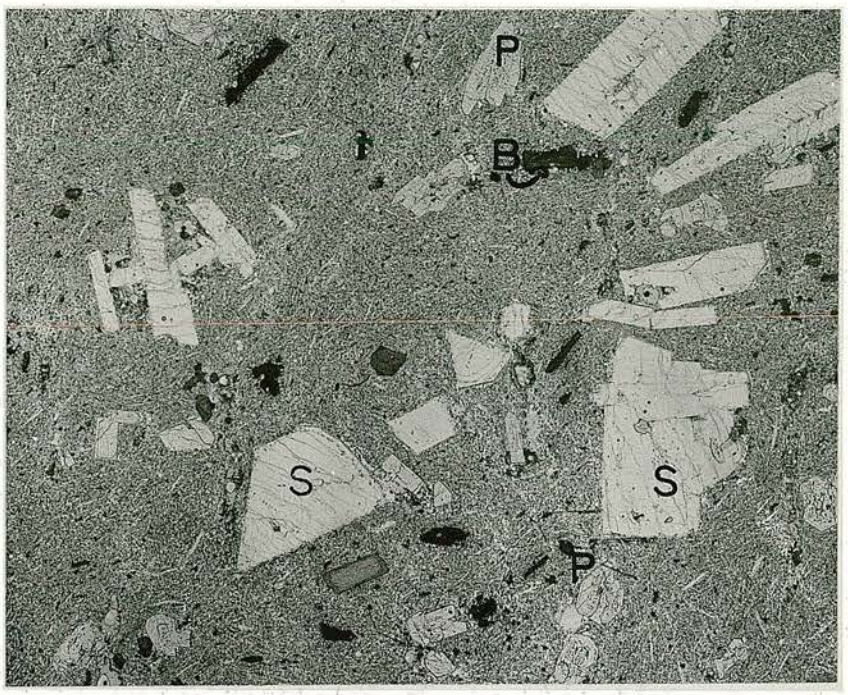
R.64: Phenocrysts of sanidine, plagioclase, clinopyroxene, biotite, and ore in a Tephritic Leucite Phonolite.

x 8

PLATE 30

R.134: Sanidine, plagioclase and clinopyroxene phenocrysts in a Tephritic Leucite Phonolite.

x 8


P
B
S
S
P

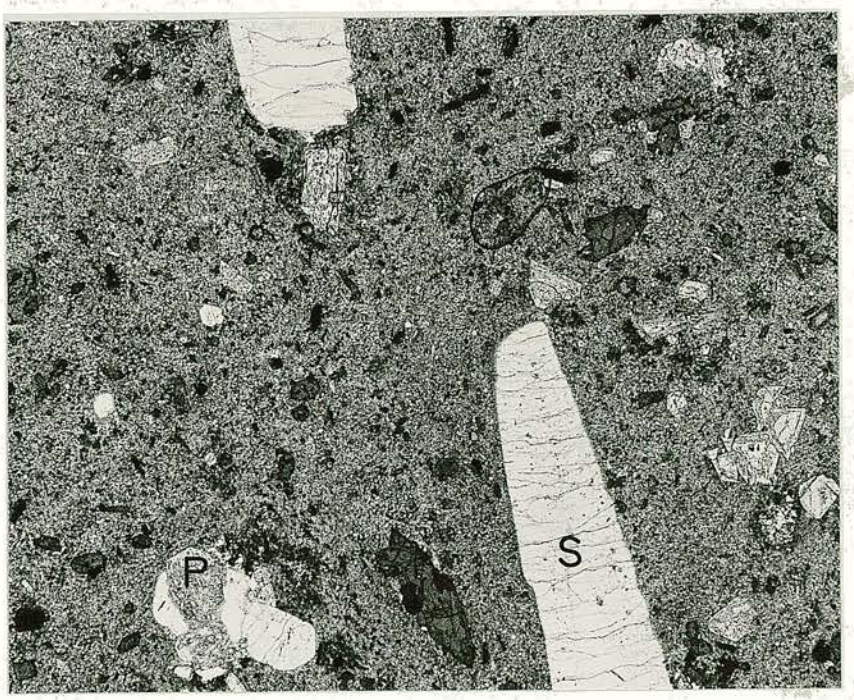

P
S

PLATE 31

R.99: Sanidine phenocrysts in Leucite Phonolite.

X 60 crossed nicols

PLATE 32

R.121: Sphene in Leucite Phonolite.

X 150



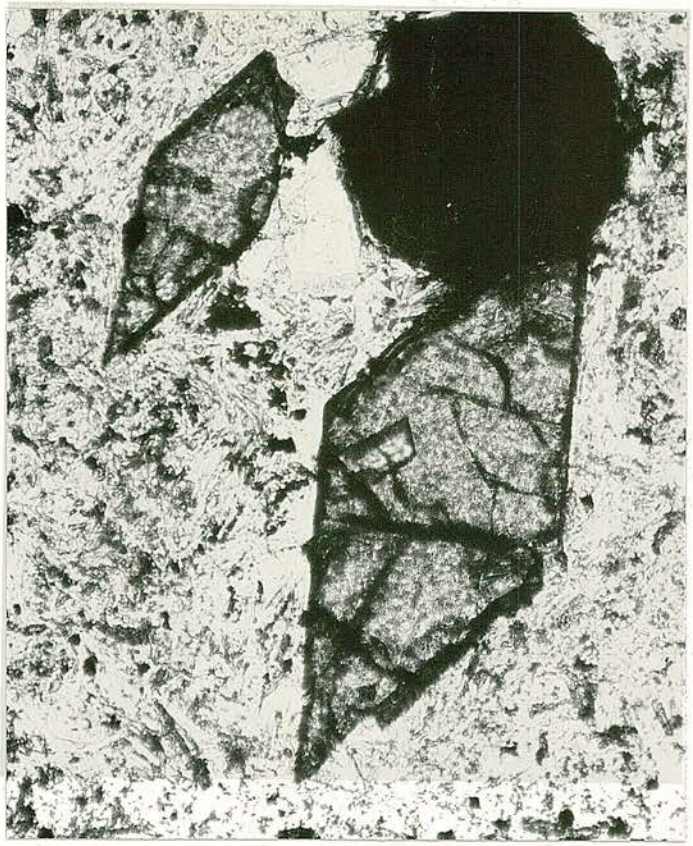


PLATE 33.

R.120: Olivine Basalt.

Note high temperature oxidation of olivine phenocrysts.

X 60

PLATE 34

R.114: Clinopyroxene and plagioclase phenocrysts in Olivine Basalt.

X 30



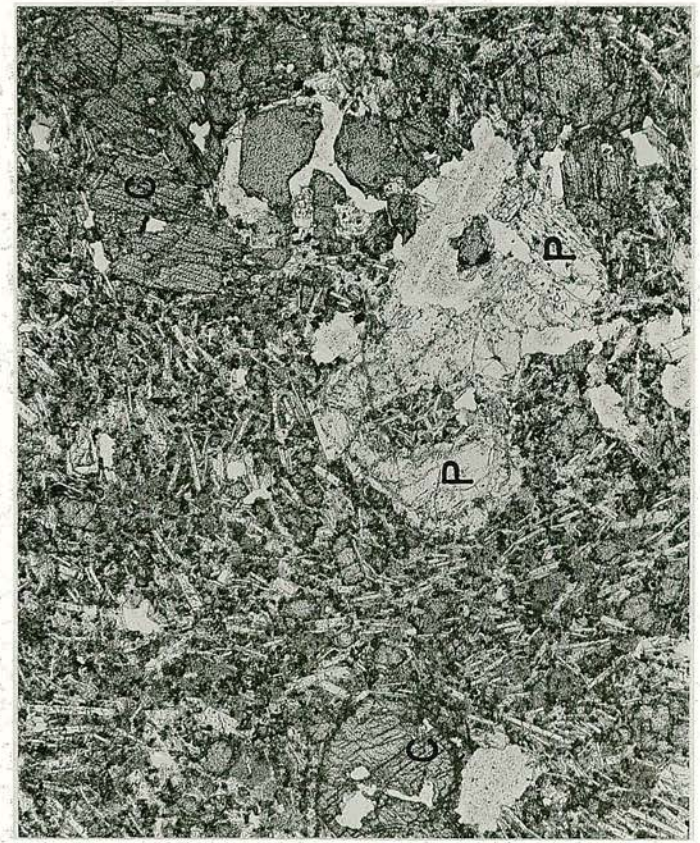

P
P
C
C

PLATE 35

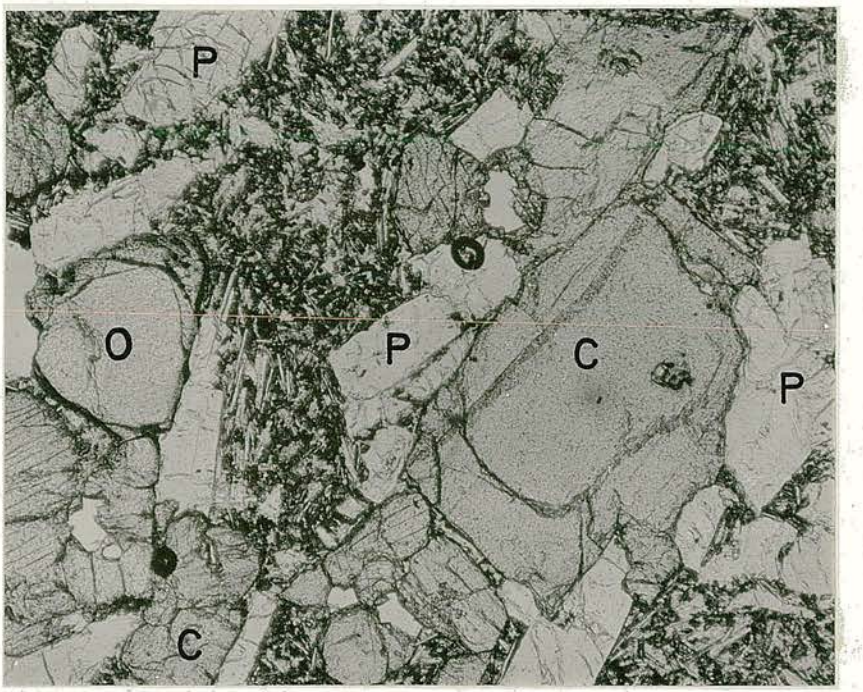
R.56: Glomeroaggregate of cpx-plagioclase-olivine in Olivine Basalt.

X 60

PLATE 36

R.56: Partially resorbed olivine phenocryst with cpx corona.

X 25


P
O
P
C
P
C

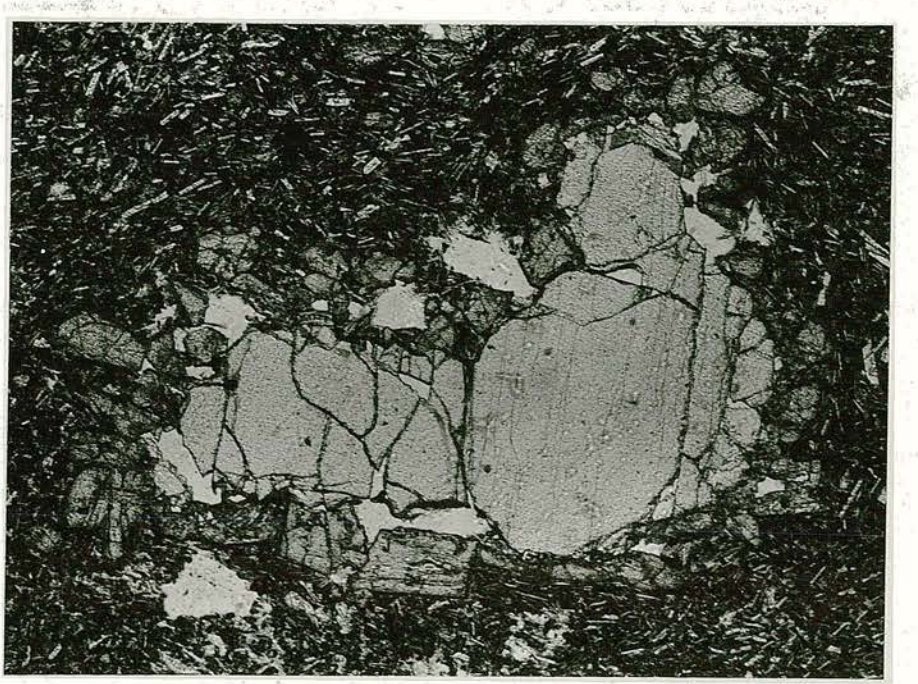


PLATE 37.

R.86: Corroded plagioclase phonocryst in Olivine Basalt.

X 60

PLATE 38

R.57: Glomeroaggregate of clinopyroxene and red spinel in Olivine Basalt.

X 60

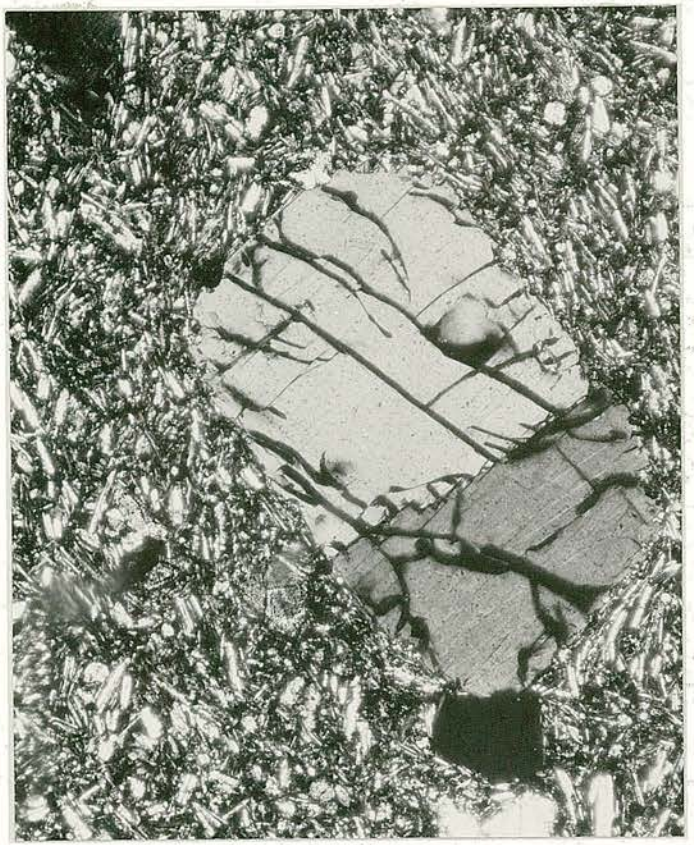




PLATE 39

R.186: Trachybasalt

X 16

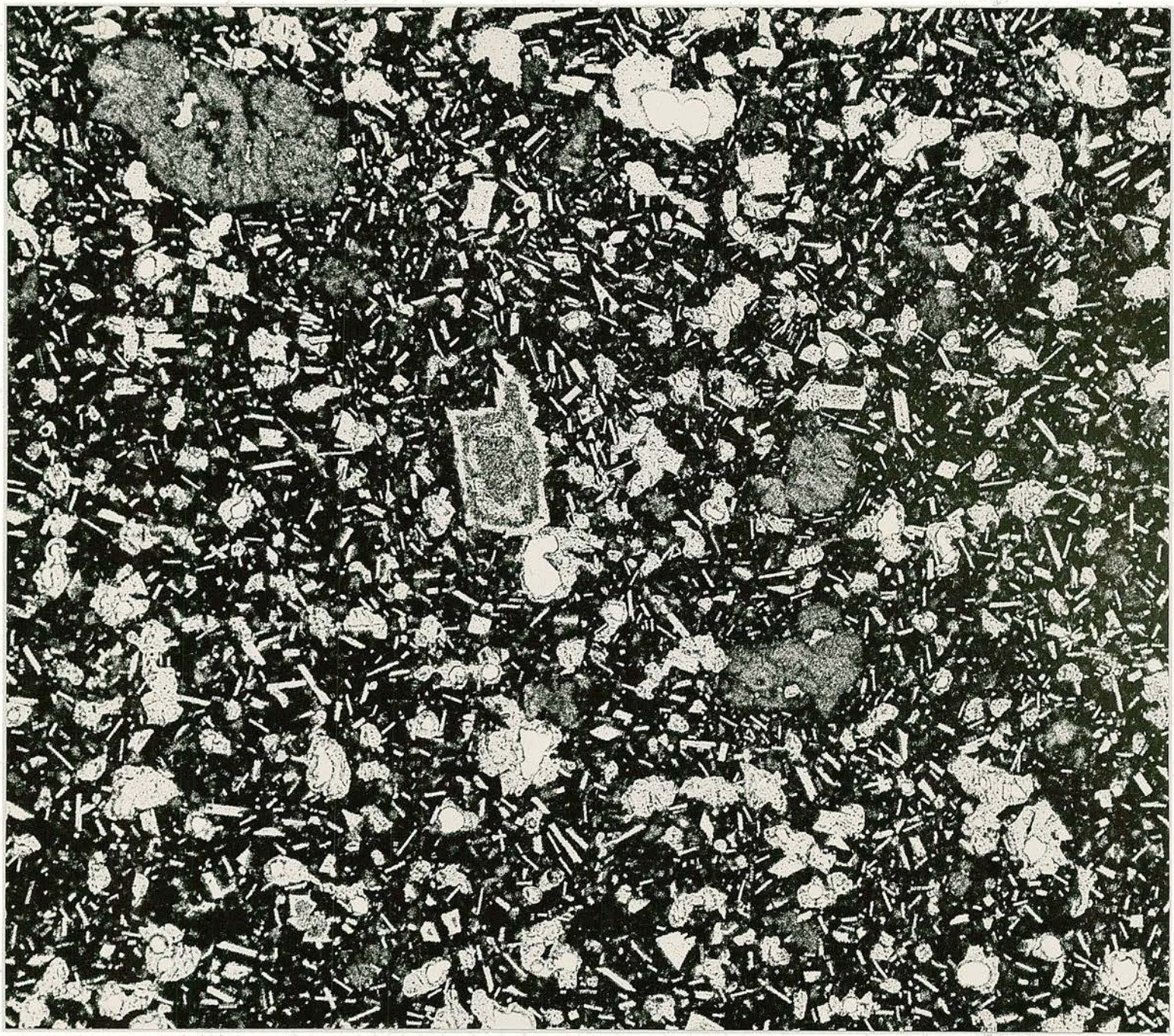


PLATE 40

R.186: Glomeroaggregate of clinopyroxene enclosing relict olivine in Trachybasalt.

Note cloudy core of plagioclase phenocryst.

X 30

PLATE 41

R.196: Biotite Augite Latite.

Note (1) plagioclase phenocrysts have spongy cores.

(2) Glomeroaggregate of biotite-cpx-plagioclase-ore (left centre).

X 7

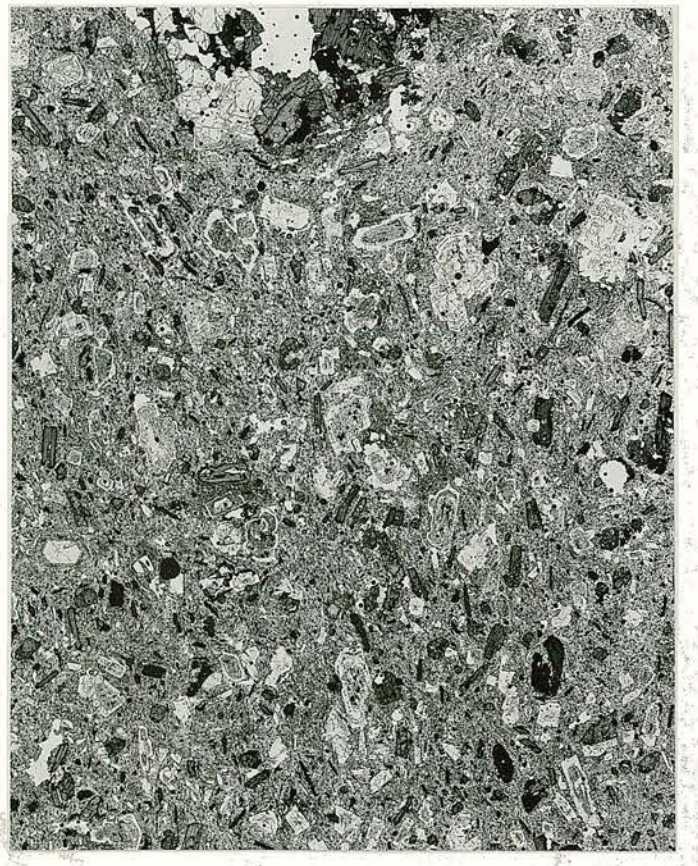




PLATE 42

R.195: Oscillatory zoning in plagioclase phenocryst in Biotite Augite Latite.

Note spongy core

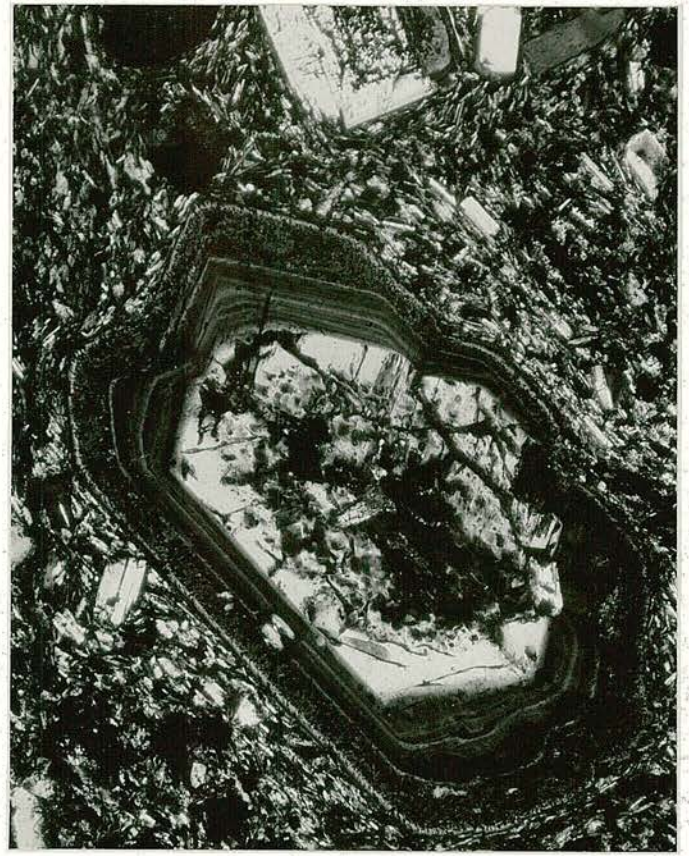
X 60 crossed nicols

PLATE 43

R.104: Plagioclase phenocryst in Biotite Augite Latite.

Note spongy core and sanidine margin.

X 60 crossed nicols



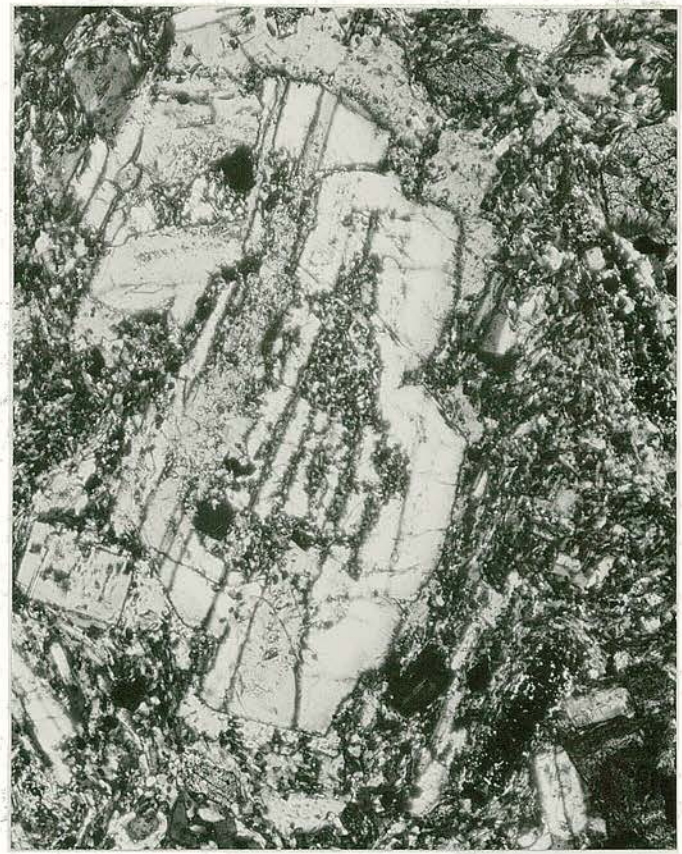


PLATE 44

R.90: Plagioclase phenocryst in Biotite Augite Latite.
Note spongy texture and oscillatory zoning.

X 60 crossed nicols

PLATE 45

R.98: Large biotite phenocryst enclosing
plagioclase laths in a Biotite Augite Latite.

X 60



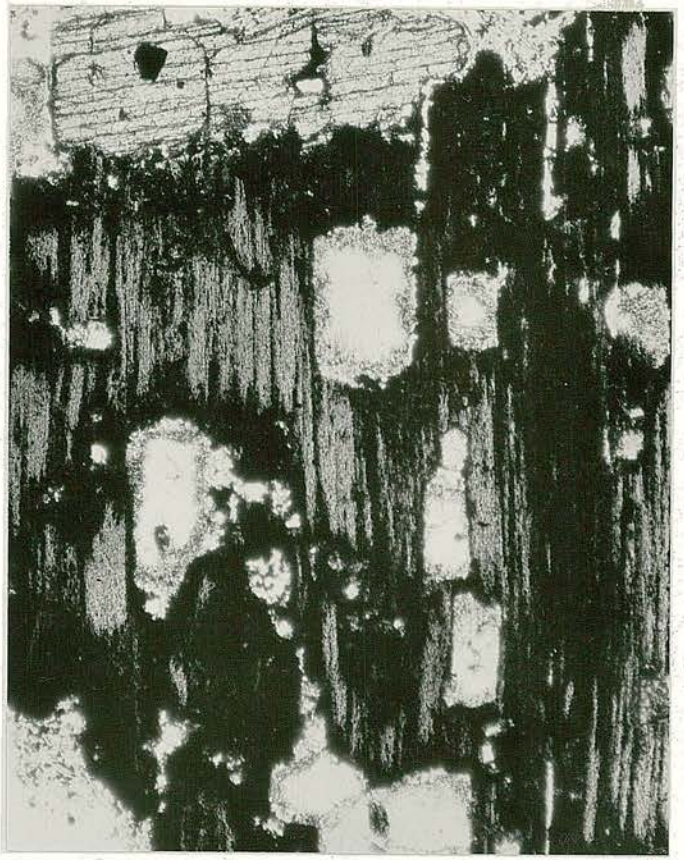


PLATE 46

R.104: Biotite Augite Latite.

Note spongy texture of plagioclase phenocrysts.

X 16

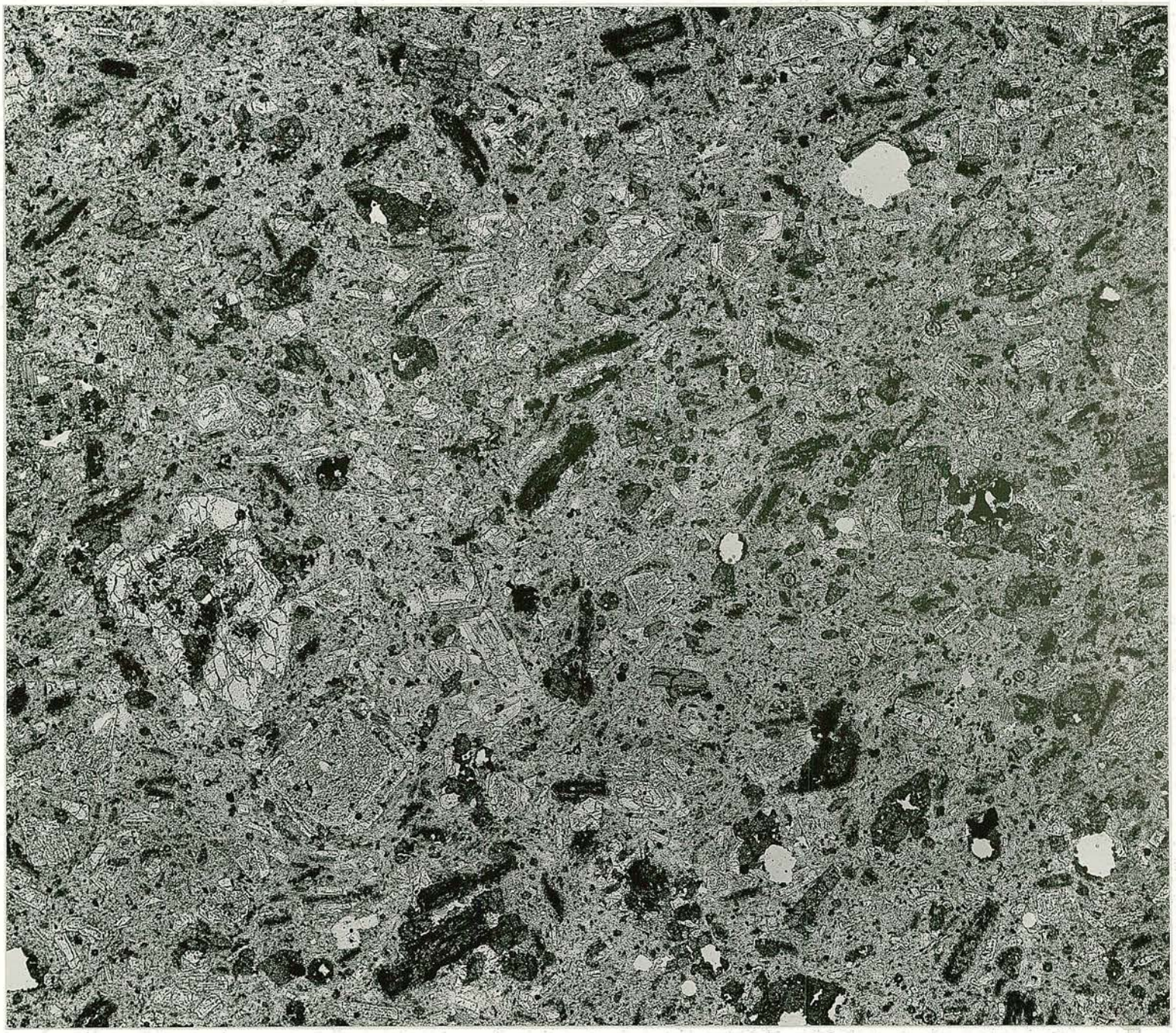


PLATE 47

R.103: Biotite Gabbro

note pronounced sub-parallel alignment of the biotite.

X 16

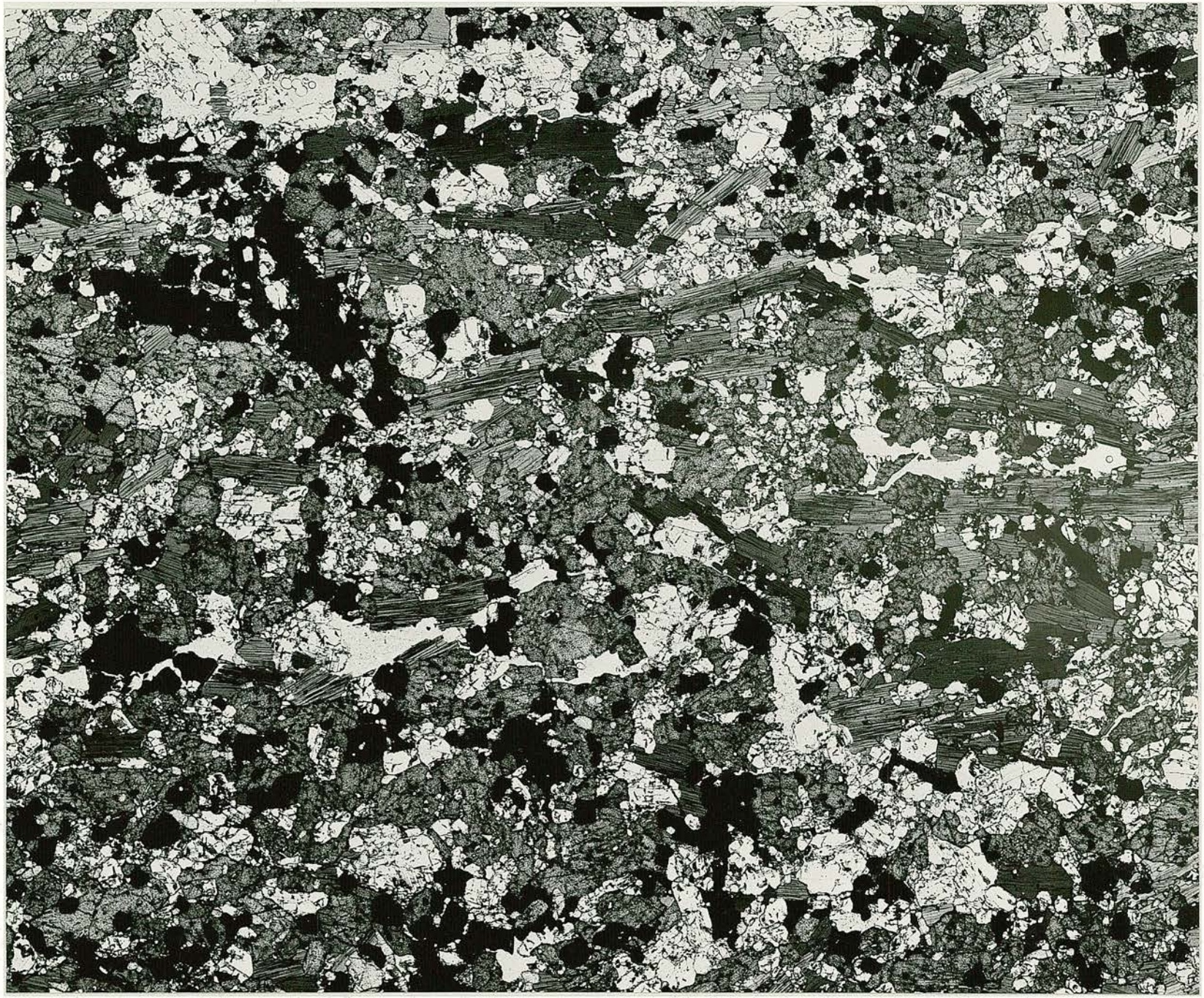


PLATE 48

R.103: Biotite Gabbro.

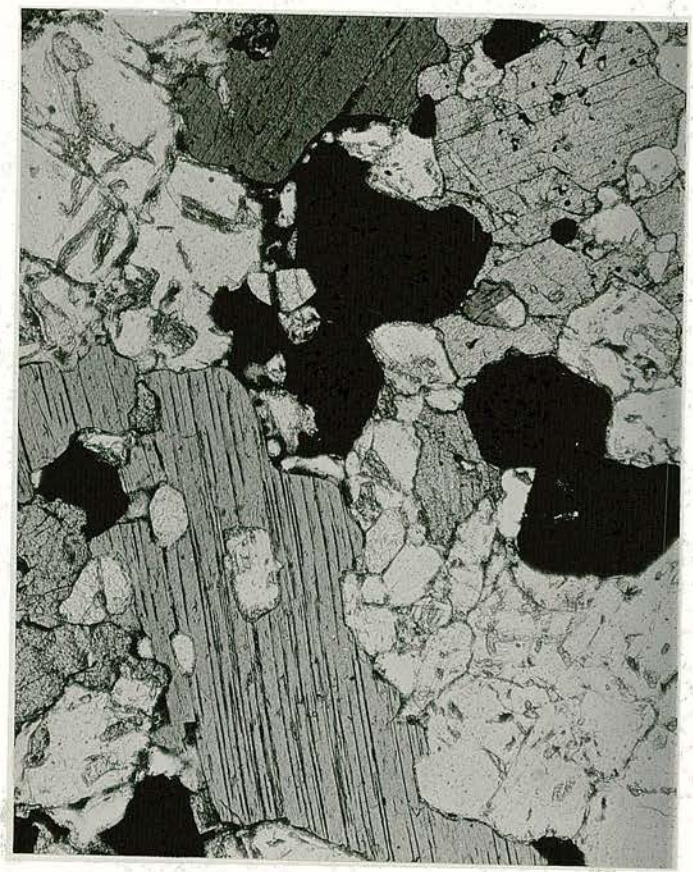
X 30

PLATE 49

R.103: Biotite Gabbro.

Note ophitic relationship between biotite and plagioclase.

X 60



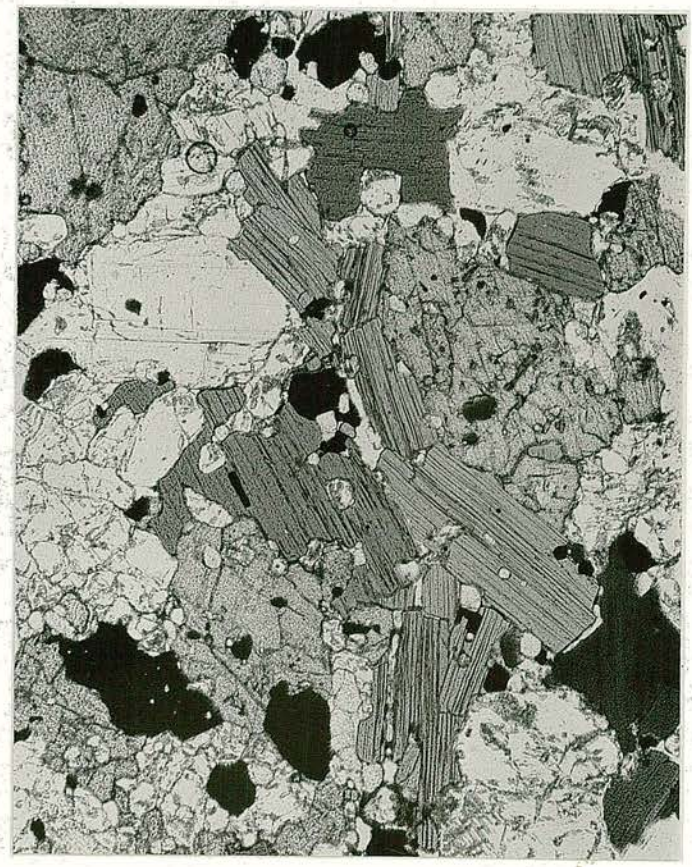
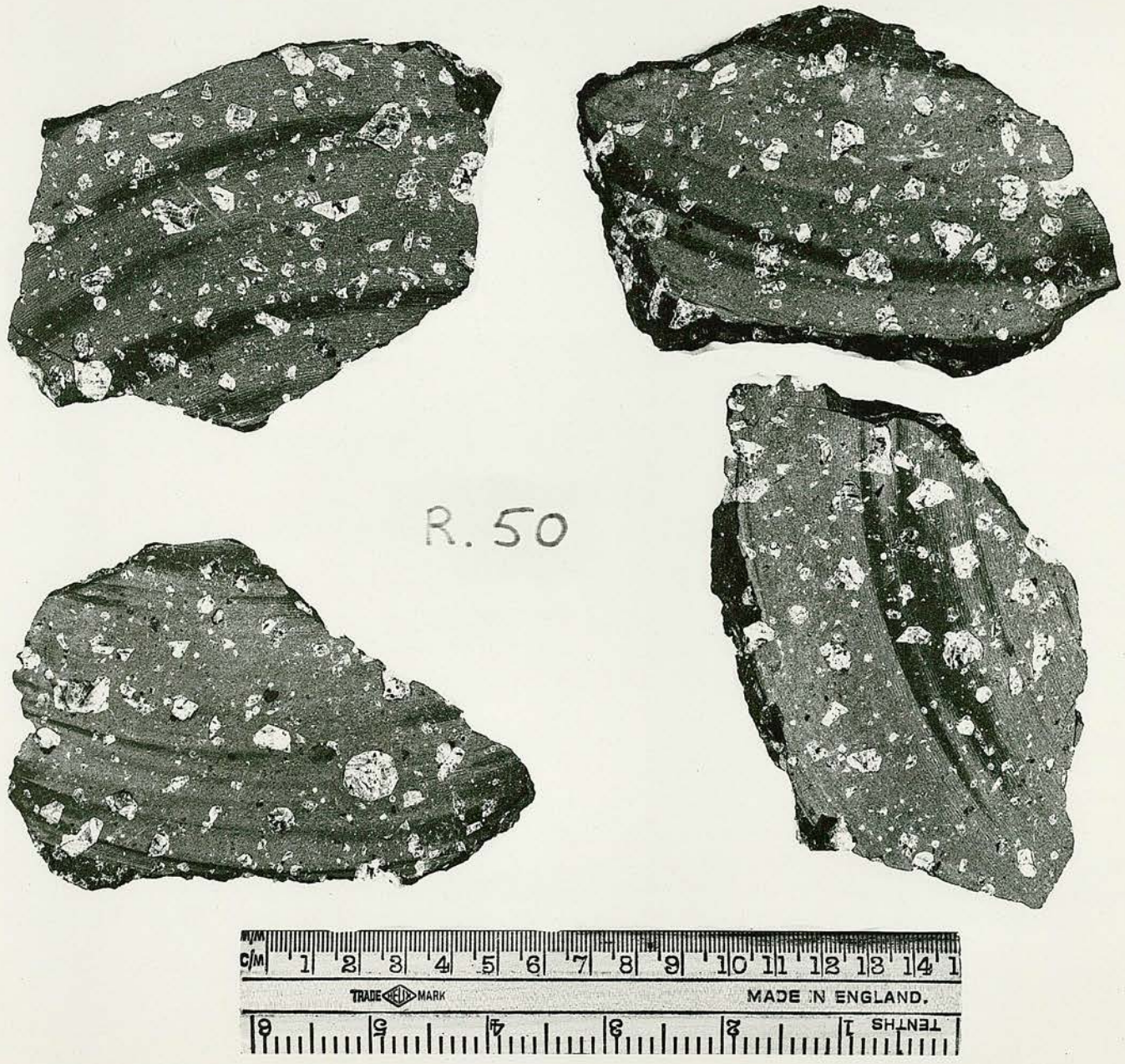


PLATE 50

R.50: Rock slabs of a leucite-cpx macrophyric Tephritic Leucitite.


R. 50
MADE IN ENGLAND.

CHAPTER 3

MINERALOGY

3:1 Introduction

The chemical composition of leucite phenocrysts from twelve macroporphyritic Roccamonfina lavas has been determined, together with distribution coefficients of the type D_{wr}^{lc} = concentration of element in leucite/concentration of element in liquid (i.e. whole rock). The variation in leucite chemistry related to variation in whole rock chemistry has also been investigated.

Variation diagrams presented in Chapter 5 suggest that fractionation of Pyroxenite, Biotite Pyroxenite, and Biotite Gabbro could produce the observed variation in the chemistry of the leucite bearing lavas of Roccamonfina, Vulsini, and Somma-Vesuvius. Pyroxenite and biotite pyroxenite nodules are not commonly found in the Roccamonfina area, so specimens from Vesuvius and the Alban Hills were used in the present study. Four clinopyroxenes and two phlogopites from pyroxenite, biotite pyroxenite, and biotitite nodules were analysed, together with biotite from the Roccamonfina biotite gabbro nodule (R.103). Trace element data are presented for a plagioclase concentrate from this gabbro nodule.

3:2 Leucite

Leucite is the most abundant phenocryst phase in the lavas of the High K series (Roccamonfina). The phenocrysts are anhedral

to euhedral and show a wide variation in size both within and between lava flows (see Chapter 2). Regular concentric bands of minute granular, prismatic and acicular inclusions of apatite, cpx, ore, and rarely plagioclase are found in some of the phenocrysts. These inclusions are too small to be easily separated from the host leucite, but as they are present in relatively small amounts, their presence should not influence the K_2O, Na_2O, Rb, Sr, and Ba data presented in this section. The zonal arrangement of inclusions (Plate 13) suggests that chemical zoning may also occur.

Previous work by Henderson (1965), and Rahman (1968) indicated that (1) there is a very limited substitution of Na for K in the ideal leucite formula and (2) the distribution coefficients of the type D_{wr}^{lc} = concentration of element in leucite/concentration of element in liquid (i.e. whole rock) show that Rb is enriched, and Sr and Ba are depleted, relative to K, in the leucite. This is the opposite relationship to that found in alkali feldspars (Berlin and Henderson, 1969).

Neither Henderson (1965) nor Rahman (1968) attempted to document the variation in leucite chemistry over a wide range of liquid (whole rock) compositions for one particular volcano. In order to do this, leucite phenocrysts were separated from 12 leucite-phyric lavas. The whole rock composition range is 5% SiO_2 and 3·5% CaO. Whole rock SiO_2 and CaO data, together with modal percent leucite in the lavas studied, are presented in Table 3-1. The methods of separation and analysis are noted in Appendix A.

Sahama (1952) postulated that the K_2O/Na_2O ratio of the leucite phenocrysts is closely related to the chemistry of the host magma. This relationship has been investigated for the Roccamonfina lavas, though it is possible that the variation postulated by Sahama (1952) may not be recognisable within the products of one volcano, but may be related only to major regional variations.

A complete chemical analysis of R.36-1c is presented in Table 3-2. Recalculation on the basis of 6 oxygens suggests that the leucite is stoichiometric within the limits of analytical error. K_2O and Na_2O data for twelve leucite samples are presented in Table 3-3. K_2O and Na_2O are converted to $KAlSi_2O_6$ and $NaAlSi_2O_6$ and plotted on this join in the system $NaAlSiO_4$-$KalSiO_4$-SiO_2 (Fig. 3-1). This illustrates the very limited substitution of Na for K in the ideal leucite formula. Comparative data from Faust (1963), and Rahman (1968), and this thesis (Aqua-1c, AB800-1c) are presented in Figs. 3-2 and 3-3. This shows that the limited substitution of Na for K is typical of leucite phenocrysts from the lavas of the Roman Region. Groundmass leucite (66/38, Rahman, 1968) from a phonolitic tephrite contains only 0·68% Na_2O, confirming Bowen and Ellestad's statement (1937) that both phenocryst and groundmass leucites from volcanic rocks seem unable to contain more than 1 - 1·5% Na_2O. Bowen and Ellestad (1937, p. 413) suggest that "phenocrystic leucites are those which are most likely to show high K_2O content, since the high temperatures (in the system Ne-Ks-SiO_2) lie towards the composition of the pure

Table 3-1

SiO_2, CaO, and volume % Leucite data for samples from which Leucite phenocrysts were separated for analysis.

Sample No.	SiO_2 (wr) wt %	CaO (wr) wt %	Vol. % Leucite
R.18	52·85	3·87	23
R.23	48·52	7·31	39
R.36	50·85	5·05	34
R.39	49·14	7·28	39
R.43	52·91	5·55	28
R.50	50·02	6·22	14
R.61	53·32	4·68	38
R.77	51·71	5·95	18
R.116	53·18	4·08	21
R.136	50·45	5·59	32
R.198	53·17	4·15	13
R.206	51·24	5·30	32

Table 3-2

Chemical analysis and formula of R.36-1c

Wt. %		No. of ions on the basis of 6 oxygens		
SiO_2	55·26	Si	2·0056	2·0056
Al_2O_3	23·26	Al	0·9932	1·0003
Fe_2O_3T	0·26	Fe^{3+}	0·0071	
MgO	n.d.	Ca	0·0062	0·9707
CaO	0·16	Na	0·0309	
Na_2O	0·44	K	0·9336	
K_2O	20·15			
TiO_2	n.d.			
MnO	n.d.			
P_2O_5	0·03			
SUM	99·56			

Table 3-3

K_2O, Na_2O, $KAlSi_2O_6$, and $NaAlSi_2O_6$ data for Roccamonfina Leucites, AB800-1c, and Aqua-1c.

Sample No.	K_2O	Na_2O	$KAlSi_2O_6$	$NaAlSi_2O_6$
R.18-1c	19·73	0·57	96·0	4·0
R.23-1c	20·01	0·61	95·9	4·1
R.36-1c	20·15	0·44	97·0	3·0
R.39-1c	20·11	0·57	96·2	3·8
R.43-1c	20·36	0·34	97·7	2·3
R.50-1c	20·09	0·53	96·4	3·6
R.61-1c	19·41	0·70	95·2	4·8
R.77-1c	20·06	0·35	97·6	2·4
R.116-1c	19·96	0·51	96·5	3·5
R.136-1c	20·04	0·48	96·7	3·3
R.198-1c	20·16	0·45	97·0	3·0
R.206-1c	20·46	0·44	97·1	2·9
AB800-1c	20·60	0·35	97·7	2·3
Aqua-1c	19·82	0·55	96·2	3·8

Fig. 4-7

Fig. 4-8

Fig. 4-9

Fig. 3-1

Recalculated analyses of Roccamonfina Leucites plotted in terms of $KAlSi_2O_6$ and $NaAlSi_2O_6$

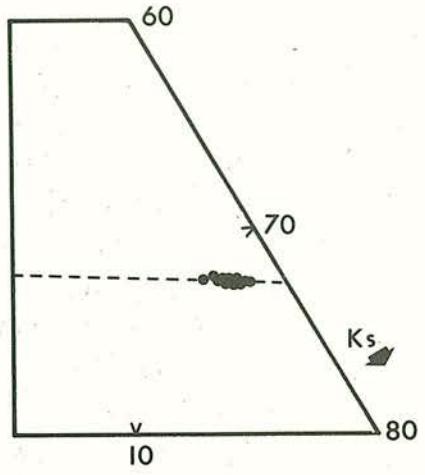
Fig. 3-2

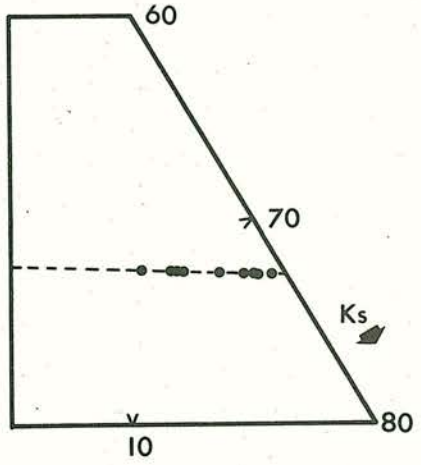
Recalculated analyses of Roman Province leucites (Faust 1963, table 6, p. 175, analyses 1-7), AB800-1c, and Aqua-1c, plotted in terms of $KAlSi_2O_6$ and $NaAlSi_2O_6$.

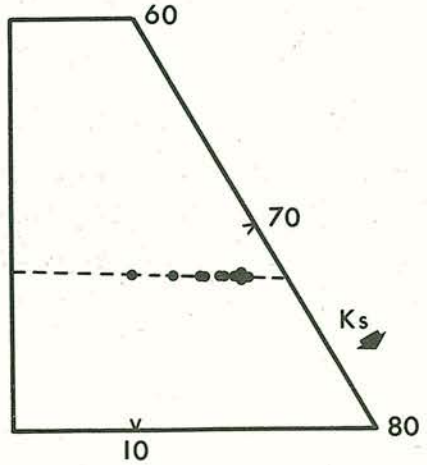
Fig. 3-3

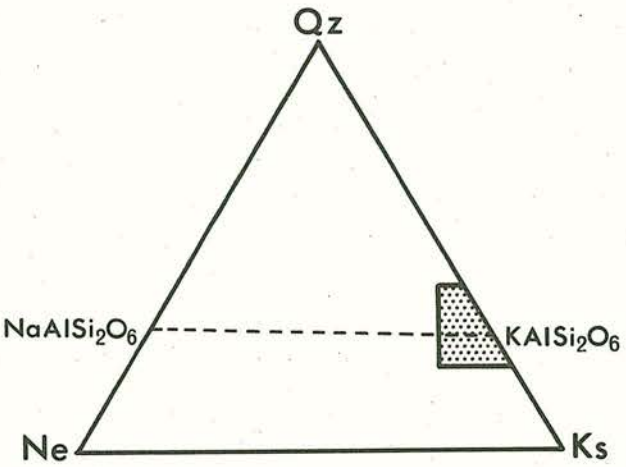
Recalculated analyses of Somma-Vesuvius leucites (Rahman, 1968) plotted in terms of $KAlSi_2O_6$ and $NaAlSi_2O_6$.

QZ - NE - KS triangle shows area (stippled) of Figs. 3-1, 3-2, 3-3.


60
70
Ks
80
10


60
70
Ks
80
10


60
70
Ks
80
10


Qz
NaAlSi2O6
KAlSi2O6
Ne
Ks

potash compound ($KAlSi_2O_6$)". It is obvious that leucites of this composition cannot be converted to pseudoleucite (K-feldspar + nepheline) by subsolidus reaction.

Table 3-4 shows the K_2O, Na_2O, Ba, Sr, and Rb concentrations for the Roccamonfina leucites together with their associated groundmass and whole rock data. K/Ba, K/Sr, and K/Rb ratios are also presented. A correlation matrix was computed for the K_2O, Na_2O, K_2O/Na_2O, Ba, Sr, and Rb data for the leucites together with SiO_2, CaO, K_2O, Na_2O, and K_2O/Na_2O data for the host rocks to see if there was any systematic variation between these variables. CaO is used as a simple index of differentiation. The only r significant at the 90% level was that between whole rock CaO and leucite K_2O/Na_2O (r = + 0·50). This indicates that as the lavas become more salic, the amount of Na substitution in the leucite increases. No other significant correlations were noted. This may be related to the fact that more than one generation of leucite phenocrysts are included in a separated sample. Electron microprobe analyses are needed to illustrate the variation in chemical composition of the different generations of leucite phenocrysts in one lava, and also the extent of chemical zoning in the larger leucite phenocrysts.

In comparison with Rahman's (1968) Somma-Vesuvius leucite analyses, the ranges of K_2O/Na_2O and Rb are very similar, but the Ba and Sr for the Roccamonfina leucites are significantly lower (see Table 3-5). Figs. 3-4 and 3-5 show the relationship between Ba(leucite) v. CaO(whole rock), and Ba(whole rock) v. CaO(whole rock) for Roccamonfina and Somma-Vesuvius (based on data

Table 3-4

Chemical analyses of Roccamonfina leucites (lc) together with their whole rock (wr) and groundmass (g) data

Sample No.		K_2O	Na_2O	Ba	Sr	Rb	K/Ba	K/Sr	K/Rb
		--wt.%--		-----ppm------			---------wt---------		
	lc	19·73	0·57	129	38	1566	1291	4309	105
R.18	wr	10·55	3·37	1824	2206	678	48	40	129
	g	8·05	4·03	2377	2719	422	28	25	158
	lc	20·01	0·61	575	61	1555	289	2723	107
R.23	wr	9·66	2·14	1823	2192	617	44	37	130
	g	7·49	2·28	2152	2544	421	29	24	148
	lc	20·15	0·44	81	34	1741	2065	4919	96
R.36	wr	10·65	2·69	1383	1851	776	64	48	114
	g	7·15	3·31	1990	2450	455	30	24	130
	lc	20·11	0·57	484	28	1428	345	5961	117
R.39	wr	9·60	2·49	1591	2027	602	50	39	132
	g	6·61	3·09	1968	2703	379	28	20	145
	lc	20·36	0·34	107	33	1523	1579	5129	111
R.43	wr	10·87	3·15	1426	1970	621	63	46	145
	g	8·38	3·78	1838	2428	421	38	29	165
	lc	20·09	0·53	200	25	1942	834	6670	86
R.50	wr	9·58	2·62	1382	1809	742	58	44	107
	g	8·13	2·74	1621	2056	603	42	33	112
	lc	19·41	0·70	89	50	1645	1810	3222	98
R.61	wr	10·28	2·88	1516	1915	633	56	45	135
	g	8·84	3·22	1817	2089	477	40	35	154
	lc	20·06	0·35	52	30	1593	3202	5550	106
R.77	wr	10·00	2·29	1329	2007	656	62	41	127
	g	9·11	2·31	1465	2191	626	52	35	121
	lc	19·96	0·51	146	59	2191	1135	2808	76
R.116	wr	11·00	2·41	932	1410	1270	98	65	72
	g	8·68	2·97	1111	1810	1045	65	40	69
	lc	20·04	0·48	310	26	1615	537	6397	103
R.136	wr	10·66	1·96	1411	1739	879	63	51	101
	g	7·62	2·42	1769	2295	634	36	28	100
	lc	20·16	0·45	40	31	1193	4183	5397	140
R.198	wr	10·30	3·60	1589	2187	497	54	39	172
	g	9·27	3·84	1797	2431	427	43	32	180
	lc	20·46	0·44	281	36	1433	604	4717	119
R.206	wr	11·51	2·78	1434	1933	760	67	49	126
	g	8·81	3·27	1766	2466	548	41	30	133

Table 3-5

Chemical composition of Roccamonfina (this thesis) and Somma-Vesuvius (Rahman, 1968) leucites

	Roccamonfina(12)			Somma-Vesuvius(6)		
ppm.	min.	mean	max.	min.	mean	max.
Ba	40	208	575	279	484	940
Sr	25	38	61	86	170	225
Rb	1193	1619	2191	932	1484	2037
K_2O/Na_2O	27·7	42·0	59·9	14·1	31·5	47·4

presented in this thesis and by Rahman, 1968). Fig. 3-4 shows the positive correlation between Ba(lc) and CaO(wr), suggesting that the leucite structure permits greater substitution of Ba at higher temperatures (presuming that the more basic rocks with higher CaO crystallised at higher temperatures). Fig. 3-5 shows that the Ba content of the leucite cannot be directly related to the concentration of Ba in the magma. Sr shows a broadly similar relationship (Figs. 3-6, 3-7).

The data presented in Table 3-6 confirms the distribution coefficients (conc. of element in lc./conc. of element in liquid(wr)) first noted by Henderson (1965). Fractionation of leucite (see Chapter 5) would thus rapidly enrich the residual liquid in Sr and Ba whilst Rb would be slightly depleted, relative to K_2O.

Figs. 3-4 to 3-7 show the relationship between leucite (lc) and whole-rock (wr) chemistry.

▲ : Roccamonfina

■ : Somma-Vesuvius (Rahman, 1968)

Fig. 3-5

Ba (wr) v. CaO (wr)

Fig. 3-7

Sr (wr) v. CaO (wr)

Fig. 3-4

Ba (lc) v. CaO (wr)

Fig. 3-6

Sr (lc) v. CaO (wr)

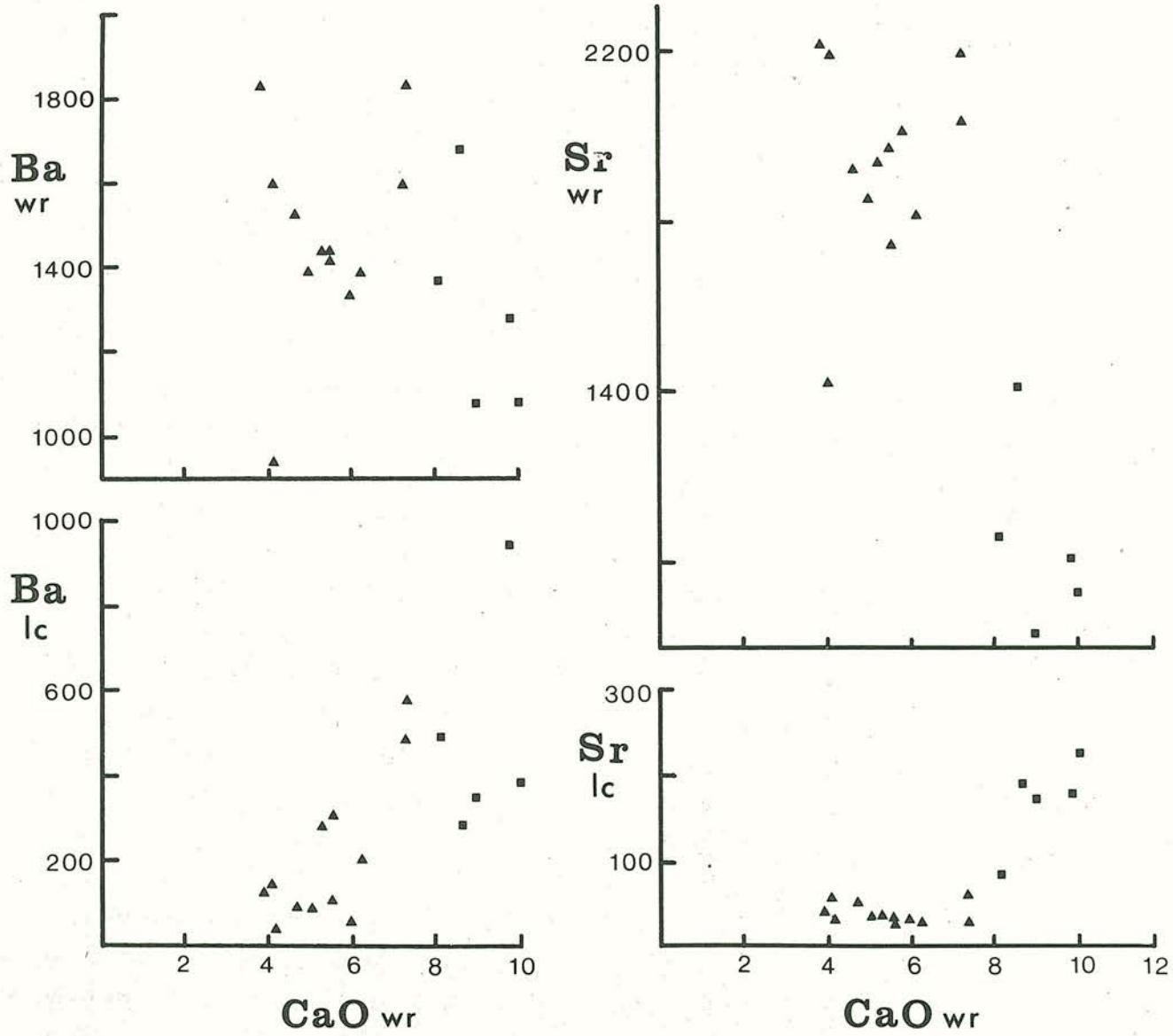

1800
Ba
wr
1400
1000
1000
Ba
lc
600
200
2
4
6
8
10
CaO wr
2200
Sr
wr
1400
300
Sr
lc
100
2
4
6
8
10
12
CaO wr

Table 3-6

Distribution coefficients of the type D^{lc}_{wr} = conc. of element in leucite/conc. of element in liquid (wr) for Roccamonfina lavas

Element	min.	mean	max.
Ba	0·02	0·14	0·32
Sr	0·01	0·02	0·04
Rb	1·73	2·28	2·62

3:3 Clinopyroxene

Chemical analyses for clinopyroxenes from three pyroxenite nodules (V-1, 14043, AB6(c)) and from one biotite pyroxenite (BP-Ariccia) are presented (Table 3-7). The petrography of these nodules is described in Appendix E, and methods of mineral separation and analysis are noted in Appendix A. The clinopyroxene analyses are recalculated on the basis of 6 oxygens; alumina (Al_2O_3) being assumed to complete the Z site (making $Si + Al_z = 2{\cdot}00$) with the remainder placed in the Y site (Table 3-8). These new analyses, together with comparative data from Rahman (1968) and Cundari and Le Maitre (1970) are presented in Fig. 3-8. According to the nomenclature of Poldervaart and Hess (1951, p. 472), Cpx-V-1, Cpx-AB6(c), and Cpx-BP(Ariccia) are diopsides, whilst Cpx-14043 lies on the border of the diopside and salite fields. The majority of the clinopyroxenes separated from the Somma-Vesuvius lavas fall within the salite field (Rahman, 1968).

Rahman (1968) noted the high Al_z of the Somma-Vesuvius clinopyroxenes. In the diopsides (Cpx-V-1, etc.) the Al_z is much lower;

Table 3-7

Clinopyroxene Analyses

Wt. %	Cpx-V-1	Cpx-14043	Cpx-AB6(c)	Cpx-BP(Ariccia)
SiO_2	51·47	49·92	51·56	52·92
TiO_2	0·67	0·93	0·48	0·41
Al_2O_3	4·09	6·80	4·47	2·57
Fe_2O_3	1·89	2·33	2·43	1·50
FeO	3·35	4·54	2·92	2·34
MnO	0·09	0·12	0·11	0·07
MgO	15·50	13·80	14·66	16·21
CaO	21·93	20·56	22·30	22·78
Na_2O	0·23	0·57	0·36	0·33
K_2O	0·08	0·12	0·09	0·11
H_2O^+	n.d.	n.d.	n.d.	n.d.
Total	99·30	99·67	99·38	99·24
ppm.				
Zr	48	103	131	79
Sr	115	241	522	351
Zn	31	39	39	22
Ni	121	90	115	139
Formula Ca	47	46	48	48
Formula Mg	46	44	45	47
Formula Fe^*	7	10	7	5

$Fe^* = Fe^{2+} + Fe^{3+} + Mn$

Table 3-8

Clinopyroxene analyses recalculated on the basis of 6 oxygens

	Cpx-V-1	Cpx-14043	Cpx-AB6(c)	Cpx-BP(Ariccia)
Si	1·892	1·836	1·895	1·938
Al^{IV}	0·108	0·164	0·105	0·062
Al^{VI}	0·069	0·130	0·088	0·049
Ti	0·019	0·026	0·013	0·012
Fe^{3+}	0·052	0·064	0·067	0·043
Mg	0·855	0·762	0·808	0·891
Fe^{2+}	0·103	0·139	0·090	0·072
Mn	0·003	0·004	0·004	0·002
Ca	0·864	0·811	0·878	0·894
Na	0·017	0·041	0·026	0·024
K	0·004	0·006	0·004	0·005
Z	2·00	2·00	2·00	2·00
WXY	1·99	1·98	1·98	1·99

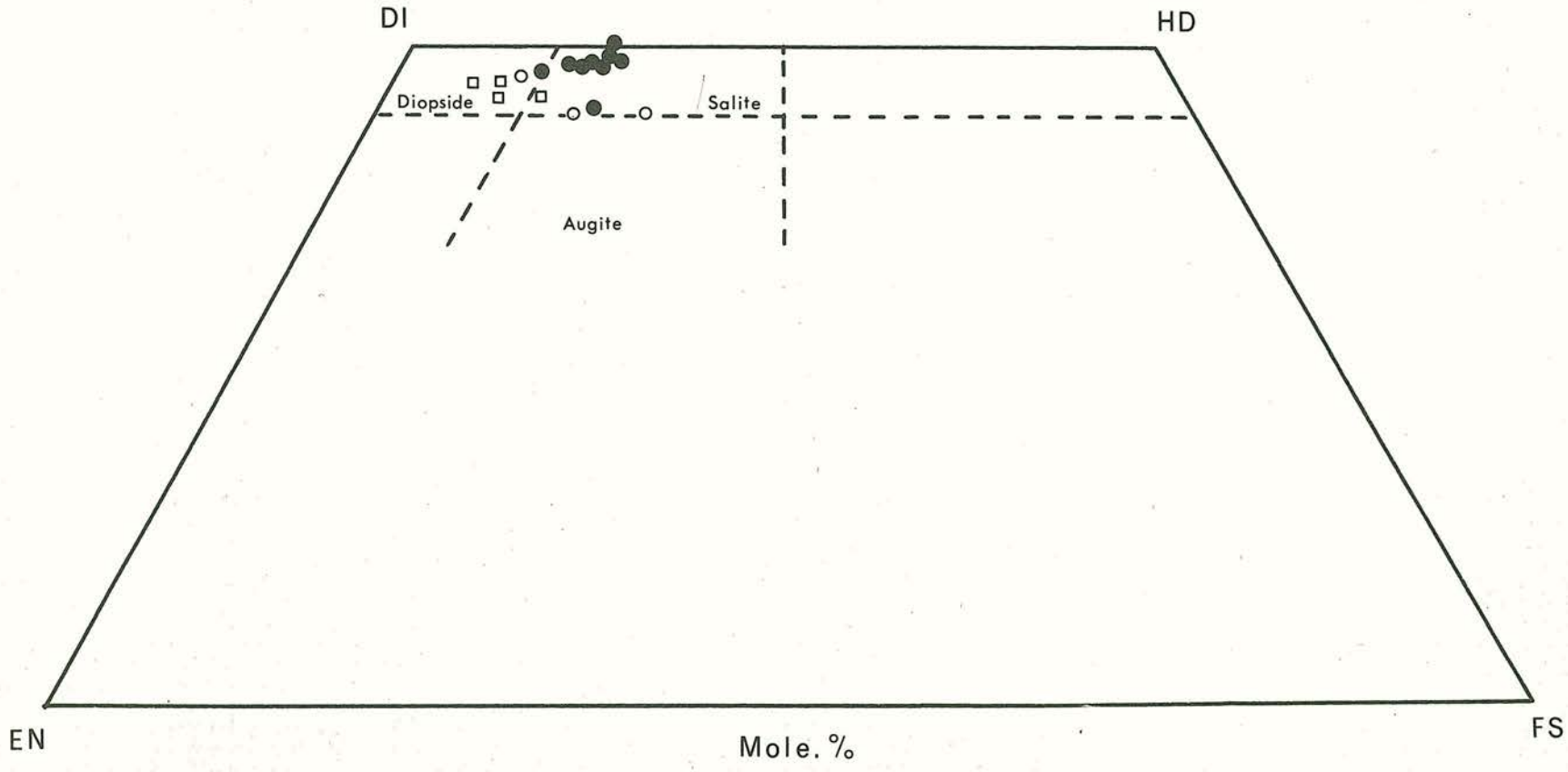
Fig. 3-8

Clinopyroxene compositions.

● : clinopyroxenes from Somma-Vesuvius lavas (Rahman, 1968).

□ : clinopyroxenes from pyroxenite and biotite-pyroxenite nodules (Table 3-7)

○ : nodule and lava clinopyroxenes (Cundari and Le Maitre, 1970, Table 2)


DI
HD
Diopside
Salite
Augite
EN
FS
Mole. %

the Al and Ti contents increase as the composition of the clinopyroxene migrates into the salite field. TiO_2 is not as high as often found in clinopyroxenes from undersaturated feldspathoidal lavas (Kushiro, 1960; Le Bas, 1962), though neither is the whole rock TiO_2 content.

Kushiro (1960), Le Bas (1962), and Aoki and Kushiro (1968) suggest that Si-Al-Ti substitution in clinopyroxenes is largely controlled by physico-chemical conditions during crystallisation. Cundari and Le Maitre (1970) state that the distribution of Al between the tetrahedral and octahedral sites in Vesuvius clinopyroxenes suggests that they crystallised under high pressure conditions when compared with those indicated for common igneous rocks (Aoki and Kushiro, 1968). Variation in PT conditions may affect the Al substitution in the Z site, but the paragenesis is also very important. On the basis of microprobe analyses, Carmichael (personal communication in Rahman, 1968) has noted that some zones in Vesuvius clinopyroxenes contain up to 20% Al_2O_3. Variation in pressure cannot explain these large zonal variations of Al_2O_3. Thus the use of Al substitution as an indicator of pressure during crystallisation should be treated with caution. The effect of magma composition and paragenesis, as well as P, T, P_{O2}, P_{H2O}, etc. on Al, and Ti substitution is not yet fully understood.

The minor element chemistry of the analysed clinopyroxenes is presented in Table 3-9, together with the mean for the Vesuvius clinopyroxenes analysed by Savelli (1967). There is a close

similarity between Cpx-V-1, Cpx-14043 (both from Vesuvius pyroxenite nodules) and the mean Vesuvius clinopyroxene data given by Savelli (1967, Table 2). The clinopyroxenes from the Alban Hills contain slightly higher Sr; perhaps reflecting the higher whole rock Sr concentrations of the Alban Hills lavas.

Table 3-9

Clinopyroxene minor element chemistry (ppm)

Element	Cpx-AB6(c)	Cpx-BP(Ariccia)	Cpx-V-1	Cpx-14043	Mean Vesuv Cpx (Savelli,1967)
Zr	131	79	48	103	120
Sr	522	351	115	241	200
Zn	39	22	31	39	30
Ni	115	139	121	90	n.d.

Clinopyroxenes were not separated from the Roccamonfina lavas because the modal percentage of cpx phenocrysts is low and because they are frequently zoned. Microprobe facilities were not available, so analysis of the Roccamonfina clinopyroxenes was not attempted. X-ray diffraction (Brown, 1960; Viswanathan, 1966) and β index methods were not used as they give inaccurate results when the clinopyroxene contains substantial quantities of Al, Fe^{3+}, and Ti.

3:4 Phlogopite and Biotite

Two phlogopites were analysed (Ph-BP(Ariccia), Ph-BAH; see Appendix E for petrographic details of the host nodules).

The Mg:Fe ratio is greater than 2:1, therefore these micas are phlogopites rather than biotites according to the nomenclature of Deer et al. (1962a). Both are brown with a faint red tinge in basal section.

Biotite from the biotite gabbro nodule (R.103) was also analysed. This mineral is brown in basal section. The chemical analyses of the micas are presented in Table 3-10.

As with the phlogopites from the ultramafic inclusions of the Dreiser Weiher (Aoki and Kushiro, 1968), the Roman Region phlogopites contain higher Al_2O_3, and lower SiO_2 and Total Fe when compared with those from eclogite nodules in kimberlite (Kushiro and Aoki, 1968), drusy cavities in alkali basalts (Aoki and Kushiro, 1968; Flower, 1969), and potassic lavas from the Leucite Hills (Carmichael, 1967). This probably reflects the higher Al_2O_3 of the host rocks. The Roman Region phlogopites (this thesis, Table 3-11; Washington, 1927) contain lower TiO_2 (mean of three phlogopites = 1·33%) than the phlogopites from the parageneses mentioned above. It should be noted that the phlogopite in the Jan Mayen Is. lavas occurs as clusters in vesicles, suggesting a late stage of crystallisation rather than the Upper Mantle origin proposed by Flower (1969).

The minor element chemistry of the analysed micas (Table 3-10) shows the considerable variation in Ba, Rb, Zn, and Ni. It is obvious that the paragenesis of the two phlogopites is different. The phlogopite (Ph-BP(Ariccia)) with Ni = 713ppm and TiO_2 = 1·91% has probably crystallised from a basic melt,

Table 3-10

Phlogopite and Biotite Analyses

Wt.%	Ph-BAH	Ph-BP(Ariccia)	Biotite(R.103)*
SiO_2	38·43	39·53	37·21
TiO_2	0·56	1·91	3·48
Al_2O_3	15·15	14·63	16·34
Fe_2O_3	4·53	2·99	5·40
FeO	2·84	4·09	8·31
MnO	0·35	0·10	n.d.
MgO	22·62	21·47	14·12
CaO	0·19	0·15	0·60
Na_2O	0·22	0·25	n.d.
K_2O	9·84	9·76	8·57
H_2O+	n.d.	n.d.	n.d.
F	n.d.	n.d.	n.d.
BaO	1·46	0·31	0·35
SUM	96·19	95·19	94·38
ppm			
Ba	13036	2775	3127
Rb	218	882	586
Zn	416	93	143
Ni	5	713	43

* SiO_2, TiO_2, Al_2O_3, Fe_2O_3, MgO, CaO and K_2O determined by G. Angell.

while the phlogopite (Ph-BAH) with 13036ppm Ba and only 5ppm Ni must have crystallised from a much more salic melt.

3:5 Plagioclase

Plagioclase compositions were determined using the Michel-Levy method (Kerr, 1959). An% was determined from the maximum extinction angle ($X \wedge 010$) curve for high temperature plagioclase (modified after Tobi, 1963). Rahman's (1968) data for Vesuvius plagioclases show a good agreement between chemical and "U" stage determinations, bearing in mind the fact that extinction angles were determined on one or two crystals while the chemical analysis will give a more average composition. It was considered that the rapid Michel-Levy method provided accurate enough results for the purpose of the present study. Compositions of plagioclases from the Roccamonfina lavas are given in Chapter 2.

The composition of the plagioclase from the biotite gabbro nodule (R.103) was calculated by determining its β index in sodium light. Trace element data for this plagioclase are compared with data for plagioclase from a Vesuvius lava (Berlin, personal communication in Rahman, 1968) in Table 3-11.

Table 3-11

Plagioclase trace element data

ppm	Plag.(R.103)	Plag.(Leucite basanite, Vesuvius)*
Ba	212	1150
Sr	2303	4500
Rb	10	n.d.

* Analyst R. Berlin (pers.comm. in Rahman, 1968).

3:6 Olivine

Olivine is only found as a major phenocryst phase in the olivine basalts of the Low K series (Roccamonfina). The composition of olivine separated from R.86 was determined by the X.R.D. method of Yoder and Sahama (1957) and Biggar (unpublished) using NaCl as an internal standard and measuring the mean distance between the olivine (130) reflection and the NaCl peak over six oscillations. The olivine from R.86 has a composition of Fo_{87}.

CHAPTER 4

CHEMISTRY OF THE LAVAS

4:1 Introduction

Major and trace element data are presented in Appendix C for 117 samples from the Roccamonfina volcano. Sample preparation and analytical methods are explained in Appendix A. Chemical analyses presented by Panichi (1922), Arevalo et al. (1962), and Gianetti (1964, 1965) have not been used in this study for two reasons:

(1) Different analytical methods were used by these authors

(2) No trace element data or modal analyses accompanied the major element data in these publications.

The distribution of analysed samples between the different lava types is as follows:

High K Series	(1) Leucitites	4
	(2) Tephritic leucitites	40
	(3) Transitional tephritic leucitites/ leucite tephrites/phonolitic leucite tephrites	20
	(4) Phonolitic leucite tephrites	14
	(5) Tephritic leucite phonolites	8
	(6) Leucite phonolites	2
Low K Series	(1) Olivine basalts	10
	(2) Trachybasalts	5
	(3) Biotite augite latites	11
	(4) Trachytic grey ash flow	2

The location of the analysed samples is shown on Map 1 (back pocket of this thesis) and a modal analysis together with brief petrographic notes for each sample is presented in Appendix B. Specimens were selected on the basis of petrography and freshness to show, as far as possible, the complete chemical variation of the Roccamonfina lavas. A number of specimens were analysed from the same lava flow to see if there were any significant intraflow variations. Three samples from the Sipicciano-Fortinella basalt flow (R.56,57,86), three from a tephritic leucitite flow near Marzano Appio (R.137,138,139), two from a latite flow (R.95,96), and two from a tephritic leucitite/leucite tephrite flow near the river Garigliano (R.81,82) were analysed. No significant variations were noted. It was impossible to study a leucite-phyric flow in great detail due to the lack of continuous exposure, but a detailed study by Locardi (personal communication) of the 1944 Vesuvius flow shows that this leucite-phyric flow is virtually homogeneous.

The main chemical differences between the High K and the Low K lava series are as follows:

(1) High K series $K_2O = 5{\cdot}5 - 11{\cdot}8\%$

Low K series $K_2O = 1{\cdot}2 - 5{\cdot}5\%$ (Grey ash flow = $7{\cdot}6\%$)

(2) Lavas of the High K series are enriched in P_2O_5, Ba, Zr, Sr, Rb, Th, and Ce relative to the Low K series.

4:2 Frequency Distribution of Major and Trace Element Data

Histograms presented in Fig. 4-1 show the distribution of the major and trace element data. The analytical data was processed using the ASCOP statistical program (E.R.C.C.). Boundaries used in histogram representation of the distribution are determined by the ASCOP system from the standard deviation and the mean for each variable. The following points emerge from a study of the histograms:

(1) K_2O, Ba, Sr, Rb, Zr, Th, P_2O_5, and the K_2O/Na_2O ratio are significantly higher in the High K series.

(2) The other oxides and trace elements have similar distributions in both series, though there is a greater predominance of samples with high CaO, MgO, and Fe_2O_3T in the Low K series.

Minimum, mean and maximum values for each chemical variable and certain ratios are presented in Table 4-1. Not much significance can be attached to mean values when dealing with such a wide variation unless the distribution is approximately normal.

4:3 C.I.P.W. Norms

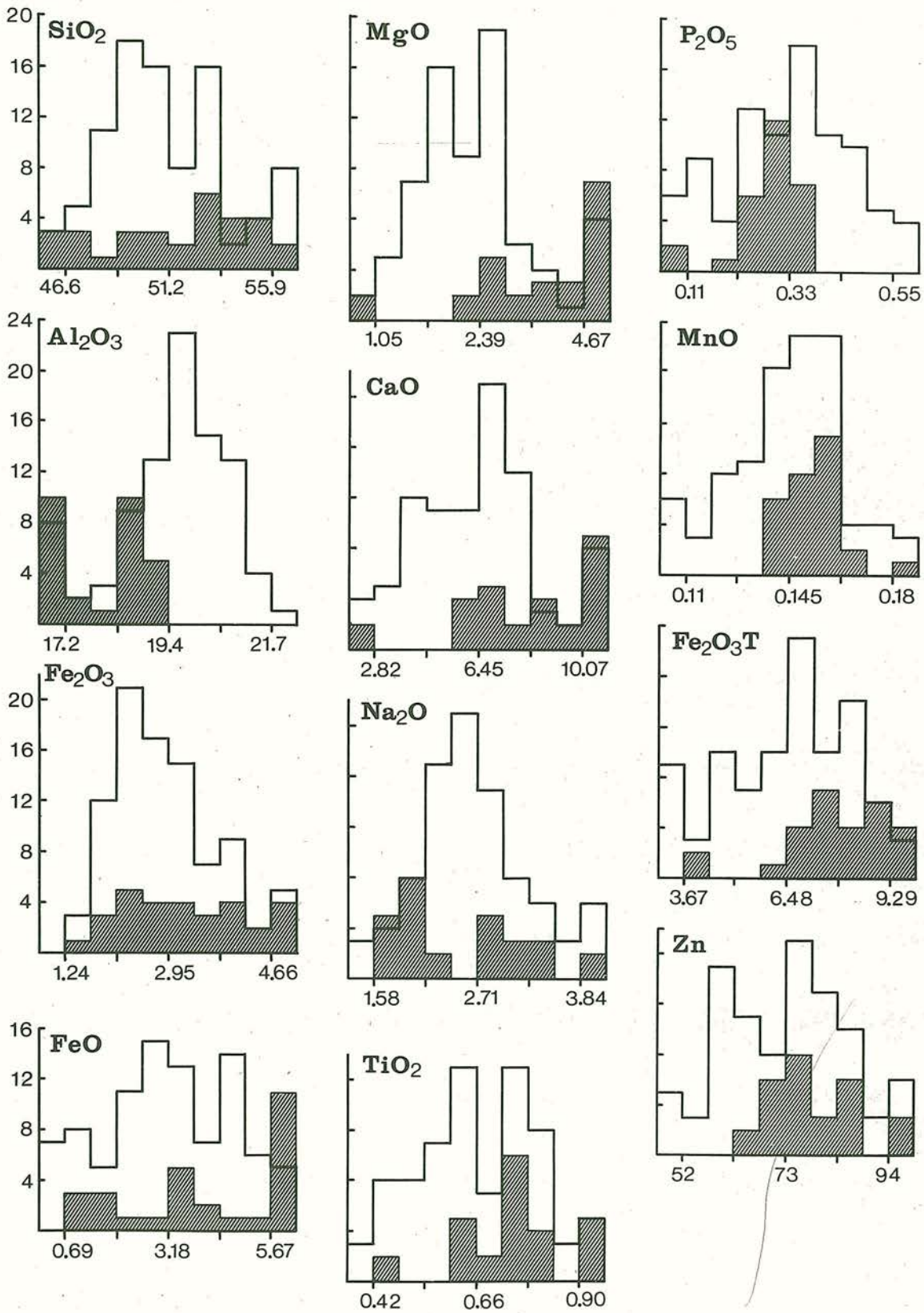
C.I.P.W. norms for the analysed samples are presented in Appendix C and summarised in Table 4:2.

The lavas of the High K series are all undersaturated with ne + lc in the norm. Differentiation Index (Thornton and Tuttle, 1960) varies from 38·9 to 85·6. From a comparison of the petrographic and normative data for the Roccamonfina lavas and

Fig. 4-1 (2 pages)

Histograms of major and trace element distributions in the Roccamonfina High K (unshaded) and Low K (shaded) lavas.

Vertical scale is frequency in units of 4.


SiO2
20
16
12
8
4
46.6
51.2
55.9
MgO
1.05
2.39
4.67
P2O5
0.11
0.33
0.55
Al2O3
24
20
16
12
8
4
17.2
19.4
21.7
CaO
2.82
6.45
10.07
MnO
0.11
0.145
0.18
Fe2O3
20
16
12
8
4
1.24
2.95
4.66
Na2O
1.58
2.71
3.84
Fe2O3T
3.67
6.48
9.29
FeO
16
12
8
4
0.69
3.18
5.67
TiO2
0.42
0.66
0.90
Zn
52
73
94

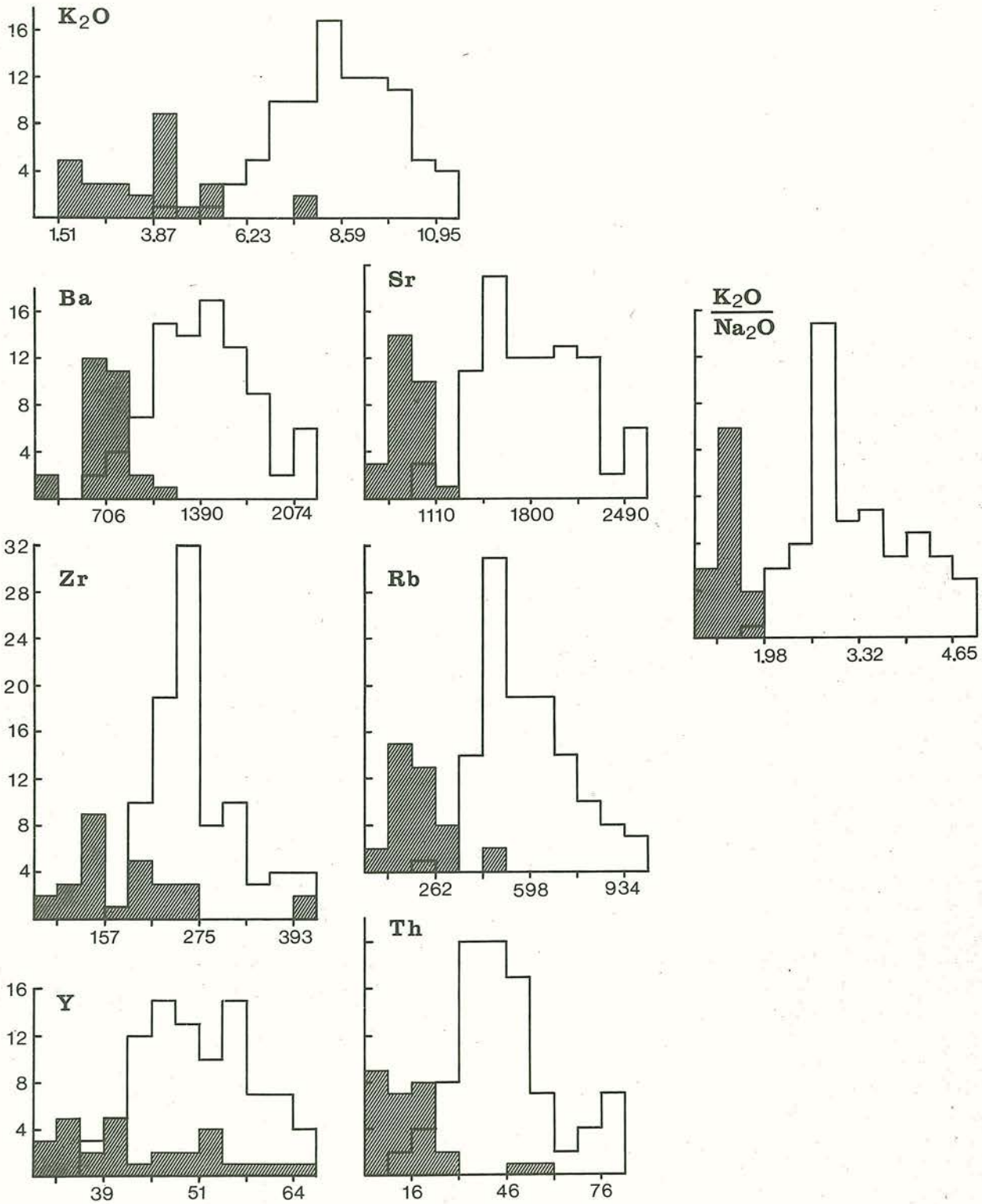

K2O
16
12
8
4
1.51
3.87
6.23
8.59
10.95
Ba
16
12
8
4
706
1390
2074
Sr
1110
1800
2490
K2O / Na2O
1.98
3.32
4.65
Zr
32
28
24
20
16
12
8
4
157
275
393
Rb
262
598
934
Y
16
12
8
4
39
51
64
Th
16
46
76

Table 4-1

Summary of Chemical Analyses

		High K Series			Low K Series		
Wt %		min.	mean	max.	min.	mean	max.
SiO_2		45·84	51·37	59·12	46·78	52·48	60·30
Al_2O_3		14·66	19·49	22·00	14·30	17·71	19·26
Fe_2O_3		1·47	2·94	8·11	1·47	3·26	5·96
FeO		0·09	3·16	6·00	0·94	4·11	6·31
Fe_2O_3T		2·21	6·45	9·92	3·77	7·82	10·44
MgO		1·60	2·31	6·79	0·62	4·68	9·02
CaO		1·86	6·37	12·41	2·19	8·50	13·37
Na_2O		1·26	2·73	5·69	1·47	2·55	4·46
K_2O		5·40	8·65	11·80	1·23	3·92	7·62
H_2O		0·35	0·95	2·37	0·24	1·04	2·69
TiO_2		0·23	0·65	1·02	0·46	0·76	1·04
P_2O_5		0·04	0·32	0·69	0·09	0·28	0·38
MnO		0·10	0·15	0·21	0·14	0·15	0·19
ppm	Ba	240	1398	2301	244	719	1130
	Zr	187	276	622	83	196	531
	Y	30	52	82	27	42	77
	Sr	156	1809	2595	187	858	1172
	Rb	329	598	1836	46	207	472
	Th	14	46	111	1	15	55
	Zn	45	74	109	65	80	122
Wt.							
$Fe_2O_3/FeO + Fe_2O_3$		0·22	0·51	0·97	0·19	0·47	0·83
$FeO + Fe_2O_3/FeO + Fe_2O_3 + MgO$		0·56	0·75	0·93	0·48	0·64	0·86
K_2O/Na_2O		1·59	3·32	5·48	0·54	1·50	1·81
K/Rb		44	127	246	42	164	244
K/Ba		30	105	3129	11	54	259
Ca/Sr		7	27	94	42	73	116
Rb/Sr		0·15	0·43	5·20	0·05	0·34	2·52

Table 4-2

Summary of C.I.P.W. Norms

	High K Series			Low K Series		
	min.	mean	max.	min.	mean	max.
Q	-	-	-	0·00	0·90	4·31
or	0·00	40·44	62·36	7·39	23·50	45·98
ab	0·00	3·92	29·99	13·57	21·79	38·19
an	5·17	15·59	24·57	8·84	25·72	34·33
lc	0·00	9·04	41·55	-	-	-
ne	0·80	10·63	17·98	0·00	0·19	1·32
di	0·00	11·67	34·12	0·32	12·28	28·97
hy	-	-	-	0·00	5·60	17·30
ol	0·00	2·27	8·08	0·00	3·44	11·71
mt	0·22	3·69	6·32	2·11	3·99	6·05
hm	0·00	0·44	8·13	0·00	0·55	4·14
il	0·45	1·78	1·98	0·89	1·47	2·01
ap	0·10	0·78	1·66	0·22	0·69	0·91
D.I.	38·9	64·1	85·6	21·7	52·2	83·7

also for the Somma-Vesuvius lavas (Savelli, 1967), it seems that the boundary between the tephritic leucitites/leucite tephrites and the phonolitic leucite tephrites is approximately delineated by the presence or absence of normative lc, the more undersaturated tephritic leucitites containing up to 41·5 lc (R.23). Normative criteria were used to confirm the classification of one fine-grained, pumiceous, phonolitic leucite tephrite (R.141).

The lavas of the Low K series vary from marginally undersaturated (0·23 ne) to oversaturated (4·31 Q). The olivine basalts plot very close to the olivine gabbro divide in the normative basalt system Qz-An-Di-Fo-Ne (Yoder and Tilley, 1962). The trachybasalts are Q normative, whilst both hy and Q normative latites are found. The highly oxidised nature of the latite specimens from Mte. S. Croce and Mte. Lattani (R.191,192,193,195) is apparent from the presence of normative hm and Q. Unoxidised specimens from a latite lava flow (R.95,96) are hy normative. Differentiation Index (Thornton and Tuttle, 1960) varies from 21·7 to 83·7.

4:4 Chemical Variation

4:4:1. Correlation Coefficients

Correlation coefficients have been computed for all possible pairs of the chemical variables (i.e. major element oxides, trace elements, and various ratios). This data is presented in Tables D-1 and D-2, Appendix D. Reference to statistical tables (Fisher and Yates, 1957) shows that values of $r > 0{\cdot}34$ for the

High K series (89 analyses) and values of $\underline{r} > 0{\cdot}59$ for the Low K series (28 analyses) are significant at the 99·9% level ($P = 0{\cdot}001$).

One of the problems associated with the interpretation of correlation coefficients between percentage variables is the constant sum factor (Chayes, 1962, 1964, 1967). An analysis of variance (Table 4-3) shows that six elements (SiO_2, Al_2O_3, Fe_2O_3, MgO, CaO, K_2O) make up 97% of the total variance in both series. Because of the constant sum factor, no great significance should be attached to negative coefficients between variables making a significant contribution to the total variance of the array. Negative values of $\underline{r}$ between the major variables and minor variables (Na_2O, TiO_2, P_2O_5, MnO, trace elements), and positive values of $\underline{r}$ between all variables are not affected by the constant sum factor.

Correlation matrices containing values of $\underline{r}$ significant at the 99·9% level are presented in Tables 4-4, 4-5. The following points should be noted:

(1) High +ve $\underline{r}$ between CaO, MgO, Fe_2O_3T, and TiO_2 in both series.

(2) High to moderate +ve $\underline{r}$ between SiO_2, Al_2O_3, Na_2O, K_2O, Zr, Y, Rb, and Th in the Low K series.

(3) High to moderate +ve $\underline{r}$ between SiO_2, Al_2O_3, Na_2O, K_2O, Zr, and Th in the High K series.

(4) High +ve $\underline{r}$ between Ba and Sr, and between Zr and Th.

(5) Variable $\underline{r}$ between <u>K and associated elements</u> in both series.

Table 4-3

Analysis of Variance

	High K Series		Low K Series	
	Variance (σ^2)	% of Total Variance	Variance (σ^2)	% of Total Variance
SiO_2	8·25	36·6	11·20	33·0
Al_2O_3	1·90	8·4	2·00	5·9
Fe_2O_3T	3·14	13·9	2·51	7·4
MgO	1·83	8·1	5·91	17·4
CaO	4·90	22·8	8·48	25·0
Na_2O	0·50	2·2	0·63	1·8
K_2O	1·96	8·7	2·68	7·9
TiO_2	0·02	*	0·46	1·3
P_2O_5	0·02	*	0·02	*
MnO	0·00	*	0·00	*

* = insignificant

Table 4-5

Correlation Matrix - Low K Series

SiO_2	1·00															
Al_2O_3	0·72	1·00														
Fe_2O_3T	-0·94	*	1·00													
MgO	-0·91	-0·81	+0·80	1·00												
CaO	-0·96	-0·81	+0·92	+0·95	1·00											
Na_2O	+0·91	+0·70	-0·91	-0·90	-0·93	1·00										
K_2O	+0·95	+0·68	-0·96	-0·89	-0·95	+0·94	1·00									
TiO_2	-0·94	*	+0·95	+0·78	+0·88	-0·83	-0·90	1·00								
P_2O_5	-0·63	*	+0·66	*	*	*	*	+0·64	1·00							
MnO	*	*	*	*	*	*	*	*	*	1·00						
Ba	*	*	*	*	*	*	*	*	+0·74	*	1·00					
Zr	+0·89	*	-0·83	-0·80	-0·89	+0·93	+0·92	-0·84	-0·69	*	-0·63	1·00				
Y	+0·79	*	-0·83	-0·73	-0·79	-0·83	-0·86	-0·79	*	*	*	+0·78	1·00			
Sr	*	*	*	*	*	*	*	*	+0·74	*	+0·70	-0·65	*	1·00		
Rb	+0·82	*	-0·86	-0·73	-0·82	+0·86	+0·83	-0·80	*	*	*	+0·89	+0·73	*	1·00	
Th	+0·84	*	-0·91	-0·73	-0·84	+0·86	+0·88	-0·79	-0·66	*	-0·65	+0·93	+0·69	-0·65	+0·88	1·00
Zn	*	*	*	*	*	*	*	*	-0·73	*	-0·77	+0·69	*	-0·71	*	+0·67	1·00

	SiO_2	Al_2O_3	Fe_2O_3T	MgO	CaO	Na_2O	K_2O	TiO_2	P_2O_5	MnO	Ba	Zr	Y	Sr	Rb	Th	Zn

* = $\underline{r}$ not significant at 99·9% level.

Table 4-4

Correlation Matrix - High K Series

	SiO_2	Al_2O_3	Fe_2O_3T	MgO	CaO	Na_2O	K_2O	TiO_2	P_2O_5	MnO	Ba	Zr	Y	Sr	Rb	Th	Zn
SiO_2	1·00																
Al_2O_3	+0·61	1·00															
Fe_2O_3T	-0·93	-0·69	1·00														
MgO	-0·82	-0·91	+0·85	1·00													
CaO	-0·89	-0·87	+0·93	+0·96	1·00												
Na_2O	+0·72	+0·62	-0·65	-0·72	-0·73	1·00											
K_2O	+0·42	+0·71	-0·65	-0·70	-0·71	*	1·00										
TiO_2	-0·91	-0·76	+0·97	+0·90	+0·95	-0·66	-0·70	1·00									
P_2O_5	-0·90	-0·67	+0·94	+0·82	+0·89	-0·65	-0·52	+0·90	1·00								
MnO	*	*	+0·43	*	*	*	*	+0·38	+0·36	1·00							
Ba	-0·41	*	*	*	*	*	*	*	*	+0·43	1·00						
Zr	+0·54	*	-0·50	-0·37	-0·42	+0·56	*	-0·49	-0·43	*	*	1·00					
Y	*	*	*	*	*	*	*	*	*	*	+0·47	1·00					
Sr	-0·40	*	*	*	*	*	*	*	*	+0·44	+0·87	*	*	1·00			
Rb	*	+0·36	-0·43	*	-0·39	*	+0·51	-0·48	*	-0·43	*	*	*	*	1·00		
Th	+0·54	*	-0·56	-0·46	-0·52	+0·61	*	-0·54	-0·47	*	*	+0·89	+0·36	*	*	1·00	
Zn	*	*	*	*	*	*	*	*	*	+0·55	*	*	*	*	*	*	1·00

* = $\underline{r}$ not significant at 99·9% level.

4:4:2 Variation Diagrams

Introduction

Chayes (1962,1964,1967) and Pearce (1968) have outlined some of the problems associated with conventional binary and ternary variation diagrams. As pointed out by Chayes (1967), the appraisal of strength of association (i.e. r) between two oxide variables by inspection of scatter diagrams must be approached with care. The comparison of various rock series by the use of simple oxide variation diagrams is also open to misinterpretation because all the other variables are not considered. As Pearce states (1968, p. 156), "Weight per-cent comparisons such as Harker and other ternary diagrams distort genetic trends by changing their slopes". Although his method of molar ratio comparisons, where one of the components (the divisor) is a constant, is theoretically ideal for simple cases, the limiting conditions (p. 148) impose severe restrictions on its use. For example, a fractionation scheme involving a Biotite Gabbro (as postulated for the Roccamonfina High K series) which incorporates all the major element components, would render the method useless. Pearce's statement (1968, p. 156) that Harker diagrams "cannot be readily used to discriminate between rival hypotheses" is not true. Fig. 4-2 adapted from Pearce's paper shows that provided mineral compositions are plotted on the Harker diagrams it is possible to draw on control lines associated with these minerals, and thereby adequately discriminate between rival hypotheses of crystal-liquid fractionation. Simple oxide variation diagrams incorporating

Fig. 4-2

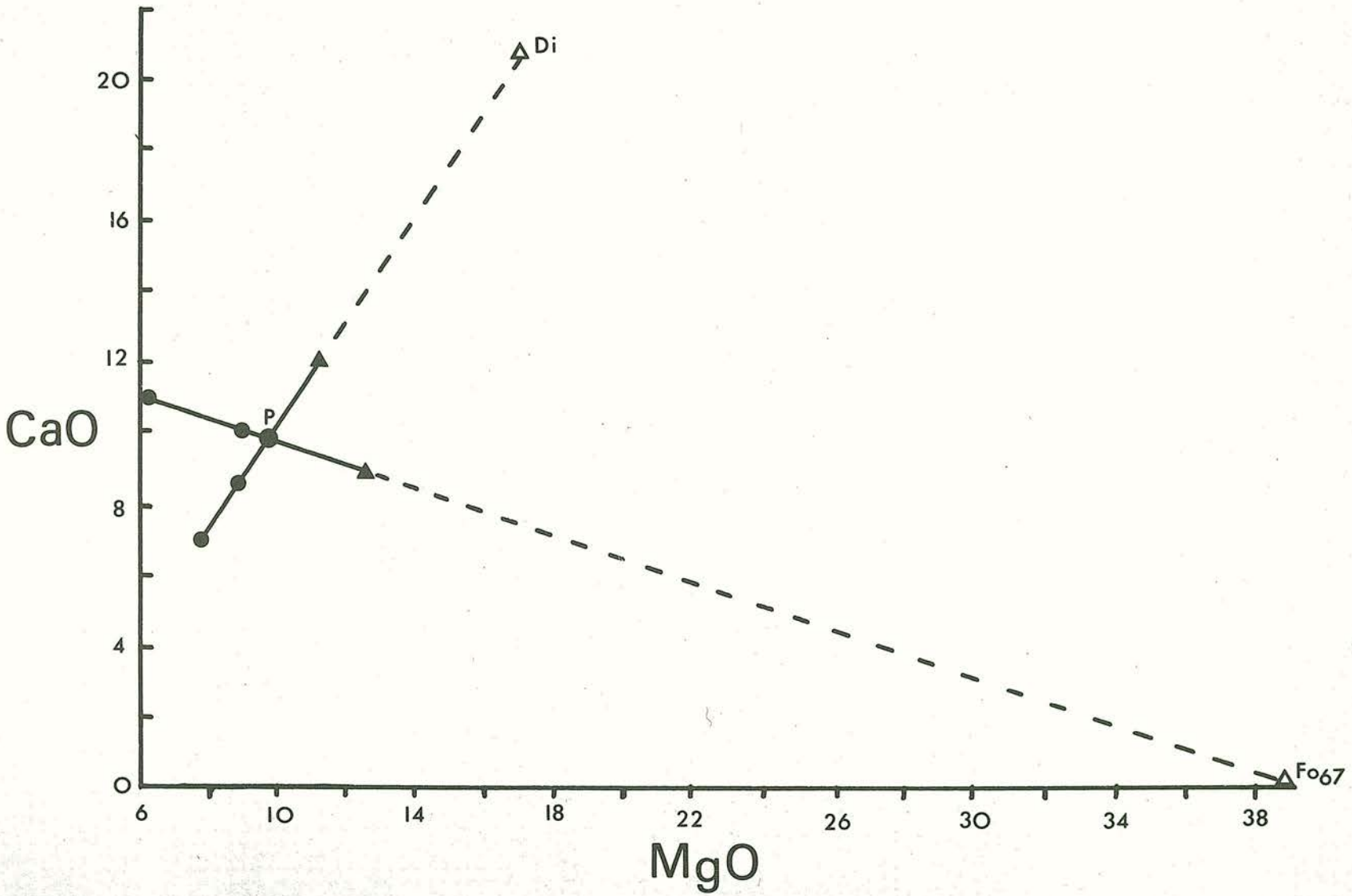
Figure adapted from Pearce (1968, Fig. 7a) to show that simple oxide variation diagrams can be used to differentiate between rival hypotheses of crystal-liquid fractionation.

Examples shown are Diopside (Di) and Olivine fractionation (Fo_{87})

P : parent magma

▲ : cumulate

● : differentiate


Di
P
Fo67
CaO
MgO
0
4
8
12
16
20
6
10
14
18
22
26
30
34
38

mineral control lines were first used by Powers (1955) for the Hawaiian lavas. Using oxide variation diagrams it is also possible to calculate the proportions of components in 2-phase and 3-phase extracts by simple graphical methods.

In this study, CaO is used as a simple index of variation for the following reasons:

(1) It has a large variance (σ^2CaO = 4·9/8·5 compared with $\sigma^2 SiO_2$ = 8·3/11·3 for the High K/Low K series respectively).

(2) It is preferred to SiO_2 because it illustrates the close correlation between CaO, MgO, TiO_2, and Fe_2O_3T.

(3) By using a simple index of variation such as CaO, it is possible to plot up mineral compositions and associated control lines.

(4) A simple variation index is preferred to the Differentiation Index (Thornton and Tuttle, 1960) or the Solidification Index (Kuno et al. 1957). By using a simple oxide index, the true relationship between chemical variables can be easily assessed. Use of D.I. or S.I. frequently complicates the issue.

The present author considers that in studying the variation within or between lava series, it is desirable to use simple oxide plots in the first instance and then it may be interesting to use more complex methods (such as C.M.A.S. projection, or P.C.A.) to show that theories proposed on the basis of the simple oxide plots are still relevant when all the variables are considered

together. However, it should be noted that if a crystal-liquid fractionation scheme can be shown to explain the observed variation on the basis of plots of all the chemical variables against one of the variables which shows a large variance, then it will also be valid for all possible combinations of the chemical variables.

Roccamonfina Variation Diagrams

Fig. 4-3 shows the major elements plotted against CaO, and Fig. 4-4 the trace element v. CaO plots; CaO being used as a simple index of variation/differentiation. The following general points should be noted:

(1) Highly significant correlation between CaO and the other major elements (except K_2O in the High K series).

(2) Parallel variation trends in the High K and Low K series (except for P_2O_5 and Al_2O_3).

(3) The High K series has higher K_2O, Ba, Zr, Sr, Rb, Th, and Ce, and lower SiO_2, and MgO for a particular value of CaO than the Low K series.

(4) Although there is a highly significant correlation between CaO and the other major elements (except K_2O), the High K series shows considerable scatter in K_2O, Ba, Sr, Rb, Th, Zr, and Ce in the CaO variation diagrams. This scatter is, however, systematic. As will be shown in the next section, there is a concomitant rise in K_2O, Ba, Sr,Rb, Zr, Th (and Ce) for a particular value of CaO.

The plots of K_2O v. SiO_2 (Fig. 4-5) and K_2O v. CaO (Fig. 4-3) illustrate the wide variation in K_2O content shown by the Roccamonfina

Fig. 4-3

Variation diagrams of major elements v. CaO

● : Roccamonfina High K lavas

△ : Roccamonfina Low K lavas

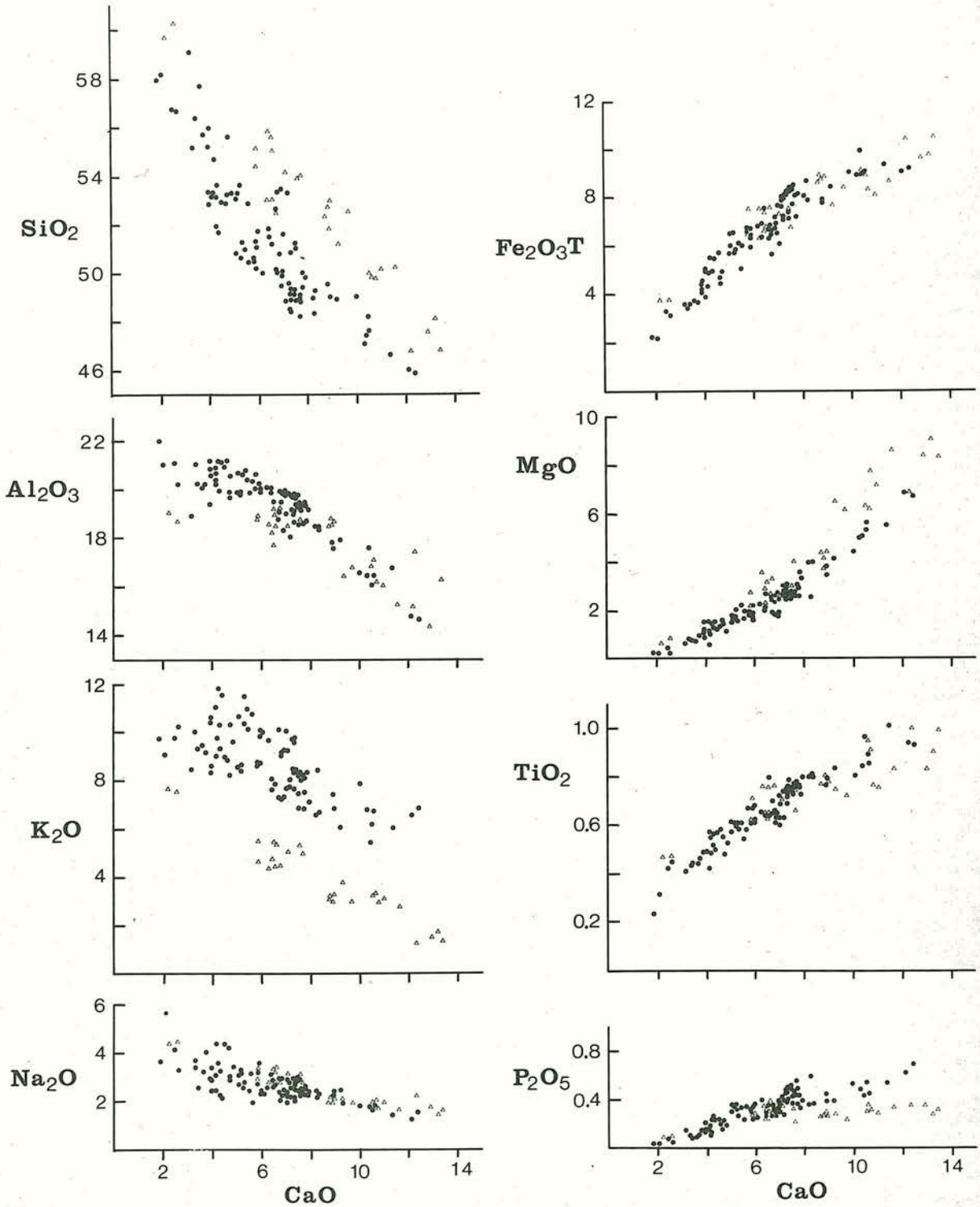

SiO2
58
54
50
46
Fe2O3T
12
8
4
Al2O3
22
18
14
MgO
10
6
2
K2O
12
8
4
TiO2
1.0
0.6
0.2
Na2O
6
4
2
P2O5
0.8
0.4
2
6
10
14
CaO
2
6
10
14
CaO

Fig. 4-4

Variation diagrams of trace elements v. CaO

● : Roccamonfina High K lavas

△ : Roccamonfina Low K lavas

□ : Biotite Gabbro (R.103)

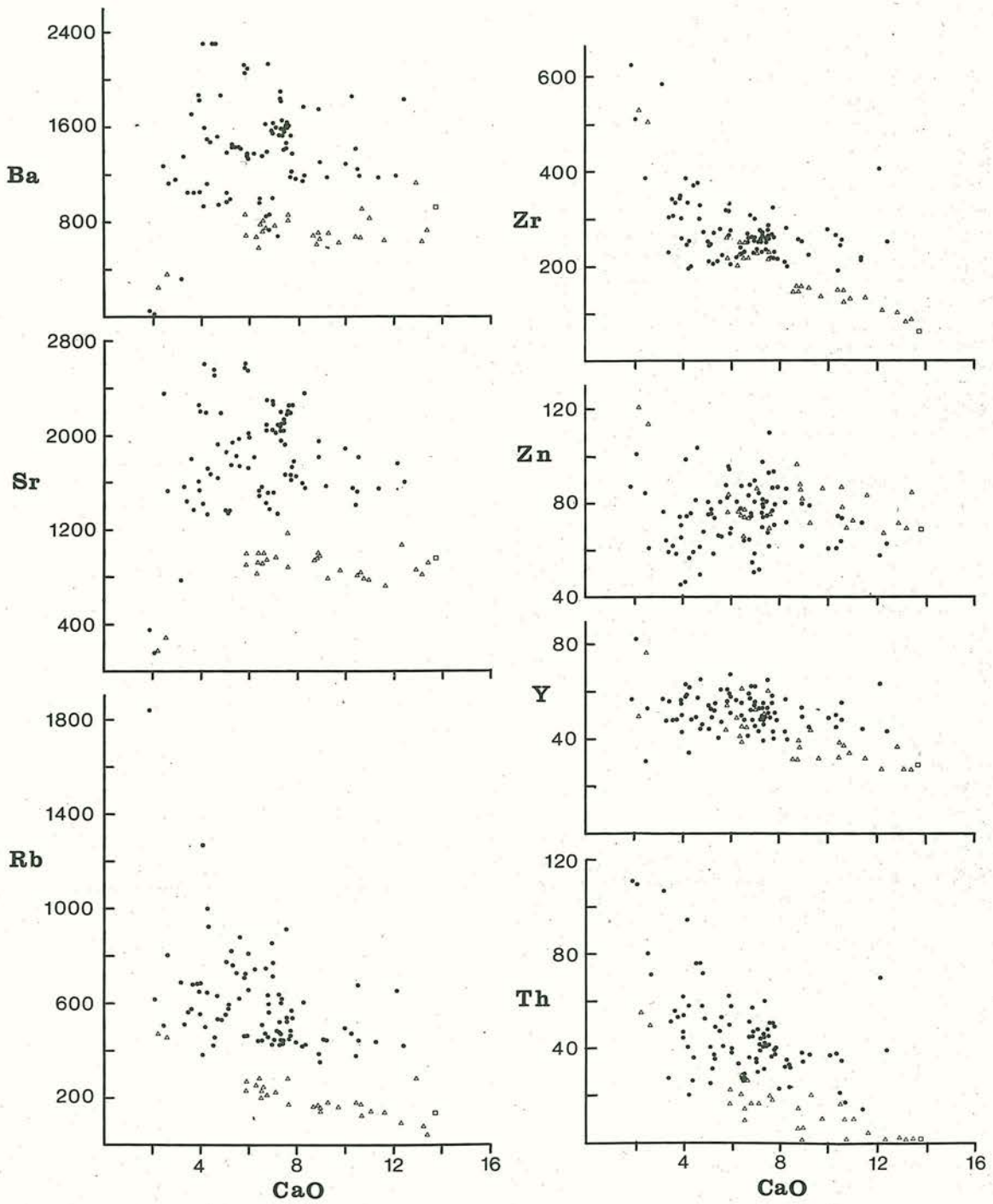

Ba
2400
1600
800
Sr
2800
2000
1200
400
Rb
1800
1400
1000
600
200
Zr
600
400
200
Zn
120
80
40
Y
80
40
Th
120
80
40
4
8
12
16
CaO
4
8
12
16
CaO

Fig. 4-4 (Contd.)

Variation diagram of Ce v. CaO for some of the Roccamonfina High K (●) and Low K (□) lavas.

Analytical data presented in Appendix C, Table C-8.

■ : Biotite Gabbro (R.103)

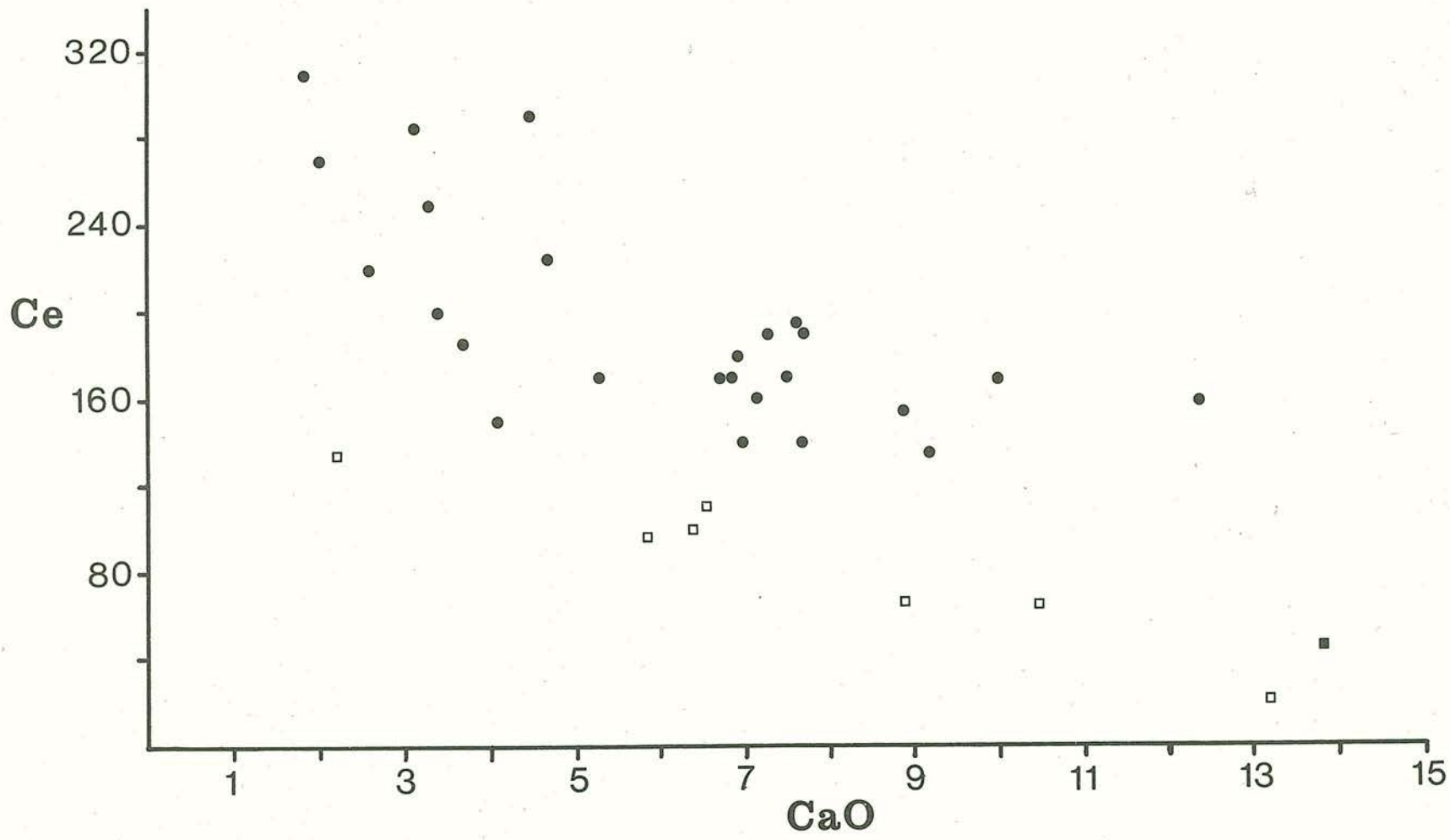

320
240
160
80
Ce
1
3
5
7
9
11
13
15
CaO

Fig. 4-5

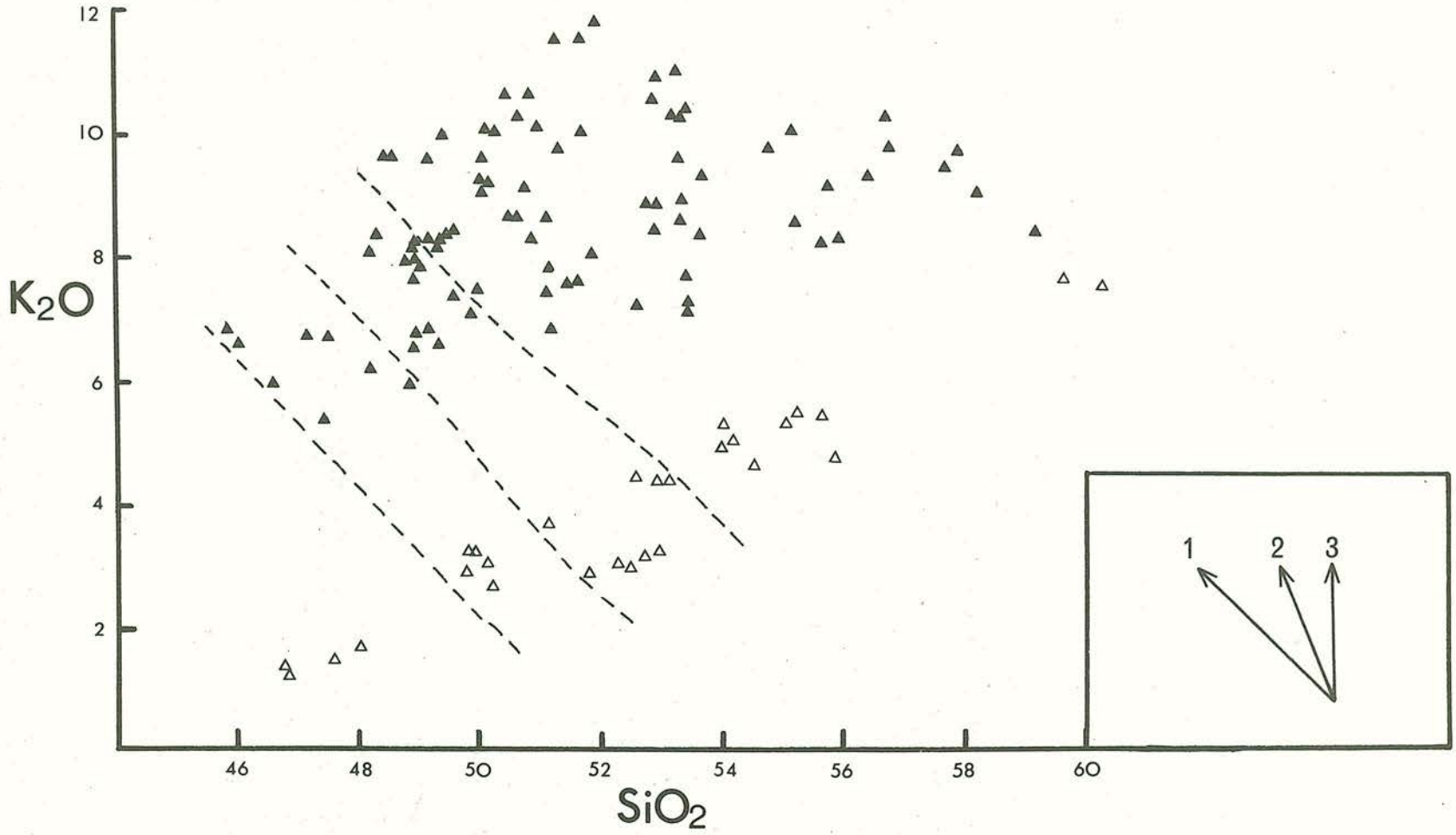
K_2O v. SiO_2 variation diagram.

▲ : Roccamonfina High K lavas

△ : Roccamonfina Low K lavas

Lavas used in the Roccamonfina Control Groups plot between the dashed lines - Group 1 on the left and Group 2 on the right.

Inset shows possible variation in the orientation of the control groups in the K_2O v. SiO_2 plot (see text).


12
10
8
6
4
2
K2O
46
48
50
52
54
56
58
60
SiO2
1
2
3

lavas. Assuming that the most basic lavas (i.e. those with the highest CaO, MgO, Fe_2O_3T) are parental to the more salic derivatives, the geochemical changes associated with rising K_2O in the most basic lavas can be illustrated as follows. Two groups of lavas have been selected to illustrate the geochemical changes with rising K_2O in (1) the "primitive" (Group 1) lavas and (2) the slightly differentiated (Group 2) lavas. The terms "primary" and "primitive" are used in this thesis in the same sense as recommended by Jamieson and Clark (1970). A primary magma is the initial magma formed at depth on partial melting, whilst the primitive lavas are the most basic lavas erupted at the surface (their compositions being closest to that of the primary magma). The two groups of lavas were selected on the basis that they represent near-liquid compositions (i.e. they do not appear to contain cumulative phenocrysts and many of the specimens are aphyric) and they have similar CaO contents. CaO is used as an index of variation/differentiation in this study, so it forms a convenient "base-level" on which to make comparisons.

The analyses used in each of the control groups are:

Group 1. R.56, 57, 86, 157, 158, 112, 131, 142, 146, 148, 151, 153, 154.

Group 2. R.90, 186, 187, 188, 189, 192, 193, 4, 6, 59, 60, 68, 81, 82, 83, 166, 180, 181, 182.

Figs. 4-6 and 4-7 show the major and trace elements plotted against K_2O for the two control groups and the correlation coefficients between K_2O and the other elements are presented in Table 4-6. The

Fig. 4-6

Roccamonfina Control Group 1 - major and trace elements plotted against K_2O.

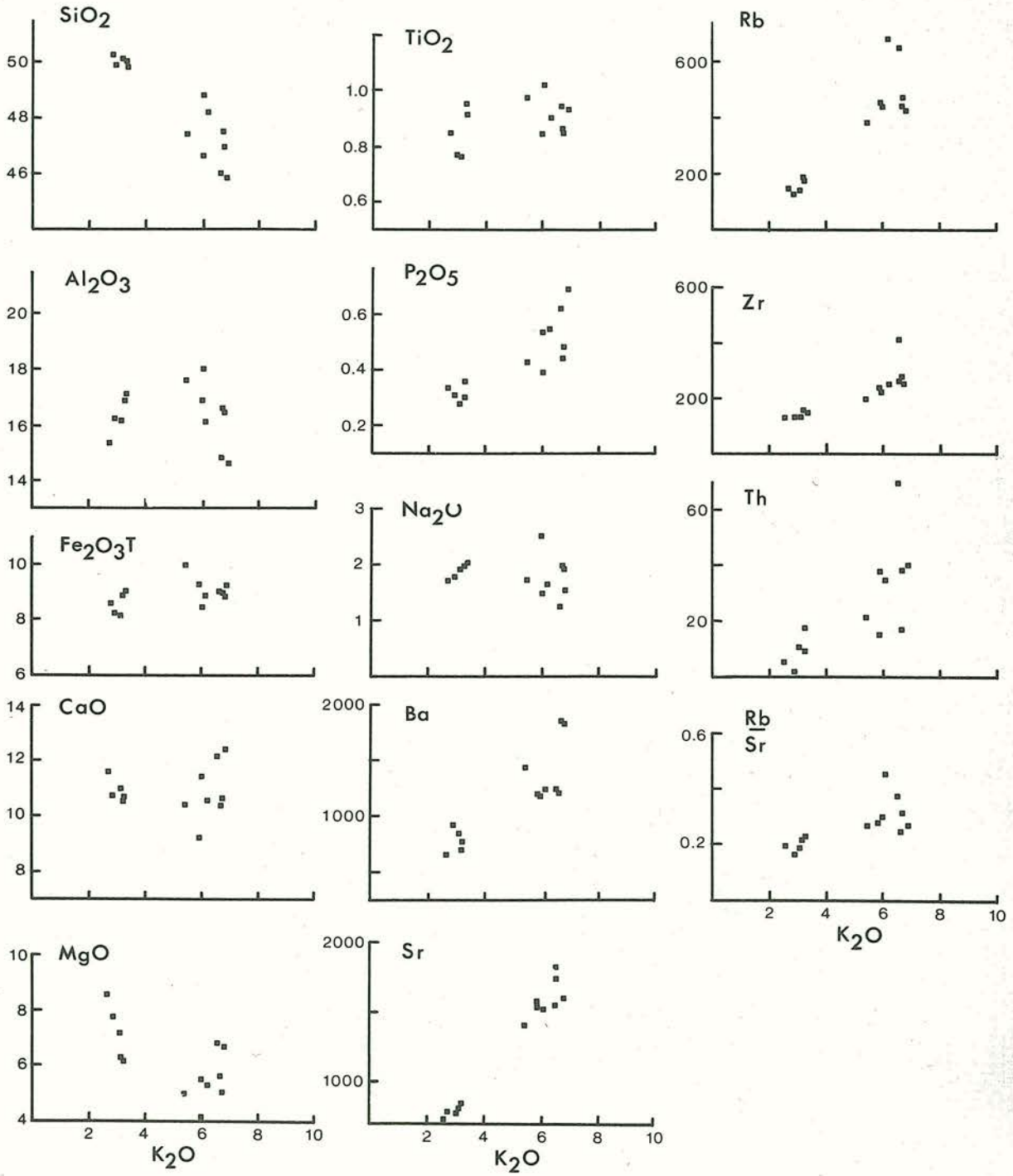

SiO2
50
48
46
TiO2
1.0
0.8
0.6
Rb
600
200
Al2O3
20
18
16
14
P2O5
0.6
0.4
0.2
600
Zr
200
Fe2O3T
10
8
6
Na2O
3
2
1
Th
60
20
CaO
14
12
10
8
2000
Ba
1000
Rb
Sr
0.6
0.2
MgO
10
8
6
4
2000
Sr
1000
2
4
6
8
10
K2O
2
4
6
8
10
K2O

Fig. 4-7

Roccamonfina Control Group 2 - major and trace elements plotted against K_2O.

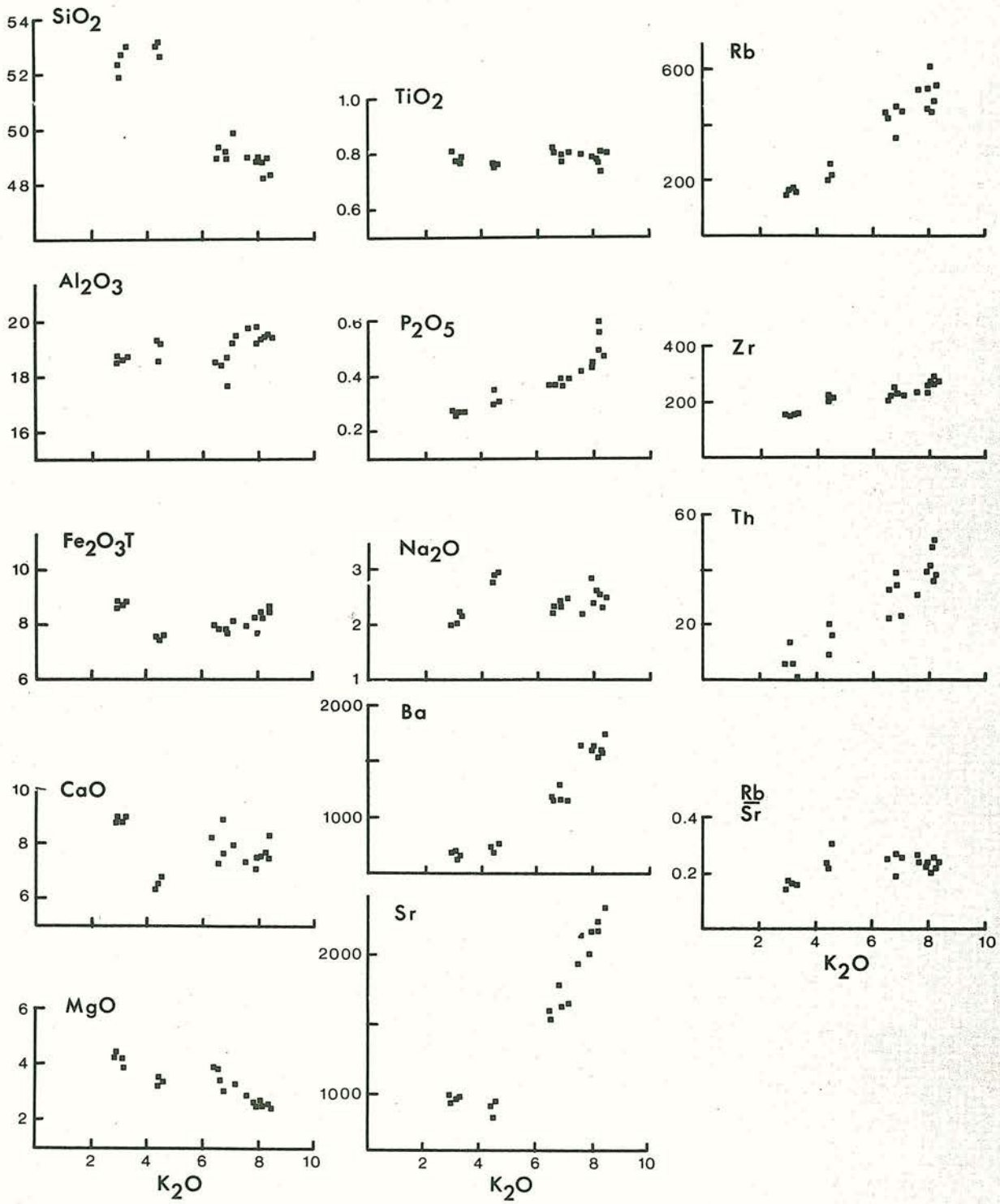

SiO2
54
52
50
48
TiO2
1.0
0.8
0.6
Rb
600
200
Al2O3
20
18
16
P2O5
0.6
0.4
0.2
Zr
400
200
Fe2O3T
10
8
6
Na2O
3
2
1
Th
60
20
Ba
2000
1000
CaO
10
8
6
Rb/Sr
0.4
0.2
Sr
2000
1000
MgO
6
4
2
2
4
6
8
10
K2O
2
4
6
8
10
K2O

Table 4-6

Roccamonfina Control Groups - Correlation with K_2O

Element	Group 1	Group 2
SiO_2	-0·90*	-0·93*
Al_2O_3	-0·10	0·45
Fe_2O_3T	0·46	-0·15
MgO	-0·62	-0·84*
CaO	-0·06	-0·22
Na_2O	-0·22	0·26
TiO_2	0·41	0·14
P_2O_5	0·84*	0·89*
Mn	-0·12	0·30
Ba	0·83*	0·96*
Zr	0·84*	0·91*
Y	0·82*	0·80*
Sr	0·98*	0·96*
Rb	0·90*	0·97*
Th	0·74''	0·91*
Zn	-0·66	0·19
Rb/Sr	0·73''	0·25

* r significant at 99·9% level

'' r significant at 99·0% level

following points should be noted:

(1) As K_2O increases, CaO, Fe_2O_3T, Al_2O_3, Na_2O, TiO_2, and Zn remain roughly constant, SiO_2 and MgO decrease, and P_2O_5, Ba, Sr, Rb, Zr, Y, and Th increase.

(2) The rise in K_2O is compensated for largely by a decrease in SiO_2 and also by a small decrease in MgO. (n.b. this is purely a result of the orientation of the control groups in the K_2O v. SiO_2 plot - see below).

(3) Enrichment factors between the end members of the two groups are as follows:

Table 4-7

(Enrichment factor = max./min. value for each group)

Element	Group 1	Group 2
K_2O	2·5	2·9
P_2O_5	2·5	2·3
Ba	2·9	2·9
Sr	2·5	2·8
Rb	5·4	4·3
Zr	3·3	1·9
Th	6·9	5·0
Y	~2·0	~2·0
Ce	~2·5	~2·5

(4) The correlation data (Table 4-6) shows the highly significant +ve correlation between K_2O, P_2O_5, Ba, Sr, Rb, Zr, Th, and Y for both control groups.

It should be noted that a number of different control-lines (groups) in the K_2O v. SiO_2 plot could have been used to illustrate K and associated element enrichment (inset, Fig. 4-5) in the primitive lavas. These are (1) increase in K_2O largely compensated for by decrease in SiO_2, CaO and other major elements relatively stable, or (2) increase in K_2O with proportional decrease in all the other major elements, or (3) stable SiO_2 with increase in K_2O compensated for by decrease in the other major elements. Reference to the K_2O v. SiO_2 plot for the Roman Region (Fig. 4-8) shows that a decrease in SiO_2 probably compensates for the greater part of the K_2O increase in the promitive lavas.

It has been shown that the variation in K and associated elements in the primitive lavas and the first differentiates of the Roccamonfina volcano is systematic. The variation of K and associated elements in the lavas of some of the other volcanoes of the Roman Region is now discussed.

<u>K and associated elements enrichment, and analysis of the K_2O v. SiO_2 plot for the lavas of the Roman Region</u>

Fig. 4-8 shows the K_2O v. SiO_2 plot containing data for the lavas of the major volcanic centres of the Roman Region (Vulsini, Vico, Alban Hills, Roccamonfina, Somma-Vesuvius, and the Phlegrean Fields). In Fig. 4-9 it can be seen that within the Roman Region each volcano appears to have a characteristic level of enrichment in K_2O. Some of the volcanoes have two series of lavas showing markedly different levels of K_2O (e.g. Roccamonfina -

BIBL. UNIV. EDINBURGH

Fig. 4-8

K_2O v. SiO_2 variation diagram for the lavas of the major volcanic centres of the Roman Region.

Roman Region primitive lavas plot between the dashed lines.

Analyses taken from the following sources:

(a) Roccamonfina (Appendix C)

(b) Somma-Vesuvius and the Phlegrean Fields (Savelli, 1967; Rahman, 1968).

(c) Alban Hills (Appendix E; Fornaseri et al., 1963).

(d) Vico (Amendolagine et al., 1963a, 1963b).

(e) Vulsini (Appendix E; Schneider, 1965; Triglia, 1966, 1969; De Fino and Mattias, 1965; Mattias, 1965).

All analyses were used.

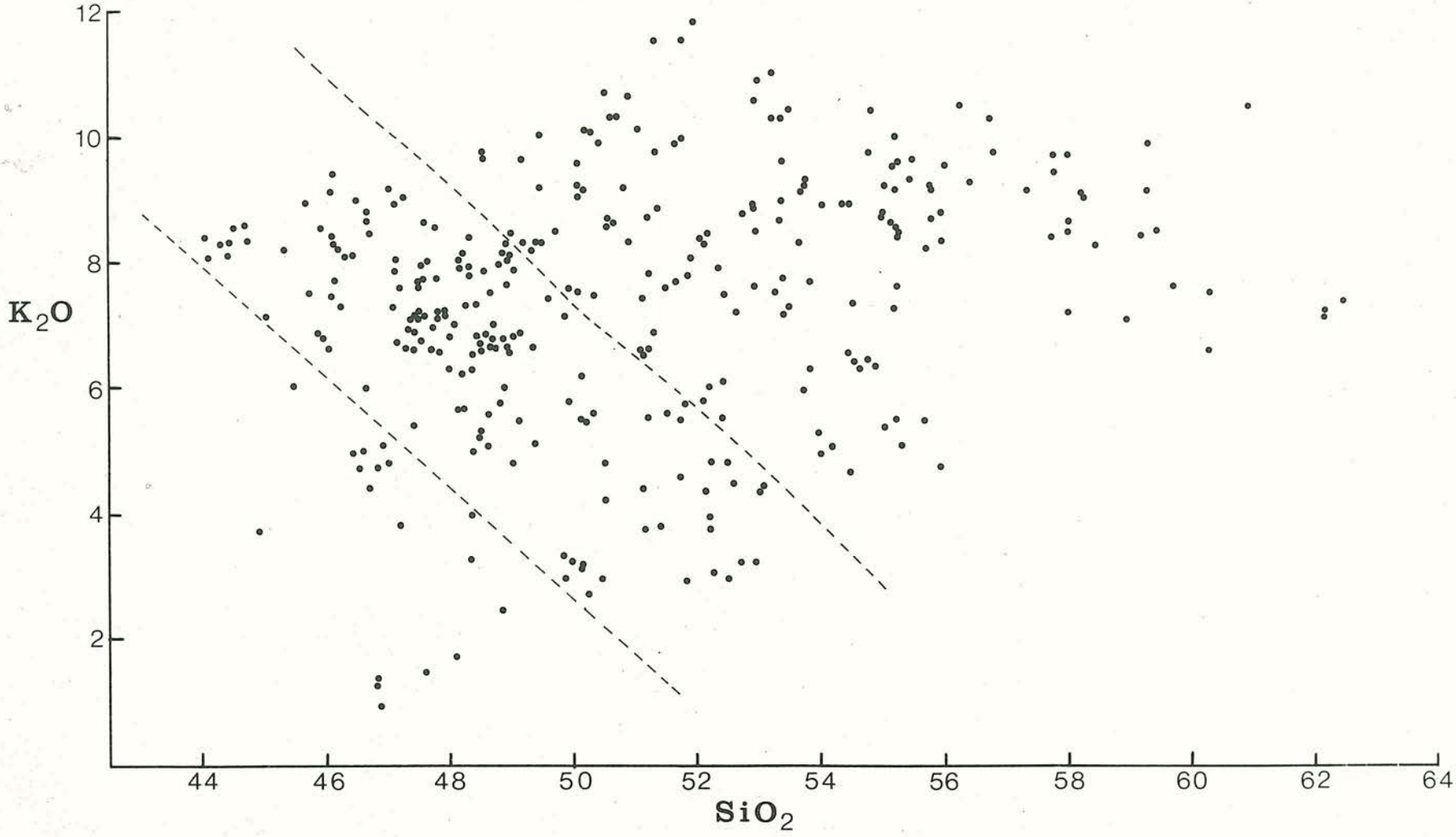

12
10
8
6
4
2
K_2O
44
46
48
50
52
54
56
58
60
62
64
SiO_2

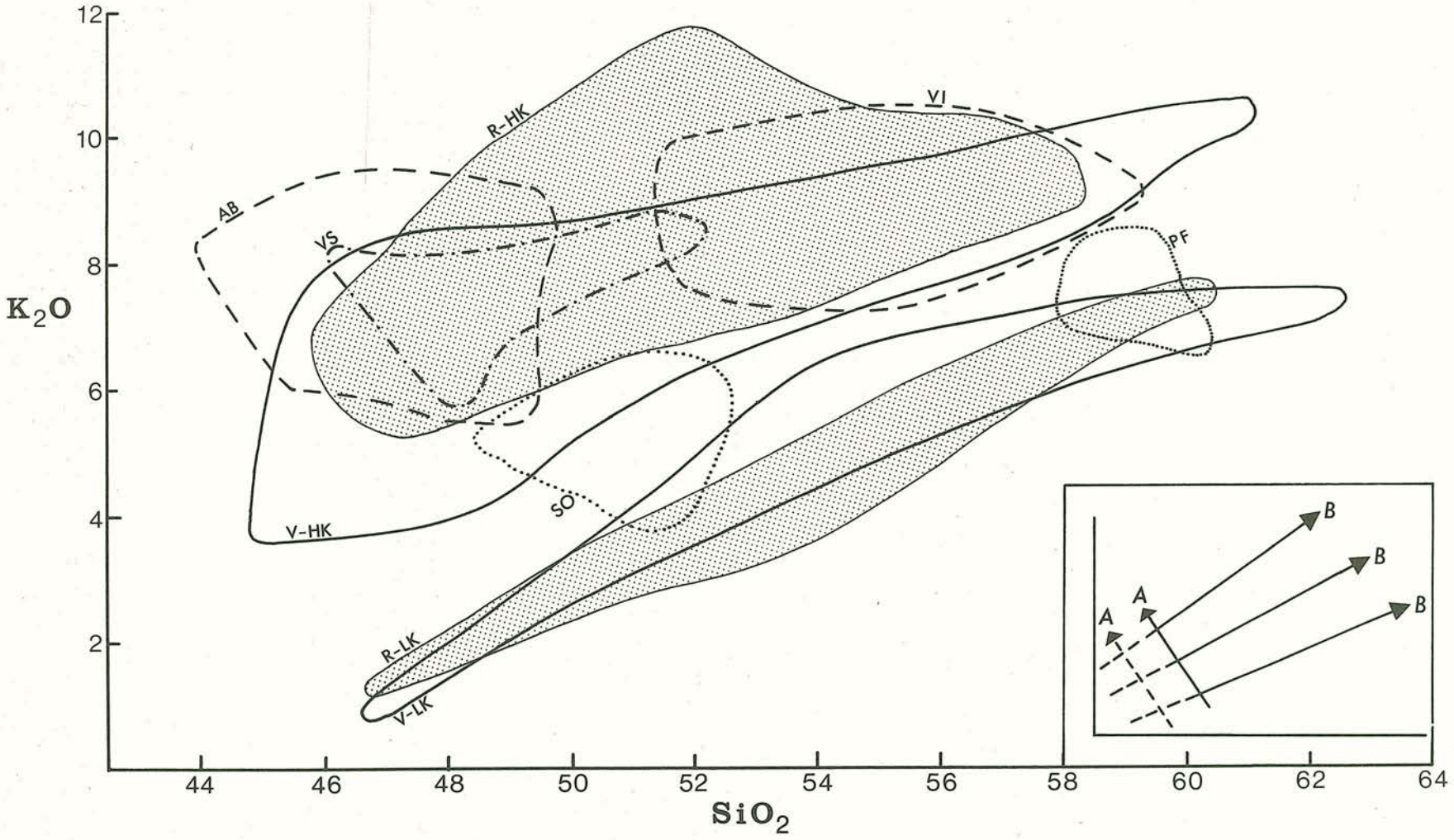
Fig. 4-9

Idealised K_2O v. SiO_2 plot for the major volcanic centres of the Roman Region.

R-LK : Roccamonfina Low K series
R-HK : Roccamonfina High K series
VS : Vesuvius
SO : Somma
PF : Phlegrean Fields
AB : Alban Hills
VI : Vico
V-LK : Vulsini Low K series
V-HK : Vulsini High K series

Source of data as for Fig. 4-8

Inset Idealised differentiation trends (see text for explanation).


12
10
8
6
4
2
K_2O
44
46
48
50
52
54
56
58
60
62
64
SiO_2
R-HK
VI
AB
VS
PF
SO
V-HK
R-LK
V-LK
A
A
B
B
B

this thesis; Vulsini - Schneider, 1965; Triglia, 1966,1969, this thesis; Somma-Vesuvius - Savelli, 1967). Both of the Roccamonfina lava series and both of the Vulsini series also show a marked differentiation towards salic derivatives, whilst the Alban Hills and Somma-Vesuvius do not.

The difference between the Somma and the Vesuvius lavas is not as marked as the difference between the two Roccamonfina lava series. According to the data of Savelli (1967), the increase in K_2O from the Somma phonolitic tephrites to the Vesuvius tephritic leucitites is accompanied by a slight enrichment in Sr and Ba (Savelli, 1967, Table 4).

Fig. 4-10 shows the K_2O v. SiO_2 plot for the Vulsini lavas. The specimens analysed by the present author are marked with a distinctive ornament. Although the difference between the High K and Low K lavas is not so marked as at Roccamonfina, they do form two distinct groups on the basis of age, petrography, and chemistry. In Fig. 4-11, SiO_2, P_2O_5, Ba, Zr, Sr, Rb, and Th are plotted against K_2O for all except two of the analyses presented in this thesis (LT.8 and LT.9 are omitted from the Latera-Vulsini control group; Latera is one of the main volcanoes within the Vulsini volcanic region) and the correlation coefficients between K_2O and the other chemical variables are presented in Table 4-8. As with the Roccamonfina control groups (Figs. 4-6, 4-7; Table 4-7), there is a concomitant rise in K_2O, P_2O_5, Ba, Zr, Y, Sr, Rb, and Th (if one aberrant point in the K_2O v. Th plot is disregarded). The orientation of the Latera-Vulsini control group

Fig. 4-10

K_2O v. SiO_2 variation diagram for the Vulsini lavas

● : Vulsini High K lavas

△ : Vulsini Low K lavas

■ : Latera-Vulsini Control Group lavas (all analyses in Table E-2 except LT8 and LT9).

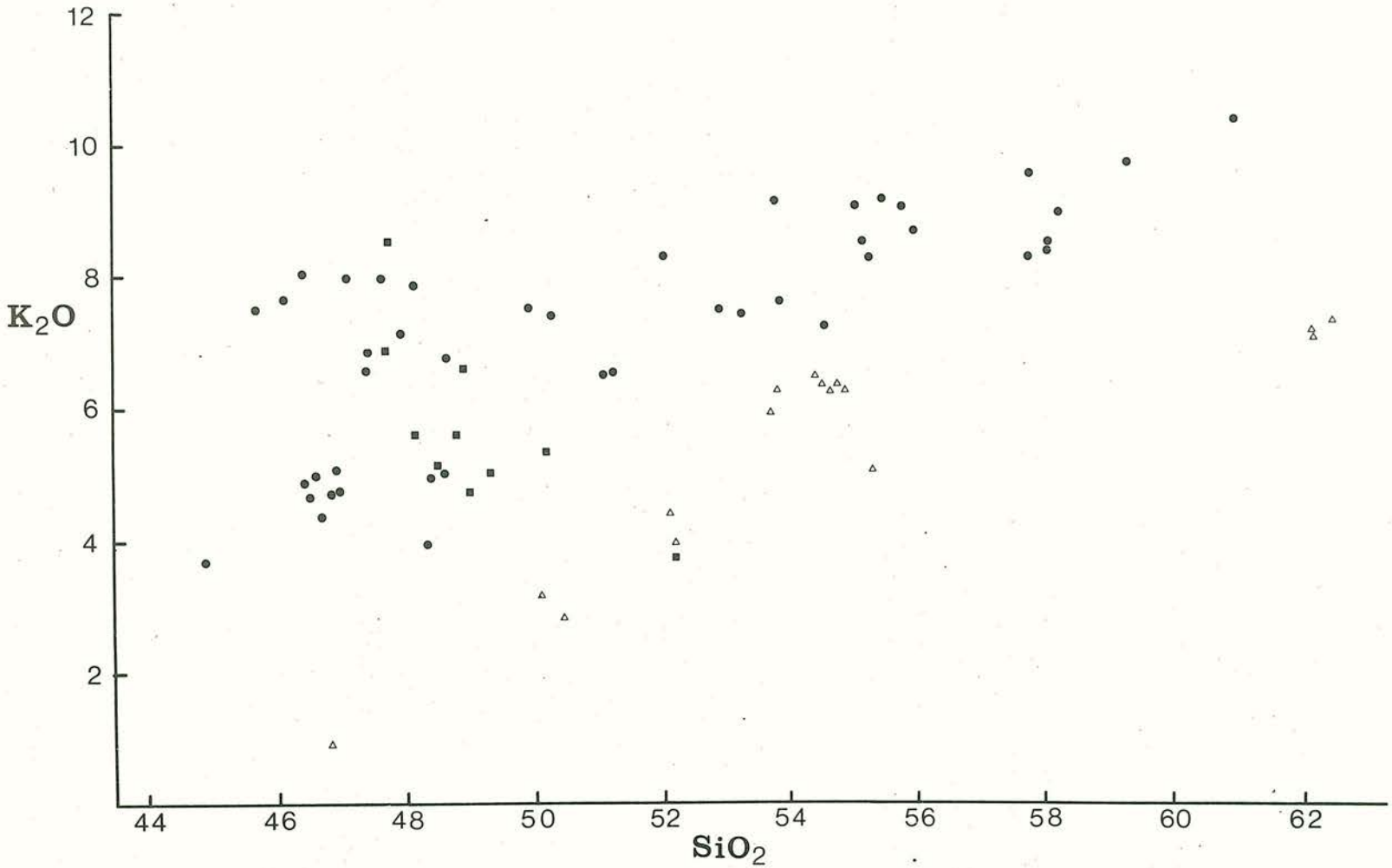

12
10
8
6
4
2
K_2O
44
46
48
50
52
54
56
58
60
62
SiO_2

Fig. 4-11

Latera-Vulsini Control Group - SiO_2, P_2O_5,
Ba, Zr, Sr, Rb, Th v. K_2O variation diagrams.

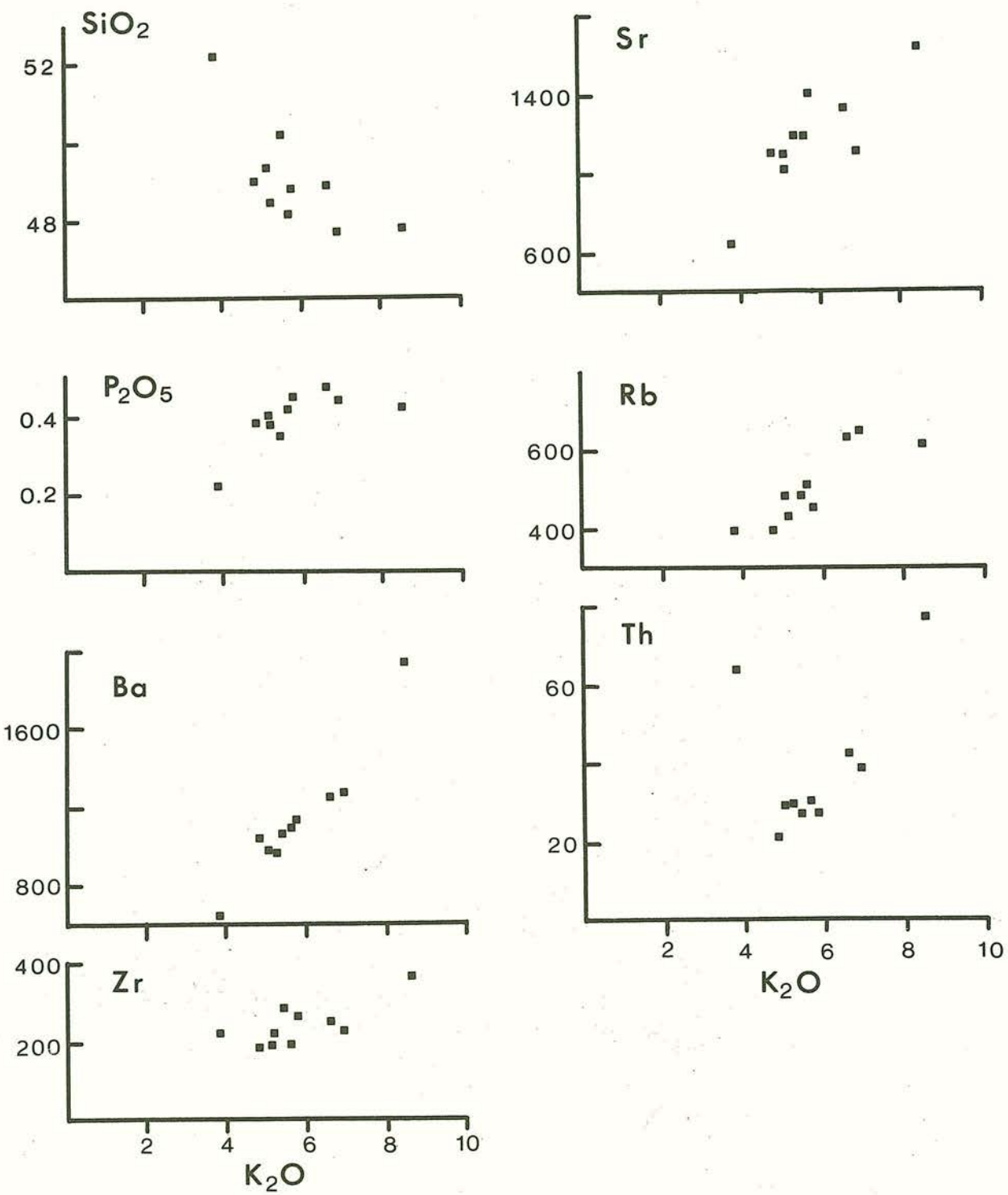

SiO2
52
48
Sr
1400
600
P2O5
0.4
0.2
Rb
600
400
Ba
1600
800
Th
60
20
Zr
400
200
2
4
6
8
10
K2O
2
4
6
8
10
K2O

Table 4-8

Latera-Vulsini Control Group - Correlation with K_2O

Element	r	Element	r
SiO_2	-0·73"	Ba	0·97*
Al_2O_3	·0·18	Zr	0·71"
Fe_2O_3	0·33	Y	0·71"
MgO	-0·51	Sr	0·84*
CaO	-0·12	Rb	0·85*
Na_2O	-0·21	Th	0·44
TiO_2	-0·05	Zn	0·62
P_2O_5	0·67"	Rb/Sr	-0·19

* r significant at 99% level
" r significant at 95% level

analyses in the K_2O v. SiO_2 plot (Fig. 4-10) is similar to that for the Roccamonfina control groups (Fig. 4-5).

The lavas of the Alban Hills show little variation towards salic derivatives. They are the most undersaturated lavas in the Roman Region (ne, lc, and often cs normative leucitites and tephritic leucitites) and they occupy the position of most extreme enrichment in K_2O in the K_2O v. SiO_2 plot for the Roman Region (Fig. 4-8). The limited trace element data available for the Alban Hills lavas (Table E-1, Appendix E) suggests that they show a similarly high enrichment in P_2O_5, Ba, Zr, Y, Sr, Rb, and Th.

It is quite clear that the primitive (i.e. most basic) lavas erupted at each of the above mentioned volcanic centres show the

same pattern of enrichment in K and associated elements. Reference to Fig. 4-8 shows that the lavas included in the Roccamonfina control groups, the Latera-Vulsini control group, and also those analyses of lavas from the Alban Hills which are presented in this thesis, all fall within a limited zone in the K_2O v. SiO_2 plot for the Roman Region. This zone includes the majority of the most basic lavas found in the Roman Region. By plotting these analyses for three different volcanic centres together it ought to be possible to check the apparent uniformity of compositional variation within the primitive lavas of the Roman Region. Fig. 4-12 shows Ba, Sr, Rb, Th, Zr, and P_2O_5 plotted against K_2O for these lavas. The highly significant correlation between K and these associated elements (Table 4-9) confirms that there is an essentially uniform relationship between K and associated elements within the primitive lavas of the Roman Region.

This is therefore the first component causing the observed distribution of data points in the K_2O v. SiO_2 plot for the Roman Region. It indicates that there is a differentiation process producing parental magmas with different levels of enrichment in K and associated elements. These parental magmas are almost certainly more basic than the most primitive lavas observed in the Roman Region, but the "serial character" (i.e. level of enrichment in K and associated elements) of the parental magmas is preserved in the basic lavas that are actually erupted. The process which provides the parental magma with its characteristic level of enrichment in K and associated elements is discussed in Chapter 6.

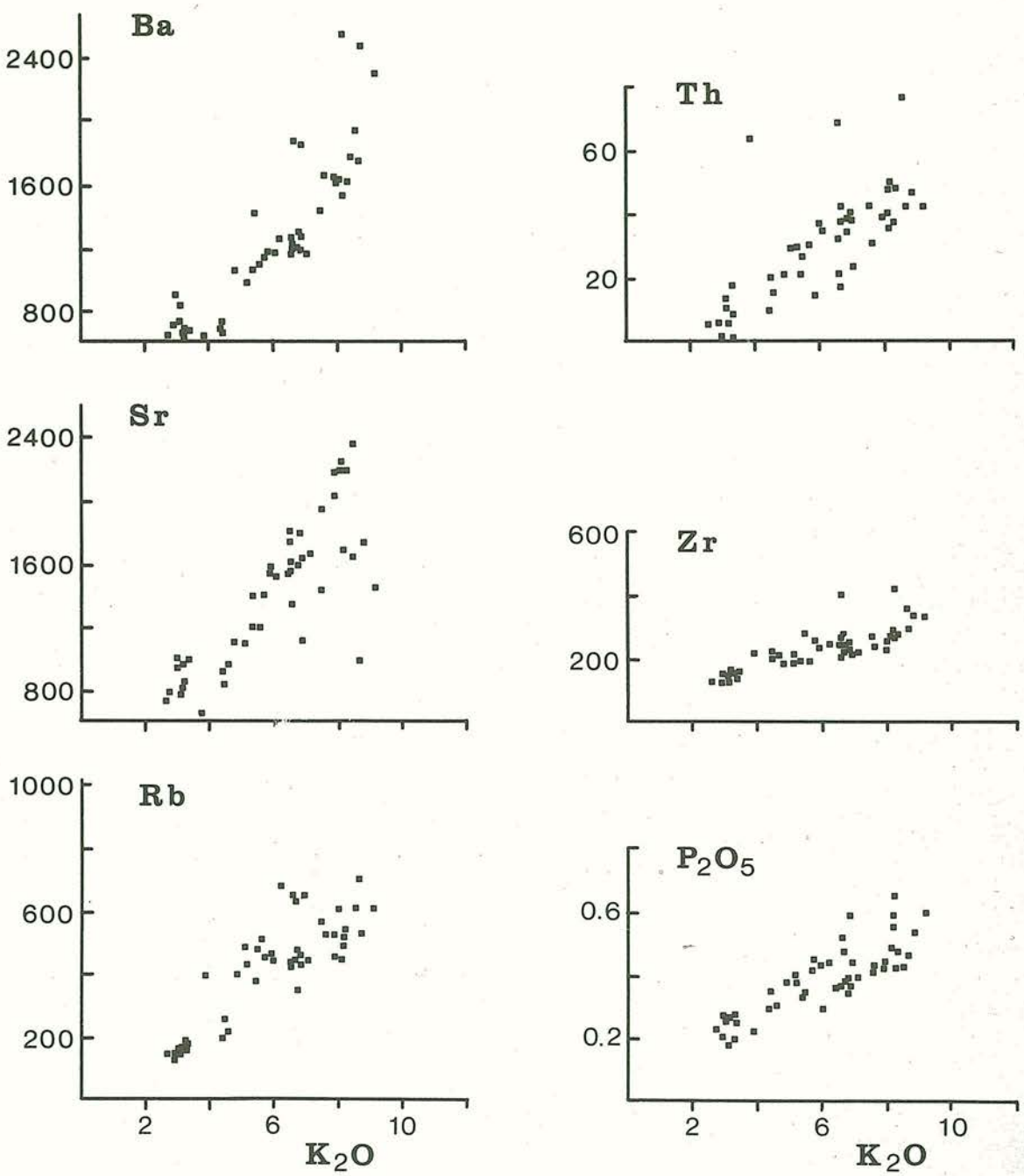

Ba
2400
1600
800
Th
60
20
Sr
2400
1600
800
Zr
600
200
Rb
1000
600
200
P_2O_5
0.6
0.2
2
6
10
K_2O
2
6
10
K_2O

Table 4-9

Roman Region Primitive Lavas - Correlation with K_2O

Element	r	Element	c
SiO_2	-0·69*	Y	0·76*
Al_2O_3	0·01	Sr	0·82*
Fe_2O_3T	0·01	Rb	0·84*
MgO	-0·33	Th	0·73*
CaO	-0·13	Zn	-0·05
Na_2O	-0·04	Rb/Sr	0·31
TiO_2	0·03	K_2O/Na_2O	0·69*
P_2O_5	0·74*	Ca/Sr	-0·71*
MnO	0·01	K/Rb	-0·41"
Ba	0·88*	K/Ba	0·00
Zr	0·79*		

* r significant at 99·9% level

" r significant at 99·0% level

It should be noted that the chemical variation observed within the group of primitive lavas of the Roman Region cannot be explained by any known low pressure differentiation process. Therefore it is assumed that the process which provides the parental magmas for each volcanic vent is an intermediate or high pressure differentiation process.

The second component controlling the distribution of data points in the K_2O v. SiO_2 plot (Fig. 4-8) can be attributed to low-pressure crystal-liquid fractionation. In some of the volcanic sequences

(e.g. Roccamonfina High K, Low K; Latera-Vulsini High K, Low K) the lavas show a marked differentiation towards salic derivatives following idealised Trend B (inset Fig. 4-9). The changes in the chemistry of the lavas along Trend B are typical of normal low-pressure crystal-liquid fractionation, i.e. there is a decrease in the "mafic" chemical variables CaO, MgO, Fe_2O_3T, TiO_2, MnO, and a concomitant rise in SiO_2, Al_2O_3, K_2O, and Na_2O. In fact CaO, MgO, etc. contours can be superimposed onto the K_2O v. SiO_2 plot approximately normal to Trend B. It will be demonstrated in Chapter 5 that the differentiation towards salic derivatives in both the Roccamonfina lava series (and also in the Latera-Vulsini lavas), along idealised Trend B (inset Fig. 4-9) can be attributed to low-pressure crystal-liquid fractionation involving the removal of phases seen in phenocryst and cumulate (nodule) assemblages.

Composition and sequence of lavas erupted at each of the volcanic centres

When a volcanic centre has two lava series showing different levels of enrichment in K and associated elements, there does not seem to be any petrological significance in the order of eruption of the lavas. For example, at Roccamonfina the High K series precedes the Low K series, whilst the Low K Somma lavas precede the higher K Vesuvius lavas, and at Latera-Vulsini the oversaturated Low K lavas were erupted during the final period of activity. Some of the volcanoes produce lava sequences with a distinct compositional gap in the K_2O v. SiO_2 plot (e.g. Roccamonfina) whilst with others the compositional gap is smaller (e.g. Latera-Vulsini). Certain

centres produced mainly-salic lavas (e.g. Vico) whilst others produced only primitive basic lavas (e.g. Alban Hills). This apparently complex situation can be explained in the following manner.

The chemical variation shown by the lavas of the Roman Region as a whole is related to two main differentiation processes. Process A produced the parental magma with a specific level of enrichment in K and associated elements. This is an intermediate or high pressure differentiation process. Process B (low-pressure crystal-liquid fractionation) controls the evolution towards salic derivatives. The composition, sequence, and volume of the lavas erupted from each volcanic vent within the Roman Region is controlled by the extent to which these two petrologically significant processes have operated. This in turn must be assumed to be controlled by local complexities of sub-volcanic thermal conditions, structure, and tectonics. As a result of these latter factors, the eruptive products at any given place or time appear to have been selected randomly from the contiuum of compositions potentially available.

4:4:3 K/Rb relationship

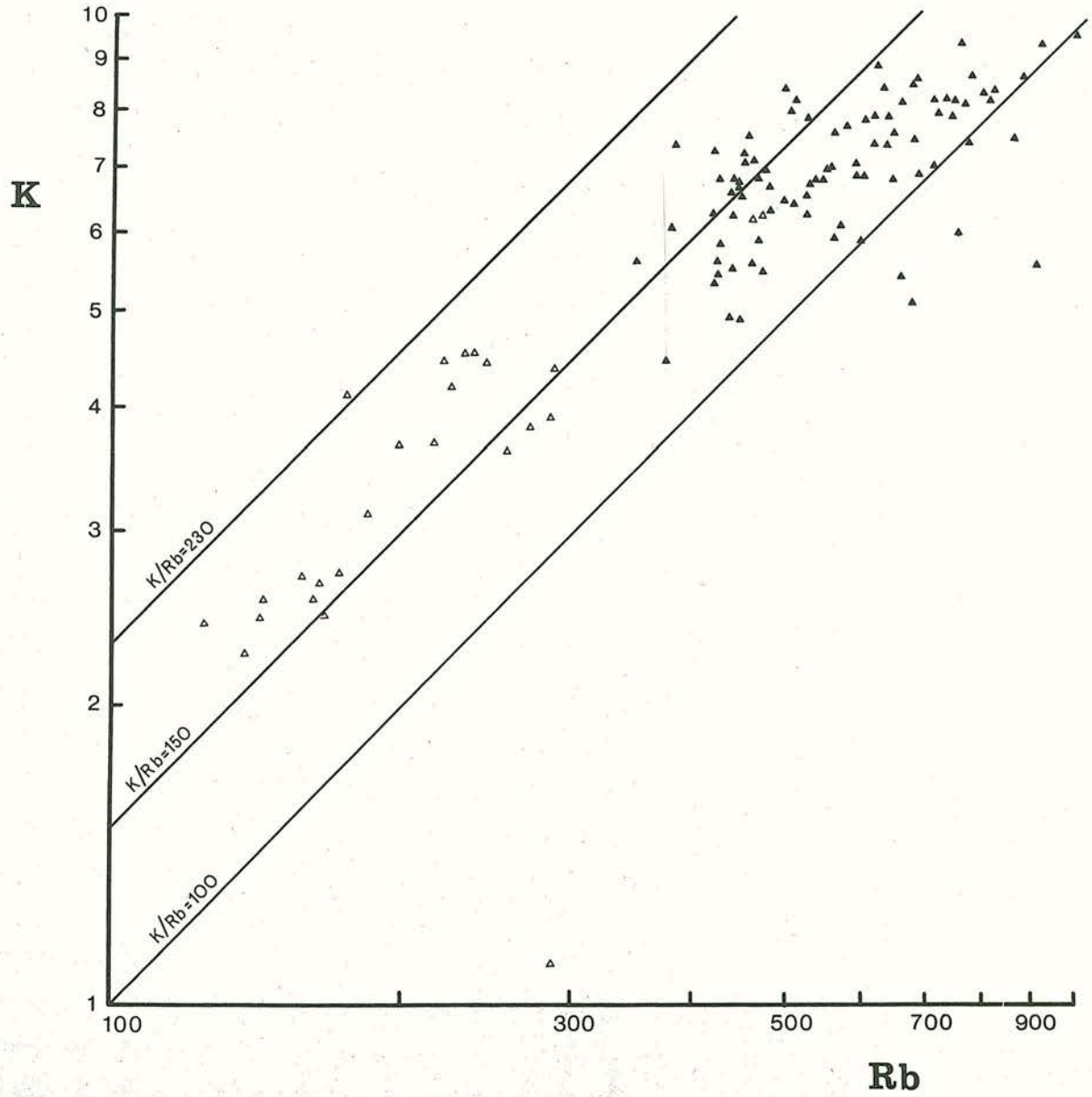
The plot of K v. Rb for the Roccamonfina lavas (Fig. 4-13) shows that the mean K/Rb for the Low K series (154) is slightly higher than that for the High K series (127), and that both series have K/Rb ratios lower than the crustal average (~230; see Erlank, 1968). Similar low K/Rb values are noted for the other volcanoes in the Roman Region (see Appendix E; Hurley et al., 1966; Savelli,

Fig. 4-13

Plot of K(wt.%) v. Rb(ppm) for the Roccamonfina lavas.

▲ : High K lavas

△ : Low K lavas


K
10
9
8
7
6
5
4
3
2
1
K/Rb=230
K/Rb=150
K/Rb=100
100
300
500
700
900
Rb

1967; Barbieri et al., 1968). The process that produced the extreme enrichment of K in the lavas of the Roman Region has obviously operated more efficiently in the case of Rb.

Bell and Powell (1969) noted that the K/Rb for the potassic lavas of the Western Rift was fairly constant at ~300, and Carmichael (1967) showed that the lavas of the Leucite Hills had K/Rb ratios in the range 190-320 (mean of 5 determinations = 287).

4:4:4 Niobium

The Nb data presented for some of the Roccamonfina lavas (see Appendix C, Table C-8) shows that Nb is enriched in the salic residual lavas and that it is present in relatively low concentrations when compared with the K-rich lavas of the Western Rift (range 80-320 ppm Nb in leucitites; Bell and Powell, 1969). On the basis of the data available, the lavas of the two Roccamonfina series appear to contain similar concentrations of Nb.

CHAPTER 5

DIFFERENTIATION OF THE LAVAS

Due to the considerable difference in K_2O content between the High K and Low K series of the Roccamonfina volcano, their differentiation will be considered separately. Reference will be made to the relevant phase relations in synthetic and pseudo-natural systems in order to illustrate and interpret the crystallisation and differentiation of the lavas and to estimate the probable stability limits of the observed phenocryst and nodule assemblages. However, the application of the results of experimental studies in simple synthetic systems for the interpretation of the crystallisation of natural magmas and the stability of phases in complex natural systems should be approached with caution. The effect of additional components considerably modifies the position of phase boundaries (Jamieson, 1969; Humphries, personal communication) and the stability limits of certain phases (e.g. increasing P_{H2O} considerably reduces the leucite phase volume in the system Ne-Ks-SiO_2-H_2O; Hamilton and MacKenzie, 1965).

5:1 Roccamonfina High K Series

Introduction

The differentiation model proposed for the leucite-bearing lavas of the High K series is based on the interpretation of the petrographic and mineralogical evidence provided by the lavas and

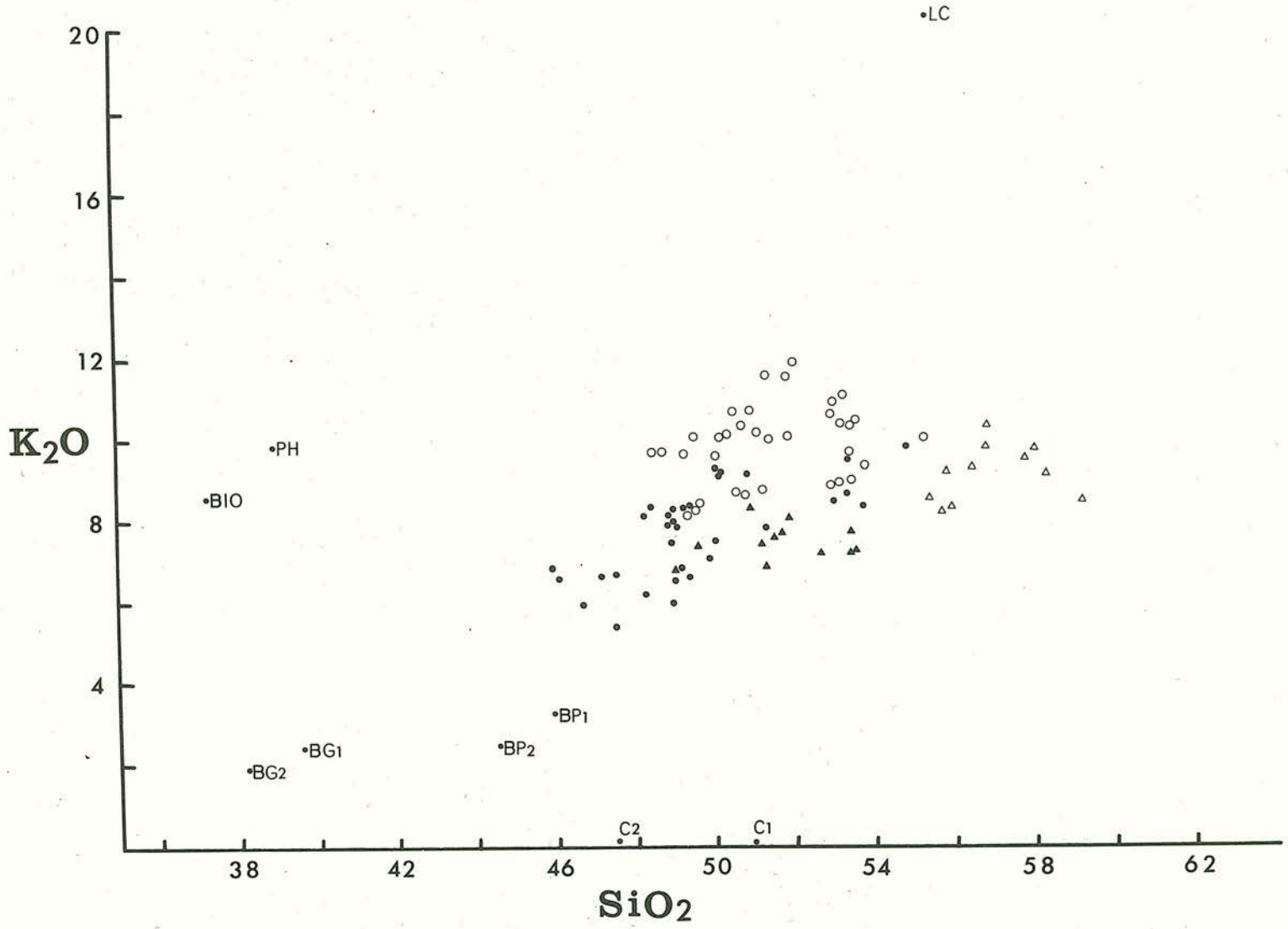
their associated nodules, and on the interpretation of simple chemical variation diagrams and extract calculations. These methods are, of course, well proven in igneous petrology, and petrogenetic conclusions based on petrography, variation diagrams, and extract calculations are usually compatible with those based on phase equilibria (Jamieson, 1970). The reader will realise in the following sections that it would be very difficult to check in detail the low pressure crystal-liquid fractionation model proposed for the lavas of the High K series by reference to the phase relations that are known for the relatively simple systems incorporating a K-rich phase (e.g. An-Lc-SiO_2, Di-Lc-SiO_2).

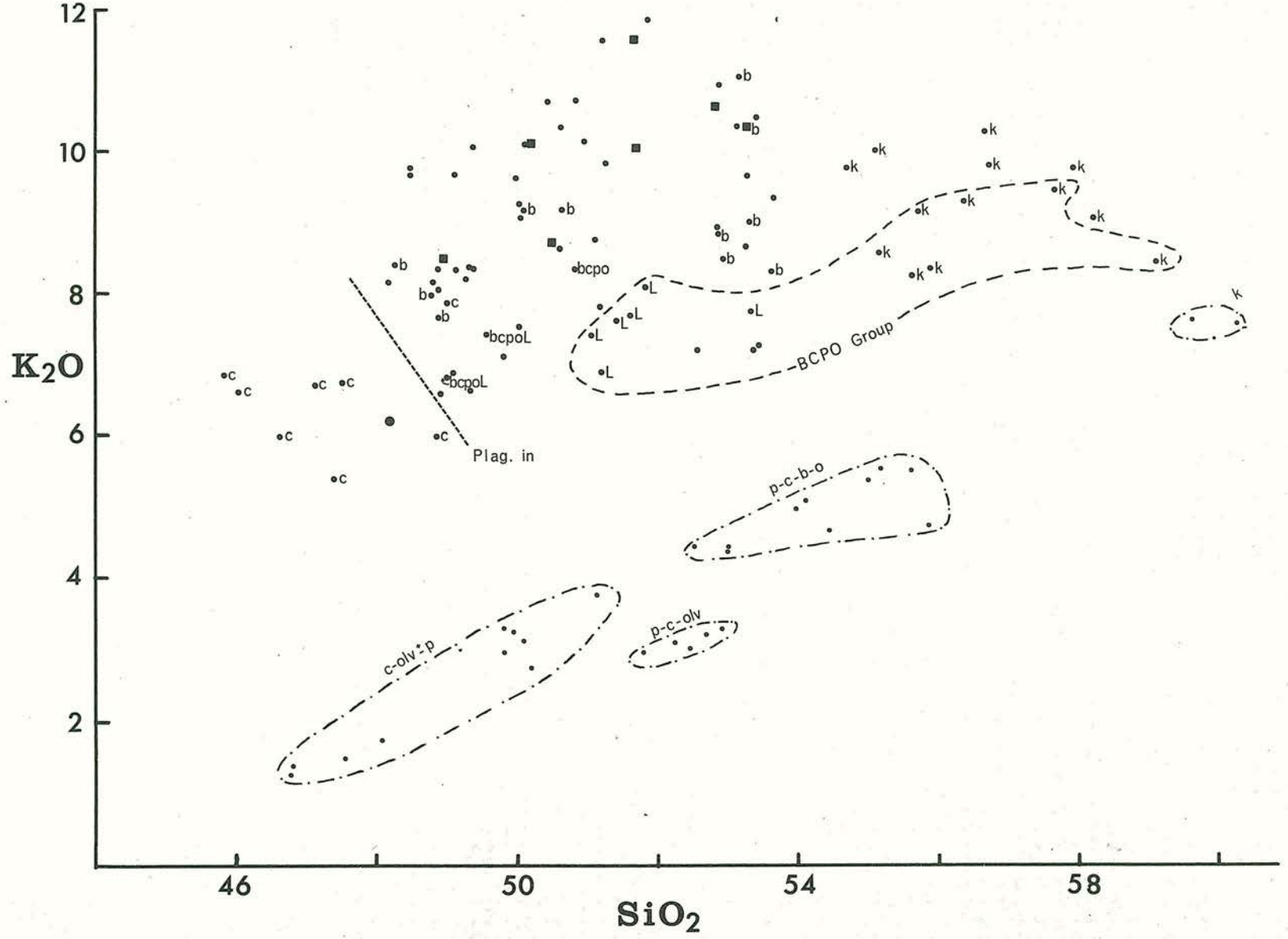
In the following sections the observed phenocryst and nodule assemblages are briefly noted, and then the relationship between these mineral assemblages (which are considered to be possible crystal extracts) and the chemical variation observed in the lavas is then discussed.

Phenocryst assemblages and other petrographic features relevant to the differentiation of the lavas of the High K series

The relationship between the main phenocryst assemblages of the lavas and their chemistry is shown in Figs. 5-1 and 5-2. In Fig. 5-1 the distribution of aphyric (microphyric), leucite macrophyric, biotite-cpx-plagioclase-ore (± leucite) phyric tephrites, and tephritic leucite phonolites/leucite phonolites is shown.

Fig. 5-2 illustrates the distribution of the lower K lavas with biotite-cpx-plagioclase-ore phenocrysts (those containing


20
16
12
8
4
K_2O
LC
PH
BIO
BP1
BG1
BP2
BG2
C2
C1
38
42
46
50
54
58
62
SiO_2


12
10
8
6
4
2
K_2O
46
50
54
58
SiO_2
BCPO Group
Plag. in
p-c-b-o
p-c-olv
c-olv±p

subsidiary leucite(L) or sanidine(k) are also indicated). This group of lavas will be referred to as the BCPO group. Fig. 5-2 also shows the distribution of lavas with clinopyroxene(c) as the main phenocryst phase, and those lavas containing rare, partially to totally resorbed biotite(b) are also noted. The remainder of the lavas are either aphyric with rare microphenocrysts of leucite, cpx, plagioclase, and ore, or porphyritic with leucite as the main macrophenocryst phase and cpx, plagioclase, ± ore as subsidiary macrophenocrysts and common microphenocrysts. Reference to the modal data presented in Appendix B shows that in these lavas, cpx-plagioclase-ore phenocrysts are present only in very small quantities (usually only in trace amounts) compared with leucite (which ranges up to 40 volume %). The wide variation in size of the leucite phenocrysts is thought to indicate a relatively long period of crystallisation prior to eruption.

The following observations are of importance when attempting to explain the differentiation of the lavas of the High K series.

(1) Some of the leucite macrophyric lavas contain glomero-aggregates of clinopyroxene-plagioclase-ore±apatite. Good examples are R.44 (Plate 14), R.183 (Plate 16), R.33, R.61 (Plate 20), R.27, R.18 and R.77. The distribution of the lavas containing these glomeroaggregates is noted in Fig. 5-2. The glomeroaggregates are sometimes surrounded by large leucite phenocrysts (Plate 14) suggesting that this cpx-plagioclase-ore±apatite assemblage may represent an earlier period of crystallisation (e.g. a period when the prevailing PT conditions prevented the crystallisation of leucite).

(2) R.131 (marked ● in Fig. 5-2) contains a small glomero-aggregate of biotite-cpx-plagioclase-ore-apatite (Plate 17) which is the same assemblage as that noted in the biotite gabbro (R.103) and in the lower K lavas of the BCPO group.

(3) The approximate position of the line marking the entry of plagioclase into the phenocryst assemblage is noted in Fig. 5-2. The significance of this observation is noted in the next section.

(4) Sanidine enters the phenocryst assemblage in those lavas with >55% SiO_2, i.e. mainly in the tephritic leucite phonolites and leucite phonolites.

(5) Apatite is a common microphenocryst phase, being most frequently associated with the cpx-plagioclase-ore±biotite glomero-aggregates and as inclusions in clinopyroxene phenocrysts where it occurs as small prismatic or needle shaped crystals (Plate 10, R.185).

(6) The distribution of aphyric/microphyric lavas is very important because these can be assumed to represent liquid compositions. R.137-139 and R.19 with >9% K_2O are the most potassium-rich aphyric tephritic leucitites analysed.

(7) It will be argued in the following sections that fractionation of biotite gabbro could produce the observed chemical variation towards salic derivatives in all the lavas of the High K series. Relics of this higher P_{H2O} assemblage in the higher K_2O leucite macro-microphyric lavas are largely absent. This could indicate that perfect fractionation has occurred or that the assemblage biotite-cpx-plagioclase-ore-apatite has been largely resorbed and disaggregated during the later period of crystallisation

under Atmospheric Pressure conditions. Rare, partially to totally resorbed biotite phenocrysts do occur in some of the lavas (see Fig. 5-2), and cpx-plagioclase-ore±apatite glomeroaggregates surrounded by "late" leucite are occasionally seen. The scarcity of relic biotite phenocrysts in the leucite macro-microphyric lavas is not surprising as biotite would be rapidly resorbed with falling P_{H2O} at the relatively high temperatures of crystallisation of potassic undersaturated lavas (Wones and Eugster, 1965; Luth, 1967). The biotite-cpx-plagioclase assemblage of the lower K_2O BCPO group (see Fig. 5-2) is similar to that of the biotite gabbro (R.103).

Nodules as possible crystal extracts

A biotite gabbro nodule found in superficial tuffaceous deposits was the only nodule found during the present survey. The petrography of this nodule is described in Chapter 2, Section 2-3. Arevalo et al. (1962) reported two nodules of similar mineralogical and chemical composition, and although there is no modal data available for these nodules, the chemical analyses (Table 5-1) show that the plagioclase content must increase from R.103→ A.5→ A.4. If these nodules are considered to be possible extracts from the K-rich magmas that produced the lavas of the High K series, the variation in the proportions of the various phases in the nodules (i.e. the crystal extracts) could explain some of the "scatter" in lava compositions noted in the next section. Arevalo et al. (1962) suggest that the biotite gabbro nodules are subvolcanic heteromorphs of the relatively leucite deficient tephritic lavas of the BCPO group (see above).

Table 5-1

Chemical Analyses of Biotite Gabbro Nodules

Wt.%	R.103	A.4*	A.5*
SiO_2	39·61	38·7	38·2
TiO_2	1·47	1·16	1·3
Al_2O_3	17·31	22·6	18·5
Fe_2O_3	7·59	4·3	8·6
FeO	6·78	5·4	5·4
MnO	0·15	0·16	0·18
MgO	6·55	5·9	5·3
CaO	13·71	17·1	15·7
Na_2O	0·76	0·6	0·6
K_2O	2·46	0·85	1·9
H_2O^+	1·86	2·6	2·5
H_2O^-	-		
P_2O_5	1·50	0·88	1·5
Total	99·75	100·25	99·58

* A.4 and A.5 from Arevalo et al. (1962).

Apart from the biotite gabbros, no other nodules have been reported from the Roccamonfina area. This may be related to the fact that the area has not been so intensively studied as for example the Alban Hills and Somma-Vesuvius - neither is the exposure so good as at these other two volcanic centres.

Pyroxenite and biotite pyroxenite nodules are the most common mafic nodules associated with the lavas and pyroclastic deposits of the Roman Region. The best examples come from the Alban Hills (Washington, 1927; Fornaseri, 1951; Fornaseri et al., 1963; this thesis, Appendix E) and Somma-Vesuvius (Lacroix, 1917; Washington, 1927; Narici, 1932; this thesis, Appendix E). The texture of these nodules suggests that they are segregations of early formed crystals and can therefore be considered as possible crystal extracts.

In order to show the relationship between nodule compositions, the compositions of various phenocryst and nodule phases, and the variation observed in the lavas of the Roccamonfina High K series, the composition of an average Somma-Vesuvius biotite pyroxenite, two average clinopyroxenes, biotite gabbros R.103 and A.5, average phlogopite, biotite-R.103, and leucite R.36-1c are plotted on the chemical variation diagrams presented in the following section. The composition of the average clinopyroxenes, phlogopite, and average Somma-Vesuvius biotite pyroxenite are noted in Table 5-2, together with the sources of the analyses used in compiling these average analyses. Analyses of biotite-R.103 and R.36-1c can be found in Chapter 3, and analyses of the biotite gabbros R.103 and A.5 are presented in Table 5-1.

Table 5-2

Average Chemical Analyses used in Variation Diagrams

Wt.%	Av. nodule cpx.[1]	Av. lava cpx.[2]	Av. phlogopite[3]	Av. Biotite Pyroxenite[4]
SiO_2	50·98	47·38	38·98	45·9
TiO_2	0·69	1·49	1·24	1·7
Al_2O_3	5·12	6·81	14·89	10·3
Fe_2O_3	2·22	3·44	3·76	3·4
FeO	3·60	4·54	3·47	)
MnO	0·11	0·13	0·23	) 3·9
MgO	14·65	13·14	22·05	13·5
CaO	21·60	22·53	0·17	17·0
Na_2O	0·39	0·47	0·24	1·0
K_2O	0·09	0·16	9·80	3·3
P_2O_5	-	-	-	0·3
SUM	99·48	100·09	94·83	100·3

1 = average of Cpx-AB6(c), CPX-V-1, Cpx-14043 (see Table 3-9)

2 = average of Somma-Vesuv lava cpxs presented by Rahman (1968) plus Analysis 4 (Narici, 1933, p. 98) and Analysis 1 (Washington and Merwin, 1921, p. 22)

3 = average of Ph-BAH, and Ph-BP(Ariccia) (see Table 3-10)

4 = average biotite pyroxenite (see Cundari and Le Maitre, 1970, p. 43).

Variation diagrams and extract calculations

Fig. 5-3 shows the relationship between the major element variation in the lavas and possible crystal extracts. The following points should be noted.

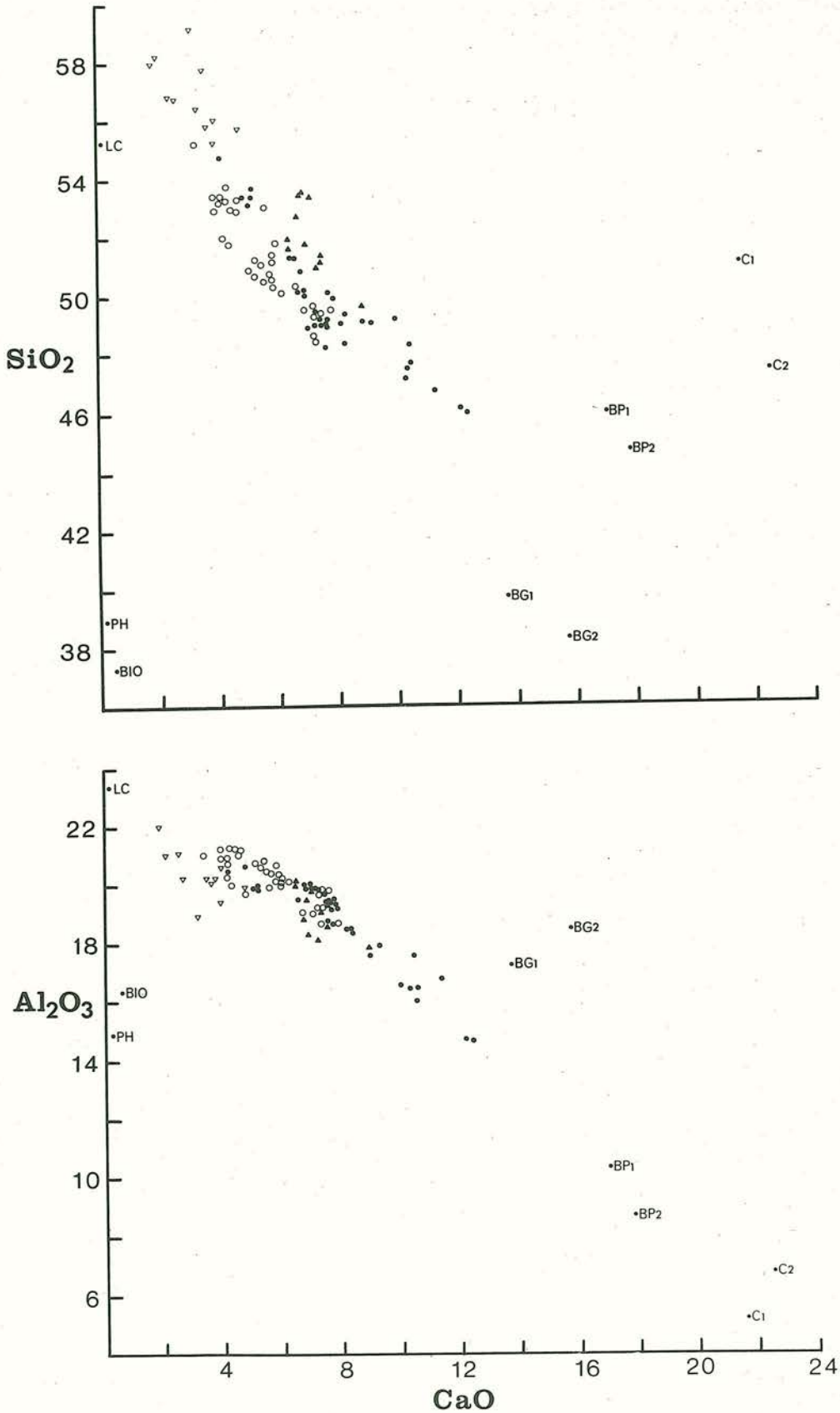
(1) Some of the variation diagrams, especially CaO v. MgO and CaO v. Fe_3O_3T show a marked change of slope at 7 - 8% CaO.

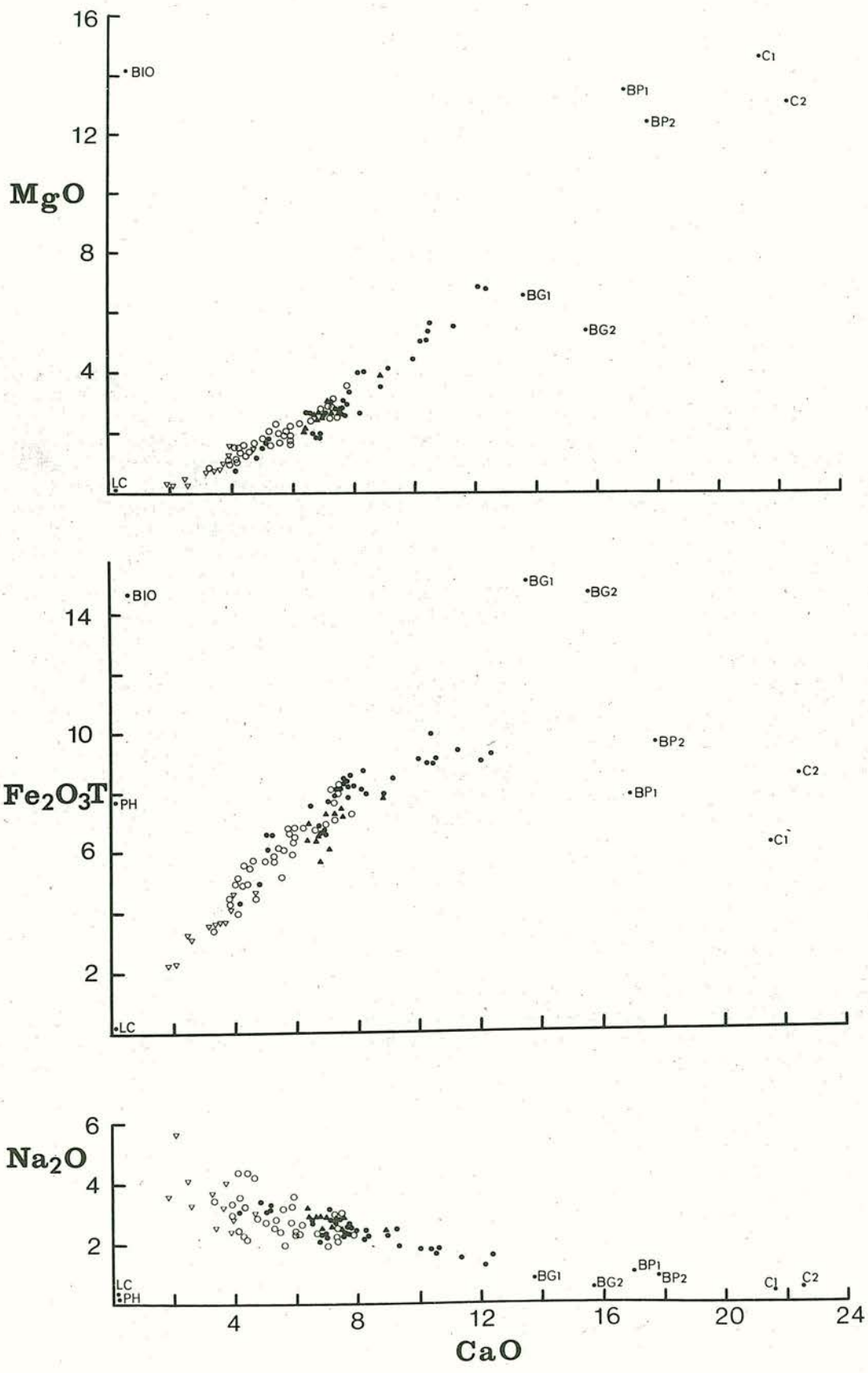
(2) Biotite pyroxenite and biotite gabbro appear to be the most plausible crystal extracts. Plagioclase enters the phenocryst assemblage at approximately 8% CaO (see above), so the "kink" in some of the variation diagrams could be related to the change over from biotite pyroxenite to biotite gabbro fractionation.

(3) The variation in K_2O (and hence SiO_2 etc.) in the primitive lavas cannot be explained by the fractionation of any of the observed phenocryst phases or nodule assemblages. This variation of K and associated elements in the primitive lavas and first differentiates has been described in Chapter 4 and will be discussed further in Chapter 6. Therefore, it is necessary to assume that the salic differentiates originated from parental magmas of varying K_2O content.

(4) Extract calculations of the type used by Bowen (1928) (Fig. 5-4) show that Na_2O is zero at 17 - 18% CaO. Therefore the most extreme possible extract has CaO = 17 - 18%. At 17 - 18% CaO, K_2O = 2 - 3%, so the proposed crystal extract must contain a K_2O-bearing mafic phase such as biotite or phlogopite.

(5) The Fe_2O_3T v. CaO plot suggests that the crystal extract contained an ore phase.


58
54
50
46
42
38
SiO2
•LC
•C1
•C2
•BP1
•BP2
•BG1
•BG2
•PH
•BIO
22
18
14
10
6
Al2O3
4
8
12
16
20
24
CaO


MgO
16
12
8
4
BIO
C1
BP1
C2
BP2
BG1
BG2
LC
Fe2O3T
14
10
6
2
BIO
BG1
BG2
BP2
C2
BP1
PH
C1
LC
Na2O
6
4
2
LC
PH
BG1
BG2
BP1
BP2
C1
C2
4
8
12
16
20
24
CaO

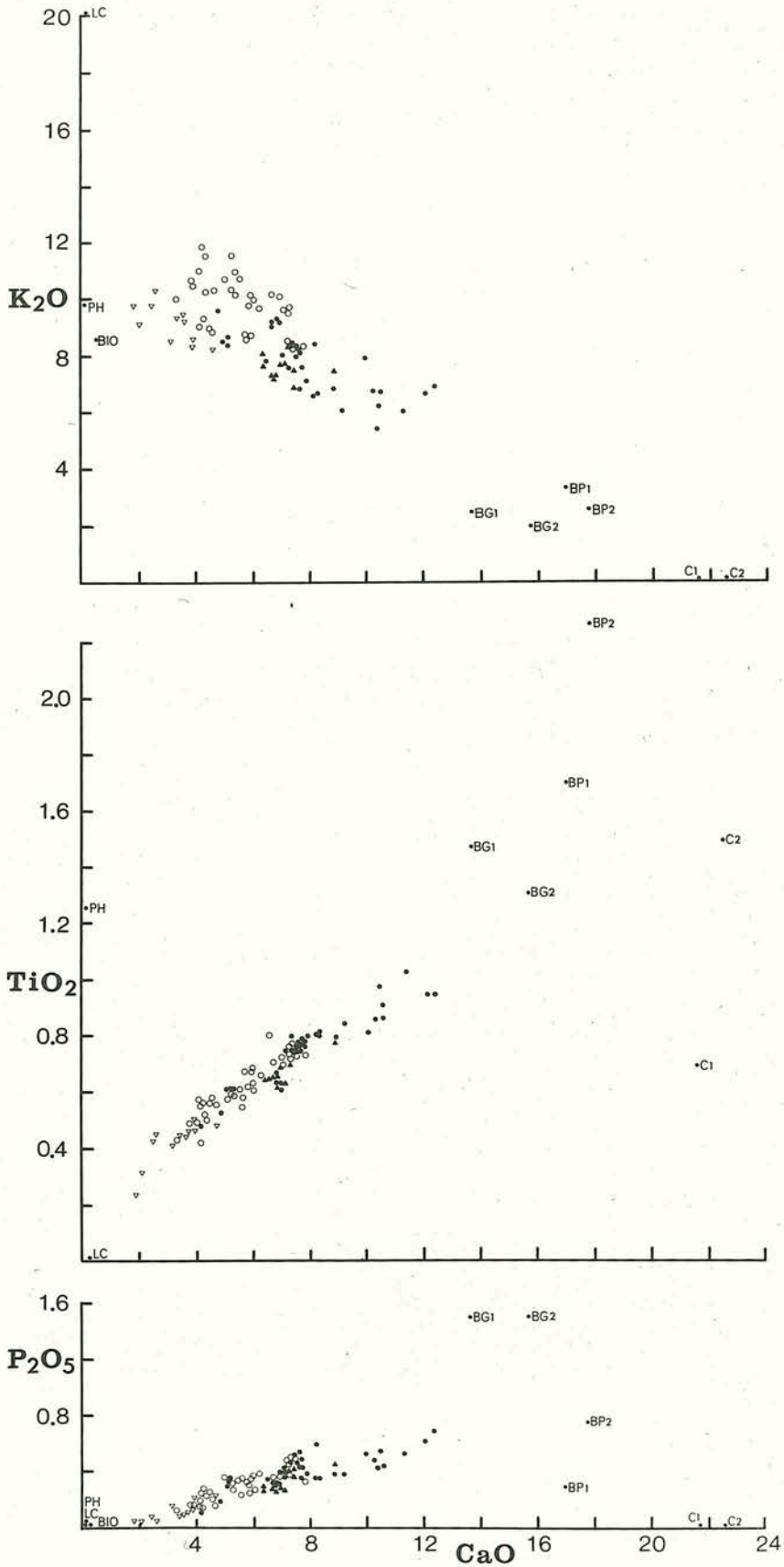

20
16
12
8
4
K2O
LC
PH
BIO
BP1
BP2
BG1
BG2
C1
C2
2.0
1.6
1.2
0.8
0.4
TiO2
1.6
0.8
P2O5
4
8
12
16
20
24
CaO

Fig. 5-4

Roccamonfina High K lavas - Extract diagram

SiO_2 = $SiO_2/2$

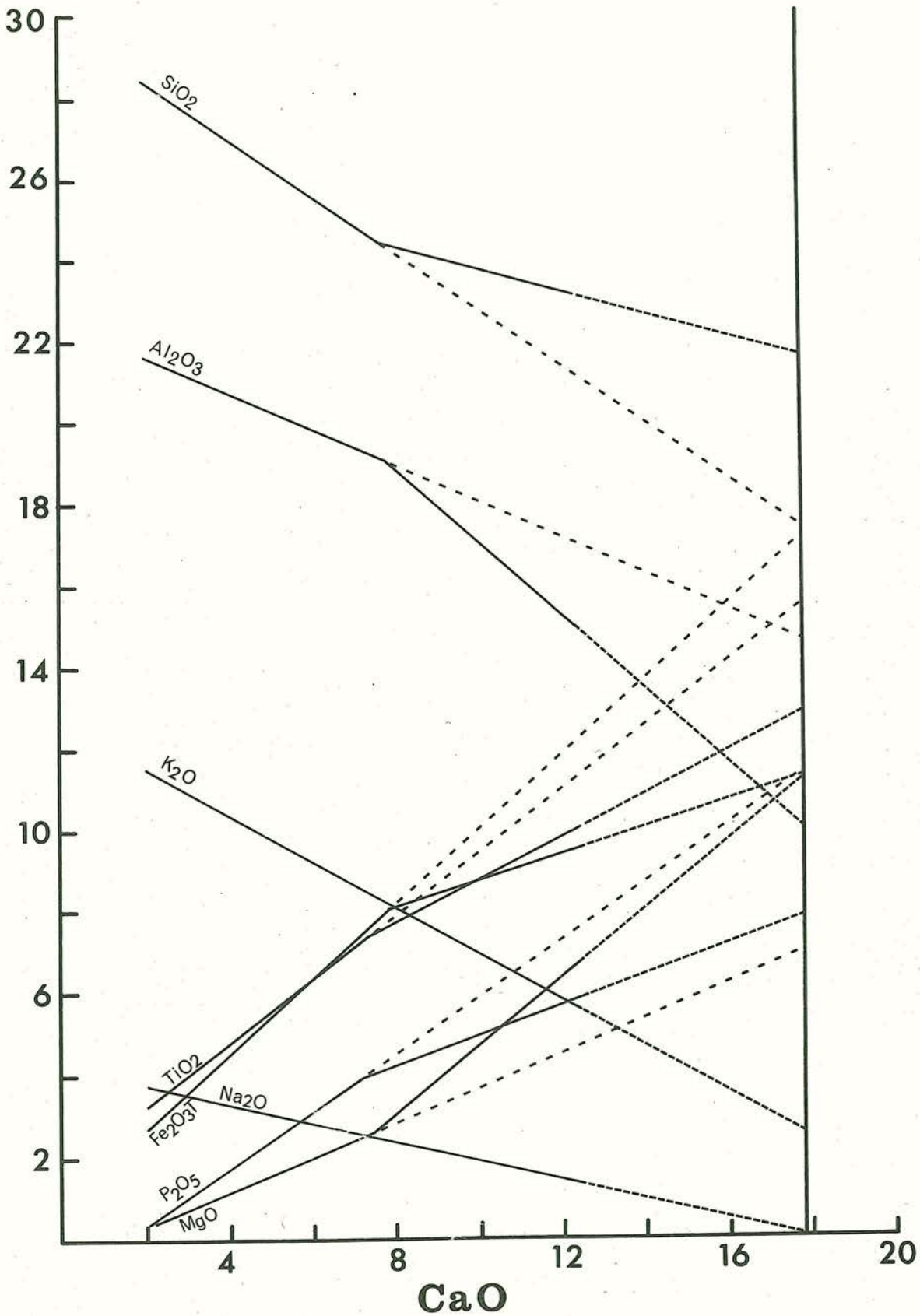
TiO_2 = TiO_2 x 10

P_2O_5 = P_2O_5 x 10

Extract diagram is based on CaO variation diagrams (Fig. 5-3).

Best-fit lines are estimated and not computed.

Compositions of most basic extracts are indicated.

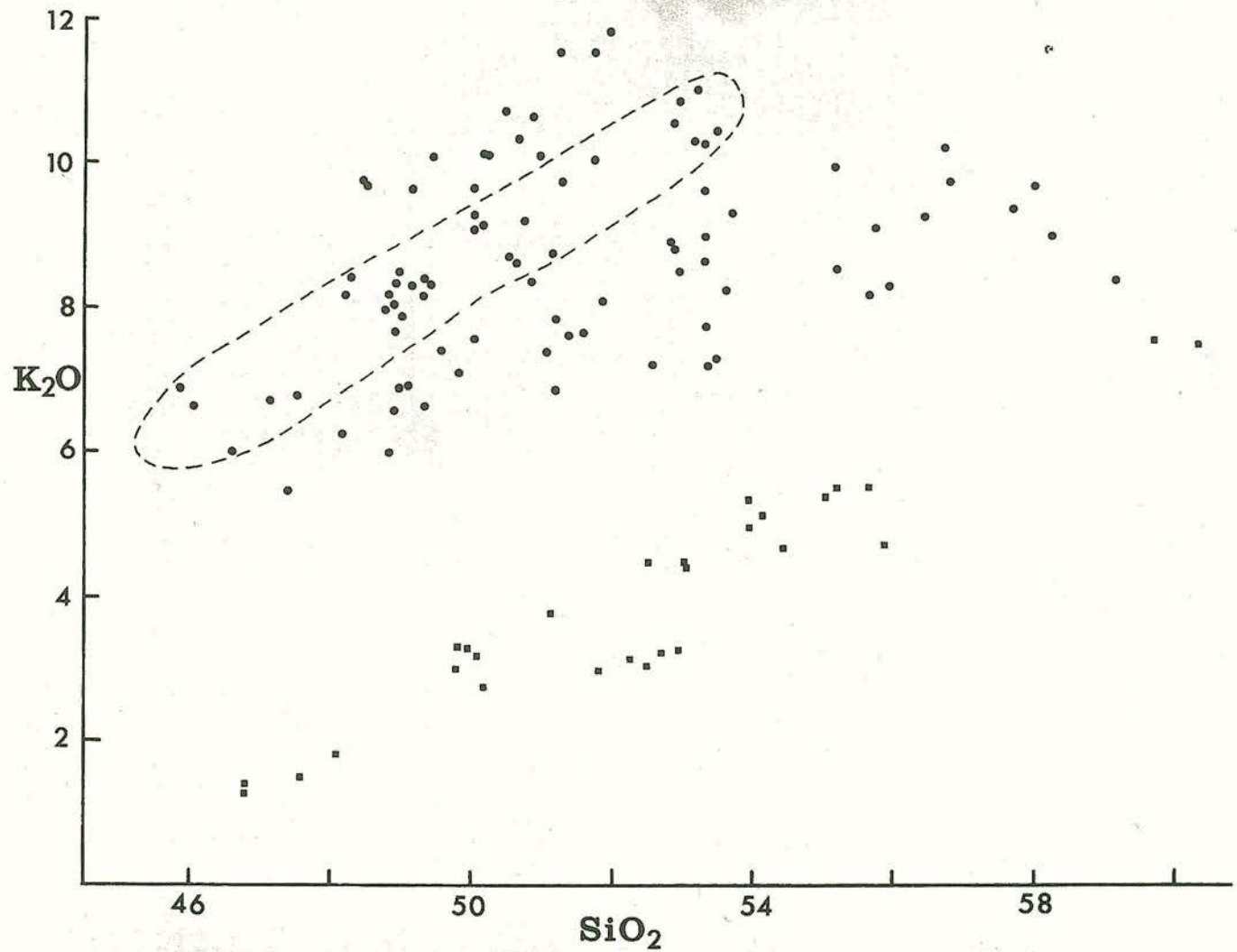

30
26
22
18
14
10
6
2
SiO2
Al2O3
K2O
TiO2
Na2O
Fe2O3T
P2O5
MgO
4
8
12
16
20
CaO

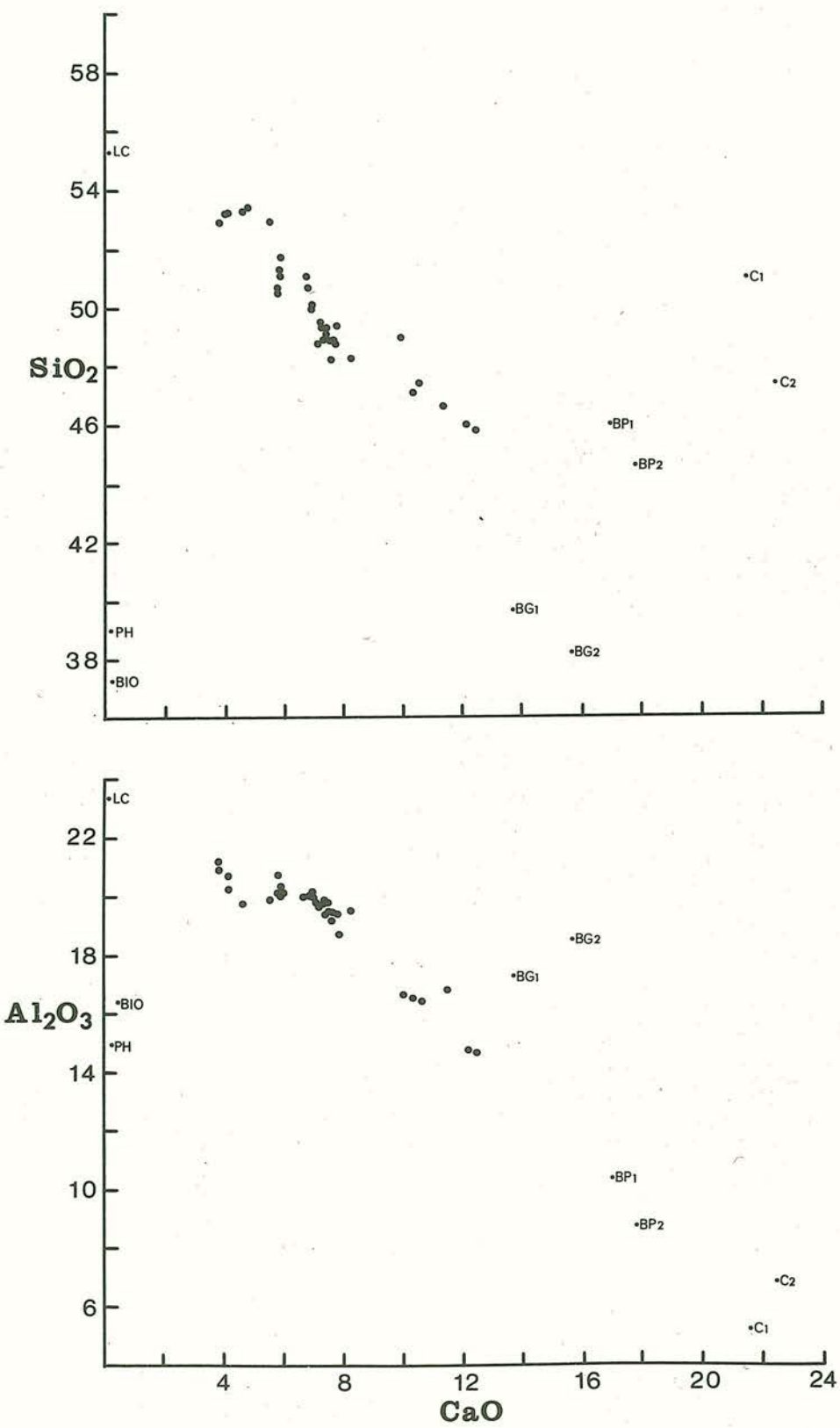
(6) The P_2O_5 v. CaO plot indicates that apatite was also included in the crystal extract.

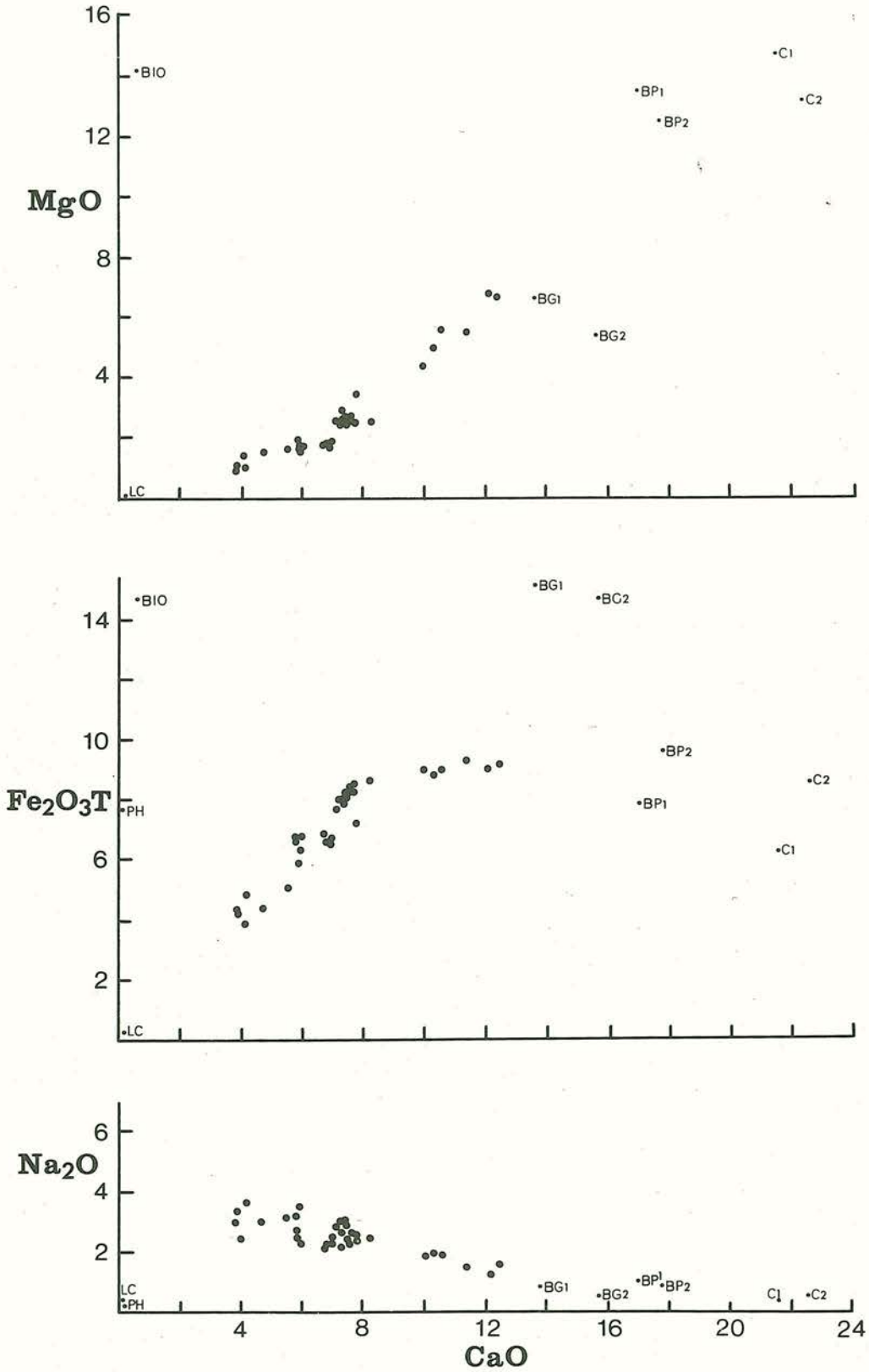
(7) The biotite gabbro (R.103) contains both a mafic K-rich phase, an ore mineral, and apatite.

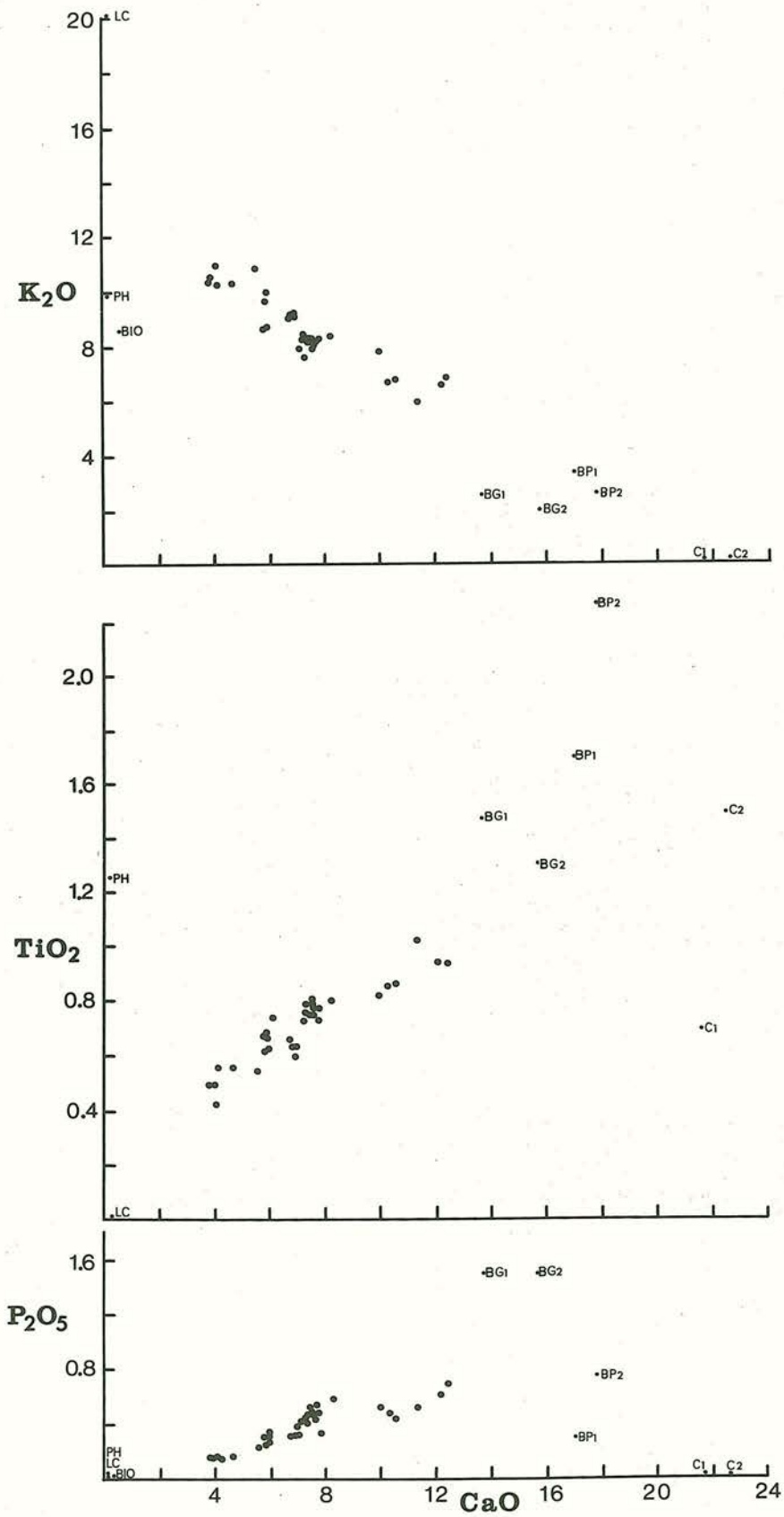
A group of lavas were selected from the K_2O v. SiO_2 plot to include the maximum number of aphyric lavas showing a similar level of K_2O enrichment (Fig. 5-5). Variation and extract diagrams (Figs. 5-6, 5-7) for this group of lavas confirm the observations noted above when all the lavas of the High K series were considered together. The variation diagrams for the select group show less scatter than the diagrams including all the lavas. This "scatter" is probably partly related to the variation in the concentration of K_2O in the parental magmas.

On the basis of the chemical variation diagrams shown above, biotite pyroxenite followed by biotite gabbro appear to be the most plausible crystal extracts for all the lavas of the High K series. The BCPO group of lavas has a similar phenocryst assemblage to the biotite gabbro suggesting that biotite gabbro fractionation under Atmospheric Pressure (AP) conditions could explain the variation within this group. However, the variation in the leucite macro-microphyric lavas cannot be explained by biotite gabbro fractionation under AP conditions because it is quite obvious from the phenocryst assemblage that these lava compositions lie within the leucite phase volume in the natural system. The wide variation and large size of the leucite phenocrysts suggests a long period of crystallisation in the leucite phase volume before


12
10
8
6
4
2
K_2O
46
50
54
58
SiO_2


58
54
50
46
42
38
SiO2
LC
PH
BIO
C1
C2
BP1
BP2
BG1
BG2
22
18
14
10
6
Al2O3
4
8
12
16
20
24
CaO


16
12
8
4
MgO
BIO
C1
BP1
C2
BP2
BG1
BG2
LC
14
10
6
2
Fe2O3T
PH
6
4
2
Na2O
4
8
12
16
20
24
CaO


20
16
12
8
4
K_2O
LC
PH
BIO
BP1
BG1
BP2
BG2
C1
C2
2.0
1.6
1.2
0.8
0.4
TiO_2
1.6
0.8
P_2O_5
4
8
12
16
20
24
CaO

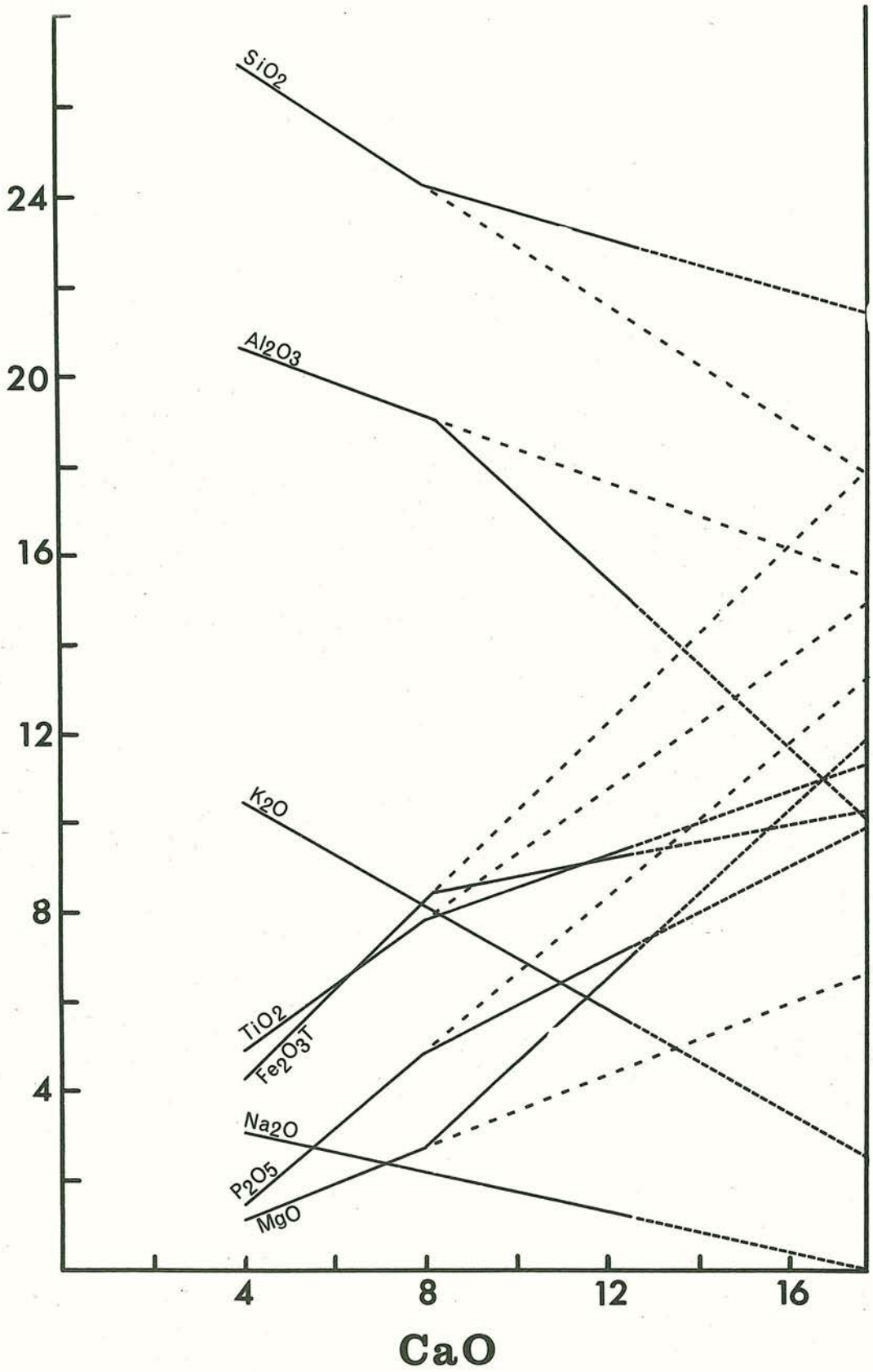

SiO2
Al2O3
K2O
TiO2
Fe2O3T
Na2O
P2O5
MgO
24
20
16
12
8
4
4
8
12
16
CaO

Fig. 5-8

Plots of Ba and Sr v. CaO for the Roccamonfina High K lavas.

Symbols as in Fig. 5-1.

□ : Biotite gabbro (R.103)

the composition of the residual liquid has migrated onto a leucite +cpx±plagioclase±ore cotectic in the natural system.

Reference to the modal data presented in Appendix B, shows that leucite is the major phenocryst phase in the leucite macro-microphyric lavas (up to 40 volume %) and that cpx-plagioclase-ore are usually present only in trace amounts. The possibility that the differentiation of the leucite macro-microphyric lavas is controlled by the fractionation of leucite is now discussed.

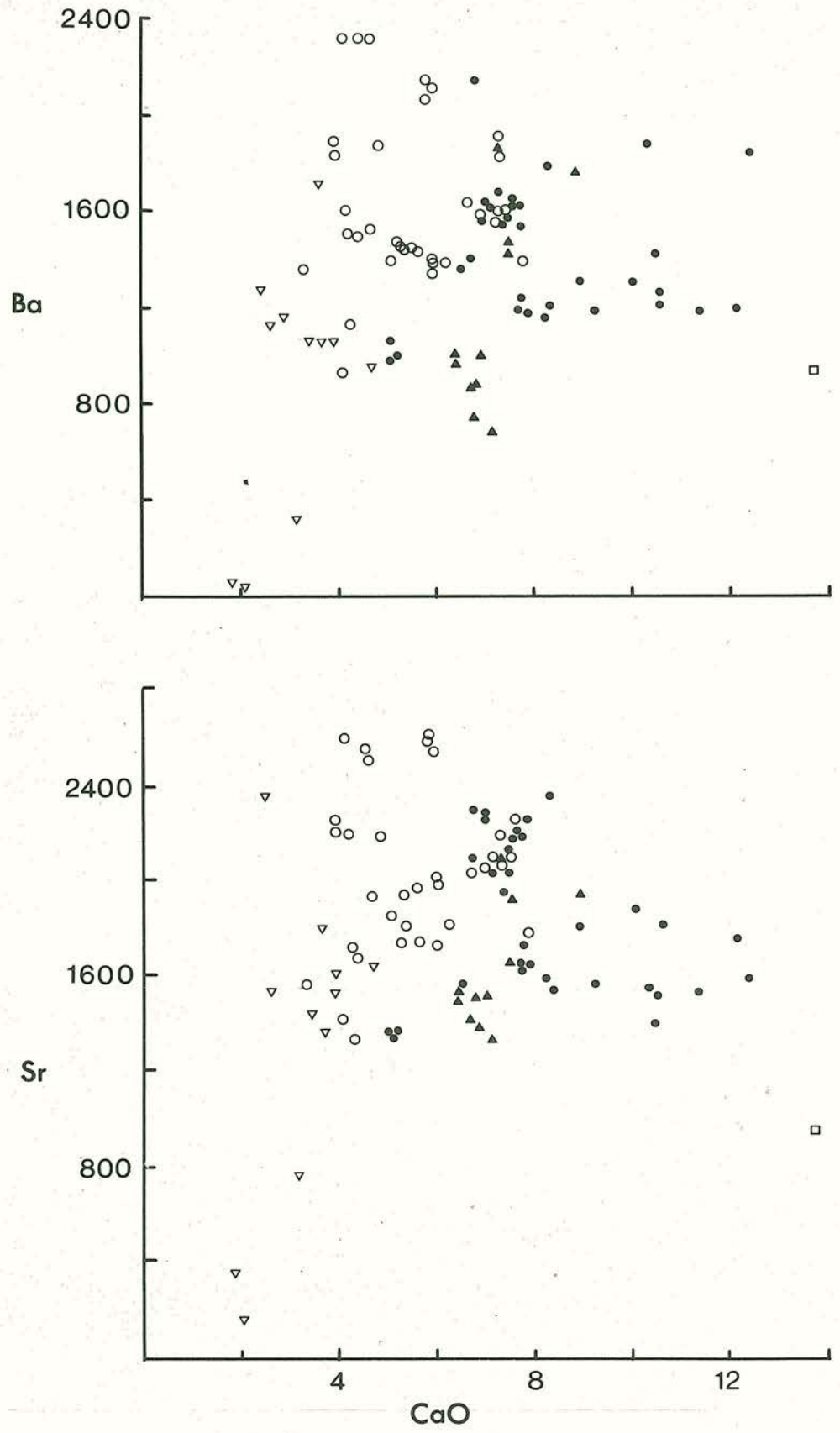
Leucite fractionation

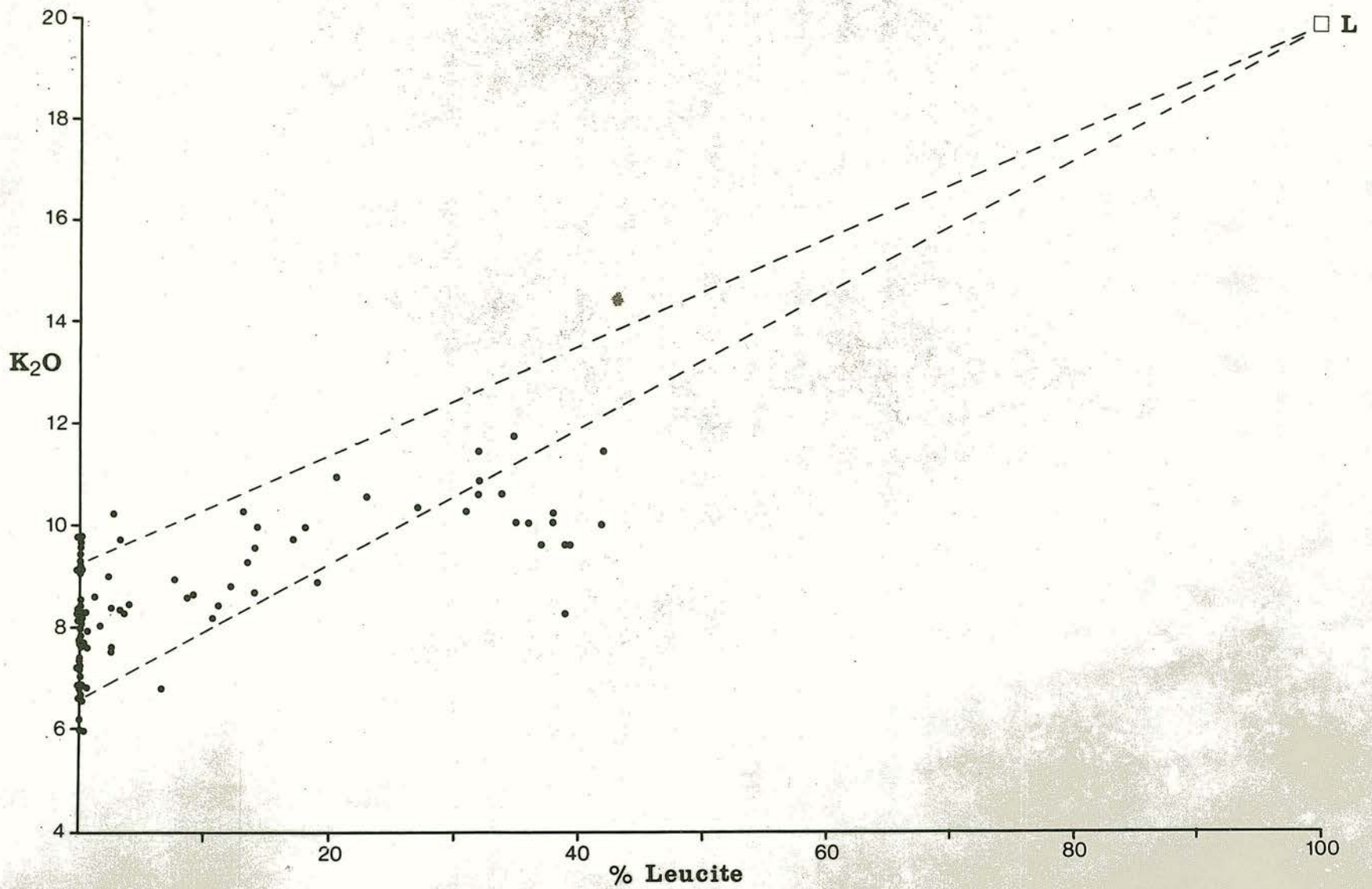
It can be seen from Figs. 5-3 (K_2O v. CaO) and 5-1 (K_2O v. SiO_2) that the macrophyric leucite-bearing lavas are concentrated towards the top of the K_2O range. It seems possible, therefore, that some of these lavas may be enriched in cumulus leucite. However, if the leucite macrophyric lavas represent true liquid compositions unmodified by leucite fractionation, then the enrichment pattern of K_2O, Ba, Sr, etc. should follow that noted for the primitive lavas and first differentiates (see Chapter 4) i.e. the lavas with the highest K_2O content should also have the highest Sr, Ba, etc. If, however, the leucite macrophyric lavas are enriched in cumulus leucite, they will have lower Sr and Ba contents than predicted by the model of parallel enrichment of K and associated elements because D^{lc}_{wr} for Sr = 0·02 and for Ba = 0·14 (see Chapter 3). By comparing the distribution of the aphyric, leucite macrophyric, and BCPO tephritic lavas in the K_2O v. SiO_2 (Fig. 5-1) and K_2O v. CaO (Fig. 5-3) plots with the distribution

of these lavas in the CaO v. Sr and CaO v. Ba plots (Fig. 5-8), it can be concluded that some of the leucite macrophyric lavas are enriched in cumulus leucite. For example, R.116, 178, 44, 33, and 136 (all with < 1750ppm Sr and with >10% K_2O) appear to be enriched in cumulus leucite whilst some of the leucite macrophyric lavas (e.g. R.23, 20, 39, 135 - all with >2000ppm Sr and >9·5% K_2O) have Sr, Ba, and K_2O contents suggesting near liquid compositions.

As leucite contains ± 20% K_2O, lavas enriched in cumulus leucite should have considerably higher K_2O values than aphyric lavas. No leucite-phyric lavas occur with K_2O<6·5% and aphyric lavas have up to 9·25% K_2O. Assuming parental magmas with 6·5 - 9·25% K_2O, the K_2O increase related to leucite cumulation can be illustrated by plotting wt.% K_2O v. volume % leucite phenocrysts. The distribution of points in Fig. 5-9 suggests that the leucite phenocrysts in the High K lavas are not completely cumulative (which would be unusual), but it is obvious that the enrichment in K_2O in some of the leucite macrophyric lavas may be partly controlled by leucite accumulation.

The question remains as to whether the leucite accumulates by flotation or by the more normal mechanism of crystal-sinking. The specific gravity contrast between leucite (2·47 - 2·50, Deer et al. 1962b) and leucite tephrites/leucitites (2·66 - 2·78, mean 2·73, Washington, 1906) suggests that leucite should fractionate by flotation. The rate of flotation would depend upon the S.G. contrast between leucite and liquid, the viscosity of the liquid, the pressure, and the size of the leucite crystals. If the leucite was crystallising in a magma chamber where a convection system had become established, this would favour the concentration


2400
1600
800
Ba
2400
1600
800
Sr
4
8
12
CaO


20
18
16
14
12
10
8
6
4
K_2O
□ L
20
40
60
80
100
% Leucite

of leucite crystals towards the top of the magma chamber. Certain geological evidence suggests that aggregation and flotation of leucite does occur.

(1) Presence of Italite nodules in pyroclastic deposits of the Alban Hills (Washington, 1927). These nodules must be large glomeroaggregates composed solely of leucite phenocrysts. They cannot represent liquid compositions as a melt of this composition would have an impossibly high liquidus temperature ($\pm$ 1680°C - pure leucite melts at 1686°C). The presence of Italite nodules indicates that leucite phenocrysts nucleated into large glomeroaggregates, but it does not indicate whether they floated, sank, or remained in situ.

(2) The leucite "rain" described by Blum (1874) during the 1845 eruption of Vesuvius was caused by the eruption of tuffaceous material composed almost totally of leucite phenocrysts. This suggests leucite flotation to the top of the magma chamber, followed by explosive eruption and fragmentation.

(3) Neubauer (1911) recorded the flotation of leucite and the sinking of clinopyroxene during the crystallisation of a leucite tephrite under experimental conditions.

(4) Buie (1941) suggested that the occurrence of a layer of Fergusite (50% pseudoleucite) at the top of a shonkinite dyke in the Highwood Mts. area, Montana, was proof that leucite floats.

(5) Sahama (1960) recorded leucite aggregates (S.G. = 2·48) in the lavas of Nyiragongo (groundmass S.G. = 3·03). He suggested that the texture of the leucite aggregates indicated that they had

crystallised slowly whilst rising through the molten lava and had accumulated in large quantities in the top part of the lava mass. He suggests that aggregation and flotation was encouraged by turbulent gas currents.

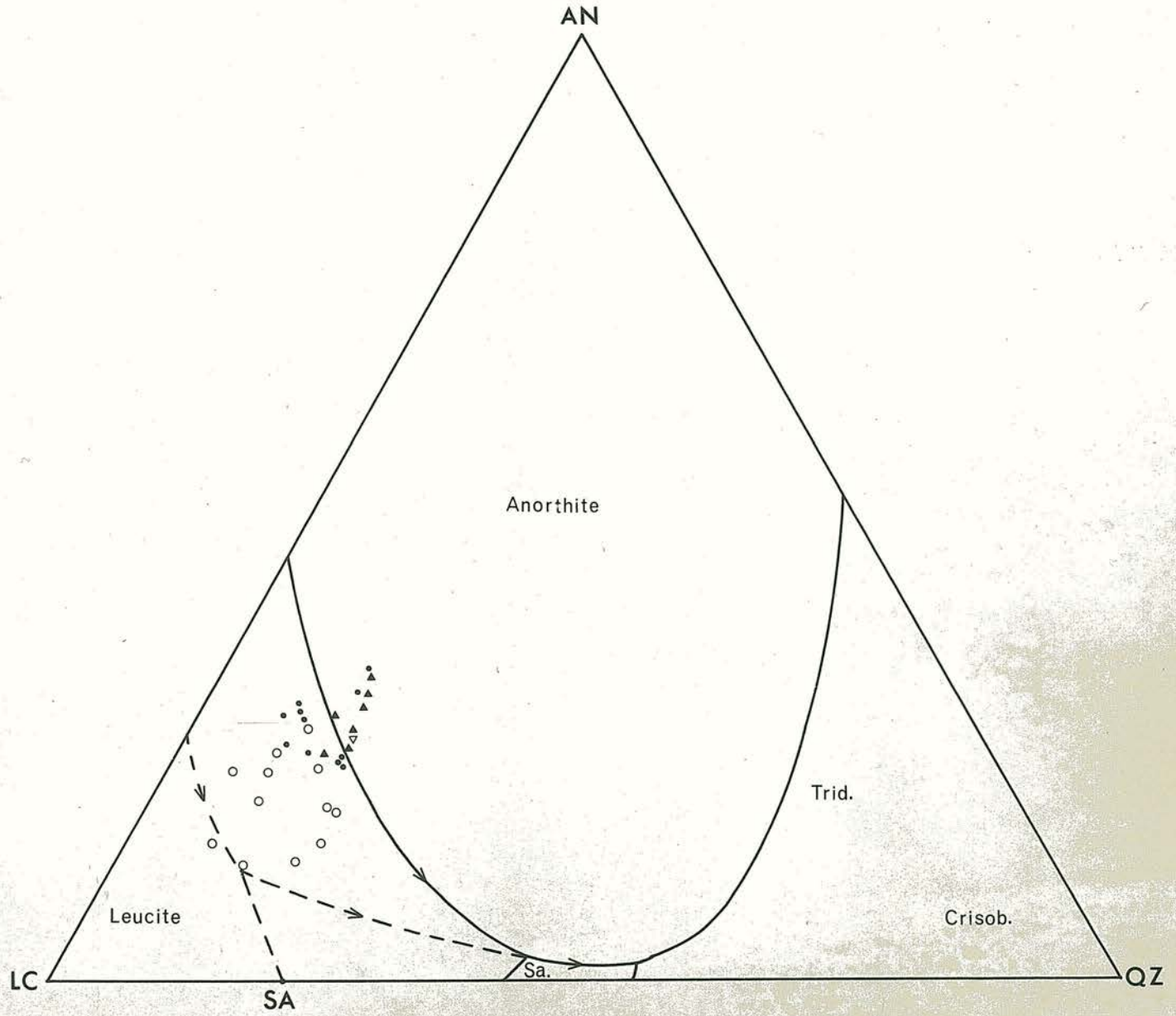
It should be noted that no obvious vertical variation in leucite content was seen in any of the leucite macrophyric lava flows in the Roccamonfina area (max. thickness ± 8m.). It was impossible to trace a leucite-phyric flow over any distance to see if there was any significant lateral variation in leucite content. A study of the leucite-phyric 1944 flow of Vesuvius (Locardi, personal communication) suggests that this flow is homogeneous.

On the basis of the evidence discussed above, it appears that leucite probably fractionates by flotation rather than by crystal-sinking and that the high K_2O content of some of the leucite macrophyric lavas is partially caused by enrichment in cumulative leucite. However, it is quite obvious from Figs. 5-3 and 5-1 that fractionation of leucite cannot explain the trend towards SiO_2 enrichment seen in these lavas (parallel to ideallised Trend B, Fig. 4-10, inset.). It certainly cannot explain the generation of leucite microphyric lavas with 53·5% SiO_2. 8·5% K_2O, and 5·0% CaO (Figs. 5-3, 5-1). It has already been noted that the chemical variation diagrams suggest that fractionation of biotite pyroxenite followed by biotite gabbro from parental magmas of varying K_2O content could explain the observed chemical variation in the lavas. If the leucite macro-microphyric lavas

and the BCPO lavas are residual liquids (only slightly modified by leucite flotation/accumulation in the case of some of the lavas of the first group) of biotite pyroxenite and biotite gabbro fractionation, then the PT conditions which would reduce the stability field of leucite are of obvious importance.

Leucite stability

Goranson (1938), Yoder et al. (1957), Hamilton and MacKenzie (1965), and Fundali (1963) have shown that the stability field of leucite is reduced by increasing P_{H2O}. In the system $KAlSi_3O_8 - H_2O$ (Goranson, 1938), the leucite field becomes narrower until at 2·6 Kb P_{H2O} and 950°C, $KAlSi_3O_8$ melts congruently to a water saturated liquid. Lindsley (1966) studied the melting relations of $KAlSi_3O_8$ and $KAlSi_2O_6$ up to 40Kb. In the dry system $KAlSi_3O_8$ (Lindsley, 1966), the field of leucite + liquid persists up to 19 ± 1Kb. When $P_{H2O}<P_{TOTAL}$ (i.e. in most natural systems) the leucite + liquid field will be intermediate between that reported by Goranson (1938) and Lindsley (1966). In the system $KAlSiO_4 - Mg_2SiO_4 - SiO_2 - H_2O$, Luth (1967) found that the stability field of leucite was depressed with increasing P_{H2O} and that lc + fo were incompatible above 1200 bars in a water saturated melt. By using the results of Luth (1967) and Goranson (1937) it is possible to predict the approximate boundaries of the leucite field in the system $CaAl_2Si_2O_8 - KAlSi_2O_6 - SiO_2 - H_2O$ at c. 2·6Kb. P_{H2O} (Figure 5-10). The AP phase boundaries are taken from Schairer and Bowen (1947). If projection distortions are not excessive (and the distribution of lavas with known phenocryst


AN
Anorthite
Trid.
Leucite
Crisob.
Sa.
LC
SA
QZ

assemblages suggests that they are not) it is possible to conclude that the leucite macro-microphyric lavas would not crystallise leucite at 2·6Kb P_{H2O} in the presence of a free vapour phase. In fact, if it is assumed that some of the leucite macrophyric lavas (e.g. R.36, 43, 206) are enriched in cumulus leucite, a P_{H2O} of 1·5 - 2·0Kb. would probably be sufficient to prevent the crystallisation of leucite.

However, the absence of amphibole in the nodule and phenocryst assemblages suggests that a free vapour phase was not present during the evolution of the lavas of the Roccamonfina High K series. The release of vast quantities of vapour during the recorded eruptions of Vesuvius can be explained by the fact that a free vapour phase could appear with release of pressure (Yoder, 1964). The presence of biotite/phlogopite in the phenocryst and nodule assemblages suggests that P_{H2O} was sufficiently high to induce the crystallisation of these hydrous phases, but not high enough to cause the crystallisation of amphibole instead of clinopyroxene. Hydrothermal melting experiments on a variety of basaltic rocks were carried out by Yoder and Tilley (1962, p. 454). The PT projection of a Hawaiite-H_2O system shows that amphibole crystallises <u>after</u> clinopyroxene and plagioclase up to 3·1Kb P_{H2O}. In the High Alumina basalt - H_2O system, amphibole crystallises after olivine, clinopyroxene, and plagioclase up to 2·6Kb P_{H2O}. In a potash-rich melt, biotite or phlogopite would probably be the first hydrous phase to crystallise.

From the above data, it can be deduced that biotite

pyroxenite and biotite gabbro fractionation could occur at P_{H2O} $\leq$ 2·5Kb (possibly as low as 1·5 - 2·0Kb) in magmas which would crystallise leucite under AP conditions. P_{TOTAL} was probably greater than P_{H2O} (i.e. there was no free vapour phase), a free vapour phase only appearing as a result of pressure release just prior to eruption. The presence of an ore mineral in the biotite gabbro and ore phenocrysts in many of the lavas suggests a fairly high P_{O2} (directly related to P_{H2O}) during the differentiation of the lavas of the High K series.

Conclusions

A polybaric model of crystal-liquid fractionation is proposed to explain the differentiation of the Roccamonfina High K series. It can be divided into three main stages:

(1) Generation of parental magmas with varying levels of enrichment in K and associated elements (see Chapters 4 and 6).

(2) Fractionation of biotite pyroxenite followed by biotite gabbro at P_{H2O} of approximately 1·5 - 2·5Kb but with $P_{H2O} < P_{TOTAL}$.

(3) Release of pressure (sometimes explosively - hence large volume of pyroclastics) followed by eruption of the lavas. The lavas with high K_2O contents are in equilibrium with leucite+clinopyroxene±plagioclase±ore; those of the lower K_2O BCPO group are in equilibrium with biotite-clinopyroxene-plagioclase-ore at AP. As pressure is released the liquidus rises, so rapid crystallisation occurs in the lavas with high K_2O. Leucite

fractionates by flotation, but not enough to alter already established compositions significantly.

Further fractionation of plagioclase + K-feldspar produces the leucite phonolites with low Ba and Sr contents.

5:2 Roccamonfina Low K Series

Phenocryst assemblages

The following main phenocryst assemblages have been recognised in the lavas of the Low K series (see Fig. 5-2).

(1) Olivine basalts - olivine+clinopyroxene; olivine+cpx+plagioclase

(2) Trachybasalts - plagioclase+clinopyroxene+olivine

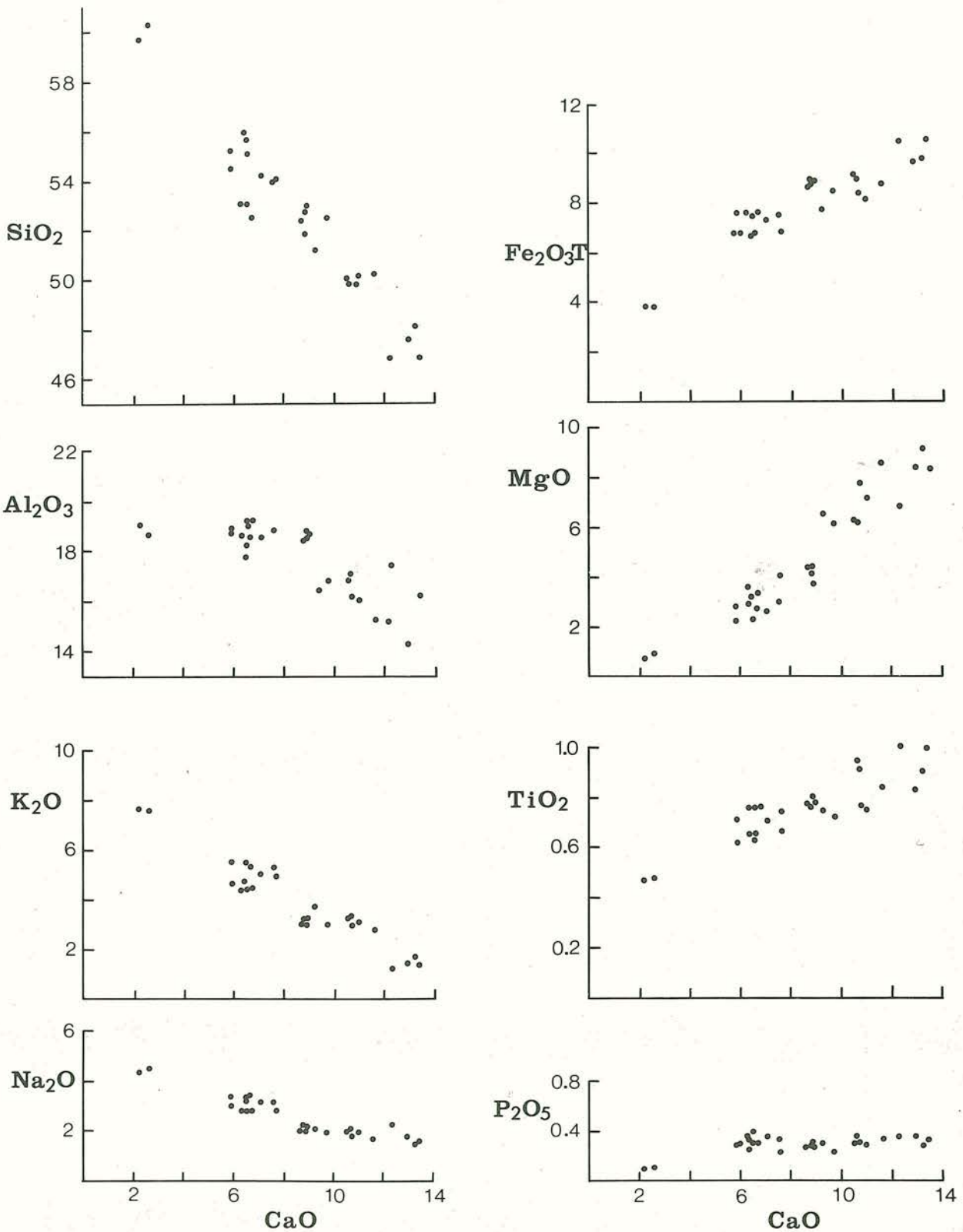
(3) Biotite augite latites - plagioclase+cpx+biotite+ore

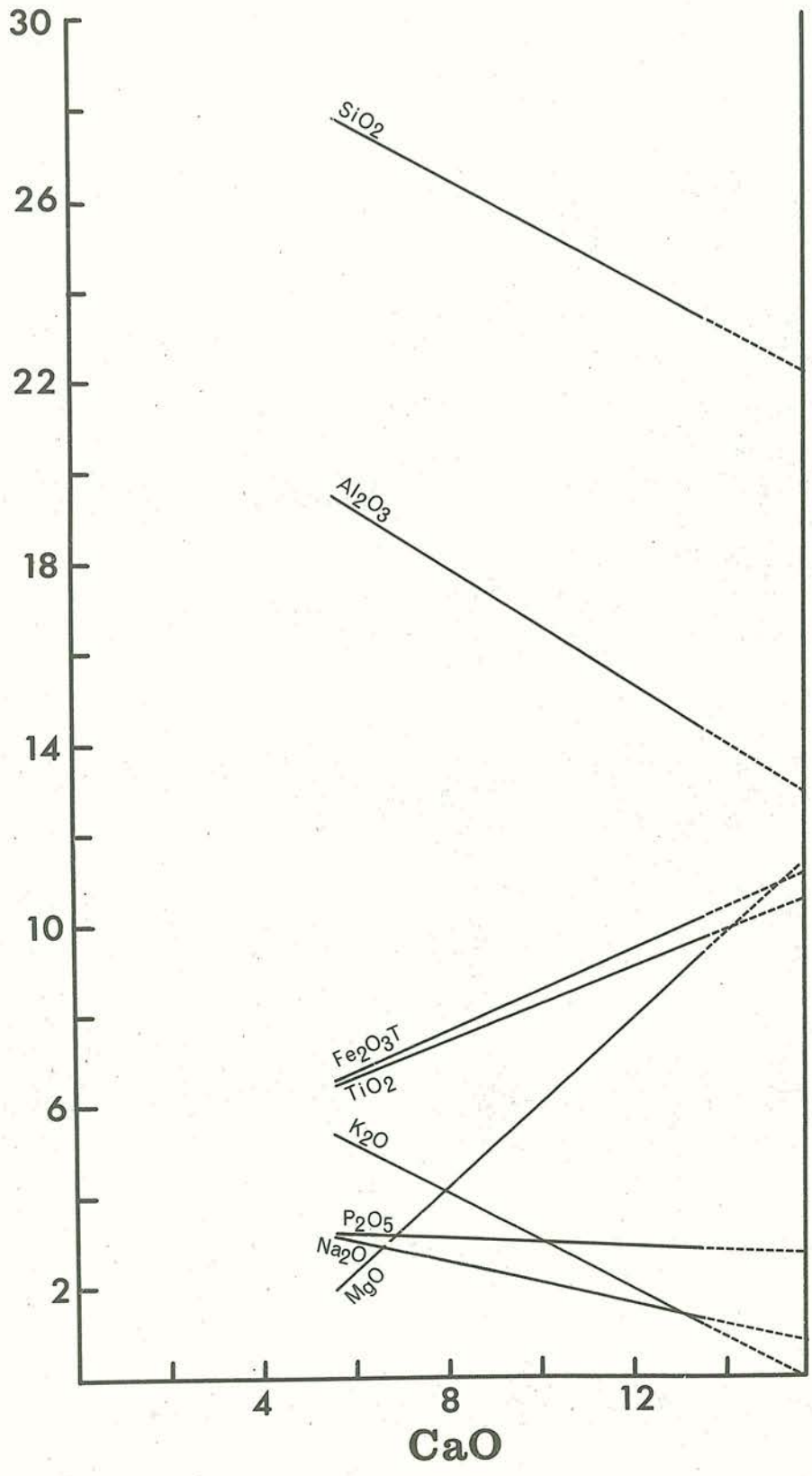
(4) Trachytic grey ash flow - rare sanidine

Differentiation

Fig. 5-11 shows that the lavas of the Low K series appear to be closely associated genetically. Extract calculations (Fig. 5-12) show that if the lavas are to be related by crystal-liquid fractionation, the first extract must be aluminous.

The chemistry, mineralogy, and petrography of basic igneous rocks have been extensively studied with reference to phase relations in synthetic systems such as $CaMgSi_2O_6 - Mg_2SiO_4 - CaAl_2Si_2O_8 - SiO_2$ (Bowen, 1914, 1928; Osborn and Tait, 1952) and also in the pseudoquaternary $C-A-M-S/R_2O_3 - XO - YO - ZO_2$ (O'Hara, 1968; Jamieson, 1970). In the pseudoquaternary C-A-M-S it has


SiO2
58
54
50
46
Fe2O3T
12
8
4
Al2O3
22
18
14
MgO
10
6
2
K2O
10
6
2
TiO2
1.0
0.6
0.2
Na2O
6
2
P2O5
0.8
0.4
2
6
10
14
CaO
2
6
10
14
CaO

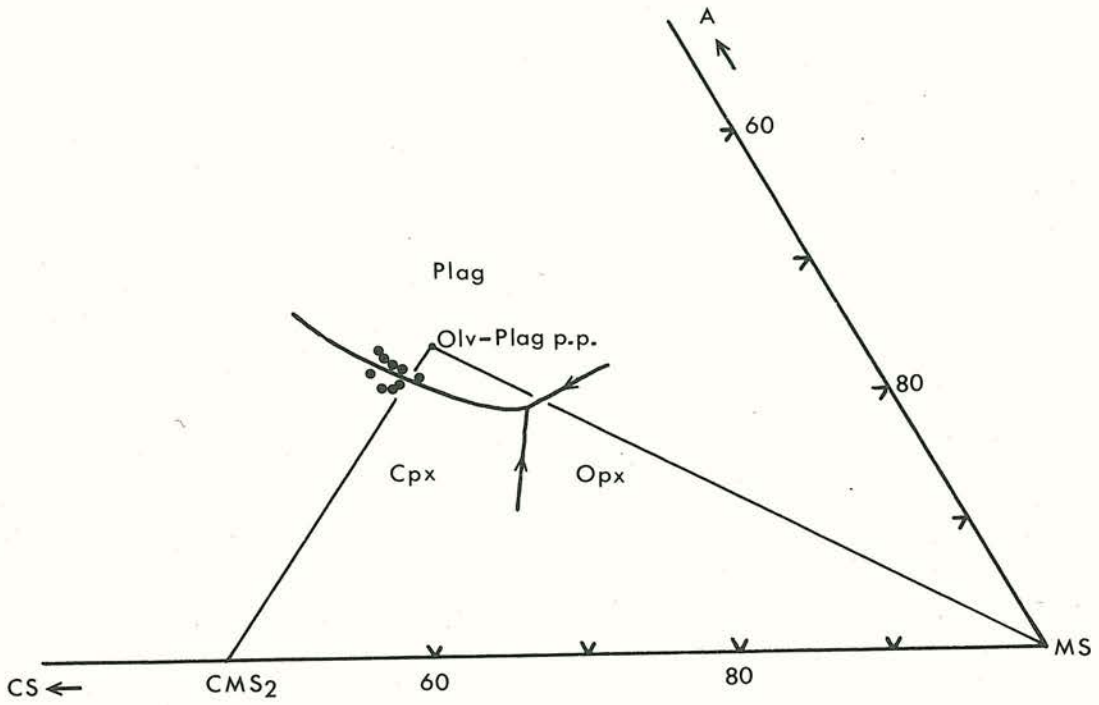

30
26
22
18
14
10
6
2
4
8
12
CaO
SiO2
Al2O3
Fe2O3T
TiO2
K2O
P2O5
Na2O
MgO

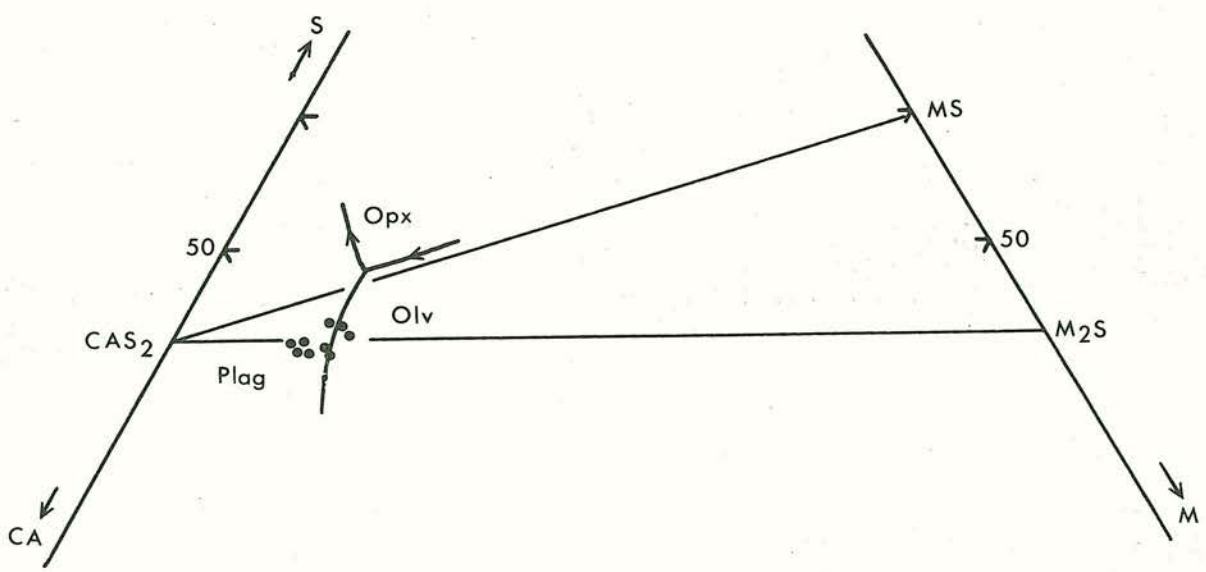
been noted that the position of the phase boundaries varies with the K_2O, TiO_2, and Fe_2O_3 content of the melts (Jamieson, 1969; Humphries, personal communication). This movement is partly the result of changing bulk composition of the melts and partly due to the projection method (O'Hara, 1968, p. 86). Fig. 5-13 shows the subprojection from or towards olivine (M_2S) into the plane CS-MS-A of the Roccamonfina olivine basalts, and Fig. 5-14 shows the subprojection from or towards diopside (CMS_2) into the plane CA-M-S. The position of the phase boundaries are taken from O'Hara (1968) and Jamieson (1970). It can be seen that the olivine basalts plot very close to the cotectic olivine+clinopyroxene+plagioclase+liquid (i.e. the Atmospheric Pressure pseudo-univariant equilibrium olivine+cpx+plagioclase+liquid), the lower K_2O group (R.114,117,119, 184) plotting further away from the cpx-plagioclase piercing point than the higher K_2O group (R.56,57,86,157,158).

The C.I.P.W. norms for the olivine basalts (Appendix C) show that they lie close to the olivine gabbro divide in the system Qz-An-Di-Fo-Ne (Yoder and Tilley, 1962).

This petrographic, extract diagram, and projection evidence suggests that fractionation of olivine gabbro from the olivine basalts could produce the observed trend towards the more salic hy and Qz normative derivatives.

A clinopyroxene inclusion containing traces of red spinel was observed in R.57. This suggests a period of fractionation at higher pressures when the cpx-spinel assemblage was stable, i.e. c. 10 - 15Kb (O'Hara, 1968).


A
60
80
Plag
Olv-Plag p.p.
Cpx
Opx
MS
CS
CMS2
60
80


S
MS
Opx
50
50
Olv
CAS2
M2S
Plag
CA
M

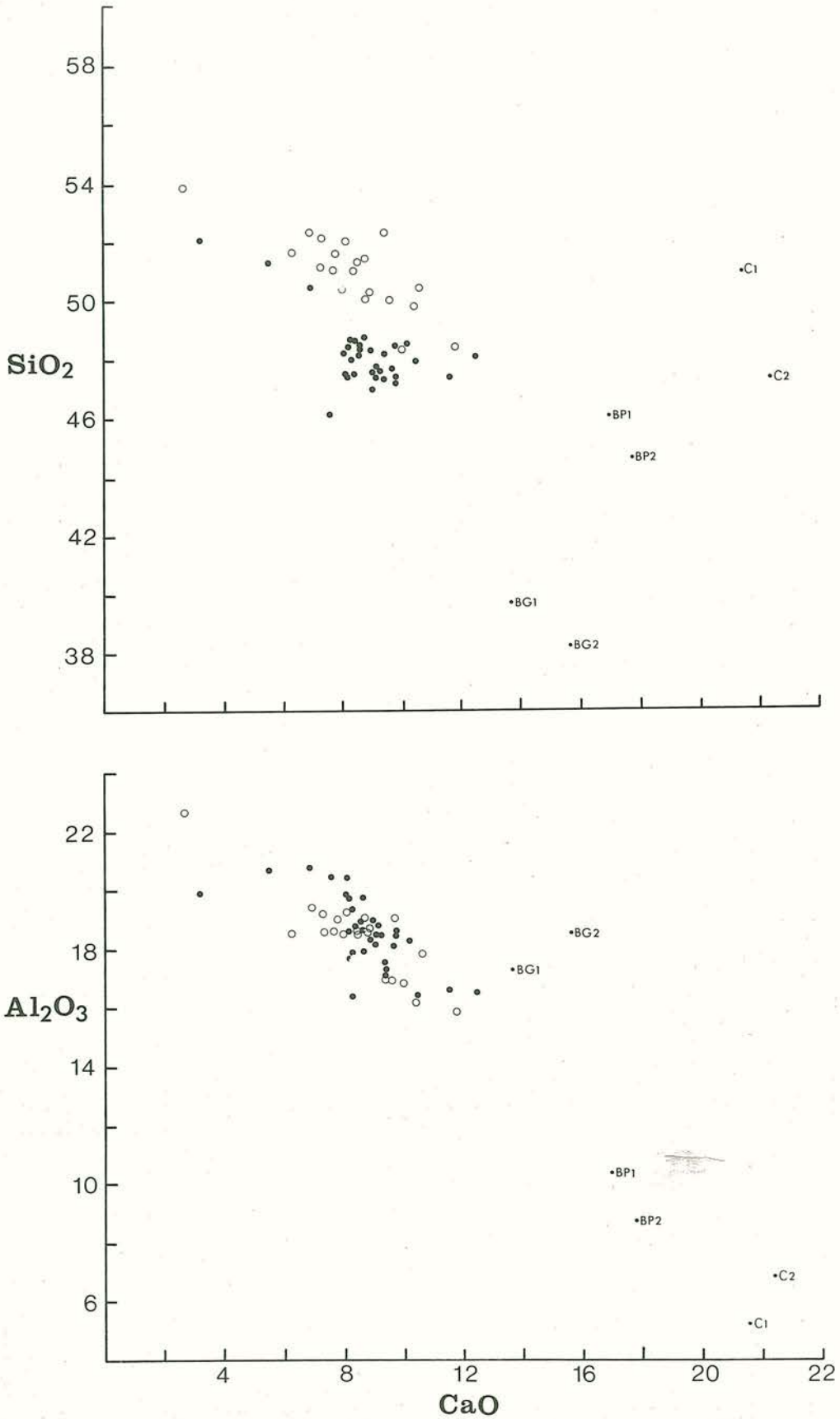
The genetic connection between the Trachytic grey ash flow and the latites is not clear. It is not even certain if the grey ash flow was erupted from the Roccamonfina volcano or whether it was erupted from a fissure to the east of the Roccamonfina area (see Chapter 1). The variation diagrams (Fig. 5-11) show a close genetic relationship between the trachytic grey ash flow and the rest of the Low K series. A similar fall off of Ba and Sr in the extreme salic differentiates is observed in the lavas of the High K series. This is presumably related to the fractionation of plagioclase + K-feldspar (see Berlin and Henderson, 1969, for $D_{wr}^{feldspar}$.)

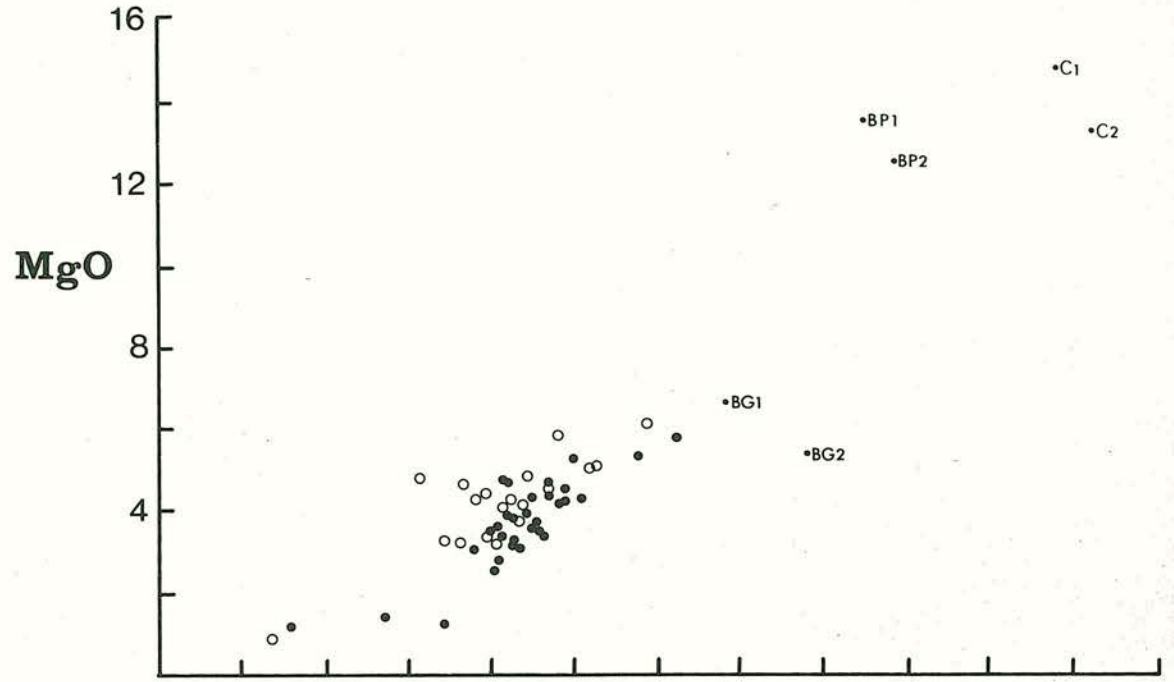
5:3 Differentiation of some of the other volcanic sequences in the Roman Region

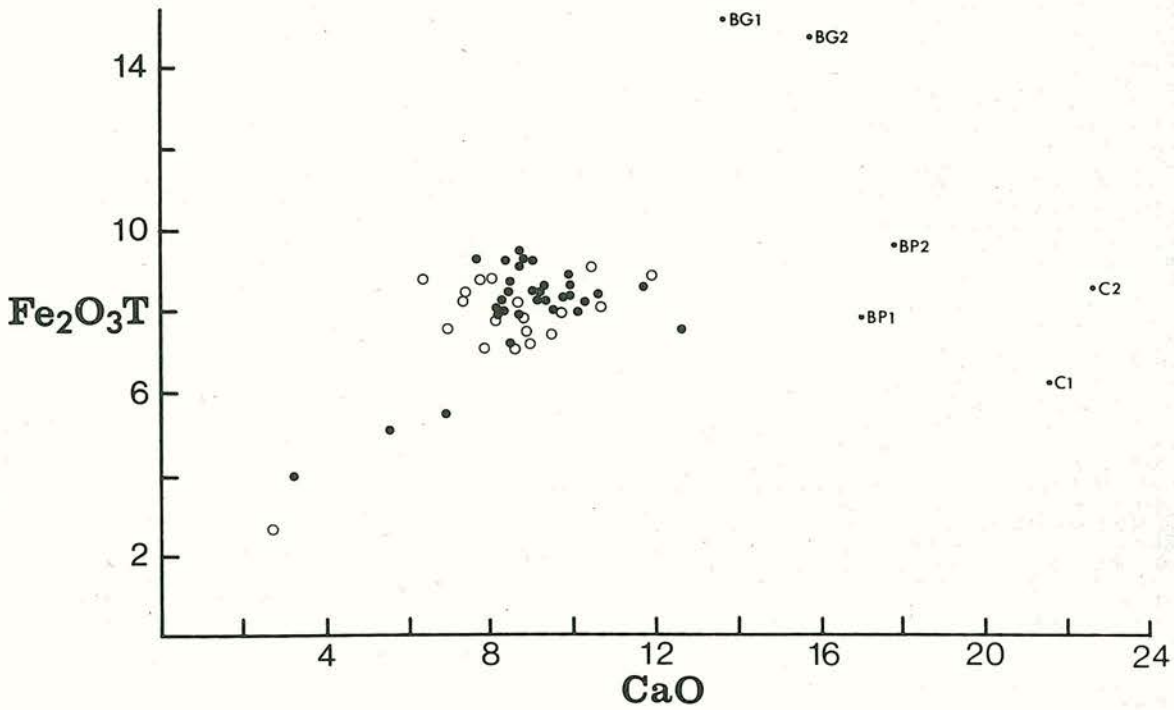
The importance of biotite pyroxenite as a possible parent/crystal cumulate for the potassic lavas of the Roman Region has been noted by Rittman (1933), Holmes and Harwood (1937), Fornaseri (1951), Fornaseri et al. (1963), and Cundari and Le Matire (1970). Cundari and Le Maitre (1970) suggested that the parental magma for the Roman Region had a composition equivalent to the average biotite pyroxenite nodule from Somma-Vesuvius (see analysis Table 5-2). Fractionation of ± 70% of a pyroxenite of slightly more basic composition (though still containing ±2·0% K_2O so that the cumulate must also contain biotite/phlogopite) under "subvolcanic" pressure regimes gave residual liquids equivalent in composition to the average Somma-Vesuvius lavas. They suggest that the marked prevalence

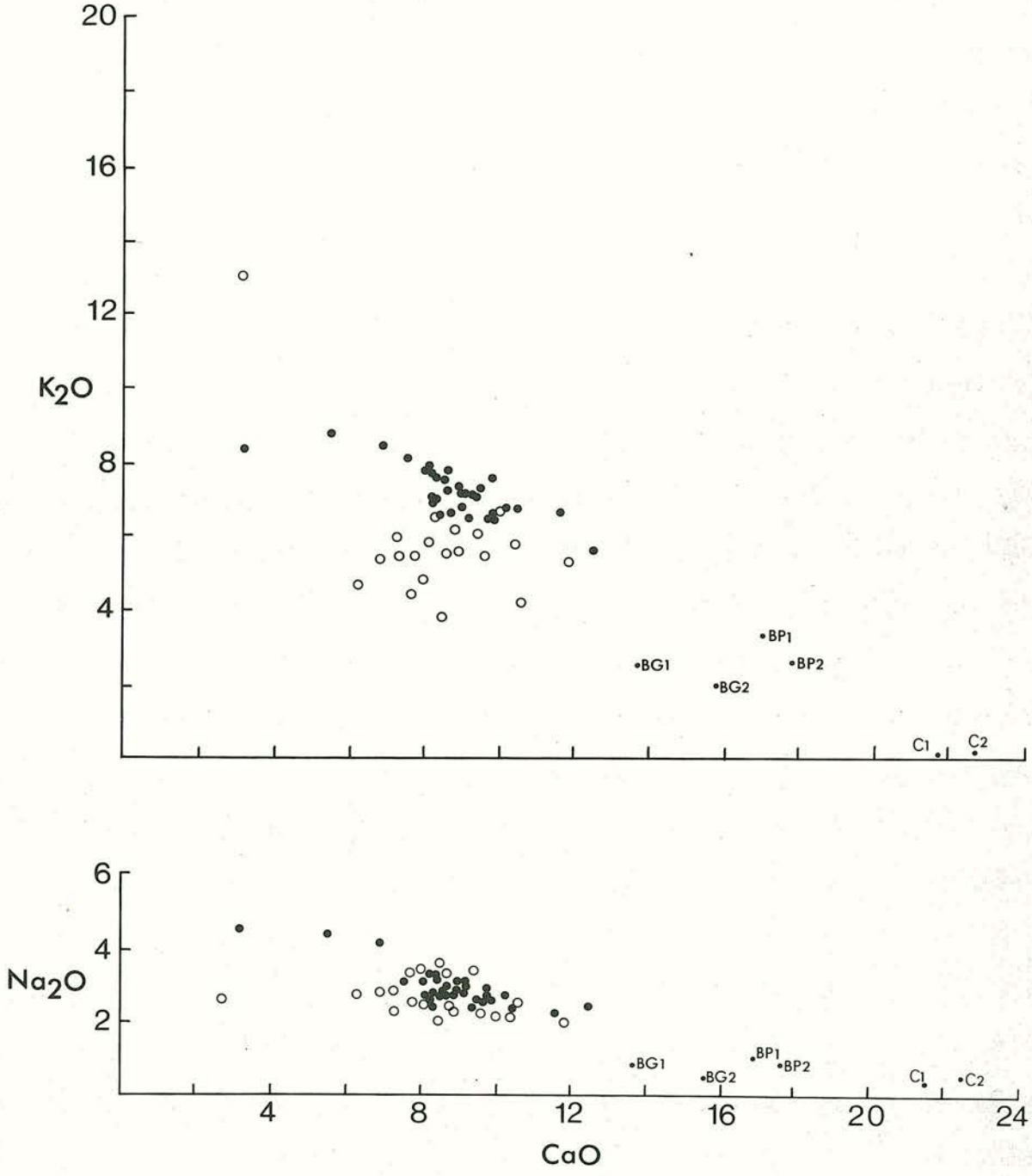
of leucocratic lavas in the Roman Region can be "attributed to extreme fractionation of a magma during its volcanic stage of evolution" (Cundari and Le Maitre, 1970). However, they make no attempt to explain the low pressure (volcanic) evolution of the lavas. On the basis of published data for some of the volcanic centres (especially the Alban Hills), it is extremely difficult to suggest a plausible mechanism of low pressure fractionation, if, indeed, any low pressure fractionation has occurred. It will be impossible to do this until further modal, petrographic, and trace element data is made available.

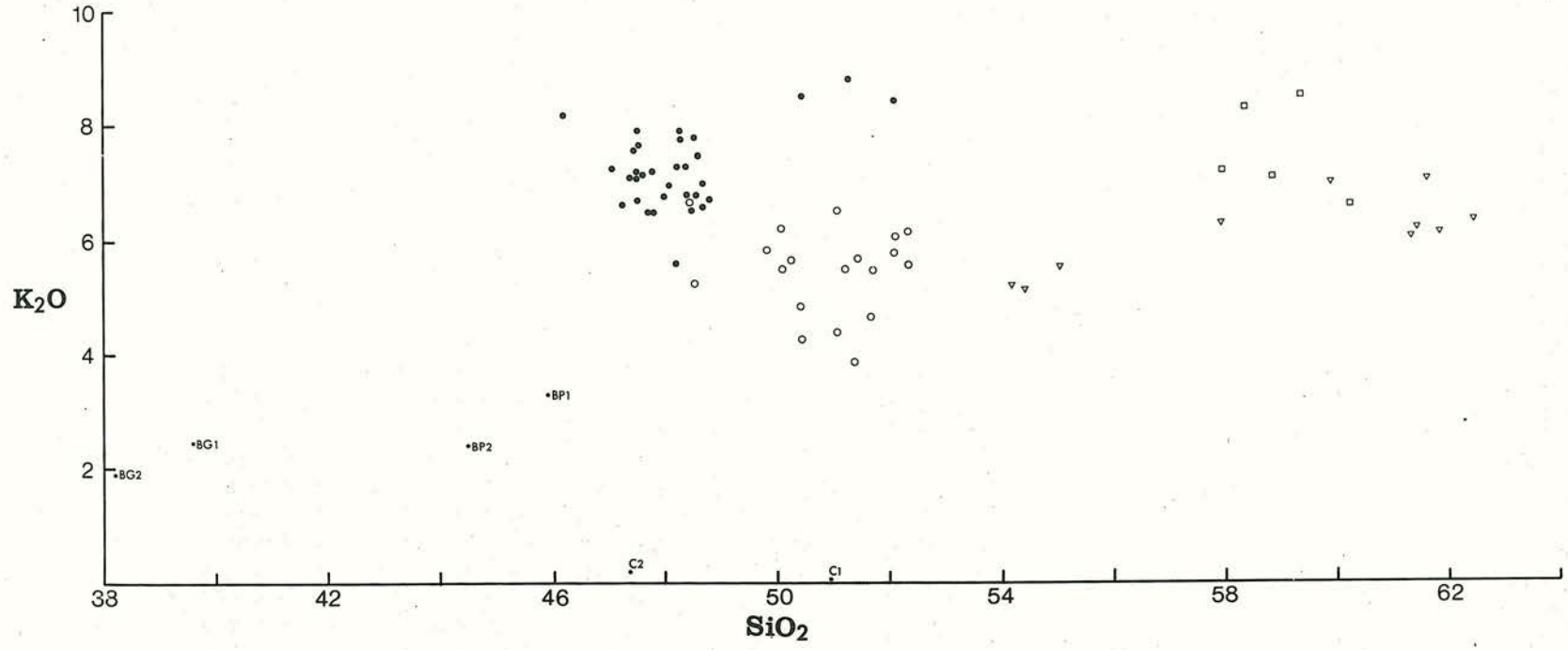
In the case of Somma Vesuvius and Vulsini it is possible to distinguish some definable trends in the analytical data. Both Somma and Vesuvius (Savelli, 1967) exhibit very little chemical variation. Fig. 5-15 shows that the variation in the Vesuvius lavas can be explained by fractionation of clinopyroxene (clinopyroxene nodules are very common amongst the ejectamente of the Vesuvius cone) and biotite pyroxenite. The variation within the Somma lavas is more difficult to understand in detail. It can be seen from the K_2O v. SiO_2 plot (Fig. 5-16) that the Phlegrean trachytes may be low pressure differentiates of a Somma-type parental magma. As noted by Cundari and Le Maitre (1970) the compositions of the glassy phonolitic products of the Plinian eruption of Vesuvius plot close to the ternary join in the system Ne-Ks-SiO_2 (Hamilton and MacKenzie, 1965) with compositions approaching the low temperature minimum for phonolitic compositions. It is interesting to note that the residual glass (Vesuv Glass -

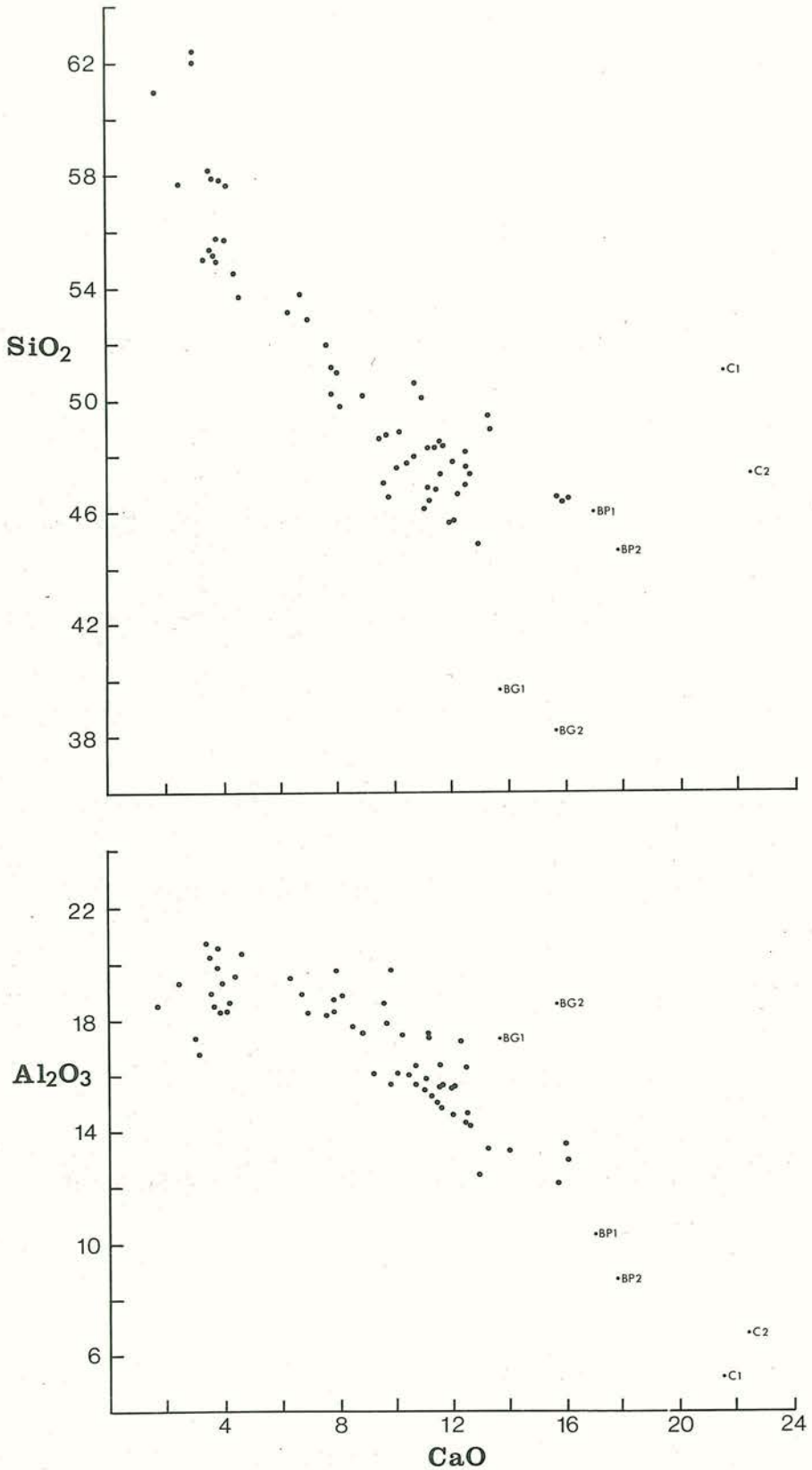

58
54
50
46
42
38
SiO2
C1
C2
BP1
BP2
BG1
BG2
22
18
14
10
6
Al2O3
4
8
12
16
20
22
CaO

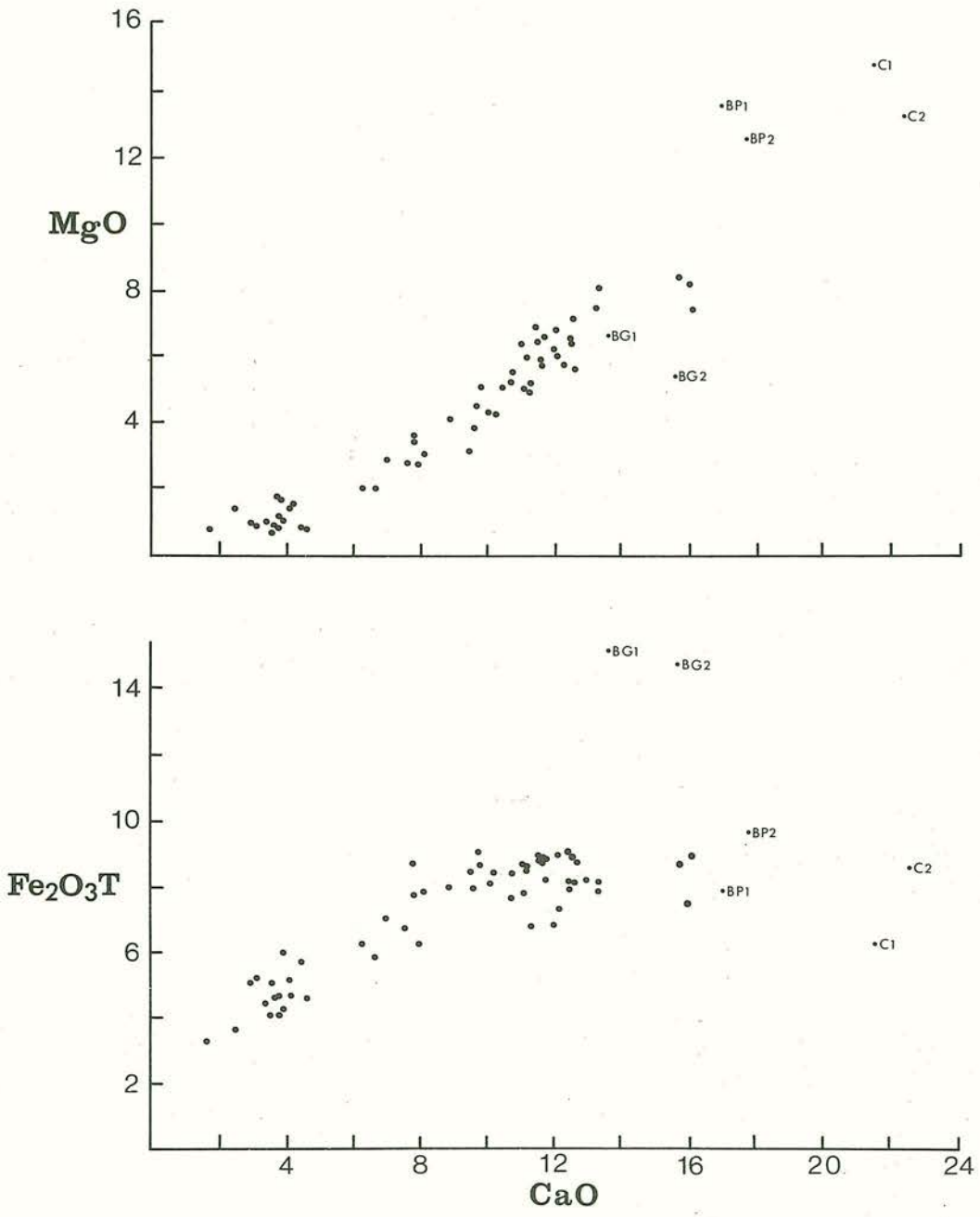

16
12
8
4
MgO
C1
BP1
C2
BP2
BG1
BG2


14
10
6
2
Fe2O3T
BG1
BG2
BP2
C2
BP1
C1
4
8
12
16
20
24
CaO


20
16
12
K_2O
8
4
BP1
BG1
BP2
BG2
C1
C2
6
4
Na_2O
2
BG1
BP1
BG2
BP2
C1
C2
4
8
12
16
20
24
CaO


10
8
6
4
2
K_2O
BG1
BG2
BP1
BP2
C2
C1
38
42
46
50
54
58
62
SiO_2


62
58
54
50
46
42
38
SiO2
C1
C2
BP1
BP2
BG1
BG2
22
18
14
10
6
Al2O3
BG2
BG1
BP1
BP2
C2
C1
4
8
12
16
20
24
CaO


16
12
8
4
MgO
•C1
•BP1
•C2
•BP2
•BG1
•BG2
14
10
6
2
Fe_2O_3T
•BG1
•BG2
•BP2
•C2
•BP1
•C1
4
8
12
16
20
24
CaO

Appendix E) from a Vesuvius leucite basanite has a similar composition. Both these facts suggest that the Plinian lavas were derived by the systematic process of crystal-liquid fractionation rather than by vapour transfer etc.

The variation diagrams for the Vulsini volcanic centre (Fig. 5-17) show similar trends to those observed in the Roccamonfina High K series (see Section 5-1 above). Biotite pyroxenite followed by biotite gabbro appear to be the most plausible crystal extracts.

5:4 Summary

A polybaric model of crystal liquid fractionation is proposed to account for the differentiation of the lavas of the Roccamonfina volcano. The basic features of this model are also applicable to the lavas of the Vulsini centre. Stage 1 is applicable to the lavas of the Roman Region in general.
Three main stages have been recognised:

(1) Derivation of parental magmas with varying contents of K and associated elements as a result of an intermediate or high pressure fractionation event.

(2)(a) Fractionation of biotite pyroxenite followed by biotite gabbro at c. 1·5 - 2·5Kb P_{H2O} to produce the lavas of the High K series.

(b) Fractionation of olivine gabbro to produce the lavas of the Low K series.

(3)(a) After pressure release, fractionation of leucite by flotation slightly modifies the composition of liquids derived from Stage 2a. Late stage fractionation of plagioclase and K-feldspar produces the phonolitic derivatives with low Ba and Sr.

(b) Same as Stage 2b above, followed by fractionation of biotite-plagioclase-clinopyroxene-ore. If the grey ash flow is derived from the same magma that produced the lavas of the Low K series, then fractionation of plagioclase + K-feldspar must have taken place to reduce Ba and Sr to the observed level.

CHAPTER 6

ENRICHMENT PROCESSES

6:1 Introduction

It has been demonstrated in the previous two chapters that the chemical variation observed within the lavas of the Roman Region can be related to two main differentiation processes. A high or medium pressure differentiation process produces parental magmas with different levels of enrichment in K and associated elements, whilst low pressure crystal-liquid fractionation controls the evolution towards salic differentiates. In this chapter it will be demonstrated that crustal assimilation and gaseous transfer processes cannot account for the chemical variation observed in the primitive lavas of the Roman Region (see Chapter 4, Section 4:4:2), nor for the geochemical characteristics of potassic undersaturated lavas in general.

The variation in the level of enrichment of K and associated elements in the primitive lavas of the Roman Region is similar to that observed in basalts, therefore it may be assumed that the mechanisms that have been proposed to explain the variation of K and associated elements in basalts (summarised by Jamieson and Clark, 1970) are also applicable to the lavas of the Roman Region. In the case of the potassic undersaturated lavas it must be assumed that the enrichment process has operated to a greater extent than in basaltic lavas. High and medium pressure (upper mantle) enrichment processes and their application to the potassic lavas of the Roman Region are discussed in the final section of this chapter.

6:2 Enrichment processes involving crustal assimilation

6:2:1 Introduction

Leucite bearing lavas are characteristically confined to continental areas though they have also been recorded in the Cape Verde Islands (Part, 1950), the Kerguelen Archipelago (Edwards, 1938), the Marquesas (Lacroix, 1931), and Tristan da Cunha (Baker et al., 1964). Of these, only Tristan da Cunha is a truly oceanic island. The potassic lavas of the Roman Region were erupted after the orogenic activity which led to the formation of the Apennines, i.e. during the period of post-orogenic relaxation of stress in the lithosphere. This close relationship between potassic undersaturated lavas, orogenesis, and the presence of continental crust obviously suggests that the high K_2O content of the lavas may be related to the assimilation of crustal material during orogenesis, and eruption during the period of post-orogenic relaxation. Alternatively, the highly alkaline nature of the lavas may be related to the possibility that continental primary magmas are generated at a greater depth than oceanic magmas because of the nature of the continental geotherm (Clark and Ringwood, 1964). As these magmas would have to traverse a considerable thickness of mantle and crust (up to 120 km.), they would be more susceptible to enrichment by wall-rock reaction processes (see below).

Enrichment processes involving the assimilation of crustal material will be discussed under the following headings:

(1) Carbonate assimilation.

(2) Assimilation and hybridisation.

(3) Significance of Sr_{87}/Sr_{86} ratios.

(4) Crustal wall-rock reaction.

6:2:2 Carbonate assimilation

Following the ideas of Daly (1910) and Shand (1922), Rittman (1933) proposed that the sequence of lavas erupted from Somma-Vesuvius was the result of the assimilation of dolomitic limestone by a parental trachytic magma already rich in potassium. According to Rittman (1933, 1962), removal of soda in volcanic gases produced the high K/Na ratios which are characteristic of these lavas. This hypothesis is still widely accepted by European geologists, e.g. Arevalo et.al., (1962), Hieke-Merlin (1964, 1967), Gianetti (1965), Schneider (1965), Marinelli and Mittempergher (1966), Marinelli (1967), Locardi and Mittempergher (1967), and Burri (1968).

Schneider (1965) and Burri (1968) have slightly modified Rittman's original carbonate assimilation theory. They suggest that the leucite-bearing lavas are produced as a result of the desilication of a potassic trachybasaltic magma rather than a trachytic magma. On the basis of major element data, Burri (1968) proposes that there is a primary "Tyrrhenian" magma typified by the potassic trachybasalts of Radicofani, Roccamonfina, Stromboli, Mte. Vulsini, Mte. Amiata etc. (see Burri, 1968). However, both trace and major element data presented in this thesis for trachybasalts from Roccamonfina (Table C-4, analyses R.186-189) and Radicofani (Table E-4) show that these two have had considerably different petrogenetic histories. This throws some doubt on Burri's proposal.

Schneider (1965) describes in detail the various mixtures of dolomitic limestone + trachybasalt (followed in some cases by fractionation of clinopyroxene) that can account for the chemistry of the leucite-bearing lavas. However, the new trace element data presented in Table 6-1 show that models similar to that proposed by Schneider (1965, p. 439) whereby 73% trachybasalt + 27% dolomitic limestone = Venanzite or Cupaellite (extremely undersaturated leucite, kalsilite, melilite bearing lavas) are impossible.

It is quite obvious that the chemical data presented in Chapter 4, Section 4:4:2, is totally inconsistent with the carbonate assimilation hypothesis. For example, extraction of 20% clinopyroxene from a syntectic magma composed of 80% trachybasalt + 20% dolomitic limestone will produce a magma with reduced SiO_2, but the K_2O, Ba, and Rb will be the same as in the parental trachybasaltic (or trachytic) magma (see Table 6-2). In order to produce the enrichment in K and associated elements that is seen in the leucite bearing lavas of the Roman Region it is necessary to extract large quantities of clinopyroxene from the syntectic magmas. A model of 85% trachybasalt + 15% dolomitic limestone followed by removal of 50% pyroxene (similar to Schneider's model, 1965, p. 437) would produce an enrichment in K_2O, Ba, and Rb of 1·70. Unfortunately it would also produce a magma with 26% Al_2O_3 and <u>minus</u> 4% MgO. The chemical data used for these models is presented in Table 6-2. Use of a trachytic rather than a trachybasaltic parent magma would give higher K_2O and Rb in the syntectic magma, but the problem of Ba and Sr enrichment becomes even more difficult to overcome. There

TABLE 6-1

Carbonate Assimilation Model I

	Trachybasalt[1]	Dolomitic Limestone[2]	Cpx[3]	Venanzite[4]	Cupaellite[4]
SiO_2	53	*	49	42	45
Al_2O_3	19	*	6	10	8
Fe_2O_3T	9	*	7	7	7
MgO	4	12	14	13	11
CaO	9	40	22	15	14
Na_2O	2	*	0·5	1	0·3
K_2O	3	*	*	8	8
TiO_2	0·8	*	1·1	0·7	1·1
P_2O_5	0·3	*	*	0·4	1·0
Ba	620	*	*	880	4220
Zr	150	*	90"	350	940
Y	30	*	*	50	100
Sr	970	270	280"	1600	3340
Rb	160	*	*	570	550
Th	5	*	*	35	85

1 = R.187, Table C-4

2 = Savelli, 1967, p. 347

3 = Mean of 2 cpx. analyses, Table 5-2

4 = Table E-3

* = insignificant

" = mean of 4 cpx. analyses, Table 3-9

TABLE 6-2

Carbonate Assimilation Models II and III

	II 80% Trachybasalt + 20% Limestone minus 20% Cpx.	III 85% Trachybasalt + 15% Limestone minus 50% Cpx.
SiO_2	41	42
Al_2O_3	18	26
Fe_2O_3T	6	6
MgO	3·5	minus 4
CaO	14	6
Na_2O	2	3
K_2O	3	5
Ba	620	1050
Sr	970	1460
Rb	160	275

N.B. Trachybasalt, Dolomitic Limestone and Cpx. analyses are presented in Table 6-1.

are numerous other reasons for rejecting the carbonate assimilation hypothesis, many of which have been noted by earlier workers. These include the following:

(1) Geochemical investigations by Savelli (1967, 1968) indicate that carbonate ejecta from Somma-Vesuvius have suffered from magmatic heat but not from reaction with the magma.

(2) The problem of the availability of enough heat energy for assimilation was noted by Bowen (1922). Recent experimental evidence (Watkinson and Wyllie, 1964, 1969) suggests that a trachytic magma would crystallise before desilication could proceed very far. By inference, the assimilation of granitic crust by carbonatite magma (Holmes, 1950; Bell and Powell, 1969) is also unlikely to produce the observed volumes of potassic undersaturated lavas.

(3) Field evidence (Tilley and Harwood, 1931; Brouwer, 1928, 1945) suggests that carbonate assimilation may only be able to produce strongly undersaturated rocks on a small scale.

(4) Leucite bearing lavas very similar to the Roman Region lavas are found in other areas where there is no possibility of limestone assimilation, e.g. in the Birunga and Toro-Ankole regions of the Western Rift (Holmes and Harwood, 1932; Bell and Powell, 1969).

(5) There is no substantial evidence, such as the presence of secondary Na-rich zeolites, that vast quantities of soda have been removed in the vapour phase, as required by Rittman (1933). The available experimental data suggests that the transportation

of large quantities of solid in the vapour phase is impossible (Luth and Tuttle, 1969).

(6) Liquidus temperatures of the undersaturated potassic lavas are almost certainly higher than those of the postulated trachytic parent magma. If carbonate assimilation was to produce these leucite bearing lavas, the trachytic magma would have to be superheated, which is unlikely.

6:2:3 Assimilation and hybridisation

Hurley et al. (1966) proposed that the mixing of a magma generated by the partial melting of granite or other salic crustal material with an alkali basaltic magma would produce the leucite bearing lavas of the Roman Region. Other crustal assimilation hypotheses have been reviewed by Bell and Powell (1969). The partial melting of granitic/granodioritic rocks and various sediments (and by inference their metamorphic equivalents) whose compositions fall within the system Qz-Ab-Or-An, has been studied by Tuttle and Bowen (1958), Winkler and Von Platen (1960, 1961), Von Platen (1965), Piwinskii and Wyllie (1968), and James and Hamilton (1969). In general, the composition of the first liquid generated on partial melting depends upon (a) P_{H2O}. As water vapour pressure rises the Ab/Or ratio of the liquid increases.

(b) An content. As the An content of the parent rock increases, the temperature of beginning of melting will rise and the liquid composition will contain a higher proportion of or, Qz, and an relative to Tuttle and Bowen's (1958) "granite

minimum". Piwinskii and Wyllie (1969) noted that there was a considerable temperature gap between the melting (at pressures up to 3Kb P_{H2O}) of the KFeldspar-NaFeldspar-Qz and the Hb-Calcic Plag-Bio assemblages in granodiorites/tonalites. Presumably when $P_{H2O} < P_{TOTAL}$, hornblende would be partially to totally replaced by clinopyroxene as a residual phase. This experimental data is probably generally applicable to conditions at the base of the crust (10kb with $P_{H2O} < P_{TOTAL}$), but the residual phases on partial melting would be garnet and clinopyroxene at this pressure. Green and Ringwood (1966) suggested that the presence of rocks of intermediate composition (Eclogite facies, Qz-KNaFeldspar-Garnet-Clinopyroxene assemblage) at the base of the continental crust was compatible with the seismic P-wave velocity data. Partial melting of this Qz-KNaFeldspar-Garnet-Clinopyroxene assemblage would not produce a liquid low in SiO_2 (as suggested by Hurley et al. (1966)). As the average crust has $SiO_2 = \pm 60\%$ (Taylor, 1964) and cpx and garnet SiO_2 contents are 50% and 39% respectively (Deer et al., 1966), the liquid would actually be richer in SiO_2 than the parental rock.

It should also be noted that except for compositions very rich in an, the first liquid produced on partial melting will always contain a substantial quantity of ab, and all the liquids will be Qz normative. It is difficult to see how the assimilation/hybridisation of such liquid compositions by an alkali basaltic magma could produce the increase in K_2O with relatively stable Na_2O and decreasing SiO_2 observed in the transition from the Roccamonfina Low K to High K series.

O'Hara (1968) has noted that the presence of thermal divides severely restricts hybridisation between two liquids either side of the divide to produce a liquid of intermediate composition. Similar restrictions apply to the assimilation of solid material. If assimilation or hybridisation does occur between two compositions either side of the divide, excess precipitation of the minerals of the divide will occur and the residual liquid will move away from the divide. In the case of hybridisation between granitic magma and alkali basaltic (under-saturated) magma (Hurley et al., 1966), an under saturated residual magma would be produced, but excess precipitation of olivine gabbro would lead to removal of Sr, which is completely contrary to the enrichment in Sr seen in the potassic undersaturated lavas. For similar reasons, the hypotheses of Holmes and Harwood (1937), Larsen (1940), and Turner and Verhoogen (1960) are considered to be incapable of producing leucite bearing lavas rich in Sr.

It is concluded that hypotheses involving the wholesale assimilation of crustal material by a basic magma are incapable of producing potassic undersaturated lavas. However, there still remains the problem of the high Sr_{87}/Sr_{86} ratios exhibited by these lavas (Hurley et al., 1966; Bell and Powell, 1969). The significance of the Sr_{87}/Sr_{86} ratios and the processes which can produce lavas with abnormally high Sr isotope ratios are discussed in the next section.

6:2:4 Significance of Sr_{87}/Sr_{86} data

In Fig. 6-1 the Sr_{87}/Sr_{86} data for the Roman Region (Hurley et al., 1966; Hoefs and Wedepohl, 1968) are compared with the Sr isotopic data for oceanic and continental basalts (Gast, 1967). Fig. 6-2 shows a histogram of Sr_{87}/Sr_{86} ratios for samples from (a) Ustica, Linosa, and Pantelleria (Barberi et al., 1969), (b) the Tertiary and Quaternary province of Tuscany (Ferrara, 1968), and (c) the Roman Region (Hurley et al., 1966; Hoefs and Wedepohl, 1968). The Sr_{87}/Sr_{86}, K/Na ratios, and other geochemical features of the Ustica, Linosa, and Pantelleria lavas suggest that they have been derived directly from the Upper Mantle and that the composition of the Upper Mantle in the western Mediterranean is not significantly different from what is considered to be normal. By inference, if the potassic lavas of the Roman Region were derived from the Upper Mantle, their geochemical peculiarities cannot be related to lateral inhomogeneity in the mantle unless inhomogeneity occurs on a relatively small scale. Samples from the Tertiary-Quaternary volcanics and intrusives of Tuscany (Ferrara, 1968) have abnormally high Sr isotope ratios which confirms the chemical and mineralogical evidence (Marinelli, 1961; Barberi et al., 1967) suggesting an anatectic origin for these rocks. The Sr_{87}/Sr_{86} ratios for the lavas of the Roman Region are intermediate between these other two groups of western Mediterranean rocks.

Wholesale assimilation of crustal material as a mechanism for producing the undersaturated potassic lavas of the Roman Region has been rejected (see above) so it is necessary to find an

Fig. 6-1

Histogram of Sr_{87}/Sr_{86} ratios for:-

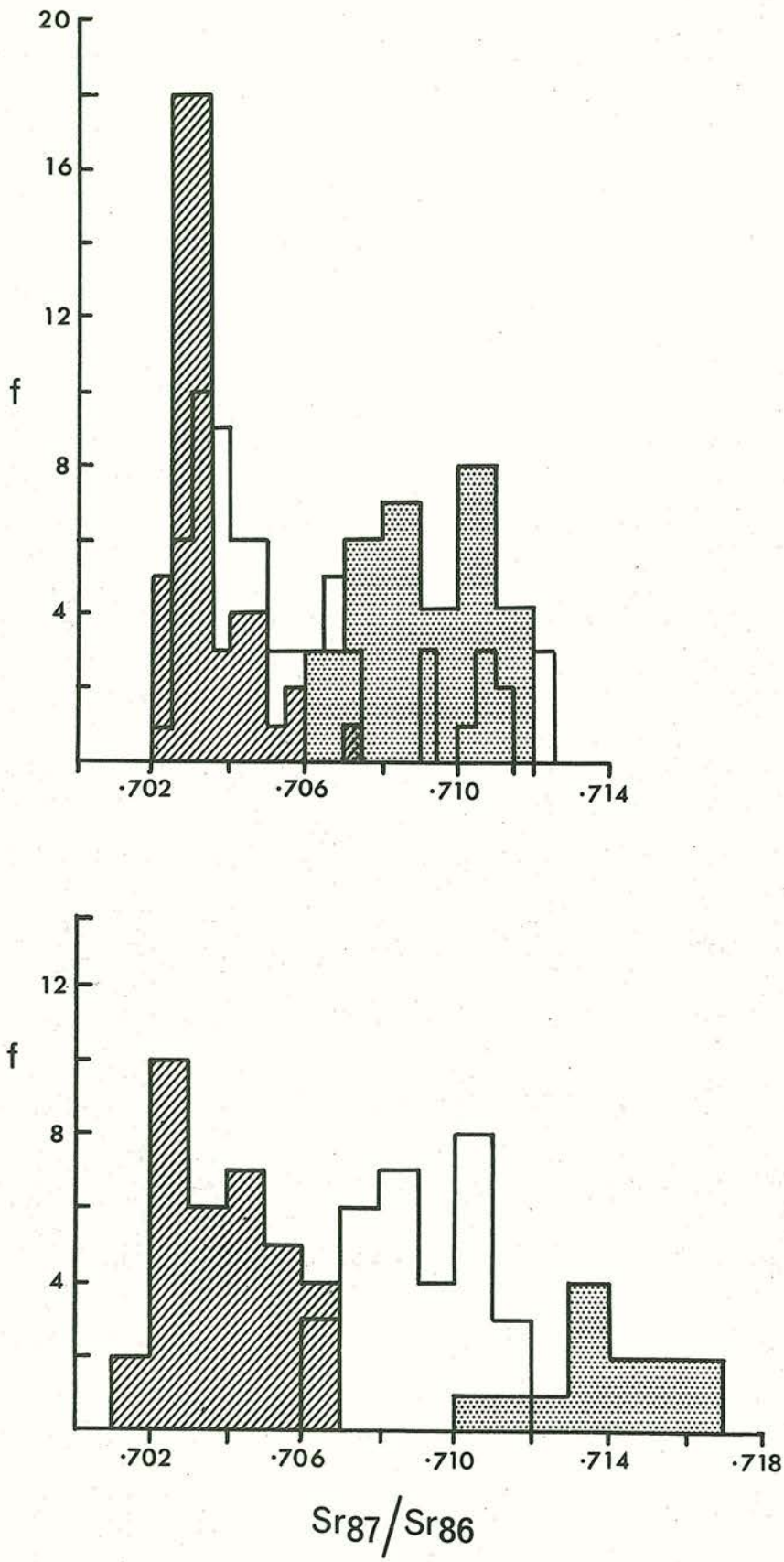
- oceanic basalts (Gast, 1967)
- continental basalts (Gast, 1967)
- Roman Region lavas (Hurley et al., 1966; Hoefs and Wedepohl, 1968)

Fig. 6-2

Histogram of Sr_{87}/Sr_{86} ratios for:-

- Ustica, Linosa and Pantelleria (Barberi et al., 1969)
- Tertiary and Quaternary provinces of Tuscany (Ferrara, 1968)
- Roman Region lavas (Hurley et al., 1966; Hoefs and Wedepohl, 1968)

Vertical scale is frequency (f).


20
16
12
f
8
4
·702
·706
·710
·714
12
f
8
4
·702
·706
·710
·714
·718
Sr87/Sr86

alternative mechanism for producing the observed high Sr isotope ratios. Heir (1964) suggested that a partial melting process operating selectively on high Rb/Sr phases such as biotite and K-feldspar could result in a concentration of radiogenic Sr_{87} in the magma. Hamilton (1968, p. 441) showed the relationship between Sr isotope ratios and Rb and Sr content in different minerals of an ancient granite. Selective assimilation of biotite (Sr_{87}/Sr_{86} = 10·36, Rb = 1867 ppm., Sr = 8 ppm) from a similar granite would substantially increase the Sr isotope and Rb/Sr ratios as well as absolute K_2O, and Rb content of the magma. Green and Ringwood (1967) suggested that the Sr isotope ratios and other geochemical features of some tholeiites from Tasmania and Antarctica could be explained by this process of selective assimilation of crustal material, which they called crustal wall-rock reaction (see next section).

It is interesting to note that the lavas from the Alban Hills (Hurley et al., 1966), i.e. those lavas in the Roman Region which have been affected most by the K and associated elements enrichment process (see Fig. 4-10) also have the highest Sr isotope ratios. The samples from Ischia have the lowest K/Na ratios and also the lowest Sr isotope ratios (Hurley et al., 1966). Presumably the lavas of the Roccamonfina High K series will have higher Sr_{87}/Sr_{86} ratios than the lavas of the Low K series.

If it is assumed that most of the K, Ba, and Rb in the Upper Mantle are held in the accessory phase phlogopite, then it seems possible that lavas with high Sr isotope ratios may be

derived directly from the mantle by the process of zone-refining or mantle wall-rock reaction (see Section 6:3:4 below). However, Powell and Bell (1970) argue that selective incorporation of phlogopite into a melt under Upper Mantle PT conditions would not produce a high Sr isotope ratio because the isotopic equilibration that occurs during metamorphism would also take place under Upper Mantle PT conditions, thus preventing the accumulation of Sr_{87} in grains of phlogopite. As there are no data available concerning the variation of Sr_{87}/Sr_{86} ratios in the minerals of upper mantle xenoliths, it is difficult to clarify this point. Another possibility is that the lavas of the Roman Region originated from a region of the upper mantle characterised by abnormally high Rb/Sr ratios. Previous episodes of partial melting and recrystallisation could have produced zones abnormally enriched in Rb bearing phases. Gast (1967) has noted that variations in Sr isotope ratios for lavas from different oceanic islands can only be related to variations in the Rb/Sr of the mantle source. Thus it seems that such factors as mantle inhomogeneity and selective melting of phlogopite may be important factors in the generation of the rather high Sr_{87}/Sr_{86} ratios observed in potassic lavas.

6:2:5 Crustal wall-rock reaction

According to Green and Ringwood (1967) lavas enriched in K and associated elements as a result of selective reaction between a magma and its wall-rock will show different geochemical characteristics if the enrichment occurs in a crustal environment than if it occurred whilst the magma was rising through the upper

mantle. These differences are related to the fact that Sr and probably also Ti become compatible elements in a low pressure environment (indeed, Ti may also be classed as a compatible element under high pressure conditions). Magmas enriched in K and associated elements under low pressure conditions should be characterised by rapidly increasing K/Sr and Rb/Sr ratios over a wide range of enrichment, whilst magmas enriched by upper mantle wall-rock reaction should have relatively stable K/Sr and Rb/Sr ratios. The fact that the correlation coefficient between Rb/Sr and K and associated elements in the primitive lavas of the Roman Region is insignificant, suggests that the variation in K and associated elements in these lavas is not related to crustal wall-rock reaction.

Other objections to the crustal wall-rock reaction process are:

(1) If there is a sharp temperature contrast between magma and wall-rock, a protective sheath of chilled magma will form on the sides of the conduit, thus preventing wall-rock reaction (Green and Ringwood, 1967).

(2) The quartz-feldspathic component of crustal material ought to form the lowest melting fraction, thus adding excess SiO_2 to the magma (O'Hara and Yoder, 1967).

(3) It requires migration of magma through a very diffuse system of small channels. As soon as these channels or conduits become enlarged it is unlikely that the crustal wall-rock reaction process could operate efficiently (Gast, 1968).

(4) There is the problem of producing equal or greater enrichment in successive batches of magma coming up the same conduit (O'Hara, 1968, p. 117).

6:3 Gaseous transfer

Some Italian geologists have relied upon the rather poorly defined process of gaseous transfer (otherwise known as volatile transfer, gaseous diffusion, pneumatolytic differentiation, or filtration) to explain the high content of K and associated elements in some of the Tertiary and Quaternary lavas of Western Italy (Marinelli, 1961, 1967; Marinelli and Mittemperghер, 1966; Locardi and Mittemperghер, 1967). As Bowen noted (1928, p. 282), "To many petrologists a volatile component is exactly like a Maxwell demon; it does just what one may wish it to do." Marinelli and Mittemperghер (1966) suggest a complex process of differentiation by "filtration" to explain the generation of the slightly undersaturated potassic trachyte of the Mediterranean "base magma" from an "anatectic" magma of similar composition to the late Tertiary acid lavas of Tuscany. They suggest that a flux of volatiles containing the metallic ions K, Fe, Mg, Mn and minor components (U, Th, F, Zr, B, Be) will migrate under a pressure gradient. These authors, together with Marinelli (1961, 1967), and Locardi and Mittemperghер (1967) all agree that although the "fundamental" potassic trachytic magma is produced by a complex process of filtration and fractional crystallisation of an anatectic magma, the strongly undersaturated potassic magmas giving the leucite

bearing or even melilite/kalsilite bearing lavas can only form if an already K-rich magma becomes desilicated as a result of the assimilation of carbonates. As noted in Section 6:2:2 above, the present writer has completely rejected the carbonate assimilation hypothesis. Savelli (1967) also rejects this hypothesis and suggests that gaseous transport (of alkalis and silica) may be important. He refers to the work of Richter and Moore (1966) in Hawaii as being a good example of gaseous transport. Unfortunately, re-analysis of the samples from the Kilauea Iki lava lake (Peck, personal communication in MacDonald, 1968) has cast doubt on Richter and Moore's original data.

Rittman (1933, 1962), in his discussion on the origin and evolution of the Somma-Vesuvius lavas suggests that following carbonate assimilation the K/Na ratio is increased as a result of the removal of soda in volcanic gases. Experimental evidence concerning the distribution of elements between silicate melt and co-existing vapour phase is very limited for major elements and non-existent for trace elements. Morey (1957), and Luth and Tuttle (1969), have shown that Na_2O and SiO_2 are preferentially concentrated in the vapour phase in equilibrium with silicate melts. However, Luth and Tuttle (1969) also noted that only small quantities of solid can be dissolved in the vapour phase in equilibrium with granitic melts (e.g. at 5kb the vapour can only dissolve 6% of solid). Therefore if there was 10% water in the melt, complete removal of this water in the vapour phase (which would be unlikely) would take with it a maximum of 0·6% solid.

Also, it is worth noting that the absence of amphibole from the phenocryst and nodule assemblages of the potassic lavas of the Roman Region suggests that there was no free vapour phase whilst the magma was undergoing differentiation at low pressure.

It is concluded that although vapour transfer could account for a slight increase in the K/Na ratio in the melt (assuming that a vapour phase existed), it cannot account for the high absolute K content. The absence of abundant soda bearing zeolites in the lavas of the Roman Region also suggests that the removal of Na in the vapour phase was only of minor importance.

6:4 Upper mantle enrichment processes

As noted at the beginning of this chapter, the chemical variation observed in the primitive lavas of the Roman Region is consistent with upper mantle enrichment processes. These are now discussed under the following headings:

(1) Enrichment factors

(2) Partial melting

(3) Crystal-liquid fractionation

(4) Zone refining/mantle wall-rock reaction

6:4:1 Enrichment factors

It is convenient to use a postulated primitive (i.e. unmodified) upper mantle composition as a base level for the calculation of enrichment factors. The garnet lherzolite in kimberlite model for the composition of the upper mantle (O'Hara, 1968, 1970) is accepted as being one of the most plausible models

for upper mantle composition. Carswell and Dawson's average of 15 garnet peridotite nodules (Table 3, 1970) is taken as being representative of the major element composition of the primitive upper mantle peridotite. The value for K_2O is probably too high because of contamination by the host kimberlite. The trace element content of the upper mantle is very difficult to assess directly from the nodule compositions because it seems likely that any fragment of the upper mantle will have lost a high proportion of its incompatible elements even if it has undergone only a very small degree of partial melting. Also, garnet lherzolite nodules in kimberlite are likely to have been contaminated by the enclosing magma which is extremely rich in incompatible elements (i.e. K, Rb, Ba, Zr, Sr, etc.) Griffin and Murthy's (1969) hypothetical K, Ba, Sr, and Rb values for anhydrous garnet peridotite are accepted for the purpose of the present study as being a reasonable estimate for the primitive upper mantle. The values for Zr and Zn are taken from Vinogradov (1962) and the Th value from Green et al. (1968).

Enrichment factors (E^1_{um} = concentration of element in lava/concentration of element in upper mantle) for K and associated elements are presented in Table 6-4 for average Roccamonfina, Alban Hills, and Latera-Vulsini analyses. Enrichment factors for average Somma and Vesuvius lavas (Savelli, 1967) and average basalts (Manson, 1967; Prinz, 1967) are presented for comparison. The basic analytical data are presented in Table 6-3. Perhaps of greater importance than the E^1_{um} factors is the variation in E

TABLE 6-4

E^{1}_{um} factors for Average Analyses - see page facing Table 6-3 for source of data

	1	2	3	4	5	6	7	8	9	10	11
K_2O	55	135	180	320	490	530	635	415	550	665	455
P_2O_5	10	25	15	15	25	20	25	30	30	25	20
Ba	15	40	55	50	100	85	115	120	155	150	80
Zr	4	5	4	6	9	7	9	9	10	11	8
Sr	30	70	55	65	105	110	145	50	60	100	80
Rb	60	125	255	415	1020	870	1060	520	540	1220	1080
Th	-	-	70	170	455	430	585	-	-	630	455
Zn	-	-	2·5	2·7	2·2	2·8	3·0	2·7	2·7	2·1	2·2

TABLE 6-5

E_{min}^{max} factors for Roman Region primitive lavas

K_2O	3·5
P_2O_5	3·0
Ba	4·0
Zr	3·5
Y	2·0
Sr	3·5
Rb	5·5
Th	~ 5·5 *
Ce	~ 3·0 **

* Th factor adjusted - see text

** Ce factor based on Roccamonfina data only - see Fig. 4-4

within the primitive lavas of the Roman Region. When dealing with E factors for a single lava sequence it is only possible to compare the concentrations of the various elements with their concentrations in a postulated upper mantle. However, by using the data presented in Chapter 4 of this thesis, it is possible to illustrate the variation of E for different elements over a wide range of enrichment. E_{min}^{max} factors for the primitive lavas of the Roman Region are presented in Table 6-5 (E_{min}^{max} = max. conc. of element in primitive lavas/min. conc. of element in primitive lavas; due to the poor precision of the Th determinations, E_{min}^{max} for Th was adjusted to 5·5). Although there is a very wide variation in the E_{um}^{1} factors for the different elements in the group of K and associated elements (see Table 6-4), the E_{min}^{max} factors for the primitive lavas of the Roman Region are all of the same order (mean = 4, range = 2·0 - 5·5). On the basis of the data for one province it is probably unwise to place too much significance on the relatively small differences between the E_{min}^{max} factors for the different elements - this should only be attempted when data are available for other provinces showing a similar variation in K and associated elements in the primitive lavas. However, the constancy of E_{min}^{max} factors for K and associated elements (K, Ba, Zr, Y, Sr, Rb, Th, Ce) shows that the enrichment process operated to approximately the same extent on all the elements in the group over a relatively wide range of enrichment. This virtually rules out crustal wall-rock reaction as the major enrichment process (see above, Section 6:2:5). The wide variation of E_{um}^{1} in the K and associated elements group suggests

that either the postulated upper mantle composition is incorrect, or that different elements were abstracted from the source rock in significantly different proportions depending upon D^{xstal}_{liquid} for the different upper mantle minerals.

6:4:2 Partial Melting

It seems probable that a large proportion of the K and associated elements in the upper mantle are held in the accessory phases phlogopite (Kushiro et al., 1967), amphibole (Oxburgh, 1964; Lambert and Wyllie, 1968), apatite and zircon. The stability of these minerals under possible upper mantle PT conditions are of obvious importance. Recent experimental evidence has shown that amphibole is probably stable down to about 85 km (Kushiro, 1969) and that phlogopite will be stable at greater depths (± 120 km., Kushiro, 1969; Yoder and Kushiro, 1969). Yoder (1969) has shown that the stability field of phlogopite expands in the presence of CO_2 which appears to be relatively insoluble in the liquid in equilibrium with phlogopite. If CO_2 is present in the upper mantle, the assumption of vapour-absent conditions will have to be re-examined. If the primary magmas for the Roman Region potassic lavas are generated in the region of the upper mantle low velocity zone (top of low velocity zone is approximately 125 km below the Italian peninsula (Ritsema, 1969)) then phlogopite, but not amphibole, would be stable at this depth if the mantle was completely solid. Partial melting of garnet peridotite containing accessory phlogopite would produce liquids with Rb/Sr ratios closest to those observed in the primitive lavas of the Roman

Region (Gast, 1968; Griffin and Murthy, 1969). The importance of the degree of partial melting to the level of enrichment of K and associated elements has been noted by Harris (1967), Gast (1968), O'Hara (1968), and Griffin and Murthy (1969). O'Hara suggests that extraction of magma is unlikely to occur before 5% liquid has been generated, so the maximum E factor related directly to partial melting will be 20. It appears that the observed enrichment of K and associated elements in the primitive lavas of the Roman Region cannot be related solely to partial melting of the postulated primitive upper mantle because the absolute levels of E^{1}_{um} are too high (see Table 6-4).

6:4:3 Crystal-liquid fractionation

Low pressure crystal-liquid fractionation cannot account for the variation of enrichment of K and associated elements observed in the primitive lavas of the Roman Region (see Chapter 5). High pressure (25-40 kb) fractionation of eclogite from primary picritic magmas will enrich the residual liquids in K and associated elements (O'Hara and Yoder, 1967). The most important geochemical features of eclogite fractionation are the increase in the K/Na ratio and the generation of ne and eventually lc normative magmas. O'Hara and Yoder (1967) suggested that the potassic mafic lavas of the Western Rift (Higazy, 1954; Bell and Powell, 1969) are the products of extensive eclogite fractionation. In comparison with the Western Rift lavas, the more leucocratic lavas of the Roman Region must have been subjected to a larger degree of crystal-liquid fractionation (olivine + pyroxenes) during the rise from the

30-40 kb zone. This extensive medium pressure fractionation is reflected in the low MgO, Cr, and Ni contents of the Roman lavas. Holmes and Harwood (1937) described some leucitites and leucite tephrites from Bufumbira that are remarkably similar to lavas found in the Roman Region, thus suggesting a common enrichment mechanism for the two provinces. However, the Roman lavas have lower TiO_2 and Nb contents than the Bufumbira lavas.

In the primitive lavas of the Roman Region, TiO_2 remains stable over a wide range of enrichment in K and associated elements suggesting that eclogite fractionation may not be the main enrichment process (assuming that the geochemical effects of this process are as postulated by O'Hara and Yoder, 1967). Alternatively, low pressure fractionation of ulvospinel from liquids saturated with Ti could have led to a depletion in this element.

6:4:4 Zone refining and mantle wall-rock reaction

The results of zone refining (Harris, 1957), mantle wall-rock reaction (Green and Ringwood, 1967), and a small degree of partial melting are virtually indistinguishable except that zone refining and mantle wall-rock reaction appear to be able to produce liquids with much higher E factors.

Mantle wall-rock reaction involves the extraction of the lowest melting fraction from the wall-rock by a magma. The subsolidus mineral assemblages of the upper mantle and the stability of the accessory phases phlogopite and amphibole are critically dependent upon P_{TOTAL}, P_{VAPOUR}, and T. Therefore the composition of the

lowest melting fraction will also vary with P and T. For example, lavas enriched in K, Rb, and Ba and with high Rb/Sr and low K/Rb ratios have probably been involved in wall-rock reaction in a PT regime where phlogopite, but not amphibole, was stable, i.e. in the garnet peridotite regime of the upper mantle at depths > 85 km.

Green (1970) has extended the original concept of wall-rock reaction to include selective migration of elements through a fluid phase (? CO_2, H_2O) or migration of a fluid phase enriched in K and associated elements. However, the question of presence or absence of a fluid phase (or free vapour phase) in the upper mantle is highly speculative.

The present author considers that a model of wall-rock reaction analogous to squeezing water out of a sponge may be more effective than the scheme whereby magma migrates upwards through major conduits. It is envisaged that liquid develops at crystal interfaces during a small degree of partial melting and then nucleates into small globules as the degree of melting increases. These diffuse globules of liquid are squeezed out of the enclosing crystal mush. The liquid migrates upwards through cooler upper mantle incorporating the lowest melting fraction and crystallising the major phases of the upper mantle which the liquid is in equilibrium with. Further concentration of K and associated elements will be brought about as the quantity of liquid decreases. This mechanism is a hybrid of zone refining and mantle wall-rock reaction, differing from the former process in that only a small and decreasing portion of the upper mantle is taken into solution.

6:5 Conclusions

The following conclusions are made concerning the K and associated elements enrichment process:

(1) E_{min}^{max} is of the same order (mean = 4, range = 2·0 - 5·5) for K, P, Ba, Zr, Y, Sr, Rb, Th, and Ce in the primitive lavas of the Roman Region.

(2) E_{um}^{1} factors for these elements are extremely variable.

(3) Ti and Nb may not have behaved as incompatible elements during the enrichment process.

(4) Crustal assimilation, gaseous transfer, crustal wall-rock reaction, and low pressure crystal-liquid fractionation cannot produce the chemical variation observed in the primitive lavas of the Roman Region.

(5) It is unlikely that partial melting of the postulated primitive upper mantle can account for the high E_{um}^{1} factors.

(6) The constant E_{min}^{max} factors suggest that the enrichment process has operated to approximately the same extent on all elements in the group over a wide range or enrichment.

(7) Extensive eclogite fractionation, zone refining, or mantle wall-rock reaction could produce the observed variation of K and associated elements in the primitive lavas of the Roman Region. It is impossible to decide between these enrichment mechanisms on objective grounds because of the assumptions that have to be made concerning the composition of the upper mantle, the behaviour of K and associated elements during these enrichment processes, the distribution of these elements between the upper mantle phases,

and the presence or absence of accessory phases such as phlogopite and amphibole.

(8) When comprehensive major and trace element data becomes available for other volcanic provinces having lava series showing different absolute levels of enrichment in K and associated elements, it may then be possible to discriminate between the effects of the enrichment processes mentioned above.

(9) If the primary magmas for the Roman Region lavas were generated at c. 120 - 140 km depth, there would be adequate opportunity for extensive eclogite fractionation/zone refing/wall-rock reaction to occur.

ACKNOWLEDGEMENTS

I wish to thank my supervisor, Dr. K.G. Cox, for suggesting the study of the potassium-rich lavas of the Roman Region and for his helpful advice and enthusiastic support. I am especially grateful to him for his constructive criticism of the manuscript of this thesis.

Messrs. G.R. Angell and M.J. Saunders provided expert tuition in X-ray fluorescence and wet chemical methods of analysis, respectively.

Dr. D.H. Doff and Mr. H.M. Moores (E.R.C.C.) provided assistance with computing problems, and Dr. R.F. Cheeney and Mr. D.J. Humphries wrote computer programs for the calculation of C.I.P.W. norms.

I am very grateful for the assistance provided by Mr. Colin Chaplin and his technical staff, especially Messrs. Ian Bowler and Robert Brown, who produced the photographs in this thesis.

Professor F.H. Stewart placed the excellent facilities of the Grant Institute of Geology at my disposal and also provided financial support from Departmental funds for field work and the transportation of rock specimens.

This work was carried out during the tenure of an N.E.R.C. Research Studentship (1967-1970).

BIBLIOGRAPHY

AIELLO, R., 1962. Studi petrografici del settore meridionale del vulcano di Roccamonfina. Rend. Acc. Sc; Fis. Mat., Napoli.

AMENDOLAGINE, M., et al., I petrischi del vulcano vicano. Periodico Min., 32, 157-83.

AMENDOLAGINE, M., et al., 1963b. Lave dell' apparato vicano. Periodico Min., 32, 197-249.

AOKI, K. and KUSHIRO, I., 1968. Some clinopyroxenes from ultramafic inclusions in Dreiser Weiher, Eifel. Contr. Mineral. and Petrol. 18, 326-337.

AREVALO, P.C., BURRI, C., and WEIBEL, M. 1962. Zur petrochemie des Roccamonfina-Vulkans (Prov. Caserta, Italien). Schweiz. Min. Petr. Mitt., 42, 237-268.

BAKER, P.E., GASS, I.G., HARRIS, P.G., and LE MAITRE, R.W. 1964. The volcanological report of the Royal Society expedition to Tristan da Cunha, 1962. Phil. Trans. R. Soc., A.256, 439-578.

BARBERI, F., INNOCENTI, F. and MAZZUOLI, R. 1967. Contributo alla conoscenza chimico-petrografica e magmatologica della rocce intrusive, vulcaniche e filoniane del Campigliese (Toscana). Mem. Soc. Geol. It., 6, 643-681.

BARBERI, F., BORSI, S., FERRARA, G. and INNOCENTI, F. 1969. Strontium isotopic composition of some recent basic volcanites of the Southern Tyrrhenian sea and Sicily channel. Contr. Mineral. and Petrol. 23, 157-172.

BARBIERI, M., FORNASERI, M. and PENTA, A. 1968. Rubidium and potassium relationship in some volcanoes of Central Italy. Chem. Geol., 3, 187-197.

BELL, K. and POWELL, J.L. 1969. Strontium isotopic studies of alkali rocks: the potassium-rich lavas of the Birunga and Toro-Ankole regions, East and Central Equatorial Africa. J. Petrol., 10, 536-572.

BERLIN, R. and HENDERSON, C.M.B. 1969. The distribution of Sr and Ba between alkali feldspar, plagioclase and groundmass phases of porphyritic trachytes and phonolites. Geochim. Cosmochim. Acta, 33, 247-255.

BLUM, J.R. 1874. Lehrbuch der Mineralogie. Stuttgart: E. Schweizer-bart'sche Verlag. pp. XV + 642.

BOWEN, N.L. 1914. The ternary system: diopside-forsterite-silica. Am. J. Sci. 38, 207-264.

BOWEN, N.L. 1922. The behaviour of inclusions in igneous rocks. Jour. Geology, 30, 513-570

BOWEN, N.L. 1928. The evolution of the igneous rocks. Princeton: Princeton University Press.

BOWEN, N.L. and ELLESTAD, R.B. 1937. Leucite and pseudoleucite. Am. Miner., 22, 409-415.

BRAUNS, R. 1922. Die phonolithischen gesteine des Laacher Seegebietes und ihre Beziehungen zu anderen gesteinen dieses gebietes. Neu. Jahrb. f. Min., B-B. 46, 1-116.

BRAUNS, R. 1928. Die chemische zusammensetzung der basaltlaven des Laacher Seegebietes. Neu. Jahrb. f. Min. B-B., 56,A, 468-498.

BROUWER, N.A. 1928. Production of trachyte and phonolite from pyroxene andesitic magma associated with limestones. Jour. Geology, 36, 545-548.

BROUWER, N.A. 1945. The association of alkali rocks and metamorphic limestone in a block ejected by the volcano Merapi (Java). Proc. Kon. Akad. Wetensch., 48, 166-189.

BROWN, G.M. 1960. The effect of ion substitution on the unit cell dimensions of the common clino-pyroxenes. Am. Miner., 45, 15-38.

BUIE, B.F. 1941. Igneous rocks of the Highwood Mountains, Montana. Pt. III, Dikes and related intrusives. Bull. geol. Soc. Am., 52, 1753-1808.

BURRI, C. 1968. Potentielle mineralbestände kalitrachybasaltisch-karbonatischer syntektika und die Zunkunft der Vesuvmagmas. Geol. Rund., 57, 744-765.

CARMICHAEL, I.S.E., 1967. The minerology and petrology of the volcanic rocks from the Leucite Hills, Wyoming. Contr. Mineral. and Petrol. 15, 24-66.

CARSWELL, D.A. and DAWSON, J.B. 1970. Garnet peridotite xenoliths in South African kimberlite pipes and their petrogenesis. Contr. Mineral. and Petrol. 25, 163-184.

CHAYES, F. 1962. Numerical correlation and petrographic variation. J. Geol. 70, 440-452.

CHAYES, F. 1964. Variance-covariance relations in some published Harker diagrams of volcanic suites. J. Petrology, 5, 219-237.

CHAYES, F. 1967. On the graphical appraisal of the strength of associations in petrographic variation diagrams. pp.322-339. in Researches in Geochemistry ed. Abelson, P.H., New York, London, Sydney: John Wiley and Sons.

CIVETTA, L., GASPARINI, P. and RAPOLLA, A. 1965. Aspetti dell' evoluzione magmatica del Vulcano di Roccamonfina attraverso misure di radioattivita. Ann. Oss. Ves., S.VI, VII.

CLARK, S.P. and RINGWOOD, A.E. 1964. Density distribution and constitution of the mantle. Rev. Geophys. 2, 35-88.

CROSS, W. 1897. Igneous rocks of the Leucite Hills and Pilot Butte, Wyoming. Am. J. Sci., 4, 115-141.

CUNDARI, A. and LE MAITRE, R.W. 1970. On the petrogeny of the leucite-bearing rocks of the Roman and Birunga volcanic regions. J. Petrology, 11, 33-47.

DALY, R.A. 1910. Origin of the alkaline rocks. Geol. Soc. Am. Bull., 21, 87-118.

DEER, W.A., HOWIE, R.A. and ZUSSMAN, J. 1962a. Rock forming minerals, Volume III. London:Longmans.

DEER, W.A., HOWIE, R.A. and ZUSSMAN, J. 1962b. Rock forming minerals, Volume II. London:Longmans.

DEER, W.A., HOWIE, R.A. and ZUSSMAN, J. 1966. An introduction to the rock-forming minerals. London:Longmans.

DE FINO, M. and MATTIAS, P.P. 1965. La lava di Ferento presso Viterbo. Periodico Min., 34, 219-33.

EDWARDS, A.B. 1938. Tertiary lavas from the Kerguelen Archipelago. Rep. B.A.N.Z. Antarc. Res. Exp., 1929-31 (Series A), 2, 72-100.

EIGENFELD, R.F.W. 1967. Zur petrogenese intermediärer effusiver magmen. Geol. Rund., 57, 296-313.

ERLANK, A.J. 1968. The terrestial abundance relationship between potassium and rubidium. p. 871-888 in Origin and Distribution of the Elements. ed. Ahrens, L.H., Oxford and New York: Pergamon.

FAUST, G.T. 1963. Phase transition in synthetic and natural leucite. Schw. Min. Petr. Mitt., 43, 165-195.

FERRARA, G. 1968. Rapporti fra la composizione isotopica dello Sr e i fenomeni anatettici nelle rocce della provincia anatettica toscana (Abstract). XXV Congr. Soc. It. Min. Petr. Napoli.

FISHER, R.A. and YATES, F. 1957. Statistical Tables for Biological, Agricultural and Medical Research. 5th Edn. Edinburgh: Oliver and Boyd.

FLOWER, M.F.J. 1969. Phlogopite from Jan Mayen Island (North Atlantic). Earth planet. Sci. Lett., 6, 461-466.

FORNASERI, M. 1951. Ricerche petrografiche sul Vulcano Laziale. I proietti inclusi nei tufi. Per. Min., 20, 211-235.

FORNASERI, M., SCHERILLO, A. and VENTRIGLIA, U. 1963. La regione vulcanica dei Colli Albani. Roma: C.N.R.

FRECHEN, J. 1962. Führer zu vulkanologisch-petrographischen Exkursionen im Siebengebirge am Rhein, Laacher Vulkangebiet, und Maaregebiet der Westeifel. E. Schweizerbart'sche Verlagsbuchhandlung, Stuttgart.

FUNDALI, R.F. 1963. Experimental studies bearing on the origin of pseudoleucite and associated problems of alkalic rock systems. Geol. Soc. Am. Bull., 74, 1101-1125.

GASPARINI, P. and ADAMS, J.A.S. 1969. K-Ar dating of Italian Plio-Pleistocene volcanic rocks. Earth Planet. Sci. Letters, 6, 225-230.

GAST, P.W. 1967. Isotope geochemistry of volcanic rocks, pp. 325-358, in Basalts: the Poldervaart treatise on rocks of basaltic composition, eds. Hess, H.H. and Poldervaart, A., New York: Interscience.

GAST, P.W. 1968. Trace element fractionation and the origin of tholeiitic and alkaline magma types. Geochim. cosmochim. Acta, 32, 1057-1086.

GIANETTI, B. 1964. Contributo alla conoscenza del vulcano di Roccamonfina, Nota 1°-Le ultime manifestazioni eruttive della caldera. Bull. Soc. Geol. Ital., 83, 87-133.

GIANETTI, B. 1965. Il vulcanismo secondario trachito-fonolitico della caldera vulcanica di Roccamonfina. Bull. Geol. Soc. Ital., 84, 69-127.

GIANETTI, B. 1966. Su due dicchi di lava del somma primitivo del vulcano di Roccamonfina. Atti. Soc. Tosc. Sc. Nat., Mem., Ser. A., 73, 647-658.

GORANSON, R.W. 1938. Silicate-water systems: phase equilibria in the $NaAlSi_3O_8$-H_2O and $KAlSi_3O_8$-H_2O systems at high temperatures and pressures. Am. Jour. Sci., 35A, 71-91.

GREEN, D.H. 1970. A review of experimental evidence on the origin of basaltic and nephelinitic magmas. Phys. Earth Planet. Int. 3, 221-235.

GREEN, D.H., MORGAN, J.W. and HEIER, K.S. 1968. Thorium, Uranium and Potassium abundances in peridotite inclusions and their host basalts. Earth Planet. Sci. Lett., 4, 155-166.

GREEN, D.H. and RINGWOOD, A.E. 1966. incorrect reference - see Ringwood, A.E. and Green, D.H. 1966.

GREEN, D.H. and RINGWOOD, A.E. 1967. The genesis of basaltic magmas. Contr. Mineral. and Petrol. 15, 103-190.

GRIFFIN, W.L. and MURTHY, V.R. 1969. Distribution of K, Rb, Sr, and Ba, in some minerals relevant to basalt genesis. Geochim. cosmochim. Acta, 33, 1389-1414.

HAMILTON, E.I. 1968. The isotopic composition of strontium applied to the problems of the origin of the alkaline rocks. pp. 437-463 in Radiometric Dating for Geologists, eds. Hamilton, E.I. and Farquhar, R.M. London, New York: Interscience.

HAMILTON, D.L. and MACKENZIE, W.S. 1965. Phase equilibrium studies in the system $NaAlSiO_4$ (nephelinite)-$KAlSiO_4$ (kalsilite)-SiO_2-H_2O. Min. Mag. Tilley Vol., 34, 214-232.

HARRIS, P.G. 1957. Zone refining and the origin of potassic basalts. Geochim. cosmochim. Acta, 12, 195-208.

HARRIS, P.G. 1967. Segregation processes in the upper mantle, pp. 305-317 in Mantles of the Earth and Terrestial planets., Ed. Runcorn, S.K., New York: Interscience.

HEIER, K.S., 1964. Rubidium/Strontium and Strontium-87/Strontium-86 ratios in deep crustal material. Nature, 202, 477-478.

HENDERSON, C.M.B. 1965. Minor element chemistry of leucite and pseudoleucite. Min. Mag., 35, 596-603.

HIEKE MERLIN, O. 1964. Le vulcaniti del settore nord-orientale del Monte Vulture (Lucania). Mem. Ist. Geol. Min. Univ. Padova, 24, 3-74.

HIEKE MERLIN, O. 1967. I prodotti vulcanici del Monte Vulture (Lucania). Mem. Ist. Geol. Min. Univ. Padova, 26, 3-67.

HIGAZY, R.A. 1954. Trace elements of volcanic ultrabasic potassic rocks of southwestern Uganda and adjoining part of the Belgian Congo. Bull. geol. Soc. Am. 65, 39-70.

HOEFS, J. and WEDEPOHL, K.H. 1969. Strontium isotope studies on young volcanic rocks from Germany and Italy. Contr. Mineral. and Petrol., 19, 328-338.

HOLMES, A. 1950. Petrogenesis of Katungite and its associates. Am. Miner. 35, 772-792.

HOLMES, A. and HARWOOD, H.F. 1932. Petrology of the volcanic fields east and south-east of Ruwenzori, Uganda. Q. Jl. geol. Soc. Lond. 88, 370-442.

HOLMES, A. and HARWOOD, H.F. 1937. The petrology of the volcanic area of Bufumbira. Mem. geol. Surv. Uganda, 3, 1-300.

HURLEY, P.M., FAIRBAIRN, H.W. and PINSON, W.H. 1966. Rb-Sr isotopic evidence in the origin of potash-rich lavas of western Italy. Earth and Planet. Sci. Lett., 1, 301-306.

IMBO, G. 1967. incorrect reference - see Hieke Merlin, O., 1967.

IMBO, G., GASPARINI, P., LUONGO, G. and RAPOLLA, A. 1968. Contributions to the volcanological researches by determination of the radioactivity of eruptive products. Bull. Volc., 32, 1-25.

JAMES, R.S. and HAMILTON, D.L. 1969. Phase relations in the system $NaAlSi_3O_8$-$KAlSi_3O_8$-$CaAl_2Si_2O_8$-SiO_2 at 1 kilobar water vapour pressure. Contr. Mineral. and Petrol., 21, 111-141.

JAMIESON, B.G. 1969. The petrology of olivine-rich basaltic rocks, Nuanetsi, Rhodesia. Univ. Edinburgh Ph.D. Thesis (unpubl.)

JAMIESON, B.G. 1970. Phase relations in some tholeiitic lavas illustrated by the system R_2O_3-XO-YO-ZO_2. Mineralog. Mag. 37, 537-554.

JAMIESON, B.G. and CLARKE, D.B. 1970. Potassium and associated elements in tholeiitic basalts. J. Petrology, 11, 183-204.

JOPLIN, G.A. 1968. The Shoshonite association: a review. Journ. Geol. Soc. Austral., 15, 275-294.

KERR, P.F. 1959. Optical Mineralogy. New York, Toronto, London: McGraw-Hill.

KHALIL, H.A. 1966. Geochemical investigations on the lavas of Ischia. Univ. Manchester Ph.D. Thesis (unpubl.)

+

KUNO, H., YAMASAKI, K., IIDA, C. and NAGASHIMA, K. 1957. Differentiation of Hawaiian magmas. Jap. Jour. Geol. Geog., 28, 179-218.

KUSHIRO, I. 1960. Si-Al relations in clinopyroxenes from igneous rocks. Am. Jour. Sci., 258, 548-554.

KUSHIRO, I. 1969. Stability of amphibole and phlogopite in the upper mantle. Yb. Carnegie Instn. Wash., 68, 245-247.

KUSHIRO, I. and AOKI, K., 1968. Origin of some eclogite inclusions in kimberlite. Am. Mineralogist, 53, 1347-1367.

KUSHIRO, I., SYONO, Y. and AKIMOTO, S. 1967. Stability of phlogopite at high pressures and possible presence of phlogopite in the Earth's upper mantle. Earth planet. Sci. Lett. 3, 197-203.

LACROIX, A. 1917. Les roches grenues d'un magma leucitique étudiées à l'aide des blocs holocristallins de la Somma. C.R. Acad. Sci., Paris., 165, 205-11.

LACROIX, A. 1931. Les phonolites nepheliniques et leucitiques de l'île Ua-pou (Archipel des Marquises). C.R. Acad. Sci., Paris, 192, 1161-1166.

LAMBERT, I.B. and WYLLIE, P.J. 1968. Stability of hornblende and a model for the low velocity zone. Nature, Lond. 219, 1240-1241.

LARSEN, E.S. 1940. Petrographic province of central Montana. Bull. geol. Soc. Am., 51, 887-948.

LE BAS, M.J. 1962. Role of aluminium in igneous clinopyroxenes with relation to their parentage. Am. Jour. Sci., 260, 267-288.

LINDSLEY, D.H. 1966. Melting relations of $KAlSi_3O_8$: effect of pressures up to 40 Kb. Am. Mineral., 51, 1793-1799.

LOCARDI, E. and MITTEMPERGHER, M. 1967. Relationship between some trace elements and magmatic processes. Geol. Rund., 57, 313-334.

LUTH, W.C. 1967. Studies in the system $KAlSiO_4$-Mg_2SiO_4-SiO_2-H_2O. I. Inferred phase relations and petrologic applications. J. Petrology., 8, 372-416.

LUTH, W.C. and TUTTLE, O.F. 1969. The hydrous vapour phase in equilibrium with granite and granite magmas, pp. 513-548. in Igneous and Metamorphic Geology, eds. Larsen, L., Manson, V. and Prinz, M. Geol. Soc. Am. Mem. 115.

MACDONALD, G.A. 1968. Composition and origin of Hawaiian lavas, pp. 477-522 in Studies in Volcanology, eds. Coats, R.R., Hay, R.L. and Anderson, C.A. Geol. Soc. Am. Mem. 116.

MANSON, V. 1967. Geochemistry of basaltic rocks: major elements, pp. 215-269 in Basalts: the Poldervaart treatise on rocks of basaltic composition, eds. Hess, H.H. and Poldervaart, A., New York: Interscience.

MARINELLI, G. 1961. Genesi e classificazione delle vulcaniti recenti toscane. Atti. Soc. Tosc. Sc. Nat., serie A, 68, 74-116.

MARINELLI, G. 1967. Genèse des magmas du volcanisme plio-quaternaire des Apennins. Geol. Rund., 57, 127-141.

MARINELLI, G. and MITTEMPERGHER, M. 1966. On the genesis of some magmas of typical mediterranean (potassic) suite. Bull. Volc., 29, 113-140.

MATTIAS, P.P. 1965. Lave dell'apparato Vulsino. Periodico Min., 34, 137-99.

MOREY, G.W. 1957. The solubility of solids in gases. Econ. Geol., 52, 225-251.

NARICI, E. 1932. Contributo alla petrografia chimica della provincia magmatica Campana e del Monte Vulture. Z. Vulk. 14, 210-47.

NEUBAUER, C. 1911. Daten zur kenntnis der silikatschmelzlösungen. Földtani Közlöny, Geol. Mitt., 41, 197-205.

O'HARA, M.J. 1968. The bearing of phase equilibria studies in synthetic and natural systems on the origin and evolution of basic and ultrabasic rocks. Earth-Sci. Rev. 4, 69-133.

O'HARA, M.J. 1970. Upper mantle composition inferred from laboratory experiments and observation of volcanic products. Phys. Earth Planet. Interiors, 3, 236-245.

O'HARA, M.J. and YODER, H.S.,Jr., 1967. Formation and fractionation of basic magma at high pressures. Scott. J. Geol. 3, 67-117.

OSBORN, E.F. and TAIT, D.B. 1952. The system diopside-forsterite-anorthite. Am. J. Sci. Bowen Volume, 413-433.

OXBURGH, E.R. 1964. Petrological evidence for the presence of amphibole in the upper mantle and its petrogenetic and geophysical implications. Geol. Mag. 101, 1-19.

PANICHI, U. 1922. Ricerche petrografiche su la regione aurunca (Vulcano di Roccamonfina). Mem. Soc. Ital. d. Sci., Ser. 3, 22, 3-124.

PART, G.M. 1950. Volcanic rocks from the Cape Verde Islands. Bull. Brit. Mus. (Nat. Hist.) Min. 1, 27-72.

PEARCE, T.H. 1968. A contribution to the theory of variation diagrams. Contr. Mineral. and Petrol., 19, 142-157.

PIWINSKI, A.J. and WYLLIE, P.J. 1968. Experimental studies of igneous rock series: a zoned pluton in the Wallowa Batholith, Oregon. J. Geology 76, 205-234.

POLDERVAART, A. and HESS, H.H. 1951. Pyroxenes in the crystallisation of basaltic magma. J. Geol. 59, 472-489.

POWELL, J.L. and BELL, K. 1970. Strontium isotopic studies of alkalic rocks: localities from Australia, Spain, and the Western United States. Contr. Mineral. and Petrol. 27, 1-10.

POWERS, H.A. 1955. Composition and origin of basaltic magma of the Hawaiian Islands. Geochim. cosmochim. Acta, 7, 77-107.

PRINZ, M. 1967. Geochemistry of basaltic rocks: trace elements, pp. 271-323 in Basalts: the Poldervaart treatise on rocks of basaltic composition, eds. Hess, H.H. and Poldervaart, A., New York: Interscience.

RAHMAN, A.A.M.S. 1968. Mineralogy of some Italian lavas. Univ. Manchester Ph.D. Thesis (unpubl.)

RINGWOOD, A.E. and GREEN, D.H. 1966. An experimental investigation of the gabbro-eclogite transformation and some geophysical implications. Tectonophysics, 3, 383-427.

RITSEMA, A.R., 1969. Seismic data of the West Mediterranean and the problem of oceanization. Trans. Kon. Ned. Geol. Mynbk. Gen. 26, 105-120.

RITTMAN, A. 1933. Die geologisch bedingte Evolution und Differentiation des Somma-Vesuvmagmas. Zeitschr. f. Vulk. 15, 8-94.

RITTMAN, A. 1962. Volcanoes and their activity. (English translation by E.A. Vincent). New York and London: Interscience.

ROEDDER, E. and COOMBS, D.S. 1967. Immiscibility in granitic melts, indicated by fluid inclusions in ejected granitic blocks from Ascension Island. J. Petrol. 8, 417-451.

SAHAMA, T.G. 1952. Leucite, potash nepheline and clinopyroxene from lavas of the south western Uganda and adjoining Belgian Congo. Am. J. Sci., Bowen vol., 457-470.

SAHAMA, T.G. 1960. Kalsilite in the lavas of Mt. Nyirangongo (Belgian Congo). J. Petrol. 1, 146-171.

SAVELLI, C. 1967. The problem of rock assimilation by Somma-Vesuvius magma. I. Composition of Somma and Vesuvius lavas. Contr. Mineral. and Petrol. 16, 328-353.

SAVELLI, C. 1968. The problem of rock assimilation by Somma-Vesuvius magma. II. Composition of sedimentary rocks and carbonate ejecta from the Vesuvius area. Contr. Mineral. and Petrol. 18, 43-64.

SCHAIRER, J.F. and BOWEN, N.L. 1947. The system anorthite—leucite—silica. Bull. Soc. Geol. Finlande, 20, 67-87.

SCHNEIDER, H. 1965. Petrographie des Lateravulkans und die magmenentwicklung der Monti Volsini. Schw. Min. Petrog. Mitt., 45, 331-455.

SEIFERT, H. 1942. Uber ein basaltischer gestein der Roccamonfina. N. Jb. Min. A. 77, 305-336.

SHAND, S.J. 1922. The problem of the alkaline rocks. South Africa Geol. Soc. Proc., 25, 19-32.

STRECKEISEN, A. 1964. Zur Klassification der eruptivgesteine. N. Jb. Mineral. Mh. 5/6, 195-222.

STRECKEISEN, A. 1966. Die klassification der eruptivgesteine. Geol. Rdsch, 55, 478-491.

TAYLOR, S.R. 1964. Abundance of chemical elements in the continental crust: a new table. Geochim. Cosmochim. Acta, 28, 1273-1285.

TEDESCO, C. 1965. Main lines of the history of the Roccamonfina volcano. Bull. Volc. 28, 1-19.

THORNTON, C.P. and TUTTLE, O.F. 1960. Chemistry of igneous rocks. I. Differentiation index. Am. Jr. Sci. 258, 664-684.

TILLEY, C.E. and HARWOOD, H.F. 1931. The dolerite-chalk contact of Scawt Hill, Co. Antrim. The production of basic alkali-rocks by the assimilation of limestone by basaltic magma. Min. Mag. 22, 439-468.

TOBI, A.C. 1963. Plagioclase determinations with the aid of the extinction angles in sections normal to (010). Am. Jr. Sci. 261, 157-167.

TRIGLIA, R. 1966. Studio geopetrografico dell'edificio vulcanico di M. Calvo (Farnese-Viterbo) Per. Min. 35, 1023-1095.

TRIGLIA, R. 1969. Studio geo-petrografico del complesso vulcanico di Latera (Vulcani Volsini) Per. Min. 38, 155-223.

TURNER, F.J. and VERHOOGEN, J. 1960. Igneous and Metamorphic petrology. New York: McGraw-Hill.

TUTTLE, O.F. and BOWEN, N.L. 1958. Origin of granite in the light of experimental studies in the system $NaAlSi_3O_8$-$KAlSi_3O_8$-SiO_2-H_2O. Geol. Soc. Amer. Mem. 74.

VINOGRADOV, A.P. 1962. Average contents of chemical elements in the principal types of igneous rocks of the Earth's crust. Geochemistry (trans. of Geokhimiya) 1962, 641-664.

VISWANATHAN, K. 1966. Unit cell dimensions and ionic substitutions in common clinopyroxenes. Am. Miner., 51, 429-442.

VON PLATEN, H. 1965. Experimental anatexis and genesis of migmatites. pp. 203-218. in Controls of Metamorphism. eds. Pitcher, W.S., and Flinn, G.S. Edinburgh and London: Oliver and Boyd.

VOROBIEVA, O.A. 1960. Alkaline rocks in the U.S.S.R. Rep. 21st. Int. Geol. Congr. (Norden) pt. 13, 7-17.

WADE, A. and PRIDER, R.T. 1940. The leucite-bearing rocks of the West Kimberley area, Western Australia. Q. Jl. geol. Soc. Lond. 96, 39-98.

WASHINGTON, H.S. 1897. Italian petrological sketches: IV, The Rocca Montina Region. Jour. Geol., 5, 241-256.

WASHINGTON, H.S. 1906. The Roman comagmatic region. Publs. Carnegie Instn. Wash. 57.

WASHINGTON, H.S. 1927. The italite locality of Villa Senni. Am. J. Sci. 14, 173-98.

WASHINGTON, H.S. and MERWIN, H.E. 1921. Note on augite from Vesuvius and Etna. Am. J. Sci. 1, 20-30.

WATKINSON, D.H. and WYLLIE, P.J. 1964. The limestone assimilation hypothesis. Nature, Lond., 204, 1053-1054.

WATKINSON, D.H. and WYLLIE, P.J. 1969. Phase equilibrium studies bearing on the limestone-assimilation hypothesis. Geol. Soc. Am. Bull., 80, 1565-1576.

WINKLER, H.G. and VON PLATEN, H. 1960. Experimentelle Gesteinsmetamorphose. III. Anatektische Ultrametamorphose kalkhaltiger Tone. Geochim. et Cosmochim. Acta. 18, 295-316.

WINKLER, H.G. and VON PLATEN, H. 1961. Experimentelle Gesteinmetamorphose. IV. Geochim. et Cosmochim. Acta. 24, 48-69.

WONES, D.R. and EUGSTER, H.P. 1965. Stability of biotite: experiment, theory and application. Am. Miner. 50, 1228-1272.

YODER, H.S., Jr. 1969. Phlogopite-H_2O-CO_2: an example of the multicomponent gas problem. Yb. Carnegie Instn. Wash. 68, 236-240.

YODER, H.S., Jr., 1964. Genesis of principal basalt magmas. Yb. Carnegie Instn. Wash. 63, 97-101.

YODER, H.S., Jr. and KUSHIRO, I. 1969. Melting of a hydrous phase: phlogopite. Am. J. Sci. Schairer Volume, 267-A, 558-582.

YODER, H.S. Jr. and SAHAMA, T.G. 1957. Olivine X-ray determinative curve. Am. Miner., 42, 475-491.

YODER, H.S. Jr. STEWART, D.B. and SMITH, J.R. 1957. Ternary feldspars. Yb. Carnegie Inst. Wash. 56, 206-214.

YODER, H.S.,Jr. and TILLEY, C.E. 1962. The origin of basalt magmas: an experimental study of natural and synthetic systems. J. Petrology, 3, 342-532.

APPENDIX A

SAMPLE PREPARATION AND ANALYTICAL METHODS

A:1 Sample preparation - crushing and grinding

A:2 X-ray spectrographic analysis

A:3 Wet chemical methods

A:4 Mineral separation and analysis

A:5 Modal analysis

APPENDIX A

SAMPLE PREPARATION AND ANALYTICAL METHODS

A:1 Sample preparation - crushing and grinding

Samples selected for analysis were washed and scrubbed with a hard brush to remove any superficial weathered material. After rinsing in deionised water and drying, they were split into pieces c.3cm. in size using a CUTROCK hydraulic splitter. After removal of weathered edges, great care was taken to retain the fine fraction produced during splitting. With leucite-phyric specimens an unrepresentative sample would have been obtained if the fine fraction (composed mainly of leucite fragments) had been rejected. The sample weight at this stage was in the range 500 - 1500g. Following the recommendations of Wager and Brown (1960), at least 500g. samples were used for most of the fine grained specimens (grainsize = < 1 mm.) and over 1000g. for most of the coarse grained leucite-phyric specimens (1 - 10mm.). The sample was reduced to < 5 mm. chips using a tungsten carbide mortar and pestle, and then cone and quartered to obtain a representative sample of c.200g. This was reduced to -100 mesh by grinding in a "Columboy" TEMA disc mill for 45 - 60 seconds. Sieving tests showed that only a very small fraction (< 1%) was > 100 mesh after grinding in the TEMA, so the sieving of samples was discontinued. The 200g. of powder was mixed and split by cone and quartering; c.100g. was placed in a clean glass bottle and the rest of the sample was discarded. The powder was dried at 110°C for 24 hours before analysis.

The only possible sources of contamination are Fe and Cr from the hydraulic splitter, W and Co from the WC mortar and pestle, and Ni and Cr from the TEMA disc mill. Ni and Cr contamination from the TEMA is considered to be the main source of contamination, reaching a maximum of c.500ppm. Ni and c.100ppm. Cr for samples ground for 60 seconds. Ni, Cr, W, and Co were not considered to be important in the present study, so the small amount of contamination incurred using the above procedures is not important.

Fitton and Gill (1970) have investigated the oxidation of samples that are ground in high velocity disc mills. The amount of oxidation is dependent upon grinding time, sample weight, and water content. Reference to Fitton and Gill (Table 2) shows that the grinding procedures used in this study will produce a negligible amount of oxidation.

A:2 X-ray Spectrographic Analysis

The general principles of X-ray spectrographic analysis have been summarised by Norrish and Chappell (1967) and Jenkins and de Vries (1967).

A:2:1 Major Elements

The method of sample preparation adopted is similar to that developed by Rose et al. (1963). A fusion mixture of 0·50g. sample: 0·50g. La_2O_3:4·00g. $Li_2B_4O_7$ was used. After fusion in a muffle furnace at 1050°C, the samples were cooled and the weight of the glass bead was made up to 5·00g. with $Li_2B_4O_7$ to maintain exactly

the 1:1:8 dilution ratio. The glass beads were reduced to -200mesh in a WC ball mill and the powders were dried at 110°C. Compressed discs with boric acid backing were prepared just before analysis. Considerable care was taken to preserve the flat surface of the fusion discs because of the shallow depth of penetration of the characteristic radiation associated with the light elements (Mg, Al, Si). This preparation method produces a homogeneous sample and reduces matrix effects so that there is a linear relationship between concentration and fluorescent intensity for all major elements with Z > 11.

Operating conditions are summarised in Table A-1. The analyses were carried out using a Philips Automatic Spectrometer (PW1212). SiO_2, Al_2O_3, Fe_2O_3T, MgO, CaO, K_2O, TiO_2, and P_2O_5 were determined together (Cr tube) and the results were computed using a Major element program written by the author (Table A-2). Using the paper tape output from the PW1212, this program performs a drift correction and then calculates m and c values for each calibration line ($y = mx + c$). The print out includes a correlation coefficient for each calibration line, recommended and computed values for the standards, and computed values for the unknowns. MnO was determined separately using the W tube.

Table A-3 shows the standards that were used and the calibration line correlation coefficients for the main batch of analyses. The recommended values of Flanagan (1969) were used for the USGS standards.

TABLE A-1

Operating conditions for XRF analysis using PW1212 Automatic Spectrometer

Element & Line	Kv	mA	Crystal	Method	Counter	Time	Collimator	Vacuum	Notes
Al Kα	60	24	PE	P	F	60	C	Y	
Ba Kα	80	24	LiF	P/B	S	30	F	N	
Ca Kα	40	24	PE	P	F	30	F	Y	
Ce Kα	80	24	LiF	P/B	F	300	F	Y	
Fe Kα	60	24	LiF	P	S	60	C	Y	
K Kα	60	24	PE	P	F	30	F	Y	
La Kα	80	24	LiF	P/B	F	300	F	Y	
Mg Kα	40	32	KAP	P-B	F	300	C	Y	Discriminate against KAP peak
Mn Kα	60	24	LiF	P-B	F	40	F	Y	
Nb Kα	80	24	LiF	P/B	S	30	F	N	
Ni Kα	80	24	LiF	P/B	S	60	F	N	
P Kα	60	24	PE	P-B	F	120	F	Y	
Rb Kα	80	24	LiF	P/B	S	60	F	N	
Si Kα	60	24	PE	P	F	60	C	Y	
Sr Kα	80	24	LiF	P/B	S	60	F	N	
Th Lα	80	24	LiF	P/B	S	120	F	N	
Ti Kα	60	24	LiF	P	F	30	C	Y	
Y Kα	80	24	LiF	P/B	S	60	F	N	Correct for Rb Kβ
Zn Kα	80	24	LiF	P/B	S	60	F	N	
Zr Kα	80	24	LiF	P/B	S	60	F	N	Correct for Sr Kβ

Tube = Cr (major elements), W (minor elements)

Discrimination = automatic except for Mg

Sample preparation = Fusion (major elements), Mylar (minor elements)

TABLE A-2 (3 pages)

Atlas Autocode X.R.F. major element program

for Philips PW 1212 Automatic Spectrometer

```
***A
JOB
GEO 022/10051212/MAJOR EL ANAL PROG PW1212 J D APPLETON
EXECUTION 30 MINUTES
OUTPUT
0 LINE PRINTER 5000 LINES
COMPILER ABC


%LIST
%BEGIN
%INTEGER S,R,CY
READ(S,R,CY)
NEWLINES(6)

%BEGIN ;  ! GLOBAL INSTR BLOCK
%INTEGER A,I,J,G
%REAL W
%ARRAY STDVAL(1:8,1:S),MINTY(1:8,1:R+1),M,C,FIRST(1:8),INTY(1:8,1:4)
%INTEGERARRAY COUNTS(1:10,1:4)
%ROUTINESPEC SUMCOUNTS
%ROUTINESPEC DRIFTCORRECTION


NEWPAGE
NEWLINES(4)
%CAPTION~PHILIPS  1212  AUTOMATIC  XRAY  SPECTROMETER
%CAPTION~PEGBOARD  FOR  CAO  K2O  FE2O3  TIO2  SIO2  AL2O3  P2O5%C
                  P2O5BK  MGO  MGOBK
%CAPTION~CORRECTED  FOR  DRIFT
%CAPTION~PROGRAM  MK  VII  WRITTEN  BY  J D APPLETON  JULY 1969

NEWLINES(2)
%CAPTION          S          R          CY~
PRINT (S,10,0)
PRINT (R,10,0)
PRINT (CY,10,0)
NEWLINES(10)
%CYCLE J=1,1,S
%CYCLE I=1,1,8
READ (STDVAL(I,J))
%REPEAT
%REPEAT

%BEGIN ; !STANDARDS BLOCK
%INTEGER K
%ARRAY STINTY(1:8,1:S),R',N,DET,SEE,REE(1:8)
%ROUTINESPEC FINDREGRESSION
A=1
%CYCLE G=1,1,S/3
SUMCOUNTS
DRIFTCORRECTION
15:   %CYCLE I=1,1,8
%CYCLE J=1,1,4
%UNLESS J=1 %THEN ->11
MINTY(I,G) = INTY(I,J)
->12
11:   K=((J-1)+(G-1)*3)
STINTY(I,K) = INTY(I,J)
12:   %REPEAT
%REPEAT
%REPEAT
```

```
FINDREGRESSION

%CAPTION KEY␣TO␣TABLE␣BELOW:~
%CAPTION M␣␣␣␣␣␣␣␣␣COEFFICIENT␣OF␣REGRESSION␣␣␣Y␣=␣M*X␣+␣C␣␣␣␣%C
        (Y=CONC␣OF␣ELEMENT␣AND␣X=INTENSITY␣VALUES)~
%CAPTION C␣␣␣␣␣␣␣␣␣POINT␣OF␣INTERSECTION␣OF␣REGRESSION␣LINE␣ON␣Y␣AXIS~
%CAPTION R␣␣␣␣␣␣␣␣␣COEFFICIENT␣OF␣CORRELATION~
%CAPTION N␣␣␣␣␣␣␣␣␣NUMBER␣OF␣STANDARDS␣USED␣IN␣REGRESSION~
NEWLINES(3)
%CAPTION␣␣␣␣␣M
SPACES(3)
%CYCLE I=1,1,8
PRINT(M(I)*1000,3,5)
%REPEAT
%CAPTION~␣␣␣␣␣C
SPACES(3)
%CYCLE I=1,1,8
PRINT(C(I),3,5)
%REPEAT
%CAPTION~␣␣␣␣␣R
SPACES(3)
%CYCLE I=1,1,8
PRINT(R'(I),5,3)
%REPEAT
%CAPTION~␣␣␣␣␣N
%CYCLE I=1,1,8
PRINT (N(I),9,0)
%REPEAT


NEWLINES(5)
%CAPTION STANDARDS␣␣␣␣␣␣␣INTENSITIES␣,␣COMPUTED␣VALUES␣,␣AND␣%C
              STANDARD␣VALUES~~~
%CAPTION~␣␣␣␣␣CAU␣␣␣␣␣␣␣␣␣K2U␣␣␣␣␣␣␣␣␣FE2U3␣␣␣␣␣␣␣␣TIU2␣␣␣␣␣␣␣␣%C
        SIU2␣␣␣␣␣␣␣␣␣AL2U3␣␣␣␣␣␣␣␣␣P2U5␣␣␣␣␣␣␣␣␣␣MGU~~
%CYCLE J=1,1,S
%CYCLE I=1,1,8
PRINT(STINTY(I,J),8,0)
SPACES(3)
%REPEAT
NEWLINE
%CYCLE I=1,1,8
W=M(I)*STINTY(I,J)+C(I)
%IF W<0 %THEN W=0
PRINT(W,4,3)
SPACES(3)
%REPEAT
NEWLINE
%CYCLE I=1,1,8
PRINT(STDVAL(I,J),4,3)
SPACES(3)
%REPEAT
NEWLINES(3)
%REPEAT



NEWLINES(5)



%ROUTINE FINDREGPESSION
%INTEGER N'
%REAL EX,EY,EXY,EX2,EY2,X,Y,VX,VY,V
%CYCLE I=1,1,8
EX=0;EY=0;EXY=0;EX2=0;EY2=0;N'=S
%CYCLE J=1,1,S
%UNLESS STDVAL(I,J)<0 %THEN ->1
N' = N'-1
->2
1:  X=STINTY(I,J);  Y=STDVAL(I,J)
EX=EX+X;EY=EY+Y;EXY=EXY+X*Y;EX2=EX2+X↑2;EY2=EY2+Y↑2
2:  %REPEAT

M(I)=(N'*EXY-EX*EY)/(N'*EX2-(EX)↑2)
C(I)=(EY-M(I)*EX)/N'
R'(I)=(N'*EXY-EX*EY)/SQRT((N'*EX2-(EX)↑2)*(N'*EY2-(EY)↑2))
N(I)=N'
%REPEAT

%END

%END ; !END OF STDS BLOCK
```

```
%BEGIN ; !SAMPLES BLOCK
%IF R=S/3 %THEN ->29
%CAPTION~SAMPLES      COMPUTED VALUES~~~
%CAPTION~      CAO      K2O      FE2O3      TIO2      %C
        SIO2      AL2O3      P2O5      MGO
NEWLINES(2)
A=2
%CYCLE G=1,1,R-S/3
SUMCOUNTS
DRIFTCORRECTION

%CYCLE J=2,1,4
%CYCLE I=1,1,8
W=M(I)*INTY(I,J)+C(I)
PRINT(W,8,3)
%REPEAT
NEWLINE
%REPEAT
NEWLINE
%REPEAT
29:  %END ; ! END OF SAMPLES BLOCK
NEWLINES(6)

%ROUTINE SUMCOUNTS
%INTEGER D,Q,A
%CYCLE I=1,1,10
%CYCLE J=1,1,4
COUNTS(I,J)=0
%REPEAT
%REPEAT
%CYCLE D=1,1,CY
%CYCLE I=1,1,10
%CYCLE J=1,1,4
READ (Q,A)
COUNTS(I,J) = COUNTS (I,J) +A
%REPEAT
%REPEAT
%REPEAT
%CYCLE J=1,1,4
COUNTS(7,J) =COUNTS(7,J) - COUNTS(8,J)
COUNTS(8,J) = COUNTS(9,J) -COUNTS(10,J)
%REPEAT
%CYCLE I=1,1,8
%CYCLE J=1,1,4
INTY(I,J) = COUNTS(I,J)
%REPEAT
%REPEAT
%END ; ! END OF ROUTINE SUMCOUNTS INC CONVERSION TO INTYS

%ROUTINE DRIFTCORRECTION
%UNLESS G=1 %THEN -> 1
-> 1 %IF A=2
%CYCLE I=1,1,8
FIRST(I) = INTY(I,1)
%REPEAT
1:  %CYCLE I=1,1,8
%CYCLE J=2,1,4
INTY(I,J) = (INTY(I,J)*FIRST(I)/INTY(I,1))
%REPEAT
%REPEAT
%END

%END ; ! END OF GLOBAL BLOCK

%ENDOFPROGRAM
```

TABLE A-3

Standards used for major element analysis, and correlation coefficients (intensity v. % oxide) for calibration lines

	DTS-1	PCC-1	BCR-1	AGV-1	GSP-1	G-2	NBS76	NBS77	NBS91	NBS1a	MG	T-1	996Bio	r
SiO_2	X	X	X	X	X			X	X		X	X		1·000
TiO_2	X	X	X	X	X	X	X		X	X	X	X		1·000
Al_2O_3	X	X	X	X	X	X			X		X	X		1·000
Fe_2O_3T	X	X	X	X	X	X	X	X	X		X	X		0·999
MnO	X	X	X	X	X	X				X	X	X		n.d.
MgO	X	X	X	X	X	X	X		X		X	X		1·000
CaO	X	X	X	X	X	X	X				X	X		1·000
K_2O	X	X	X	X	X	X	X	X				X	X	1·000
P_2O_5	X	X	X	X	X	X	X				X	X		0·989

Accuracy and Precision. Jamieson (1969) has noted the accuracy of the major element analytical methods used at Edinburgh University. In order to estimate the precision of the XRF analytical methods, seven fusions of R.150-P were prepared. The results of this precision test are presented in Table A-4 together with comparative data from Jamieson (1969), and Strong (1970), who used the same sample preparation and analytical methods. The precision data is compared with that obtained by Rose et al. (1963) using XRF methods and by Gould (1966) using "rapid" wet chemical methods (Table A-4).

A:2:2 Trace Elements

Trace element determinations were carried out on rock powders supported by mylar using the PW1212. The peak/background method of Anderman and Kemp (1958) reduces absorption effects to an acceptable level. Correlation coefficients for trace element calibration lines are presented in Table A-5. The low values obtained are mainly related to the uncertainty regarding the correct concentrations of elements in some standards (see variation in data presented by Flanagan, 1969). Ba, Zr, Y, Sr, Rb, Th, and Zn were determined on all samples, and Ni, La, Ce, and Nb on selected samples. The operating conditions are given in Table A-1, and precision data (together with comparative data from Strong, 1969) are presented in Table A-6. The accuracy of the trace element analytical method used at the Grant Institute of Geology can be estimated by comparing Edinburgh values for international standards reported in Flanagan (1969, Table 3) with mean values (Flanagan, 1969, Table 5).

TABLE A-4

Precision of XRF Major Element Analyses

	$\bar{x}$	R	s	C(%)
SiO_2	48·37	0·41	0·153	0·32
TiO_2	0·81	0·02	0·009	1·11
Al_2O_3	16·34	0·42	0·178	1·09
Fe_2O_3T	8·74	0·24	0·081	0·93
MnO	0·14	0·01	0·005	3·70
MgO	4·45	0·23	0·082	1·85
CaO	9·73	0·07	0·025	0·26
K_2O	7·71	0·10	0·038	0·49
P_2O_5	0·48	0·05	0·016	3·40

$\bar{x}$ mean of 7 determinations R range = max. - min. concentration
s standard deviation C relative deviation (100 s/$\bar{x}$)

	Jamieson (1969)		Strong (1970)		Rose et al. (1963)		Gould (1966)	
	$\bar{x}$	C	$\bar{x}$	C	Comp.range	C	$\bar{x}$	C
SiO_2	49·35	0·64	47·05	0·27	50-75	0·50	71·78	0·46
TiO_2	2·31	0·82	2·38	1·14	0·1-2·0	2·14	0·59	1·86
Al_2O_3	9·04	1·07	13·23	0·60	10-20	1·02	13·12	1·22
Fe_2O_3T	11·47	1·83	12·70	1·18	1-12	0·95	4·13	0·97
MnO	0·144	2·36	-	-	0·01-0·5	3·13	0·073	4·11
MgO	14·74	1·90	9·21	1·09	0·4-10	2·07	0·59	6·47
CaO	7·27	1·07	11·36	0·53	1-12	0·97	1·48	2·57
K_2O	1·56*	1·41	1·25	0·76	-	-	-	-
P_2O_5	0·46*	1·4	0·43	4·65	-	-	-	-

* wet chemical determinations

TABLE A-5

Trace Element Calibration Line Correlation Coefficients

	r
Ba	0·997
Zr	0·998
Y	0·931
Sr	0·994
Rb	0·995
Th	0·989
Zn	0·903
Ni	0·995

r = correlation coefficient between concentration and Peak/Background ratio

TABLE A-6

Precision of XRF Trace Element Analyses

	$\bar{x}$	R	s	C(%)
Ba	1291	66	21·27	1·7
Zr	291	17	7·11	2·5
Y	57	13	3·90	6·9
Sr	1867	68	24·59	1·3
Rb	483	40	15·99	3·3
Th	31	18	6·57	21·1
Zn	62	11	3·55	5·7

$\bar{x}$ mean of 7 determinations
R range = max. - min. concentration
s standard deviation
C relative deviation ($100s/\bar{x}$)

Strong (1970)

	$\bar{x}$	C
Ba	381	6
Zr	201	5
Y	-	-
Sr	512	2
Rb	29	20
Th	-	-
Zn	93	5



A:3 Wet Chemical Methods

FeO was determined by Wilson's (1955) cold solution method using PTFE crucibles. Excess vanadate was titrated against ammonium ferrous sulphate using sodium diphenylamine β sulphonate as an indicator.

Na_2O was determined using an EEL flame photometer (Vincent, 1960). The sample solutions were diluted to give concentrations in the range 1 - 25ppm Na_2O; the exact concentration of Na_2O was determined by bracketing between standard solutions. The effect of CaO concentration on the Na_2O determination was investigated. It was found that 10% CaO in the solution produced a reading equivalent to ± 0·02% Na_2O using two Na filters in the photometer. The interference of CaO on the Na_2O reading was disregarded because most of the samples analysed contained <10% CaO, some of the $CaSO_4$ remains as an insoluble residue after dissolution, and because $CaSO_4$ is not very volatile. The accuracy of this method can be estimated from the following data:

Duplicate determination of GSP-1 2·90g 2·94g Na_2O

Recommended value (Flanagan, 1969) 2·88g Na_2O

H_2O was determined gravimetrically by heating 1g. of the rock powder with 3g. of flux ($PbO:PbCrO_4$ = 2:1) in a pyrex tube. The water given off was collected and weighed (Shapiro and Brannock, 1962).

CO_2 was determined by the Pressometric method (Welcher, 1963, p. 1191).

Al_2O_3 in three clinopyroxene samples was determined by Atomic

Absorption Spectroscopy in the presence of La_2O_3 and KCl. The wet chemical results are compared with the XRF results in Table A-7 below.

TABLE A-7

Sample	XRF(wt%)	AA(wt%)
Cpx-BP (Ariccia)	2·55	2·16 2·51 2·20
Cpx-V.1.	4·07	4·05
Cpx-14043	6·69	6·51

The precision of the FeO and Na_2O determinations is presented in Table A-8 below.

TABLE A-8

Element	n	$\bar{x}$	R	S	C(%)
FeO	7	4·19	0·12	0·042	1·01
Na_2O	7	1·79	0·02	0·008	0·44

M. Saunders kindly determined Ba and Sr in three samples by atomic absorption spectroscopy. The AA results are compared with the authors XRF results in Table A-9.

TABLE A-9

Sample	XRF		AA	
	BaO	SrO	BaO	SrO
R.146	0·131	0·186	0·121	0·165
R.39	0·179	0·240	0·166	0·230
R.73	0·256	0·307	0·250	0·278

The AA results were determined using synthetic standards whilst the XRF data were determined using G1, W1, and other USGS standards.

A:4 Mineral separation and analysis

A;4:1 Leucite

Fresh rock chips were crushed down to <0·2mm. in a steel roller mill, thus releasing the macro-leucite phenocrysts from the groundmass. This material was washed to remove the fine dust fraction and the leucite was separated from the groundmass by using the Frantz magnetic separator (vertical position, full power). It was possible to get a sample ± 80% pure by this method as only the leucite phenocrysts were released from the groundmass by the coarse crushing method. The partially purified leucite was then crushed to -50mesh and repeatedly passed through the Frantz magnetic separator to remove clinopyroxene and groundmass particles. A portion of this was then taken and any remaining impurities were removed by hand-picking. The purified leucite was crushed to -125 mesh for analysis.

R.36-1c was analysed for major elements and all the leucite samples were analysed for Ba, Sr, and Rb using XRF techniques (see A-2 above). K_2O, and Na_2O were determined by flame photometry (see A-3 above). Special Na_2O standards were prepared so that standard and sample solutions contained similar concentrations of K_2O. The Sr values of R.18-1c and R.61-1c were corrected for plagioclase impurities (4% and 3·5% respectively).

A:4:2 Clinopyroxene and phlogopite/biotite

Separation of these minerals from nodules was carried out using the Frantz magnetic separator, and the Syntron vibrating table. Final purification was by hand picking. The minerals were analysed

by the methods described in sections A-1, 2, 3 above. Phlogopite-BP(Ariccia) was corrected for 2% clinopyroxene impurity, and Bio-R.103 for 4%. The percentage impurity was determined by point counting.

A:5 Modal Analysis

Modal data was obtained by point counting on rock slabs and thin sections. Rock slab point counting was carried out on samples containing a low percentage of large leucite phenocrysts. Most of the thin section modal analyses were performed by counting 1200-4500 points on a Shadowmaster projection microscope. A few thin sections were also determined using the less rapid Swift point counter. The modal data (expressed as volume %) are presented in Appendix B.

References cited.

ANDERMAN, G. and KEMP, J.W. 1958. Scattered X-rays as internal standards in X-ray emission spectroscopy. Analyt. Chem., 30, 1306-1309.

FITTON, J.G. and GILL, R.C.O. 1970. The oxidation of ferrous iron in rocks during mechanical grinding. Geochim. cosmochim. Acta, 34, 518-524.

FLANAGAN, F.J. 1969. U.S. Geological Survey Standards - II. First compilation of data for the new U.S.G.S. rocks. Geochim. cosmochim. Acta, 33, 81-120.

GOULD, D. 1966. Geochemical and mineralogical studies of the granitic gneiss and associated rocks of Western Ardgour, Argyll. Univ. Edinburgh Ph.D. thesis (unpubl.)

JAMIESON, B.G. 1969. The petrology of olivine-rich basaltic rocks, Nuanetsi, Rhodesia. Univ. Edinburgh Ph.D. thesis (unpubl.)

JENKINS, R. and DE VRIES, J.L. 1967. Practical X-ray Spectrometry. Philips Technical Library, Eindhoven, 181pp.

NORRISH, K. and CHAPPELL, B.W. 1967. X-ray fluorescence Spectrography. in Physical methods in determinative mineralogy (ed. J. Zussman) London and New York: Academic Press.

ROSE, H.J., ADLER, I. and FLANAGAN, F.J. 1963. X-ray fluorescence analysis of the light elements in rocks and minerals. Appl. Spectrosc., 17, 81-85.

SHAPIRO, L. and BRANNOCK, W.W. 1962. Rapid analysis of silicate, carbonate and phosphate rocks. U.S. Geol. Surv. Bull. 1144-A.

STRONG, D.F. 1970. Petrology of the lavas of Grande Comore. Univ. Edinburgh Ph.D. thesis (unpubl.)

VINCENT, E.A. 1960. Analysis by gravimetric and volumetric methods, flame photometry, colorimetry and related techniques, pp. 33-80 in Methods in Geochemistry, eds. Smales, A.A. and Wager, L.R. New York and London: Interscience.

WAGER, L.R. and BROWN, G.M. 1960. Collection and preparation of material for analyses, pp. 4-32 in Methods in Geochemistry, eds. Smales, A.A. and Wager, L.R. New York and London: Interscience.

WELCHER, F.J. (ed.) 1963. Standard methods of chemical analysis. Volume Two, Part A. 6th edn., New Jersey: D. Van Nostrand Co.

WILSON, A.D. 1955. A new method for the determination of ferrous iron in rocks and minerals. Bull. geol. Surv. Gt. Br., 9, 56-58.

APPENDIX B

Modal data and petrographic notes for Roccamonfina lavas (R)

Table B-1. High K lavas.

L : leucitite

TL : tephritic leucitite

LT : leucite tephrite

PLT : phonolitic leucite tephrite

TLP : tephritic leucite phonolite

LP : leucite phonolite

T : trachyte

Transitional samples are indicated as follows -TL/PLT

Symbols are as indicated in Fig. 5-1.

Table B-2. Low K lavas.

OB : olivine basalt

TB : trachybasalt

BAL : biotite augite latite

GAF : grey ash flow

TABLE B-1

Petrography of analysed samples from the High K Series

Rock No.	Rock Type	Symbol	Volume °/o Phenocrysts							Groundmass Mineralogy					Comments
			Lc.	Cpx.	Plag.	Ore	Bio.	Kspar	Others	Lc.	Cpx.	Plag.	Ore	Kspar.	
2	TL	○	39.0	7.0	2.0	tr	-	-	Ap	X	X	X	X	?	Ap in cpx phenos. Zoned, hourglass cpx. Lc→ 12mm. Fine grndmass.
4	TL	●	2.5	2.0	tr	tr	tr	-	-	X	X	X	X	?	Rare bio marginally altered to ore. Quench lc in gndmass. Microphenо plag.
6	TL	●	0.5	tr	-	tr	tr	-	-	X	X	X	X	-	Rare resorbed bio.
7	TL	○	31.0	2.0	1.5	tr	-	-	Ap	X	X	X	X	-	Glomero cpx-plag-ore. Lc enclosing plag.
11	TLP	▽	-	tr	tr	-	tr	tr	-	X	X	X	X	X	Microphenо plag with kspar mantles. Small °/o lc in gnd.
14	TLP	▽	-	1.9	2.9	tr	0.8	tr	Ol Hb Ap	X	X	X	X	X	Poikilitic kspar with acicular cpx. Glomero cpx-plag--resorbed bio- ore- 2° Hb. Kspar margins to plag.
15	TL/LT	○	14.0	2.5	1.5	0.5	-	-	-	X	X	X	X	?	Glomero cpx-plag-ore+late leucite
18	TL/PLT	○	23.0	3.2	tr	tr	-	-	Ap	X	X	X	X	X	Glomero c-p-o+late lc. Note development of kspar at plag-lc contacts. Pleochroic, zoned cpx.
19	TL	●	2.2	tr	tr	tr	-	-	-	X	X	X	X	?	Microphenos in devitrified brown glassy matrix.
20	TL	○	37.0	2.6	tr	tr	-	-	Ap	X	X	X	X	-	Ap needles in coarse cpx-rich gndmass.
21	PLT	○	10.6	tr	tr	tr	-	-	-	X	X	X	X	X	Pegmatitic veins of kspar + aeg-augite. Subsolidus alteration of lc phenos to kspar.
23	TL	○	39.0	2.0	-	0.5	-	-	Ap	X	X	X	X	-	Cpx and lc zoned with inclusions. Coarse gndmass.
24	TL/PLT	○	27.0	1.9	0.4	tr	-	-	Ap	X	X	X	X	X	Rare glomero c-p-o. Plag phenos zoned with kspar mantles. Max. lc= 10mm. Pleochroic yellow-green cpx.
27	TL	○	9.0	tr	tr	tr	-	-	-	X	X	X	X	?	Glomero c-p-o-ap+late lc. Max lc = 2.5mm.
29	TLP	▽	3.3	tr	tr	tr	-	tr	-	X	X	X	X	X	Plag with kspar mantles. Aeg-augite microphenos.
33	TL	○	36.0	4.5	0.5	0.5	-	-	Ol	X	X	X	X	-	Glomero c-p-o-ap. Max lc = 13mm. Fine gndmass.
36	TL	○	34.0	1.2	0.7	-	-	-	Ol	X	X	X	X	X	Cpx plag inclusions in large lc pheno.
37	PLT	▲	-	6.7	3.3	tr	0.8	-	Ol Ap Hb	X	X	X	X	X	Bio-cpx-plag-ore phyric. Glomero cpx-bio-2°Hb. Acicular cpx + altered bio in poikilitic kspar.
39	TL	○	39.0	11.0	tr	tr	-	-	Ap	X	X	X	X	-	Zoned, hourglass cpx in fine groundmass.
41	TL	○	38.0	6.8	tr	tr	-	-	-	X	X	X	X	-	Macro leucite phyric 0.25-5.0mm.
42	PLT	▲	-	6.1	4.5	tr	1.7	-	Ap	X	X	X	X	X	Abundant glomero c-p-b-o-ap. 2°Hb after cpx.
43	TL	○	28.0	3.0	1.0	tr	-	-	Ap	X	X	X	X	X	Macro, micro lc + cpx. Rare plag phenos. Fine gndmass.
44	TL	○	42.0	4.7	1.6	tr	-	-	Ap	X	X	X	X	-	Glomero c-p-o+late lc. Development of Ksp. at lc/plag. contacts.
47	PLT	▲	-	6.6	5.7	tr	0.9	-	Ap	X	X	X	X	X	Glomero c-p-o-b-ap. 2°Hb after cpx. Cloudy apatite.
48	TL	○	35.0	1.2	1.2	-	-	-	Ap	X	X	X	X	?	Lc 0.25-4.0mm
50	TL	○	14.0	tr	tr	tr	-	-	-	X	X	X	X	X	Macro lc and micro c-p-o in fine gndmass.
53	PLT	▲	tr	9.6	3.6	-	0.9	tr	Ap Ol Hb	X	X	X	X	X	Rare lc and olv phenos. Plag with kspar mantles. Tachytic gndmass. 2°Hb after cpx. Bio altered to ore.

TABLE B-1 (contd.)

Rock No.	Rock Type	Symbol	Volume °/o Phenocrysts							Groundmass Mineralogy					Comments
			Lc.	Cpx.	Plag.	Ore	Bio.	Kspar	Others	Lc.	Cpx.	Plag.	Ore	Kspar.	
55	PLT/TL	●	2.6	tr	tr	-	-	-	-	X	X	X	X	-	Microphyric. Cpx xstallised before lc.
59	TL/LT	●	tr	tr	tr	-	-	-	Ol	X	X	X	X	-	Interstitial 2° calcite. Microphenos in fine gndmass.
60	TL/LT	●	6.5	12.6	2.1	tr	tr	-	-	X	X	X	X	-	Interstitial calcite. Bio altered to ore. Glomero c-p-o-lc
61	TL/PLT	○	38.0	9.6	10.4	tr	tr	-	Ap	X	X	X	X	X	Glomero c-p-o-ap-lc. Kspar at plag/lc margins.
64	TLP	▽	-	1.4	4.8	tr	tr	6.4	-	X	X	X	X	X	Large (4mm) kspar phenos- zoned with plag inclusions.
68	TL	●	2.5	0.5	tr	tr	tr	-	-	X	X	X	X	-	Quenched groundmass lc.
69	TL	○	8.5	1.0	0.8	0.3	-	-	-	X	X	X	X	X	Glomero c-p-o-bio(altered to ore) ± late leucite.
72	PLT	○	9.5	2.0	1.5	-	-	-	Ap	X	X	X	X	X	Glomero c-p-o-late lc. Zoned plag with kspar margins.
73	PLT	○	7.5	1.0	1.6	0.3	tr	-	Ap	X	X	X	X	X	Rare relic bio partially altered to ore. Max lc = 4mm.
76	TL	●	3.5	1.0	-	-	-	-	-	X	X	X	X	?	Zones of inclusions in macro leucites.
77	TL	○	18.0	2.5	0.5	0.5	-	-	Ap	X	X	X	X	X	Glomero c-p-o-ap±late lc.
79	TL	○	17.1	2.1	tr	tr	-	-	Ap	X	X	X	X	?	Max lc = 6mm. Fine gndmass.
81	TL/LT	●	tr	tr	tr	-	-	-	-	X	X	X	X	-	Micropheno cpx,plag,lc. Quench leucite. 2° calcite.
82	TL/LT	●	tr	tr	tr	-	-	-	-	X	X	X	X	-	As above.
83	TL/LT	●	tr	tr	tr	-	-	-	-	X	X	X	X	-	Macro/micro cpx,plag,lc. Rare resorbed olv. Zoned plag.
91	PLT	○	12.1	1.8	0.9	tr	tr	-	Ap	X	X	X	X	X	Glomero c-p-o±bio±ap-late leucite. Max lc = 4mm.
97	T	▽	-	1.2	3.7	0.7	1.2	5.0	-	-	X	X	X	X	Kspar upto 10mm long. Trachytic matrix. Rare glomero cpx-plag- bio-ore.
99	LP	▽	-	-	-	--	-	3.8	-	X	X	X	X	X	Rare small (2mm) kspar phenos in trachytic matrix.
105	TLP	▽	tr	5.6	4.4	0.8	tr	8.9	Ap	X	X	X	X	X	Bio partially to totally altered to ore.
106	LT/PLT	▲	tr	4.4	2.7	tr	2.3	-	-	X	X	X	X	X	Glomero c-p-o-bio. Mgtite octahedra. Plag and cpx zoned.
107	LT/PLT	▲	1.1	4.0	4.5	tr	1.4	-	Ap	X	X	X	X	X	Cpx-plag-bio-ap glomero. Plag glomero.
108	LT/PLT	▲	1.6	2.5	2.5	tr	1.1	-	Ol	X	X	X	X	X	Resorbed olv surrounded by small cpx, ore, iddingsite.
111	TLP	▽	-	2.5	3.6	tr	3.9	tr	-	X	X	X	X	X	Glomero plag. Zoned plag and cpx. Rare kspar phenos.
112	L	●	-	6.6	-	-	tr	-	Ol	X	X	X	X	?	Rare resorbed bio and olv. Note colour varn. in pleochr. cpx.
116	TL/PLT	○	20.5	2.2	1.7	tr	tr	-	Ap	X	X	X	X	X	Macro lc+ microlc,cpx,plag(Zoned with kspar mantles-max 3mm) Kspar pseudomorph after lc. Max lc = 10mm.
121	LP	▽	-	tr	-	-	-	2.0	Sp Hauyne	X	X	X	X	X	Rare cpx and kspar phenos in trachytic matrix.
122	PLT	●	3.2	1.0	1.8	tr	tr	-	Ap	X	X	X	X	X	Rare altered bio. Glomero lc-c-p-o-ap.
123	PLT	●	1.1	tr	tr	tr	-	-	-	X	X	X	X	X	As above.
128	PLT	●	3.9	0.7	1.9	tr	tr	-	-	X	X	X	X	X	Glomero c-p-o-lc. Rare macro lc.(upto 4mm.)
129	PLT	○	13.4	1.5	1.5	tr	-	-	Ap	X	X	X	X	X	Note complex lc-plag glomeroaggregate.
131	TL	●	-	15.4	tr	-	tr	-	Ol	X	X	X	X	-	Resorbed bio and olv. Rare c-p-bio glomero.
132	TL/LT	▲	tr	7.0	0.8	tr	2.0	-	Ap	X	X	X	X	-	Rare lc and apatite phenos. Glomero cpx surrounded by bio.
134	TLP	▽	-	4.3	4.1	0.6	tr	9.0	Ap 2°Hb	X	X	X	X	X	Bio totally altered to ore. Kspar upto 7mm.,frequently in glomeros, zoned and Carlsbad twinned. Abundant clouded apatite

TABLE B-1 (contd.)

Rock No.	Rock Type	Symbol	Volume °/o Phenocrysts							Groundmass Mineralogy					Comments
			Lc.	Cpx.	Plag.	Ore	Bio.	Kspar	Others	Lc.	Cpx.	Plag.	Ore	Kspar	
136	TL	○	32.0	4.0	tr	-	-	-	Ap	X	X	X	X	-	Lc phenos 0.25-6mm. Kspar develops at lc/plag boundaries.
137	TL	●	-	tr	tr	tr	tr	-	Ap	X	X	X	X	X	Olv in gndmass. Ap in cpx phenos. Bio altered to ore.
138	TL	●	tr	tr	tr	-	-	-	Ap	X	X	X	X	X	Olv in gndmass. Cpx pleochroic yellow-green and zoned.
139	TL	●	tr	tr	-	-	-	-	Ap Ol	X	X	X	X	X	Olv with corona of cpx. Ore pseudo after bio.
140	TL	▲	tr	12.0	tr	tr	3.5	-	Ap	X	X	X	X	-	Note apatite phenos. Cpx zoned and bio altered.
141	PLT	●	tr	tr	-	-	tr	-	Ap	X	X	X	X	X	Pumiceous specimen. Microphenos in brown devitrified matrix.
142	TL/LT	●	-	tr	-	-	-	-	-	X	X	X	X	-	Bio and apatite in gndmass.
146	TL/LT	●	-	3.2	-	-	tr	-	-	X	X	X	X	-	Interstitial phlogopitic mica. Rare resorbed bio.
148	TL	●	-	1.0	-	-	-	-	-	X	X	X	X	X	2^{o}Hb after gndmass cpx.
150	TL	●	-	0.7	-	-	-	-	Ol	X	X	X	X	X	Mgtite-kspar pseudomorphs after biotite.Poikilitic late kspar.
151	L	●	-	tr	-	tr	-	-	-	X	X	X	X	-	Microphenos of cpx.
153	L	●	-	3.4	-	-	-	-	-	X	X	X	X	X	Rare phenos of cpx and olv. Gndmass and pheno olv iddingsitised
154	L	●	-	tr	-	-	-	-	-	X	X	-	X	-	Interstitial phlogo mica. Quench leucite.
155	PLT	○	14.2	1.0	tr	-	tr	1.3	Hauyne	X	X	X	X	X	Plag phenos with kspar mantles. Gndmass slightly altered.
163	LT	●	tr	tr	tr	tr	-	-	Ap	X	X	X	X	X	Rare macro leucite. Kspar mantles gndmass plag.
165	TL	●	4.5	tr	-	-	-	-	-	X	X	X	X	?	Microphenos of leucite. Max 1mm.
166	TL	●	-	tr	-	-	-	-	-	X	X	X	X	-	Gndmass olivine. Large glomero cpx. Max cpx = 3mm.
170	LT/PLT	▲	0.5	5.2	2.7	tr	2.9	-	Ap	X	X	X	X	X	Glomero plag. Bio marginally resorbed.
177	TL	○	10.6	3.3	0.3	0.3	-	-	-	X	X	X	X	X	Rare glomero zoned c-p-o+late leucite.
178	TL	○	34.8	1.4	1.4	tr	-	-	Ap	X	X	X	X	X	Max lc = 8mm. Ap needles in lc phenos.
179	TLP	▽	2.6	tr	tr	-	-	3.5	Sp	X	X	X	X	X	Gndmass plag with kspar mantles. Rare kspar phenos (max 5mm)
180	TL	●	tr	tr	-	-	-	-	-	X	X	X	X	-	Rare microphenos lc + cpx. Quench leucite. Dyke rock.
181	TL	●	tr	tr	-	-	-	-	-	X	X	X	X	-	As above. Different dyke.
182	TL	●	tr	tr	-	-	-	-	-	X	X	X	X	-	As above. Margin of dyke R.181
183	TL	○	11.0	tr	-	-	-	-	-	X	X	X	X	-	Glomeroaggregate of plag-cpx-ore-apatite.
185	TL	○	42.0	5.0	-	-	-	-	Ol	X	X	X	X	-	Rare olv pheno with cpx mantle. Ap occurs as inclusions in lc. and cpx.
198	TL/PLT	○	13.0	2.7	tr	tr	-	-	Ap	X	X	X	X	X	Oscillatory zoned cpx. Ap inclusions in cpx.
206	TL	○	32.0	3.5	tr	0.8	-	-	Ap	X	X	X	X	-	Max lc pheno = 9mm. Fine gndmass. Ap needles in lc phenos.
209	LT/PLT	▲	tr	6.0	4.1	tr	1.5	-	Ap	X	X	X	X	X	Biotite marginally altered tp ore. Zoned plag and cpx phenos. Glomero cpx-plag-ore-bio-apatite.

TABLE B-2 Petrography of analysed specimens from Low K Series.

Rock No.	Rock Type	Volume °/o Phenocrysts						Groundmass Mineralogy					Comments
		Olv.	Cpx.	Plag.	Ore	Bio.	Kspar.	Olv.	Cpx.	Plag.	Ore	Kspar.	
56	OB	3.7	7.5	tr	-	tr	-	X	X	X	X		Olivine with cpx corona. Large biotite with cpx inclusions. Glomero cpx-plag-ore
57	OB	2.9	8.3	-	-	-	-	X	X	X	X		Only macrophenos counted. Glomero cpx with small red spinels.
67	GAF	-	-	-	-	-	tr	-	-	-		X	XRD suggests bulk of ash flow is Kspar.
86	OB	1.3	3.7	tr	-	tr	-	X	X	X	X		Only macrophenos counted. Olivine Fo87. Colourless cpx and rare pale green cpx. Plag zoned with inclusions. Very vesicular.
90	BAL	-	10.1	15.8	tr	4.1	-	-	X	X	X	X	Glomero cpx-plag-bio-ore in trachytic groundmass. Zoned, spongy plag phenos with cpx inclusions. Rare apatite phenos.
95	BAL	-	0.5	3.7	tr	0.8	-	-	X	X	X	X	Euhedral phenos in trachytic groundmass.
96	BAL	-	0.6	3.4	tr	0.8	-	-	X	X	X	X	Primary bio altered to ore. Secondary bio in trachytic gndmass.
98	BAL	tr	1.7	3.4	tr	1.5	-	-	X	X	X	X	Large bio enclosing plag. Glomero cpx-bio-plag-ore in trachytic groundmass.
101	TB	tr	5.0	1.7	-	-	-	X	X	X	X		Only macrophenos counted. Brown devitrified glassy matrix. Very vesicular.
104	BAL	-	4.5	5.5	tr	1.6	tr	-	X	X	X	X	Aggregate of late kspar. Glomero c-p-b-o in trachytic matrix
109	BAL	-	4.6	5.3	tr	1.4	-	-	X	X	X	X	Plag phenos with kspar mantles - normal and oscillatory zoning.
114	OB	tr	3.4	tr	-	-	-	X	X	X	X		Rare glomero cpx-plag. Secondary red brown bio near vesicles. Olivine marginally iddingsitised. Coarse intergranular gndmass.
117	OB	1.1	1.3	-	-	-	-	X	X	X	X		Only macrophenos counted. Fine, vesicular, microphenos olv+cpx.
119	OB	2.5	1.4	-	-	-	-	X	X	X	X		Abundant microphenos olv + cpx. Quench olivine.
157	OB	4.3	4.2	-	-	-	-	X	X	X	X		Very vesicular. Olivine marginally to totally iddingsitised.
158	OB	tr	tr	-	-	-	-	X	X	X	X		Abundant microphenos cpx + olivine
160	OB	1.2	1.0	tr	-	-	-	-	X	X	X		Olivine enclosed by cpx. Rare plag glomero.
162	BAL	tr	tr	tr	-	tr	-	-	X	X	X	X	Rare microphenos in fine groundmass.
184	OB	2.6	4.7	-	-	-	-	X	X	X	X		Only macrophenos counted. Large cpx (1-3mm) shows oscillatory zoning. Olivine →0.5mm and marginally iddingsitised.
186	TB	tr	15.0	21.0	-	-	-	X	X	X	X		Plag phenos zoned; large variation in size; some of cores show alteration and inclusions. Olivine often skeletal.
187	TB	tr	15.0	21.0	-	-	-	X	X	X	X		As above.
188	TB	"	"	"	-	tr	-	X	X	X	X		Glomero cpx-plag-ore-bio. Plag shows oscillatory zoning.
189	TB	"	"	"	-	tr	-	X	X	X	X		Large corroded biotite. Rare glomero cpx-plag-bio.
191	BAL	-	8.4	14.0	tr	5.5	-	-	X	X	X	X	Large glomero cpx-plag-bio. Rare apatite phenos. Some of plag. phenos have kspar mantles. Plag phenos with spongy cores.

APPENDIX C

Tables of chemical data for the Roccamonfina lavas (R)

Abbreviations : FEE = Total iron as Fe_2O_3;

FM = $FeO + Fe_2O_3/FeO + Fe_2O_3 + MgO$; FF = $Fe_2O_3/FeO + Fe_2O_3$;

KNA = K_2O/Na_2O; KBA = K/Ba; KSR = K/Sr; KRB = K/Rb;

THK = Th/K; ZT = Zr/Th; CS = Ca/Sr; RBSR = Rb/Sr.

C-1 High K lavas - major elements

C-2 High K lavas - trace elements and ratios

C-3 High K lavas - groundmass major, trace and ratio data

C-4 Low K lavas - major elements

C-5 Low K lavas - trace elements and ratios

C-6 High K lavas - C.I.P.W. norms

C-7 Low K lavas - C.I.P.W. norms

C-8 CO_2, Ce, and Nb data

C-9 Biotite Gabbro

TABLE C-1

S.N.	SIO2	AL2O3	FE2O3	FEO	MGO	CAO	NA2O	K2O	H2O	TIO2	P2O5	MNO	BAO	SRO	TOTAL
2	49.38	18.71	2.53	4.19	3.48	7.82	2.28	8.31	0.95	0.73	0.33	0.14	0.15	0.21	99.2
4	48.91	19.78	4.09	3.45	2.89	7.32	2.17	7.63	1.50	0.79	0.41	0.15	0.19	0.23	99.5
6	48.83	19.76	3.14	4.07	2.58	7.09	2.83	7.95	0.98	0.74	0.42	0.15	0.18	0.24	99.0
7	50.65	20.71	1.80	3.52	1.98	5.25	2.54	10.31	0.97	0.59	0.32	0.11	0.16	0.21	99.1
11	56.42	20.25	3.16	0.34	0.72	3.41	2.53	9.28	2.20	0.44	0.09	0.12	0.12	0.17	99.2
14	55.75	20.24	2.10	1.39	0.91	3.69	4.04	9.15	0.99	0.46	0.11	0.14	0.12	0.16	99.2
15	51.13	20.30	2.46	3.87	1.81	5.89	3.54	8.72	0.56	0.68	0.34	0.19	0.23	0.30	100.0
18	52.85	20.91	2.15	1.86	0.93	3.87	3.37	10.55	1.14	0.49	0.15	0.15	0.20	0.26	98.9
19	50.05	19.98	5.62	1.05	1.85	6.74	2.04	9.03	1.29	0.66	0.32	0.15	0.16	0.27	99.2
20	48.49	19.18	2.25	4.81	2.74	7.27	2.10	9.65	0.70	0.75	0.48	0.15	0.21	0.24	99.0
21	53.31	20.62	1.71	2.90	1.04	4.83	3.41	9.60	0.63	0.53	0.19	0.14	0.21	0.26	99.4
23	48.52	19.21	2.48	4.93	2.78	7.31	2.14	9.66	0.86	0.76	0.51	0.16	0.20	0.26	99.8
24	53.43	21.20	3.60	0.75	1.04	3.87	2.93	10.41	1.27	0.49	0.15	0.15	0.21	0.27	99.8
27	50.54	20.10	3.00	3.27	1.77	5.82	3.26	8.66	1.06	0.67	0.31	0.17	0.23	0.30	99.2
29	56.75	21.09	3.16	0.09	0.42	2.45	4.17	9.76	1.56	0.42	0.08	0.16	0.14	0.28	100.5
33	50.22	20.05	3.44	2.62	2.17	5.94	2.31	10.06	0.66	0.61	0.36	0.12	0.15	0.20	98.9
36	50.85	20.72	1.72	3.56	1.73	5.05	2.69	10.65	0.65	0.57	0.35	0.12	0.15	0.22	99.0
37	53.45	18.36	3.99	1.54	2.59	6.84	2.47	7.26	1.52	0.61	0.26	0.12	0.08	0.16	99.3
39	49.14	18.69	3.23	3.49	2.98	7.28	2.49	9.60	0.56	0.72	0.38	0.15	0.18	0.24	99.1
41	50.17	19.10	3.00	3.33	2.38	6.71	2.38	10.07	0.79	0.70	0.35	0.14	0.18	0.24	99.5
42	52.58	18.83	3.16	2.81	2.42	6.71	2.89	7.18	1.09	0.65	0.27	0.13	0.10	0.17	99.0
43	52.91	19.91	2.25	2.51	1.60	5.55	3.15	10.87	0.50	0.54	0.23	0.14	0.16	0.23	100.6
44	51.71	21.20	1.99	2.68	1.48	4.35	2.10	11.50	1.16	0.50	0.24	0.11	0.17	0.20	99.4
47	53.39	19.49	3.43	2.76	2.34	6.71	2.96	7.20	0.80	0.65	0.30	0.15	0.10	0.18	100.5
48	51.00	20.47	1.89	3.79	2.18	5.45	2.44	10.10	0.58	0.61	0.34	0.12	0.16	0.22	99.3
50	50.02	20.12	2.34	4.02	2.23	6.22	2.62	9.58	0.83	0.65	0.39	0.14	0.15	0.21	99.5
53	53.34	18.04	3.89	1.91	2.96	7.15	2.55	7.71	0.92	0.63	0.27	0.14	0.08	0.16	99.7
55	50.01	19.47	2.65	4.90	2.91	7.74	2.56	7.51	0.63	0.77	0.43	0.16	0.14	0.20	100.1
59	48.93	18.48	1.68	5.66	3.93	8.21	2.21	6.55	0.73	0.80	0.36	0.15	0.13	0.19	98.0
60	49.01	17.60	2.44	4.83	3.42	8.92	2.31	6.83	0.89	0.79	0.39	0.14	0.14	0.21	97.9
61	53.32	19.67	2.37	1.83	1.52	4.68	2.88	10.28	0.90	0.55	0.16	0.11	0.17	0.23	98.7
64	57.70	20.10	2.51	1.02	0.69	3.59	3.25	9.44	0.44	0.44	0.10	0.10	0.19	0.21	99.8
68	48.27	19.47	3.49	4.64	2.49	8.25	2.48	8.39	0.61	0.80	0.59	0.18	0.20	0.28	100.1
69	50.60	20.69	2.27	3.99	1.91	5.83	2.75	8.64	0.83	0.67	0.31	0.18	0.24	0.31	99.2
72	52.88	21.02	2.75	2.44	1.22	4.47	4.37	8.86	0.66	0.57	0.24	0.20	0.26	0.30	100.2
73	53.34	20.91	2.12	2.65	1.11	4.11	4.40	8.97	0.66	0.57	0.19	0.18	0.26	0.31	99.8
76	49.35	19.74	1.69	5.67	2.61	7.31	2.69	8.32	0.67	0.75	0.47	0.16	0.17	0.24	99.8
77	51.71	20.11	3.30	2.74	1.56	5.95	2.29	10.00	1.49	0.62	0.26	0.14	0.15	0.24	100.6
79	51.29	20.03	2.80	2.78	1.67	5.87	2.41	9.76	1.34	0.61	0.25	0.13	0.15	0.23	99.3
81	49.81	19.18	1.90	5.63	3.33	7.91	2.46	7.07	0.73	0.80	0.39	0.16	0.13	0.20	99.7

TABLE C-1 (contd.)

S.N.	SIO2	AL2O3	FE2O3	FEO	MGO	CAO	NA2O	K2O	H2O	TIO2	P2O5	MNO	BAO	SRO	TOTAL
82	49.09	18.72	1.66	5.49	2.97	7.72	2.33	6.84	0.78	0.77	0.36	0.13	0.13	0.19	97.2
83	49.32	18.39	1.56	5.67	3.87	8.28	2.29	6.61	0.55	0.81	0.36	0.14	0.13	0.18	98.2
91	52.87	21.23	3.21	2.20	1.33	4.58	4.25	8.83	0.52	0.58	0.20	0.21	0.26	0.30	100.6
97	59.12	18.86	2.36	1.05	0.62	3.14	3.68	8.43	0.97	0.41	0.15	0.10	0.03	0.09	99.0
99	57.94	22.00	1.68	0.48	0.19	1.86	3.66	9.72	1.79	0.23	0.04	0.14	0.01	0.04	99.8
105	55.92	19.39	2.65	1.26	1.13	3.92	2.85	8.31	1.93	0.46	0.15	0.10	0.13	0.19	98.4
106	51.60	19.83	4.92	2.03	2.45	6.97	2.86	7.65	0.94	0.69	0.29	0.16	0.11	0.18	100.7
107	51.45	19.91	4.07	1.99	2.08	6.40	2.86	7.58	0.95	0.64	0.27	0.12	0.11	0.18	98.6
108	51.85	20.11	4.45	2.21	1.95	6.40	3.18	8.04	0.62	0.64	0.29	0.16	0.11	0.18	100.2
111	55.17	20.62	4.09	0.42	1.51	3.94	2.43	8.55	2.37	0.50	0.21	0.12	0.12	0.18	100.2
112	46.61	16.77	2.63	6.00	5.49	11.35	1.47	5.99	1.25	1.02	0.53	0.15	0.13	0.18	99.6
116	53.18	20.71	2.54	1.21	1.48	4.08	2.41	11.00	1.12	0.42	0.15	0.10	0.10	0.17	98.7
121	58.22	21.03	1.47	0.67	0.16	2.05	5.69	9.05	0.35	0.31	0.04	0.16	0.00	0.02	99.2
122	53.64	20.00	3.08	3.12	1.60	5.17	3.31	8.35	1.03	0.61	0.35	0.16	0.11	0.16	100.7
123	53.31	19.85	2.04	4.01	1.63	5.13	3.24	8.62	1.01	0.61	0.33	0.16	0.11	0.16	100.2
128	52.94	19.88	2.80	2.89	1.47	5.05	3.08	8.48	0.84	0.61	0.30	0.15	0.12	0.16	98.8
129	53.70	19.97	2.36	2.82	1.29	4.27	3.23	9.31	0.98	0.56	0.26	0.15	0.12	0.16	99.2
131	48.18	16.06	3.34	4.97	5.31	10.52	1.63	6.20	0.91	0.90	0.54	0.15	0.14	0.18	99.0
132	50.86	19.13	3.17	3.62	2.70	7.31	2.84	8.31	0.56	0.69	0.40	0.16	0.20	0.25	100.2
134	55.65	19.91	3.23	1.28	1.41	4.70	2.92	8.22	2.07	0.48	0.23	0.13	0.11	0.19	100.5
136	50.45	20.40	2.78	2.93	1.91	5.59	1.96	10.66	1.19	0.58	0.34	0.12	0.16	0.21	99.3
137	50.13	19.93	2.32	3.79	1.89	6.96	2.36	9.15	0.99	0.63	0.31	0.14	0.18	0.27	99.1
138	50.03	20.01	2.56	3.71	1.73	6.94	2.46	9.22	0.77	0.60	0.38	0.15	0.17	0.27	99.0
139	50.74	19.95	3.60	2.72	1.83	6.81	2.29	9.16	0.74	0.63	0.31	0.15	0.24	0.25	99.4
140	49.56	17.93	3.93	3.43	3.77	8.87	2.43	7.39	0.67	0.77	0.44	0.16	0.20	0.23	99.8
141	54.74	20.37	2.23	1.84	0.56	4.14	3.08	9.74	1.25	0.48	0.12	0.14	0.20	0.19	99.1
142	47.40	17.58	4.83	4.59	4.97	10.37	1.74	5.40	0.44	0.97	0.43	0.16	0.16	0.17	99.2
146	48.85	17.94	2.80	5.05	4.08	9.19	2.50	5.97	0.97	0.84	0.39	0.16	0.13	0.19	99.1
148	47.50	16.37	3.99	4.49	5.59	10.55	1.87	6.73	0.99	0.86	0.44	0.15	0.13	0.21	99.9
150	49.00	16.62	4.35	4.18	4.37	10.01	1.86	7.86	0.64	0.81	0.53	0.16	0.14	0.22	100.8
151	47.13	16.47	8.11	0.68	4.99	10.31	1.95	6.69	1.09	0.85	0.48	0.15	0.21	0.18	99.3
153	46.01	14.75	6.35	2.40	6.79	12.13	1.26	6.62	0.92	0.94	0.62	0.13	0.13	0.21	99.3
154	45.84	14.66	4.02	4.66	6.72	12.41	1.56	6.85	0.49	0.94	0.69	0.16	0.20	0.19	99.4
155	55.16	21.04	1.98	1.28	0.77	3.28	3.47	9.99	1.16	0.43	0.11	0.13	0.15	0.18	99.1
163	51.18	19.51	2.28	4.72	2.63	6.50	2.69	7.80	0.66	0.80	0.35	0.14	0.15	0.18	99.6
165	49.14	19.40	2.77	4.85	2.72	7.44	3.01	8.30	0.37	0.75	0.52	0.17	0.17	0.25	99.9
166	48.19	19.42	2.72	5.03	2.55	7.66	2.58	8.13	0.95	0.77	0.55	0.17	0.18	0.27	99.2
170	51.21	19.32	3.78	3.29	2.65	7.51	2.88	6.85	1.41	0.74	0.43	0.15	0.16	0.20	100.6
177	49.28	19.81	3.11	4.57	2.43	7.45	2.98	8.18	0.47	0.75	0.49	0.17	0.18	0.25	100.1
178	51.90	21.20	2.54	2.11	1.46	4.25	2.18	11.80	0.69	0.51	0.26	0.10	0.17	0.20	99.4
179	56.70	20.24	2.50	0.55	0.26	2.58	3.29	10.24	1.72	0.45	0.05	0.13	0.13	0.18	99.0
180	48.92	19.47	2.35	5.44	2.62	7.54	2.28	8.30	0.86	0.80	0.47	0.15	0.18	0.26	99.6
181	48.77	19.44	2.17	5.68	2.53	7.72	2.57	8.15	0.99	0.77	0.49	0.18	0.17	0.26	99.9
182	48.88	19.16	1.98	5.72	2.73	7.57	2.35	7.99	1.30	0.78	0.44	0.16	0.18	0.26	99.5
183	49.55	19.70	2.18	5.24	2.46	7.24	2.91	8.45	0.48	0.73	0.45	0.16	0.17	0.25	100.0
185	49.38	18.96	3.28	3.23	2.71	6.96	1.93	10.02	0.99	0.72	0.37	0.13	0.18	0.24	99.1
198	53.17	20.23	2.65	2.04	1.02	4.15	3.60	10.30	0.67	0.55	0.15	0.14	0.18	0.26	99.1
206	51.24	20.75	2.83	2.69	1.51	5.30	2.78	11.51	0.55	0.58	0.27	0.14	0.16	0.23	100.5
209	51.09	18.59	3.80	2.98	2.72	7.50	2.45	7.38	1.08	0.73	0.37	0.13	0.16	0.23	99.2

TABLE C-2

S.No.	BA	ZR	Y	SR	RB	TH	ZN	FEE	FM	FF	KNA	KBA	KSR	KRB	THK	ZT	CS	RBSR
2	1377	233	51	1784	542	40	79	7.18	0.66	0.38	3.64	50	39	127	5.80	6	31	0.30
4	1660	233	53	1945	526	31	97	7.92	0.72	0.54	3.52	38	33	120	4.90	8	27	0.27
6	1606	235	43	2022	448	39	84	7.66	0.74	0.44	2.81	41	33	147	5.91	6	25	0.22
7	1447	206	52	1741	819	35	58	5.71	0.73	0.34	4.06	59	49	104	4.09	6	22	0.47
11	1064	306	56	1418	562	51	59	3.54	0.83	0.90	3.67	72	54	137	6.62	6	17	0.40
14	1051	332	48	1368	682	53	58	3.64	0.79	0.60	2.26	72	56	111	6.98	6	19	0.50
15	2085	333	59	2552	460	58	94	6.76	0.78	0.39	2.46	35	28	157	8.01	6	16	0.18
18	1824	345	56	2206	678	62	65	4.21	0.81	0.54	3.13	48	40	129	7.08	6	13	0.31
19	1395	324	57	2286	634	45	87	6.79	0.78	0.84	4.43	54	33	118	6.00	7	21	0.28
20	1900	251	46	2068	634	41	81	7.59	0.72	0.32	4.60	42	39	126	5.12	6	25	0.31
21	1867	271	46	2191	527	53	67	4.93	0.82	0.37	2.82	43	36	151	6.65	5	16	0.24
23	1823	269	55	2192	617	42	74	7.95	0.73	0.33	4.51	44	37	130	5.24	6	24	0.28
24	1868	302	50	2252	674	47	74	4.43	0.81	0.83	3.55	46	38	128	5.44	6	12	0.30
27	2048	320	56	2567	453	70	82	6.63	0.78	0.48	2.66	35	28	159	9.74	5	16	0.18
29	1265	386	30	2344	506	80	84	3.26	0.89	0.97	2.34	64	35	160	9.88	5	7	0.22
33	1361	204	51	1720	810	38	67	6.35	0.74	0.57	4.35	61	49	103	4.55	5	25	0.47
36	1383	207	44	1851	776	40	75	5.67	0.75	0.33	3.96	64	48	114	4.53	5	19	0.42
37	740	260	48	1379	561	47	54	5.70	0.68	0.72	2.94	81	44	107	7.80	6	35	0.41
39	1591	277	48	2027	602	60	78	7.10	0.69	0.48	3.86	50	39	132	7.53	5	26	0.30
41	1630	271	59	2043	744	51	83	6.70	0.73	0.47	4.23	51	41	112	6.10	5	23	0.36
42	857	252	41	1422	470	36	64	6.28	0.71	0.53	2.48	70	42	127	6.04	7	34	0.33
43	1426	281	61	1970	621	53	80	5.04	0.75	0.47	3.45	63	46	145	5.87	5	20	0.32
44	1491	198	48	1677	921	36	59	4.96	0.76	0.43	5.48	64	57	104	3.77	6	19	0.55
47	865	260	52	1512	594	45	74	6.49	0.73	0.55	2.43	69	40	101	7.53	6	32	0.39
48	1428	208	40	1831	728	47	66	6.10	0.72	0.33	4.14	59	46	115	5.61	4	21	0.40
50	1382	222	56	1809	742	33	80	6.80	0.74	0.37	3.66	58	44	107	4.15	7	25	0.41
53	675	250	53	1328	482	44	51	6.01	0.66	0.67	3.02	95	48	133	6.88	6	38	0.36
55	1231	217	40	1730	570	37	70	8.09	0.72	0.35	2.93	51	36	109	5.94	6	32	0.33
59	1145	210	43	1587	418	32	80	7.96	0.65	0.23	2.96	47	34	130	5.89	7	37	0.26
60	1295	256	53	1807	351	34	79	7.80	0.68	0.34	2.96	44	31	162	6.00	8	35	0.19
61	1516	300	44	1915	633	72	61	4.40	0.73	0.56	3.57	56	45	135	8.44	4	17	0.33
64	1710	306	48	1791	575	56	62	3.64	0.84	0.71	2.90	46	44	136	7.15	5	14	0.32
68	1775	280	57	2348	604	35	71	8.64	0.77	0.43	3.38	39	30	115	5.03	8	25	0.26
69	2126	317	61	2595	710	62	87	6.70	0.77	0.36	3.14	34	28	101	8.65	5	16	0.27
72	2301	369	49	2564	418	76	81	5.46	0.81	0.53	2.03	32	29	176	10.33	5	12	0.16
73	2298	384	58	2593	383	94	98	5.06	0.81	0.44	2.04	32	29	194	12.63	4	11	0.15
76	1529	228	39	2030	466	45	79	7.98	0.74	0.23	3.09	45	34	148	6.52	5	26	0.23
77	1329	274	67	2007	656	39	69	6.34	0.79	0.55	4.37	62	41	127	4.70	7	21	0.33
79	1374	267	58	1981	717	50	95	5.89	0.77	0.50	4.05	59	41	113	6.17	5	21	0.36
81	1159	214	48	1651	437	23	86	8.15	0.69	0.25	2.87	51	36	134	3.92	9	34	0.26

TABLE C-2 (contd.)

S.N.	BA	ZR	Y	SR	RB	TH	ZN	FEE	FM	FF	KNA	KBA	KSR	KRB	THK	ZT	CS	RBSR
82	1177	218	43	1624	460	39	86	7.75	0.71	0.23	2.94	48	35	123	6.87	6	34	0.28
83	1197	200	40	1552	419	22	86	7.85	0.65	0.22	2.89	46	35	131	4.01	9	38	0.27
91	2296	377	58	2499	453	76	103	5.65	0.80	0.59	2.08	32	29	162	10.37	5	13	0.18
97	313	587	57	772	684	107	76	3.53	0.85	0.69	2.29	224	91	102	15.29	5	29	0.89
99	54	622	57	353	1836	111	87	2.21	0.92	0.78	2.66	1494	229	44	13.76	6	38	5.20
105	1158	348	55	1599	647	54	45	4.05	0.78	0.68	2.92	60	43	107	7.83	6	18	0.40
106	997	227	45	1522	421	30	89	7.17	0.74	0.71	2.67	64	42	151	4.72	8	33	0.28
107	999	227	50	1527	441	26	87	6.28	0.74	0.67	2.65	63	41	143	4.13	9	30	0.29
108	964	238	55	1490	440	29	77	6.90	0.77	0.67	2.53	69	45	152	4.35	8	31	0.30
111	1063	258	43	1534	556	44	70	4.56	0.75	0.91	3.52	67	46	128	6.20	6	18	0.36
112	1175	217	44	1538	437	14	71	9.29	0.61	0.30	4.07	42	32	114	2.82	16	53	0.28
116	932	246	58	1410	1270	42	46	3.88	0.72	0.68	4.56	98	65	72	4.60	6	21	0.90
121	24	511	82	156	616	109	100	2.21	0.93	0.69	1.59	3130	482	122	14.51	5	94	3.95
122	996	245	49	1359	592	37	75	6.54	0.79	0.50	2.52	70	51	117	5.34	7	27	0.44
123	974	245	53	1363	588	31	77	6.49	0.79	0.34	2.66	73	52	122	4.33	8	27	0.43
128	1056	250	54	1348	553	25	80	6.01	0.79	0.49	2.75	67	52	127	3.55	10	27	0.41
129	1117	250	62	1334	645	26	75	5.49	0.80	0.46	2.88	69	58	120	3.36	10	23	0.48
131	1245	246	55	1520	677	34	63	8.86	0.61	0.40	3.80	41	34	76	6.61	7	49	0.45
132	1830	264	48	2096	427	46	69	7.19	0.72	0.47	2.93	38	33	162	6.67	6	25	0.20
134	954	329	65	1626	533	58	48	4.65	0.76	0.72	2.82	72	42	128	8.50	6	21	0.33
136	1411	224	47	1739	879	41	65	6.03	0.75	0.49	5.44	63	51	101	4.63	5	23	0.51
137	1634	254	54	2282	771	35	58	6.53	0.76	0.38	3.88	46	33	99	4.61	7	22	0.34
138	1542	260	62	2273	858	36	50	6.68	0.78	0.41	3.75	50	34	89	4.70	7	22	0.38
139	2126	308	62	2086	454	57	75	6.62	0.78	0.57	4.00	36	36	167	7.50	5	23	0.22
140	1751	256	49	1943	382	38	61	7.74	0.66	0.53	3.04	35	32	161	6.20	7	33	0.20
141	1792	187	38	1626	329	20	70	4.27	0.88	0.55	3.16	45	50	246	2.47	9	18	0.20
142	1413	191	45	1404	375	21	74	9.92	0.65	0.51	3.10	32	32	120	4.69	9	53	0.27
146	1166	224	45	1567	447	37	78	8.41	0.66	0.36	2.39	42	32	111	7.47	6	42	0.29
148	1188	257	48	1806	440	17	73	8.97	0.60	0.47	3.60	47	31	127	3.04	15	42	0.24
150	1291	278	49	1880	496	37	60	8.99	0.66	0.51	4.23	51	35	132	5.67	8	38	0.26
151	1860	267	50	1545	473	38	60	8.86	0.64	0.92	3.43	30	36	117	6.84	7	48	0.31
153	1178	405	63	1749	654	69	57	9.01	0.56	0.73	5.25	47	31	84	12.56	6	50	0.37
154	1824	251	43	1594	422	39	62	9.19	0.56	0.46	4.39	31	36	135	6.86	6	56	0.26
155	1354	230	48	1560	509	27	64	3.40	0.81	0.61	2.88	61	53	163	3.26	9	15	0.33
163	1354	230	48	1560	509	27	64	7.52	0.73	0.33	2.90	48	41	127	4.17	9	30	0.33
165	1561	257	53	2119	443	49	80	8.15	0.74	0.36	2.76	44	33	156	7.11	5	25	0.21
166	1615	268	58	2248	445	48	76	8.30	0.75	0.35	3.15	42	30	152	7.11	6	24	0.20
170	1418	274	65	1662	909	41	67	7.43	0.73	0.53	2.38	40	34	63	7.21	7	32	0.55
177	1587	251	49	2096	445	41	74	8.18	0.76	0.40	2.74	43	32	153	6.04	6	25	0.21
178	1499	194	34	1706	1002	45	56	4.88	0.76	0.55	5.41	65	57	98	4.59	4	18	0.59
179	1124	340	53	1532	801	71	61	3.11	0.92	0.82	3.11	76	55	106	8.35	5	12	0.52
180	1604	259	51	2180	534	50	93	8.39	0.75	0.30	3.64	43	32	129	7.26	5	25	0.24
181	1523	271	55	2179	479	37	93	8.47	0.76	0.28	3.17	44	31	141	5.47	7	25	0.22
182	1626	259	49	2192	526	50	109	8.33	0.74	0.26	3.40	41	30	126	7.54	5	25	0.24
183	1542	256	48	2078	474	41	76	8.00	0.75	0.29	2.90	45	34	148	5.85	6	25	0.23
185	1571	300	55	2043	711	48	80	6.87	0.71	0.50	5.19	53	41	117	5.77	6	24	0.35
198	1589	334	63	2187	497	58	74	4.91	0.82	0.57	2.86	54	39	172	6.78	6	14	0.23
206	1434	271	55	1933	760	49	73	5.82	0.79	0.51	4.14	67	49	126	5.13	6	20	0.39
209	1464	284	49	1923	754	45	61	7.11	0.71	0.56	3.01	42	32	81	7.35	6	28	0.39

TABLE C-3

S.N.	SIO2	AL2O3	FE2O3	FEO	MGO	CAO	NA2O	K2O	H2O	TIO2	P2O5	MNO	BAO	SRO	TOTAL
18	53.10	20.19	3.17	2.36	1.10	4.98	4.03	8.04	0.86	0.66	0.18	0.20	0.27	0.32	99.5
23	47.41	18.09	3.00	6.01	3.44	8.80	2.28	7.49	0.77	0.92	0.52	0.18	0.24	0.30	99.5
36	49.70	20.10	3.01	4.50	2.69	7.01	3.31	7.15	0.61	0.78	0.40	0.16	0.22	0.29	99.9
39	47.70	17.39	4.13	4.63	3.64	9.27	3.09	6.61	0.46	0.94	0.46	0.19	0.22	0.32	99.0
43	52.40	18.81	2.00	3.03	1.92	6.83	3.78	8.38	0.42	0.70	0.24	0.15	0.21	0.29	99.2
50	49.90	19.62	2.69	4.47	2.66	7.17	2.74	8.13	0.66	0.74	0.40	0.14	0.18	0.24	99.7
61	53.29	19.29	2.85	2.11	1.57	5.36	3.22	8.84	1.07	0.62	0.19	0.15	0.20	0.25	99.0
77	50.62	19.82	3.29	2.95	1.72	6.37	2.31	9.11	1.36	0.67	0.29	0.13	0.16	0.26	99.1
116	52.92	20.07	3.27	1.52	1.72	5.27	2.97	8.68	1.28	0.52	0.20	0.14	0.12	0.21	98.9
136	48.60	19.31	3.60	3.96	2.70	7.62	2.42	7.62	1.25	0.79	0.42	0.16	0.20	0.27	98.9
198	53.32	19.96	2.91	2.25	0.90	4.61	3.84	9.27	0.69	0.63	0.15	0.14	0.20	0.29	99.2
206	50.26	19.10	3.77	3.30	1.90	6.82	3.27	8.81	0.41	0.77	0.29	0.16	0.20	0.29	99.3

S.N.	BA	ZR	Y	SR	RB	TH	ZN
18	2377	438	68	2719	422	70	71
23	2152	347	70	2544	421	33	83
36	1990	324	55	2450	455	56	87
39	1968	404	69	2703	379	64	101
43	1838	388	66	2428	421	65	94
50	1621	261	50	2056	603	46	90
61	1817	360	59	2089	477	75	82
77	1465	316	57	2191	626	59	87
116	1111	319	55	1810	1045	61	59
136	1769	299	52	2295	634	56	95
198	1797	393	68	2431	427	67	95
206	1766	362	70	2466	548	52	91

FEE	FM	FF	KNA	KBA	KSR	KRB	THK	ZT	CS	RBSR
5.79	0.83	0.57	2.00	28	25	158	10.49	6	13	0.16
9.67	0.72	0.33	3.29	29	24	148	5.31	11	25	0.17
8.00	0.74	0.40	2.16	30	24	130	9.44	6	20	0.19
9.27	0.71	0.47	2.14	28	20	145	11.67	6	25	0.14
5.36	0.72	0.40	2.22	38	29	165	9.35	6	20	0.17
7.65	0.73	0.38	2.97	42	33	112	6.82	6	25	0.29
5.19	0.76	0.57	2.75	40	35	154	10.22	5	18	0.23
6.56	0.78	0.53	3.94	52	35	121	7.80	5	21	0.29
4.96	0.74	0.68	2.92	65	40	69	8.47	5	21	0.58
8.00	0.74	0.48	3.15	36	28	100	8.85	5	24	0.28
5.41	0.85	0.56	2.41	43	32	180	8.71	6	14	0.18
7.43	0.79	0.53	2.69	41	30	133	7.11	7	20	0.22

TABLE C-4

S.N.	SIO2	AL2 03	FE2O3	FEO	MGO	CAO	NA2O	K2O	H2O	TIO2	P2O5	MNO	BAO	SRO	TOTAL
56	49.95	16.91	2.04	6.23	6.24	10.53	1.97	3.24	0.58	0.95	0.30	0.15	0.08	0.10	99.3
57	50.21	15.25	2.19	5.78	8.52	11.61	1.68	2.72	0.26	0.84	0.33	0.15	0.07	0.09	99.7
67	60.30	18.69	2.75	0.94	0.86	2.55	4.46	7.53	0.62	0.47	0.10	0.17	0.04	0.03	99.5
86	49.81	17.09	2.35	5.90	6.12	10.61	2.02	3.29	0.80	0.91	0.35	0.15	0.08	0.10	99.6
90	53.04	19.23	3.83	3.31	3.15	6.51	2.77	4.41	2.01	0.76	0.30	0.14	0.08	0.11	99.6
95	54.14	18.55	3.36	3.53	2.57	7.03	3.11	5.07	0.68	0.70	0.35	0.15	0.09	0.12	99.4
96	55.03	18.53	2.74	3.57	2.55	6.55	3.39	5.37	0.29	0.65	0.38	0.16	0.09	0.12	99.4
98	55.19	18.91	3.90	2.32	2.14	5.85	3.37	5.50	0.40	0.62	0.28	0.14	0.10	0.12	98.8
101	52.49	16.81	1.47	6.18	6.10	9.70	1.94	2.99	0.47	0.72	0.23	0.14	0.07	0.10	99.4
104	53.95	18.82	3.50	3.62	2.93	7.55	3.11	5.30	0.24	0.74	0.32	0.16	0.10	0.14	100.5
109	55.66	19.07	4.68	1.75	2.34	6.49	3.36	5.48	0.52	0.63	0.30	0.16	0.09	0.12	100.6
114	46.78	17.46	3.62	6.06	6.78	12.30	2.26	1.23	1.07	1.04	0.36	0.17	0.10	0.13	99.4
117	46.80	16.28	3.44	6.31	8.33	13.37	1.61	1.35	0.55	1.00	0.31	0.16	0.08	0.11	99.7
119	48.06	15.15	2.88	6.15	9.02	13.20	1.47	1.70	0.33	0.91	0.28	0.16	0.07	0.10	99.5
157	49.78	16.14	3.12	4.65	7.73	10.73	1.77	2.92	1.23	0.77	0.31	0.15	0.10	0.09	99.5
158	50.10	16.07	4.10	3.60	7.15	10.97	1.93	3.10	1.17	0.76	0.28	0.16	0.09	0.09	99.6
160	51.15	16.42	3.35	3.89	6.48	9.24	2.08	3.75	1.56	0.75	0.28	0.15	0.08	0.09	99.3
162	53.98	17.70	2.49	3.82	4.00	7.62	2.74	4.96	1.57	0.66	0.21	0.14	0.09	0.10	100.1
184	47.57	14.30	3.37	5.54	8.40	12.91	1.79	1.44	2.69	0.83	0.35	0.16	0.13	0.10	99.6
186	52.95	18.73	2.17	5.96	3.78	8.91	2.14	3.26	0.95	0.78	0.27	0.16	0.07	0.12	100.2
187	52.72	18.55	2.03	5.99	4.16	8.80	2.18	3.20	0.76	0.77	0.27	0.16	0.07	0.12	99.8
188	52.28	18.47	1.79	6.10	4.32	8.71	2.00	3.08	0.98	0.77	0.26	0.15	0.08	0.11	99.1
189	51.81	18.81	2.36	5.80	4.36	8.85	1.99	2.94	0.91	0.81	0.27	0.14	0.08	0.12	99.2
191	54.45	18.80	5.91	1.45	2.75	5.85	2.97	4.64	2.05	0.71	0.29	0.16	0.08	0.11	100.2
192	53.02	18.61	5.96	1.39	3.56	6.29	2.79	4.37	2.52	0.76	0.35	0.16	0.08	0.10	100.0
193	52.54	19.26	4.03	3.17	3.31	6.70	2.86	4.45	1.85	0.76	0.30	0.15	0.08	0.11	99.6
195	55.89	18.22	5.11	1.08	2.85	6.38	3.20	4.74	0.72	0.64	0.25	0.14	0.07	0.11	99.4
210	59.66	19.06	2.69	0.97	0.62	2.19	4.36	7.62	1.29	0.46	0.09	0.19	0.03	0.02	99.2

TABLE C-5

S.N.	BA	ZR	Y	SR	RB	TH	ZN	FEE	FM	FF	KNA	KBA	KSR	KRB	THK	ZT	CS	RBSR
56	676	150	32	814	180	17	86	8.96	0.57	0.25	1.64	40	33	149	6.32	9	92	0.22
57	641	131	31	721	137	4	83	8.61	0.48	0.27	1.62	35	31	165	1.77	33	115	0.19
67	348	507	77	286	459	49	113	3.79	0.81	0.75	1.69	180	219	136	7.84	10	64	1.60
86	675	150	38	836	172	9	78	8.90	0.57	0.28	1.63	40	33	159	3.30	17	91	0.21
90	732	215	39	910	199	9	65	7.50	0.69	0.54	1.59	50	40	184	2.46	24	51	0.22
95	789	232	52	974	225	16	86	7.28	0.73	0.49	1.63	53	43	187	3.80	15	52	0.23
96	816	249	45	997	244	26	77	6.70	0.71	0.43	1.58	55	45	183	5.83	10	47	0.24
98	869	257	55	990	233	16	76	6.48	0.74	0.63	1.63	53	46	196	3.50	16	42	0.24
101	628	135	32	840	166	10	86	8.33	0.56	0.19	1.54	40	30	149	4.03	14	83	0.20
104	865	233	49	1172	288	19	69	7.52	0.71	0.49	1.70	51	38	153	4.32	12	46	0.25
109	792	251	61	1000	237	14	74	6.62	0.73	0.73	1.63	57	45	192	3.08	18	46	0.24
114	878	107	27	1063	94	1	67	10.35	0.59	0.37	0.54	12	10	109	0.98	107	83	0.0
117	735	87	27	911	46	1	84	10.44	0.54	0.35	0.84	15	12	244	0.89	87	105	0.05
119	640	83	27	811	77	1	69	9.71	0.50	0.32	1.16	22	17	183	0.71	83	116	0.09
157	909	123	37	784	125	1	69	8.28	0.50	0.40	1.65	27	31	194	0.41	123	98	0.1
158	833	128	34	774	143	10	72	8.10	0.52	0.53	1.61	31	33	180	3.89	13	101	0.18
160	705	157	44	784	183	20	71	7.67	0.53	0.46	1.80	44	40	170	6.43	8	84	0.23
162	816	214	60	843	175	18	75	6.73	0.61	0.39	1.81	50	49	235	4.37	12	65	0.21
184	1130	102	37	856	288	2	71	9.52	0.51	0.38	0.80	11	14	41	1.67	51	108	0.34
186	658	155	36	975	157	1	82	8.79	0.68	0.27	1.52	41	28	172	0.37	155	65	0.16
187	623	149	31	973	164	6	86	8.68	0.66	0.25	1.47	43	27	162	2.26	25	65	0.17
188	702	148	31	943	162	14	96	8.56	0.65	0.23	1.54	36	27	158	5.48	11	66	0.17
189	709	152	39	1000	142	6	88	8.80	0.65	0.29	1.48	34	24	172	2.46	25	63	0.14
191	686	214	44	898	272	22	82	7.52	0.73	0.80	1.56	56	43	142	5.71	10	47	0.30
192	680	199	49	828	256	20	76	7.50	0.67	0.81	1.57	53	44	142	5.51	10	54	0.31
193	757	216	45	940	215	16	74	7.55	0.69	0.56	1.56	49	39	172	4.33	14	51	0.23
195	585	226	41	913	285	27	75	6.31	0.68	0.83	1.48	67	43	138	6.86	8	50	0.31
210	244	531	51	187	472	55	122	3.77	0.86	0.73	1.75	259	338	134	8.70	10	84	2.52

TABLE C-6

C.I.P.W. Norms - Roccamonfina High K Series

Sample Number	or	ab	an	lc	ne	di	ol	mt	hm	il	ap	Rest	D.I.
2	30·20	0·00	16·61	15·62	10·67	17·09	3·85	3·74	0·00	1·42	0·80	-	56·5
4	44·06	0·00	22·21	1·64	10·18	10·03	3·27	6·07	0·00	1·54	0·99	-	55·9
6	36·59	0·00	18·16	9·03	13·28	12·53	3·28	4·66	0·00	1·44	1·02	-	58·9
7	35·74	0·00	14·98	20·79	11·90	8·06	3·94	2·67	0·00	1·15	0·77	-	68·4
11	56·65	18·76	17·03	0·00	1·82	0·05	1·28	0·22	3·11	0·86	0·22	-	77·2
14	55·16	11·97	10·27	0·00	12·40	5·60	0·00	3·11	0·00	0·89	0·27	0·33wo	79·5
15	44·28	0·00	13·89	6·11	16·40	11·07	2·53	3·60	0·00	1·31	0·81	-	66·8
18	53·50	0·00	11·06	8·23	15·86	6·50	0·33	3·20	0·00	0·96	0·36	-	77·6
19	44·77	0·00	19·16	7·78	9·58	10·19	0·00	2·01	4·37	1·28	0·78	0·08wo	62·1
20	19·09	0·00	14·71	30·67	9·83	15·90	3·86	3·33	0·00	1·45	1·16	-	59·6
21	55·77	0·00	12·76	1·50	15·89	8·95	1·12	2·52	0·00	1·02	0·46	-	73·2
23	6·60	0·00	14·91	41·55	10·24	16·04	4·13	3·75	0·00	1·51	1·26	-	58·4
24	60·83	0·00	14·22	1·47	13·69	3·69	0·65	1·52	2·62	0·95	0·36	-	76·0
27	46·33	0·00	14·98	4·75	15·30	10·54	1·59	4·45	0·00	1·30	0·75	-	66·4
29	58·52	13·97	10·15	0·00	11·83	0·90	0·45	0·00	3·21	0·54	0·19		84·3
33	36·57	0·00	14·93	18·90	10·81	10·35	1·29	5·09	0·00	1·18	0·87	-	66·3
36	34·93	0·00	13·27	22·95	12·58	8·24	3·53	2·54	0·00	1·10	0·85	-	70·5
37	43·99	14·68	18·01	0·00	13·66	11·82	0·79	3·68	1·55	1·19	0·63	-	62·3
39	22·23	0·00	11·67	27·85	11·62	18·41	1·15	4·77	0·00	1·39	0·92	-	61·7
41	28·72	0·00	11·89	24·94	11·10	16·11	0·62	4·42	0·00	1·35	0·84	-	64·8
42	43·44	11·56	17·61	0·00	7·30	11·86	1·63	4·69	0·00	1·26	0·65	-	62·3
43	38·82	0·00	8·11	20·10	14·49	12·62	0·00	3·27	0·00	1·03	0·55	1·02wo	73·4
44	39·95	0·00	14·76	23·08	9·83	4·90	2·98	2·95	0·00	0·97	0·58	-	72·9
47	42·77	12·58	18·73	0·00	6·82	10·48	1·66	5·00	0·00	1·24	0·71	-	62·2
48	37·94	0·00	15·31	17·78	11·36	8·39	4·45	2·78	0·00	1·18	0·82	-	67·1
50	33·00	0·00	15·09	19·26	12·21	11·26	3·53	3·45	0·00	1·26	0·94	-	64·5
53	46·20	9·17	15·22	0·00	6·89	14·76	0·44	4·85	0·60	1·21	0·65	-	62·3
55	40·92	0·00	19·62	3·01	11·84	13·37	4·85	3·88	0·00	1·48	1·03	-	55·8
59	39·89	0·09	21·81	0·00	10·39	14·78	8·08	2·51	0·00	1·57	0·88	-	50·4
60	37·12	0·00	18·07	3·60	10·94	20·67	3·43	3·66	0·00	1·55	0·95	-	51·7
61	56·22	0·00	10·66	4·80	13·55	9·73	0·00	3·53	0·00	1·07	0·39	0·06wo	74·6

[contd.

TABLE C-6 (Contd.)

Sample Number	or	ab	an	lc	ne	di	ol	mt	hm	il	ap	Rest	D.I.
64	56·34	17·17	12·50	0·00	5·74	3·74	0·00	2·36	0·91	0·84	0·24	0·15wo	79·3
68	24·64	0·00	17·37	19·91	11·47	16·43	2·12	5·11	0·00	1·53	1·41		56·0
69	46·69	0·00	18·98	4·26	12·87	7·38	4·40	3·36	0·00	1·30	0·75		63·8
72	52·87	2·85	11·69	0·00	18·69	7·40	0·82	4·03	0·00	1·09	0·57		74·4
73	53·73	3·45	10·96	0·00	18·58	7·36	1·26	3·12	0·00	1·10	0·46		75·8
76	30·53	0·00	17·43	15·09	12·48	13·48	5·94	2·48	0·00	1·44	1·13		58·1
77	45·08	0·00	15·26	11·60	10·64	10·40	0·36	4·85	0·00	1·19	0·62		67·3
79	44·57	0·00	15·37	11·36	11·31	10·56	0·89	4·16	0·00	1·19	0·61		67·2
81	40·68	0·00	20·69	1·30	11·43	13·62	7·00	2·79	0·00	1·54	0·94		53·4
82	42·04	1·15	21·24	0·00	10·49	13·58	6·59	2·50	0·00	1·52	0·89		53·7
83	40·12	0·10	20·93	0·00	10·73	15·70	7·65	2·32	0·00	1·58	0·88		50·9
91	52·44	2·94	12·84	0·00	17·98	6·92	0·62	4·68	0·00	1·11	0·48		73·4
97	50·86	29·99	10·26	0·00	0·98	3·40	0·00	2·58	0·63	0·79	0·36	0·15wo	81·8
99	58·64	21·46	9·15	0·00	5·51	0·00	0·34	1·37	0·77	0·45	0·10	2·22 c	85·6
105	51·05	22·71	16·19	0·00	1·28	2·53	1·23	3·17	0·57	0·91	0·37		75·0
106	45·45	5·15	18·78	0·00	10·39	10·96	0·74	5·09	1·43	1·32	0·69		61·0
107	45·78	7·85	19·61	0·00	9·20	8·86	0·85	5·08	0·67	1·25	0·66		63·0
108	47·85	4·33	16·97	0·00	12·33	10·19	0·12	5·83	0·46	1·22	0·69		64·5
111	51·78	19·60	18·63	0·00	0·80	0·00	2·70	0·30	3·98	0·97	0·51	0·72 c	72·2
112	15·37	0·00	21·90	16·26	6·87	25·98	6·48	3·89	0·00	1·98	1·28		38·5
116	55·29	0·00	13·59	9·02	11·35	4·99	1·03	3·09	0·48	0·82	0·37		75·7
121	54·10	20·02	5·17	0·00	15·54	0·87	0·00	1·80	0·24	0·60	0·10	1·56wo	89·7
122	49·64	9·48	15·14	0·00	10·13	6·81	2·31	4·49	0·00	1·17	0·83		69·2
123	51·48	5·77	14·31	0·00	11·88	7·69	3·91	2·99	0·00	1·17	0·79		69·1
128	51·28	8·24	15·73	0·00	9·98	6·62	2·07	4·15	0·00	1·19	0·73		69·5
129	56·18	5·79	12·76	0·00	11·98	5·86	2·22	3·49	0·00	1·09	0·63		74·0
131	29·61	0·00	18·59	6·13	7·63	25·25	4·79	4·95	0·00	1·75	1·31		43·4
132	41·57	0·00	15·03	6·22	13·12	15·28	1·88	4·63	0·00	1·32	0·95		60·9
134	49·48	19·08	17·26	0·00	3·30	3·86	1·25	3·22	1·07	0·93	0·55		71·9
136	35·40	0·00	15·73	22·75	9·19	8·62	2·24	4·12	0·00	1·13	0·82		67·3
137	34·99	0·00	17·16	15·96	11·07	13·58	1·82	3·44	0·00	1·22	0·75		62·0
138	35·18	0·00	16·69	16·10	11·53	13·18	1·45	3·79	0·00	1·16	0·92		62·8

[Contd.

TABLE C-6 (contd.)

Sample Number	or	ab	an	lc	ne	di	ol	mt	hm	il	ap	Rest	D.I.
139	42·60	0·00	17·40	9·78	10·68	12·17	0·08	5·31	0·00	1·22	0·75		63·1
140	35·85	0·00	16·40	6·58	11·28	20·08	1·49	5·77	0·00	1·48	1·06		53·7
141	59·01	6·79	13·32	0·00	10·80	5·02	0·00	3·31	0·00	0·93	0·29	0·52wo	76·6
142	32·38	1·01	24·57	0·00	7·55	20·05	4·44	7·11	0·00	1·87	1·03		40·9
146	36·07	1·48	20·55	0·00	10·92	190·8	5·17	4·15	0·00	1·63	0·94		48·5
148	17·85	0·00	16·63	17·63	8·69	26·95	3·68	5·87	0·00	1·66	1·06		44·2
150	22·91	0·00	13·82	18·53	8·54	25·93	1·14	6·32	0·00	1·54	1·26		50·0
151	24·41	0·00	16·78	12·53	9·13	25·31	0·68	0·22	8·13	1·65	1·16		46·1
153	7·96	0·00	15·33	25·02	5·89	32·90	1·39	5·54	2·65	1·82	1·50		38·9
154	0·00	0·00	12·96	32·21	7·26	34·12	3·43	5·91	0·00	1·81	1·66	0·64cs	39·5
155	60·43	6·98	12·62	0·00	12·50	2·79	0·64	2·94	0·00	0·84	0·27		79·9
163	46·74	2·64	18·38	0·00	11·07	9·89	5·54	3·35	0·00	1·54	0·84		60·5
165	29·62	0·00	15·05	15·58	13·92	15·44	3·65	4·05	0·00	1·44	1·24		59·1
166	29·10	0·00	17·79	15·70	12·09	14·37	4·09	4·03	0·00	1·50	1·33		56·9
170	40·96	8·20	19·79	0·00	8·91	12·05	2·10	5·55	0·00	1·42	1·03		58·1
177	32·60	0·00	16·64	12·63	13·76	14·27	2·94	4·54	0·00	1·44	1·17		59·0
178	39·63	0·00	13·43	24·50	10·16	5·27	1·66	3·74	0·00	0·98	0·63		74·3
179	62·36	13·03	10·53	0·00	8·48	1·44	0·00	0·92	1·94	0·88	0·12	0·30wo	83·9
180	30·88	0·00	18·67	14·86	10·62	13·72	5·12	3·46	0·00	1·54	1·13		56·4
181	28·69	0·00	17·70	15·84	11·96	14·94	5·01	3·19	0·00	1·48	1·18		56·5
182	32·24	0·00	18·53	12·55	11·01	14·34	5·81	2·93	0·00	1·51	1·07		55·8
183	30·66	0·00	15·88	15·47	13·46	14·46	4·41	3·19	0·00	1·40	1·08		59·6
185	26·40	0·00	13·78	26·79	9·05	15·54	1·28	4·86	0·00	1·40	0·90		62·2
198	56·15	0·00	8·80	4·66	16·84	7·34	0·00	3·92	0·00	1·07	0·36	0·87wo	77·7
206	27·36	0·00	10·19	32·09	12·79	11·70	0·02	4·12	0·00	1·11	0·64		72·2
209	44·58	5·53	18·33	0·00	8·49	13·86	1·25	5·63	0·00	1·42	0·92		58·6
Biotite Gabbro R.103													
103	14·84	0·25	37·31	0·00	3·42	17·61	8·86	11·23	0·00	2·85	3·63		18·51

TABLE C-7

C.I.P.W. Norms - Roccamonfina Low K Series

Sample Number	Qz	or	ab	an	ne	di	hy	ol	mt	hm	il	ap	D.I.
56	0·00	19·43	16·92	28·14	0·00	18·58	0·85	10·52	3·00	0·00	1·83	0·72	36·3
57	0·00	16·18	14·31	26·21	0·00	23·87	4·00	9·83	3·20	0·00	1·61	0·79	30·5
67	0·00	45·02	38·19	8·84	0·00	2·57	0·23	0·52	2·25	1·23	0·90	0·24	83·2
86	0·00	19·71	16·99	28·24	0·19	18·48	0·00	10·35	3·45	0·00	1·75	0·84	36·9
90	2·12	26·73	24·04	27·71	0·00	2·83	8·67	0·00	5·70	0·00	1·48	0·73	52·9
95	0·00	30·39	26·70	21·99	0·00	8·93	4·35	0·51	4·94	0·00	1·35	0·84	57·1
96	0·00	32·07	28·99	19·69	0·00	8·64	0·86	3·57	4·02	0·00	1·25	0·91	61·1
98	0·95	33·07	29·02	20·58	0·00	5·72	3·03	0·00	5·75	0·00	1·20	0·67	63·0
101	0·27	17·88	16·61	28·67	0·00	15·18	17·30	0·00	2·16	0·00	1·38	0·55	34·8
104	0·00	31·30	23·87	21·73	1·32	11·10	0·00	3·45	5·07	0·00	1·40	0·76	56·5
109	0·00	32·43	28·84	20·50	0·00	7·66	2·38	0·29	4·40	1·56	1·21	0·72	61·3
114	0·00	7·39	19·03	34·44	0·23	20·47	0·00	10·22	5·34	0·00	2·01	0·87	26·6
117	0·00	8·06	13·57	33·54	0·10	25·33	0·00	11·71	5·04	0·00	1·92	0·74	21·7
119	0·00	10·14	12·56	30·01	0·00	27·59	2·35	10·71	4·22	0·00	1·75	0·67	22·7
157	0·00	17·58	15·26	27·99	0·00	19·43	6·46	6·42	4·61	0·00	1·49	0·75	32·9
158	0·00	18·65	16·62	26·50	0·00	21·32	4·60	4·11	6·05	0·00	1·47	0·68	35·3
160	0·00	22·71	18·04	24·99	0·00	16·08	7·70	3·36	4·98	0·00	1·46	0·68	40·7
162	0·00	29·74	23·53	21·66	0·00	12·30	4·05	2·86	3·66	0·00	1·70	0·50	53·3
184	0·00	8·82	15·67	27·65	0·00	28·97	3·86	7·51	5·05	0·00	1·63	0·86	24·5
186	2·65	19·43	18·27	32·15	0·00	8·78	13·40	0·00	3·17	0·00	1·49	0·65	40·4
187	1·99	19·13	18·66	31·74	0·00	8·74	14·63	0·00	2·98	0·00	1·48	0·65	39·8
188	2·52	18·58	17·27	32·99	0·00	7·83	16·04	0·00	2·65	0·00	1·49	0·63	38·4
189	2·65	17·69	17·15	34·33	0·00	7·15	15·33	0·00	3·48	0·00	1·57	0·65	37·5
191	4·31	27·98	25·65	24·76	0·00	2·28	5·93	0·00	3·20	3·82	1·38	0·70	57·9
192	3·13	26·55	24·27	26·06	0·00	2·86	7·79	0·00	2·88	4·14	1·48	0·85	53·9
193	0·74	26·95	24·80	27·23	0·00	3·94	8·14	0·00	5·99	0·00	1·48	0·73	52·5
195	3·85	28·43	27·49	21·67	0·00	6·85	4·03	0·00	2·11	3·73	1·23	0·60	59·8
210	0·00	45·98	37·67	10·14	0·00	0·32	0·88	0·39	2·46	1·05	0·89	0·22	83·7

TABLE C-8

Roccamonfina lavas - CO_2, Ce, and Nb data

Sample No.	CO_2	Ce	Nb	Sample No.	CO_2	Ce	Nb
11	-	200	-	146	-	135	-
14	-	-	29	150	-	170	25
23	-	190	-	154	-	160	-
36	-	-	21	155	-	250	-
37	-	170	-	160	-	195	24
42	-	170	-	170	-	-	34
53	-	160	-	180	-	220	-
59	1·51	-	-	181	-	-	20
60	1·09	155	-	182	-	190	-
64	-	185	30	206	-	170	-
72	-	290	30	209	-	170	-
81	1·06	-	-				
82	1·52	140	-	56	-	64	12
83	1·10	-	-	96	-	110	-
97	0·17	285	-	117	-	-	2
99	-	325	44	119	-	20	-
105	0·26	-	-	186	-	65	-
106	-	140	-	191	-	95	-
116	-	150	17	192	-	-	19
121	-	270	-	195	-	100	-
122	-	-	51	210	-	135	159
134	-	225	-				
138	-	180	5	103	-	45	-

Table C-9

Chemical analysis of biotite gabbro (R.103)

SiO_2	39·61
TiO_2	1·47
Al_2O_3	17·31
Fe_2O_3	7·59
FeO	6·78
MnO	0·15
MgO	6·55
CaO	13·71
Na_2O	0·76
K_2O	2·46
P_2O_5	1·50
H_{20+}	1·86
Total	99·75

Ba	925
Zr	59
Y	29
Sr	958
Rb	137
Th	1
Zn	68
Ce	45

APPENDIX D

CORRELATION MATRICES

Table D-1 Roccamonfina High K lavas

Table D-2 Roccamonfina Low K lavas

SI	= SiO_2	AL	= Al_2O_3	FEE	= Fe_2O_3
FE	= FeO	MG	= MgO	CA	= CaO
NA	= Na_2O	K	= K_2O	H	= H_2O
TI	= TiO_2	P	= P_2O_5	MN	= MnO

TOTFE = Total iron as Fe_2O_3

FR = Fe_2O_3/Fe_2O_3 + FeO

FM = Fe_2O_3 + FeO/Fe_2O_3 + FeO + MgO

KNA = K_2O/Na_2O

KRB = K/Rb

KBA = K/Ba

CASR = Ca/Sr

RBSR = Rb/Sr

TABLE D-1

CORRELATION MATRIX FOR DATA MATRIX ROCCA 1

	SI H RB KBA	AL TI TH CASR	FEE P ZN RBSR	FE MN TOTFE	MG BA FR	CA ZR FM	NA Y KNA	K SR KRB
SI	1.000000 0.384134 0.289222 0.370651	0.605530 -0.909745 0.536107 -0.292882	-0.285748 -0.903115 -0.129488 0.414335	-0.770450 -0.328318 -0.925663	-0.819342 -0.409421 0.571711	-0.885269 0.541434 0.777256	0.719276 0.167079 -0.415138	0.423873 -0.398135 0.032668
AL	0.605530 0.146012 0.358695 0.199420	1.000000 -0.764788 0.325163 -0.614121	0.483665 0.673818 0.195857 0.246175	-0.406400 -0.052740 -0.689542	-0.911534 0.064174 0.143347	-0.869291 0.182994 0.829342	0.622191 0.111080 -0.182642	0.713200 0.118480 0.125339
FEE	-0.285748 0.142198 -0.184541 -0.193456	-0.483665 0.346741 -0.149225 0.248203	1.000000 0.298767 -0.180000 -0.201049	-0.271227 0.072928 0.339471	0.451619 0.042610 0.554613	0.448743 -0.023132 -0.390595	-0.366707 0.055618 0.155597	-0.366523 0.012934 -0.072528
FE	-0.770450 -0.471714 -0.328873 -0.259516	-0.406400 0.781590 -0.479875 0.238129	-0.271227 0.775190 0.284812 -0.315177	1.000000 0.392484 0.813284	0.589319 0.260561 -0.913673	0.676213 -0.498338 -0.549906	-0.443052 -0.208465 0.091632	-0.441410 0.287128 0.040156
MG	-0.819342 -0.252244 -0.325288 -0.247741	-0.911534 0.898484 -0.456824 0.594967	0.451619 0.816431 -0.068468 -0.275589	0.589319 0.179787 0.848927	1.000000 0.076299 -0.319101	0.960354 -0.365930 -0.932132	-0.716989 -0.203627 0.276775	-0.702264 0.016862 -0.148207
CA	-0.885269 -0.305452 -0.389138 -0.308158	-0.869291 0.950501 -0.515338 0.530405	0.448743 0.887049 -0.012076 -0.357167	0.676213 0.276264 0.932106	0.960354 0.167022 -0.401102	1.000000 -0.422552 -0.887711	-0.725804 -0.154963 0.249670	-0.709169 0.147287 -0.079794
NA	0.719276 -0.076364 -0.006278 0.478669	0.622191 -0.663697 0.609539 -0.192963	-0.366707 -0.654955 0.290730 0.362116	-0.443052 0.252908 -0.654656	-0.716989 -0.095709 0.236667	-0.725804 0.555073 0.761175	1.000000 0.251858 -0.727446	0.283490 -0.093507 0.325070
K	0.423873 0.055296 0.508068 0.075485	0.713200 -0.696564 0.308113 -0.608016	-0.366523 -0.521746 -0.103309 0.143886	-0.441410 -0.327013 -0.652941	-0.702264 0.165367 0.171563	-0.709169 0.134505 0.597482	0.283490 0.129264 0.378706	1.000000 0.178796 0.024167
H	0.384134 1.000000 0.270663 -0.034459	0.146012 -0.343920 0.076352 -0.212652	0.142198 -0.366314 -0.222441 0.130356	-0.471714 -0.353364 -0.375019	-0.252244 -0.304430 0.528790	-0.305452 0.182859 0.217000	-0.076364 0.051261 0.067633	0.055296 -0.207234 -0.237632
TI	-0.909745 -0.343920 -0.479931 -0.380174	-0.764788 1.000000 -0.542725 0.420247	0.346741 0.899140 0.139895 -0.458265	0.781590 0.377852 0.973422	0.898484 0.276506 -0.520094	0.950501 -0.486554 -0.822278	-0.663697 -0.202265 0.179154	-0.696564 0.260462 0.002602
P	-0.903115 -0.366314 -0.296601 -0.314806	-0.673818 0.899140 -0.468305 0.366538	0.298767 1.000000 0.066969 -0.354051	0.775190 0.363068 0.938165	0.816431 0.276045 -0.542044	0.887049 -0.427064 -0.741714	-0.654955 -0.121379 0.301147	-0.521746 0.274449 -0.089070
MN	-0.328318 -0.353364 -0.427996 0.021565	-0.052740 0.377852 0.048292 0.084813	0.072928 0.363068 0.548451 -0.108250	0.392484 1.000000 0.427642	0.179787 0.425947 -0.276535	0.276264 0.078235 -0.006960	0.252908 0.142713 -0.420129	-0.327013 0.437535 0.391206
BA	-0.409421 -0.304430 -0.316570 -0.495915	0.064174 0.276506 -0.072024 -0.479147	0.042610 0.276045 0.154139 -0.566760	0.260561 0.425947 0.280392	0.076299 1.000000 -0.278539	0.167022 -0.240654 -0.076461	-0.095709 -0.091775 0.170010	0.165367 0.872768 0.449645

TABLE D-1 (contd.)

ZR	0.541434	0.182994	-0.023132	-0.498338	-0.365930	-0.422552	0.555073	0.134505
	0.182859	-0.486554	-0.427064	0.078235	-0.240654	1.000000	0.473106	-0.198729
	0.322872	0.887857	0.166924	-0.500984	0.460801	0.498312	-0.316335	-0.119549
	0.542664	0.048523	0.614696					
Y	0.167079	0.111080	0.055618	-0.208465	-0.203627	-0.154963	0.251858	0.129264
	0.051261	-0.202265	-0.121379	0.142713	-0.091775	0.473106	1.000000	-0.052795
	0.211167	0.360899	0.100827	-0.170099	0.152744	0.255977	-0.070123	-0.181895
	0.411699	0.137695	0.324101					
SR	-0.398135	0.118480	0.012934	0.287128	0.016862	0.147287	-0.093507	0.178796
	-0.207234	0.260462	0.274449	0.437535	0.872768	-0.198729	-0.052795	1.000000
	-0.300874	-0.038946	0.200447	0.288414	-0.277693	-0.048172	0.150661	0.386987
	-0.559896	-0.596237	-0.629488					
RB	0.289222	0.358695	-0.184541	-0.328873	-0.325288	-0.389138	-0.006278	0.508068
	0.270663	-0.479931	-0.296601	-0.427996	-0.316570	0.322872	0.211167	-0.300874
	1.000000	0.306083	-0.236772	-0.432951	0.203765	0.282603	0.356855	-0.730252
	0.293257	-0.110695	0.627575					
TH	0.536107	0.325163	-0.149225	-0.479875	-0.456824	-0.515338	0.609539	0.308113
	0.076352	-0.542725	-0.468305	0.048292	-0.072024	0.887857	0.360899	-0.038946
	0.306083	1.000000	0.196348	-0.559167	0.375863	0.528221	-0.258082	-0.033607
	0.499819	-0.091044	0.517961					
ZN	-0.129488	0.195857	-0.180000	0.284812	-0.068468	-0.012076	0.290730	-0.103309
	-0.222441	0.139895	0.066969	0.548451	0.154139	0.166924	0.100827	0.200447
	-0.236772	0.196348	1.000000	0.169517	-0.267497	0.190743	-0.308734	0.299074
	0.226379	0.052508	0.122070					
TOTFE	-0.925663	-0.689542	0.339471	0.813284	0.848927	0.932106	-0.654656	-0.652941
	-0.375019	0.973422	0.938165	0.427642	0.280392	-0.500984	-0.170099	0.288414
	-0.432951	-0.559167	0.169517	1.000000	-0.557607	-0.773521	0.183610	-0.004603
	-0.370561	0.382757	-0.429546					
FR	0.571711	0.143347	0.554613	-0.913673	-0.319101	-0.401102	0.236667	0.171563
	0.528790	-0.520094	-0.542044	-0.276535	-0.278539	0.460801	0.152744	-0.277693
	0.203765	0.375863	-0.267497	-0.557607	1.000000	0.341670	-0.063637	-0.074863
	0.191390	-0.072161	0.243750					
FM	0.777256	0.829342	-0.390595	-0.549906	-0.932132	-0.887711	0.761175	0.597482
	0.217000	-0.822278	-0.741714	-0.006960	-0.076461	0.498312	0.255977	-0.048172
	0.282603	0.528221	0.190743	-0.773521	0.341670	1.000000	-0.346313	0.185340
	0.379790	-0.451879	0.388832					
KNA	-0.415138	-0.182642	0.155597	0.091632	0.276775	0.249670	-0.727446	0.378706
	0.067633	0.179154	0.301147	-0.420129	0.170010	-0.316335	-0.070123	0.150661
	0.356855	-0.258082	-0.308734	0.183610	-0.063637	-0.346313	1.000000	-0.325794
	-0.242995	-0.064304	-0.143621					
KRB	0.032668	0.125339	-0.072528	0.040156	-0.148207	-0.079794	0.325070	0.024167
	-0.237632	0.002602	-0.089070	0.391206	0.449645	-0.119549	-0.181895	0.386987
	-0.730252	-0.033607	0.299074	-0.004603	-0.074863	0.185340	-0.325794	1.000000
	-0.166345	-0.257125	-0.386675					
KBA	0.370651	0.199420	-0.193456	-0.259516	-0.247741	-0.308158	0.478669	0.075485
	-0.034459	-0.380174	-0.314806	0.021565	-0.495915	0.542664	0.411699	-0.559896
	0.293257	0.499819	0.226379	-0.370561	0.191390	0.379790	-0.242995	-0.166345
	1.000000	0.562875	0.868012					
CASR	-0.292882	-0.614121	0.248203	0.238129	0.594967	0.530405	-0.192963	-0.608016
	-0.212652	0.420247	0.366538	0.084813	-0.479147	0.048523	0.137695	-0.596237
	-0.110695	-0.091044	0.052508	0.382757	-0.072161	-0.451879	-0.064304	-0.257125
	0.562875	1.000000	0.411859					
RBSR	0.414335	0.246175	-0.201049	-0.315177	-0.275589	-0.357167	0.362116	0.143886
	0.130356	-0.458265	-0.354051	-0.108250	-0.566760	0.614696	0.324101	-0.629488
	0.627575	0.517961	0.122070	-0.429546	0.243750	0.388832	-0.143621	-0.386675
	0.868012	0.411859	1.000000					

TABLE D-2

CORRELATION MATRIX FOR DATA MATRIX ROCCA 2

	SI H RB KBA	AL TI TH CASR	FEE P ZN RBSR	FE MN TOTFE	MG BA FR	CA ZR FM	NA Y KNA	K SR KRB
SI	1.000000	0.717527	0.133227	-0.777688	-0.913907	-0.960822	0.905757	0.954570
	-0.093920	-0.935509	-0.631710	0.180176	-0.571789	0.897030	0.791514	-0.411440
	0.819825	0.845130	0.571563	-0.944422	0.624876	0.874821	0.642251	0.025587
	0.791285	-0.664145	0.657802					
AL	0.717527	1.000000	0.230805	-0.534924	-0.913269	-0.806767	0.702821	0.682679
	-0.008646	-0.519009	-0.246856	0.035276	-0.323375	0.572541	0.513003	0.114421
	0.436462	0.476786	0.284716	-0.548292	0.453441	0.882774	0.409333	0.165896
	0.420280	-0.900163	0.257970					
FEE	0.133227	0.230805	1.000000	-0.678653	-0.245106	-0.270733	0.308375	0.198765
	0.457542	-0.136308	0.231107	0.077902	0.180871	0.090626	0.265298	0.154161
	0.215368	0.140657	-0.355243	-0.180757	0.818031	0.243313	-0.065531	-0.082981
	-0.024068	-0.391267	-0.064752					
FE	-0.777688	-0.534924	-0.678653	1.000000	0.734145	0.834053	-0.847416	-0.827411
	-0.244709	0.781511	0.364380	-0.216424	0.301144	-0.748736	-0.767022	0.347483
	-0.759877	-0.753150	-0.205066	0.845032	-0.964087	-0.704082	-0.440719	0.040046
	-0.621238	0.586372	-0.525043					
MG	-0.913907	-0.913269	-0.245106	0.734145	1.000000	0.952925	-0.901263	-0.888880
	-0.004396	0.779877	0.418299	-0.143825	0.401874	-0.801143	-0.733938	0.134040
	-0.725931	-0.727194	-0.431103	0.804660	-0.616152	-0.970233	-0.510088	-0.029103
	-0.643939	0.863380	-0.497732					
CA	-0.960822	-0.806767	-0.270733	0.834053	0.952925	1.000000	-0.926292	-0.951723
	-0.086615	0.875786	0.543887	-0.179500	0.517378	-0.889644	-0.787261	0.366012
	-0.816650	-0.842717	-0.503755	0.919792	-0.704648	-0.916893	-0.608332	-0.003892
	-0.768191	0.743334	-0.636671					
NA	0.905757	0.702821	0.308375	-0.847416	-0.901263	-0.926292	1.000000	0.938416
	-0.019218	-0.826515	-0.483302	0.348371	-0.426863	0.930765	0.829115	-0.371434
	0.859502	0.862601	0.461521	-0.910281	0.749002	0.910290	0.401629	-0.067439
	0.787227	-0.662787	0.687548					
K	0.954570	0.682679	0.198765	-0.827411	-0.888880	-0.951723	0.938416	1.000000
	-0.059276	-0.896711	-0.543597	0.213908	-0.488187	0.921360	0.856641	-0.425852
	0.831093	0.875762	0.486817	-0.963293	0.673887	0.849182	0.685417	0.085234
	0.795377	-0.634431	0.667185					
H	-0.093920	-0.008646	0.457542	-0.244709	-0.004396	-0.086615	-0.019218	-0.059276
	1.000000	-0.007852	0.070063	0.049339	0.225710	-0.032975	0.057262	-0.100200
	0.178227	0.008901	-0.177853	0.005414	0.308205	-0.015678	-0.106785	-0.373413
	-0.018427	-0.052858	0.058566					
TI	-0.935509	-0.519009	-0.136308	0.781511	0.779877	0.875786	-0.826515	-0.896711
	-0.007852	1.000000	0.641486	-0.154922	0.428236	-0.838864	-0.788983	0.473938
	-0.804054	-0.791392	-0.493420	0.947298	-0.617343	-0.726693	-0.633448	-0.010197
	-0.749174	0.526281	-0.652852					
P	-0.631710	-0.246856	0.231107	0.364380	0.418299	0.543887	-0.483302	-0.543597
	0.070063	0.641486	1.000000	-0.273002	0.738743	-0.695513	-0.434582	0.741003
	-0.550408	-0.664606	-0.735874	0.656203	-0.260579	-0.436288	-0.351463	-0.011972
	-0.786657	0.032241	-0.765503					
MN	0.180176	0.035276	0.077902	-0.216424	-0.143825	-0.179500	0.348371	0.213908
	0.049339	-0.154922	-0.273002	1.000000	-0.352921	0.449895	0.116013	-0.484581
	0.431161	0.408420	0.452607	-0.233101	0.269003	0.308539	-0.232091	-0.338434
	0.560153	0.180789	0.647409					
BA	-0.571789	-0.323375	0.180871	0.301144	0.401874	0.517378	-0.426863	-0.488187
	0.225710	0.428236	0.738743	-0.352921	1.000000	-0.627652	-0.219890	0.698990
	-0.448812	-0.648785	-0.772754	0.534948	-0.239120	-0.446288	-0.362914	-0.026265
	-0.763928	0.028798	-0.697959					

TABLE D-2 (contd.)

ZR	0.897030	0.572541	0.090626	-0.748736	-0.801143	-0.889644	0.930765	0.921360
	-0.032975	-0.838864	-0.695513	0.449895	-0.627652	1.000000	0.780600	-0.648780
	0.895873	0.926182	0.686299	-0.936667	0.629424	0.834050	0.458618	-0.091169
	0.944239	-0.424905	0.880495					
Y	0.791514	0.513003	0.265298	-0.767022	-0.733938	-0.787261	0.829115	0.856641
	0.057262	-0.788983	-0.434582	0.116013	-0.219890	0.780600	1.000000	-0.333596
	0.726669	0.693895	0.310467	-0.833986	0.648354	0.685885	0.519480	0.082642
	0.585568	-0.568961	0.491336					
SR	-0.411440	0.114421	0.154161	0.347483	0.134040	0.366012	-0.371434	-0.425852
	-0.100200	0.473938	0.741003	-0.484581	0.698990	-0.648780	-0.333596	1.000000
	-0.570483	-0.654289	-0.709858	0.577556	-0.285102	-0.193730	-0.259088	0.172134
	-0.797310	-0.338346	-0.853194					
RB	0.819825	0.436462	0.215368	-0.759877	-0.725931	-0.816650	0.859502	0.831093
	0.178227	-0.804054	-0.550408	0.431161	-0.448812	0.895873	0.726669	-0.570483
	1.000000	0.883579	0.568289	-0.860769	0.670980	0.749348	0.378230	-0.430256
	0.835451	-0.405443	0.812997					
TH	0.845130	0.476786	0.140657	-0.753150	-0.727194	-0.842717	0.862601	0.875762
	0.008901	-0.791392	-0.664606	0.408420	-0.648785	0.926182	0.693895	-0.654289
	0.883579	1.000000	0.669201	-0.906153	0.640300	0.726852	0.490798	-0.150131
	0.899504	-0.377041	0.835476					
ZN	0.571563	0.284716	-0.355243	-0.205066	-0.431103	-0.503755	0.461521	0.486817
	-0.177853	-0.493420	-0.735874	0.452607	-0.772754	0.686299	0.310467	-0.709858
	0.568289	0.669201	1.000000	-0.533238	0.112737	0.511798	0.251476	-0.120052
	0.791847	-0.007656	0.792968					
TOTFE	-0.944422	-0.548292	-0.180757	0.845032	0.804660	0.919792	-0.910281	-0.963293
	0.005414	0.947298	0.656203	-0.233101	0.534948	-0.936667	-0.833986	0.577556
	-0.860769	-0.906153	-0.533238	1.000000	-0.695468	-0.765708	-0.637884	-0.006787
	-0.849433	0.500364	-0.750236					
FR	0.624876	0.453441	0.818031	-0.964087	-0.616152	-0.704648	0.749002	0.673887
	0.308205	-0.617343	-0.260579	0.269003	-0.239120	0.629424	0.648354	-0.285102
	0.670980	0.640300	0.112737	-0.695468	1.000000	0.619829	0.239910	-0.106324
	0.518557	-0.508947	0.448088					
FM	0.874821	0.882774	0.243313	-0.704082	-0.970233	-0.916893	0.910290	0.849182
	-0.015678	-0.726693	-0.436288	0.308539	-0.446288	0.834050	0.685885	-0.193730
	0.749348	0.726852	0.511798	-0.765708	0.619829	1.000000	0.361146	-0.035064
	0.703874	-0.782365	0.587655					
KNA	0.642251	0.409333	-0.065531	-0.440719	-0.510088	-0.608332	0.401629	0.685417
	-0.106785	-0.633448	-0.351463	-0.232091	-0.362914	0.458618	0.519480	-0.259088
	0.378230	0.490798	0.251476	-0.637884	0.239910	0.361146	1.000000	0.336052
	0.400697	-0.388556	0.250148					
KRB	0.025587	0.165896	-0.082981	0.040046	-0.029103	-0.003892	-0.067439	0.085234
	-0.373413	-0.010197	-0.011972	-0.338434	-0.026265	-0.091169	0.082642	0.172134
	-0.430256	-0.150131	-0.120052	-0.006787	-0.106324	-0.035064	0.336052	1.000000
	-0.142546	-0.116690	-0.271153					
KBA	0.791285	0.420280	-0.024068	-0.621238	-0.643939	-0.768191	0.787227	0.795377
	-0.018427	-0.749174	-0.786657	0.560153	-0.763928	0.944239	0.585568	-0.797310
	0.835451	0.899504	0.791847	-0.849433	0.518557	0.703874	0.400697	-0.142546
	1.000000	-0.188194	0.973043					
CASR	-0.664145	-0.900163	-0.391267	0.586372	0.863380	0.743334	-0.662787	-0.634431
	-0.052858	0.526281	0.032241	0.180789	0.028798	-0.424905	-0.568961	-0.338346
	-0.405443	-0.377041	-0.007656	0.500364	-0.508947	-0.782365	-0.388556	-0.116690
	-0.188194	1.000000	-0.017278					
RBSR	0.657802	0.257970	-0.064752	-0.525043	-0.497732	-0.636671	0.687548	0.667185
	0.058566	-0.652852	-0.765503	0.647409	-0.697959	0.880495	0.491336	-0.853194
	0.812997	0.835476	0.792968	-0.750236	0.448088	0.587655	0.250148	-0.271153
	0.973043	-0.017278	1.000000					

APPENDIX E

MISCELLANEOUS DATA

E:1 Alban Hills

E:2 Latera-Vulsini

E:3 Radicofani

E:4 Pyroxenite, biotite pyroxenite and biotitite nodules.

E:5 Miscellaneous analyses.

APPENDIX E

MISCELLANEOUS DATA

Introduction

Specimens were collected for comparative purposes from the Alban Hills, Latera-Vulsini, and Radicofani. The location, petrography, and chemistry of some of the specimens collected is presented in the following sections together with notes on pyroxenite, and biotite pyroxenite nodules, Venanzite, Cupaellite, and a residual glass from a Vesuvius leucite basanite.

E:1 Alban Hills (AB)

Chemical analyses are presented in Table E-1. Reference should be made to the Italian Geological Survey map of the Alban Hills (Sheet 150) and also to Fornaseri et al. (1963).

AB100 Fine grained nepheline leucitite; small quarry below monument near road from Velletri to Nemi; Group sc_1'; microphenocrysts of leucite and elongate, very pale green cpx in a groundmass of lc-cpx-ore-ne-interstitial phlogopite.

AB200 Vesicular nepheline olivine leucitite; below Maschio dell'Artemisio on the road from Velletri to Nemi; Group β^7; rare microphenocrysts of cpx and leucite in granular groundmass of lc-cpx-olv-ore-interstitial nepheline.

AB400 Fine grained nepheline leucitite; near Nemi on road down into Nemi from the Marino-Velletri road; Group β^7; rare phenocrysts of leucite and cpx in groundmass of equidimensional leucite, cpx, ore, ne, and interstitial phlogopitic mica.

AB800 Olivine leucitite; M.Cavo; Group β^6; coarse grained leucitite with euhedral phenocrysts of cpx, leucite and euhedral olivine in leucite-cpx-ore-plag groundmass. Contains glomero-aggregates of leucite-cpx-olivine (see Plate A-1).

AB810 Ignore this analysis.

AB900 Fine grained leucitite; quarry on road up to Rocca Priora from Rocca di Papa; Group β^7; very rare phenocrysts of leucite and cpx in fine matrix of "quench" leucite-cpx-ore + small quantity of plag, ne, and interstitial phlogopitic mica.

E:2 Latera-Vulsini(LT)

Latera is one of the main volcanoes included in the Vulsini group. It is situated 2 km west of Lake Bolsena and has been described in detail by Schneider (1965). The reader is also referred to Triglia (1966, 1969), De Fino and Mattias (1965), and Mattias (1965) for further information concerning Latera-Vulsini. Sample localities are described with reference to the maps in Schneider (1965). Analyses of 12 specimens from Latera are presented in Table E-2. A specimen of a leucite macrophyric lava was also collected from Aquapendente which is situated on the northern margin of the Vulsini centre. An analysis of this lava is presented in Table E-3.

LT-1 Tephritic leucitite; north east margin of Calveglio di Latera vicoite outcrop; vesicular block in chaotic red foam lava; rare phenocrysts of cpx, leucite and plagioclase.

LT-2 Cpx-phyric tephritic leucitite; location as LT-1; eu-subhedral phenocrysts of zoned cpx and rare resorbed olivine with cpx-ore-iddingsite coronas.

LT-3 Leucite-bearing pyroxenitic sommaite; location as LT-1; holocrystalline rock composed of eu-subhedral cpx set in sub-anhedral bytownite, leucite, sanidine, biotite, and ore with accessory apatite and rare resorbed olivines with cpx-biotite-ore coronas.

LT-5 Cpx-phyric leucite tephrite; location as LT-1; contains rare euhedral cpx phenocrysts, rare leucite and resorbed olivine phenocrysts in a fine cpx-plag-ore-leucite groundmass.

LT-6 Cpx-phyric leucite tephrite; 1·5km south of M.S. Magno on the Valentano to Latera road; dark vesicular block in tuffs/ashes; petrography as LT-5 above.

LT-7 Tephritic leucitite; location as LT-6; fine grained basic block in tuffs/ashes.

LT-8 Vicoite (foam lava); roadside exposure west of Fosso delle Route; dark foam lava containing microphenocrysts of plagioclase, cpx, biotite, and leucite in extremely vesicular devitrified matrix.

LT-9 Tephritic leucite phonolite; location as LT-8; inclusion in foam lava; rare cpx, plag, biotite, ore phenocrysts in groundmass of sanidine > plagioclase ≫ leucite.

LT-14 Trachybasalt; M.Rosso near Lago Mezzano; scoriaceous trachybasalt containing numerous microphenocrysts of cpx, olivine, and plag in a microcrystalline groundmass.

LT-15 Leucite tephrite (basanite); 1·5km east of Valentano -

ottajanite of M. Felcete; coarsely crystalline with < 5% olivine

LT-16 Dark pumiceous leucite tephrite; ash-cinder cone of M. Starnina.

LT-17 Leucite tephrite (ottajanite); roadside 1·5km S.S.W. of Valentano; rare microphenocrysts of cpx, plagioclase and olivine in microcrystalline groundmass.

Aqua leucite macrophyric phonolitic leucite tephrite; roadside on northern margin of Aquapendente.

E:3 Radicofani (RA)

Analyses of 8 specimens from the volcanic neck of Radicofani are presented in Table E-4. Innocenti (1967) has published a detailed geological and petrographic account of the Radicofani neck to which the interested reader is referred. Specimens RA6, RA7 and RA8 are trachybasalts from the columnar jointed outer zone. They are composed of olivine, cpx and plagioclase phenocrysts in a groundmass of cpx, plag, sanidine and ore. RA4 and RA5 are olivine latites from near the centre of the neck and they contain small phenocrysts of olivine (showing evidence of high temperature oxidation) and cpx in a glassy matrix. RA1 is a specimen of red, vesicular olivine latite which crops out just below and to the west of the fort. RA2 and RA3 are vesicular trachybasalts.

E:4 Pyroxenite, biotite pyroxenite and biotitite nodules

Analyses of clinopyroxenes from two Vesuvius (V-1, 14043) and one Alban Hills (AB6(c)) pyroxenite nodules are presented in

Table 3-7. V-1 (dark green in H.S.) and 14043 (black in H.S.) are ejected blocks (3" in diameter) from near the summit of Vesuvius. In T.S. they are composed of eu-subhedral crystals of clinopyroxene with accessory (<1%) olivine in V-1 and a small amount of interstitial glass in 14043.

AB6(c) was collected from a pyroclastics horizon near Albalonga (Group v^2). It is composed of sub-anhedral, green (apparently unzoned) clinopyroxene with <1% interstitial biotite, ore and leucite. Plate A-2 shows the wide range in size of the cpx crystals - the texture indicates that the nodule represents a segregation of early formed crystals (i.e. the nodule is a large glomeroaggregate). The texture of the Vesuvius nodules is similar.

Phlogopite and cpx analyses for minerals separated from a "biotite pyroxenite" collected from the peperino of Ariccia (Alban Hills) are presented in Tables 3-10 and 3-7. This nodule is composed of 68% elongate green cpx (max. 2mm in length) and 38% red brown phlogopitic mica. There is a marked sub-parallel alignment of the minerals in this nodule and the mica shows an ophitic relationship to the pyroxene. Plate A-3 shows another biotite pyroxenite from the Alban Hills (AB6(a)). This contains accessory olivine, ore and apatite and again shows the ophitic relationship between mica and pyroxene.

Ph-BAH (analysis presented in Table 3-10) was separated from a "biotitite" nodule collected from the peperino of Ariccia. This nodule is composed almost entirely of black mica and is similar to

the Type A biotitite described by Washington (1927, p. 187).

E:5 Miscellaneous data

Chemical analyses of Venanzite, Cupaellite, and Vesuv glass are presented in Table E-3. Mittempergher (1965) has presented a detailed description of Venanzite (melilite, olivine, diopside, leucite, kalsilite, phlogopite) and Rodolico (1937) has described the extremely undersaturated melilite bearing lava called Cupaellite (otherwise known as Coppaelite, from Coppaeli di Sotto near Rieti, Central Italy).

The Vesuv glass was separated from a leucite basanite specimen from Vesuvius. Coordinates in the system Qz-Ne-Ks for this glass are Qz = 33·30, Ne = 38·40, Ks = 28·30 (wt%).

Additional References

INNOCENTI, F. 1967. Studio chimico-petrografico delle vulcaniti di Radicofani. Rend. Soc. Min. Ital., 23, 99-128.

MITTEMPERGHER, M. 1965. Vulcanismo e petrogenesi nella zona di San Venanzo (Umbria). Atti. Soc. Tosc. Sc. Nat. Serie A., LXXII, 437-479.

RODOLICO, F. 1937. Le rocce vulcaniche di San Venanzo e Cupaello. Boll. Soc. Geol. It., 56, 33-66.

TABLE E-1

S.N.	SIO2	AL2O3	FE2O3	FEO	MGO	CAO	NA2O	K2O	H2O	TIO2	P2O5	MNO	BAO	SRO	TOTAL
100	45.35	14.59	7.98	1.82	5.43	10.57	1.71	8.20	1.90	0.92	0.65	0.16	0.28	0.20	99.8
200	47.58	14.84	3.40	4.10	6.29	10.49	0.98	8.66	1.21	0.78	0.46	0.12	0.19	0.12	99.2
400	46.68	17.13	4.12	3.97	4.57	9.37	2.10	8.81	0.35	0.89	0.53	0.14	0.28	0.20	99.1
800	49.31	13.87	2.25	4.43	7.96	10.69	1.41	7.53	0.29	0.75	0.42	0.13	0.16	0.17	99.4
810	48.34	13.19	3.43	4.24	8.21	11.46	1.51	6.52	0.30	0.77	0.45	0.13	0.18	0.19	98.9
900	46.08	13.99	5.14	3.21	6.66	11.15	1.47	9.15	0.36	0.87	0.60	0.13	0.26	0.17	99.2

S.N.	BA	ZR	Y	SR	RB	TH	ZN	FEE	FM	FF	KNA	KBA	KSR	KRB	THK	ZT	CS	RBSR
100	2539	423	68	1693	521	47	75	10.00	0.64	0.81	4.80	27	40	131	6.91	9	45	0.31
200	1670	295	53	989	697	42	56	7.95	0.54	0.45	8.84	43	73	103	5.84	7	76	0.70
400	2474	335	58	1715	531	46	63	8.53	0.64	0.51	4.20	30	43	138	6.29	7	39	0.31
800	1420	263	46	1435	565	42	54	7.17	0.46	0.34	5.34	44	44	111	6.72	6	53	0.39
810	1608	303	47	1567	458	45	62	8.14	0.48	0.45	4.32	34	35	118	8.32	7	52	0.29
900	2291	331	50	1453	605	42	61	8.70	0.56	0.62	6.22	33	52	126	5.53	8	55	0.42

TABLE E-2

S.N.	SIO2	AL2O3	FE2O3	FEO	MGO	CAO	NA2O	K2O	H2O	TIO2	P2O5	MNO	BAO	SRO	TOTAL
1	48.92	17.46	7.21	1.07	4.29	10.19	1.62	6.59	0.44	0.84	0.47	0.13	0.14	0.16	99.5
2	47.69	14.64	5.17	2.66	6.48	12.49	1.00	6.92	0.59	0.75	0.44	0.12	0.14	0.13	99.2
3	49.01	13.98	4.55	2.92	7.47	13.27	1.11	4.80	0.41	0.77	0.38	0.14	0.12	0.13	99.1
5	48.16	14.39	5.54	2.31	7.16	12.54	1.21	5.63	0.46	0.77	0.42	0.13	0.12	0.14	99.0
6	49.34	13.32	4.08	3.65	8.06	13.31	1.11	5.08	0.59	0.72	0.40	0.13	0.11	0.12	100.0
7	47.75	16.00	3.56	3.93	5.11	10.44	1.72	8.53	0.59	0.75	0.42	0.14	0.22	0.19	99.3
8	52.91	18.22	4.09	2.69	2.92	6.98	2.35	7.71	0.55	0.82	0.40	0.13	0.14	0.15	100.1
9	55.75	18.35	2.61	2.25	1.44	4.11	2.60	9.17	0.63	0.61	0.25	0.12	0.14	0.14	98.2
14	52.17	15.98	3.05	3.25	7.46	10.09	2.45	3.78	0.44	0.75	0.22	0.11	0.07	0.08	99.9
15	48.46	15.63	3.04	5.18	6.63	11.71	1.49	5.17	0.58	0.90	0.38	0.15	0.11	0.13	99.6
16	50.19	17.57	4.08	3.44	4.15	8.90	2.73	5.44	1.24	0.81	0.35	0.13	0.12	0.14	99.3
17	48.77	17.90	5.36	3.34	4.49	9.67	1.90	5.74	0.57	0.94	0.45	0.15	0.13	0.17	99.6

S.N.	BA	ZR	Y	SR	RB	TH	ZN	FEE	FM	FF	KNA	KBA	KSR	KRB	THK	ZT	CS	RBSR
1	1255	251	42	1335	627	42	71	8.40	0.66	0.87	4.07	44	41	87	7.68	6	55	0.47
2	1273	224	36	1105	653	39	72	8.12	0.55	0.66	6.92	45	52	88	6.79	6	81	0.59
3	1045	193	35	1101	389	21	59	7.79	0.50	0.61	4.32	38	36	102	5.27	9	86	0.35
5	1089	196	38	1194	513	30	62	8.10	0.52	0.71	4.65	43	39	91	6.42	7	75	0.43
6	979	196	33	1020	485	29	52	8.13	0.49	0.53	4.58	43	41	87	6.88	7	93	0.48
7	1930	366	48	1639	610	77	75	7.92	0.59	0.48	4.96	37	43	116	10.88	5	46	0.37
8	1287	322	57	1259	687	53	78	7.08	0.70	0.60	3.28	50	51	93	8.28	6	40	0.55
9	1288	356	60	1168	660	68	50	5.11	0.77	0.54	3.53	59	65	115	8.93	5	25	0.57
14	640	226	33	640	390	64	60	6.66	0.46	0.48	1.54	49	49	80	20.40	4	113	0.61
15	973	225	34	1097	430	29	61	8.79	0.55	0.37	3.47	44	39	100	6.76	8	76	0.39
16	1056	285	45	1198	482	27	76	7.90	0.64	0.54	1.99	43	38	94	5.98	11	53	0.40
17	1126	265	42	1411	453	27	77	9.07	0.66	0.62	3.02	42	34	105	5.67	10	49	0.32

TABLE E-3

	Aqua	Venanzite	Cupaellite	Vesuv Glass
SiO_2	55·42	42·47	44·58	55·33
Al_2O_3	20·17	10·29	7·48	19·63
TiO_2	0·49	0·73	1·08	0·97
Fe_2O_3	2·21	1·57	4·08	2·52
FeO	1·66	5·21	2·77	0·57
MnO	0·14	0·11	0·11	0·12
MgO	0·71	12·84	10·83	1·28
CaO	3·57	14·83	14·39	2·11
Na_2O	3·84	1·11	0·28	7·20
K_2O	9·29	8·05	7·54	7·22
P_2O_5	0·12	0·41	1·02	0·26
H_2O+	0·89	0·70	4·27	2·17
CO_2	n.d.	0·73	0·41	n.d.
BaO	0·25	0·10	0·47	0·31
SrO	0·19	0·19	0·40	-
	99·0	99·3	99·7	99·7
Ba	601	884	4224	2771
Zr	63	348	938	488
Y	1610	45	99	26
Sr	454	1600	3341	431
Rb	144	569	552	165
Th	80	35	85	n.d.
Zn	183	81	130	94

TABLE E-4

S.N.	SIO2	AL2O3	FE2O3	FEO	MGO	CAO	NA2O	K2O	H2O	TIO2	P2O5	MNO	BAO	SRO	TOTAL
1	54.22	15.13	3.97	2.41	8.25	7.22	1.57	4.15	0.74	1.02	0.26	0.11	0.09	0.04	99.2
2	53.23	16.46	0.82	5.66	7.93	8.58	1.98	2.94	0.62	0.89	0.24	0.12	0.08	0.04	99.6
3	53.72	15.63	2.64	3.94	7.95	8.11	1.78	3.70	0.51	0.96	0.24	0.11	0.08	0.04	99.4
4	54.83	14.09	2.79	3.02	9.27	6.45	1.44	5.24	0.42	1.10	0.31	0.10	0.09	0.04	99.2
5	55.12	14.04	5.05	1.11	8.74	6.44	1.49	5.43	0.53	1.14	0.31	0.10	0.09	0.04	99.6
6	54.02	15.90	0.16	5.87	8.15	8.25	1.90	3.39	0.44	0.94	0.23	0.11	0.08	0.04	99.5
7	53.21	16.04	0.61	5.79	7.87	8.37	1.93	3.28	0.55	0.92	0.24	0.11	0.08	0.04	99.0
8	52.58	15.96	1.11	5.08	8.03	8.23	1.96	3.20	1.05	0.88	0.23	0.11	0.08	0.04	98.5

S.N.	BA	ZR	Y	SR	RB	TH	ZN
1	764	326	20	338	382	59	78
2	690	197	21	332	213	39	77
3	729	258	20	340	308	48	70
4	829	419	28	368	509	71	70
5	824	434	30	369	492	57	72
6	751	240	24	336	255	33	68
7	759	225	24	327	246	33	57
8	749	215	22	325	250	23	58

FEE	FM	FF	KNA	KBA	KSR	KRB	THK	ZT	CS	RBSR
6.65	0.44	0.62	2.64	45	102	90	17.13	6	153	1.13
7.10	0.45	0.13	1.48	35	73	115	15.98	5	185	0.64
7.01	0.45	0.40	2.08	42	90	100	15.63	5	170	0.91
6.14	0.39	0.48	3.64	52	118	85	16.32	6	125	1.38
6.28	0.41	0.82	3.64	55	122	92	12.65	8	125	1.33
6.68	0.43	0.03	1.78	37	84	110	11.73	7	175	0.76
7.04	0.45	0.10	1.70	36	83	111	12.12	7	183	0.75
6.75	0.44	0.18	1.63	35	82	106	8.66	9	181	0.77

PLATE A-1

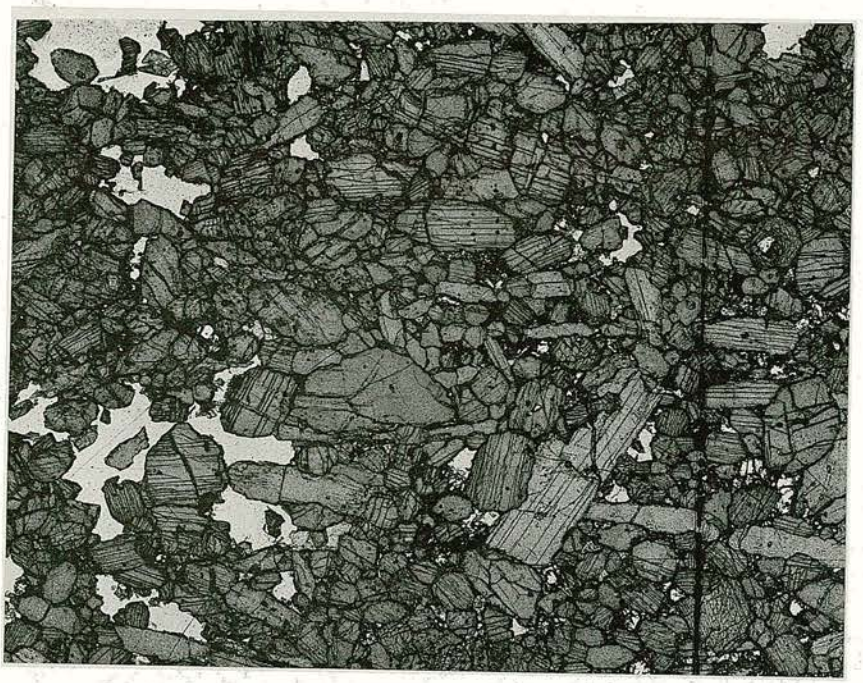
AB800 Olivine leucitite

x 7

PLATE A-2

AB6(c) Pyroxenite

x 8



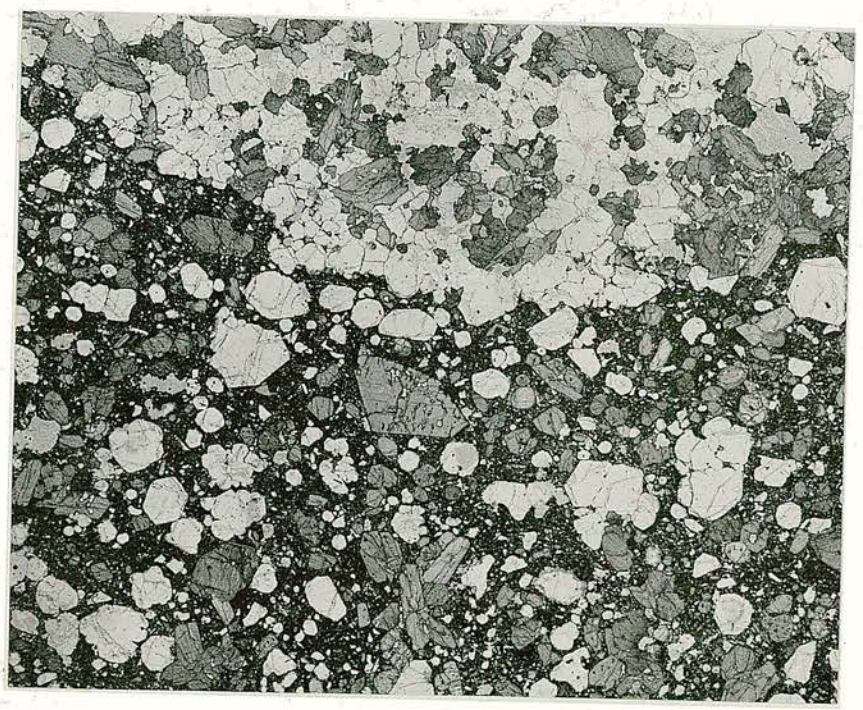


PLATE A-3

AB6(a) Biotite Pyroxenite

x 8

